VOLUME 1 Si, Ge, C (Diamond), GaAs, GaP, GaSb, InAs, InP, InSb

HANDBOOK SERIES ON

SEMICONDUCTOR PARAMETERS

HANDBOOK SERIES ON SEMICONDUCTOR PARAMETERS

edited by M. Levinshtein, S. Rumyantsev and M. Shur

Vol. 1: Si, Ge, C (Diamond), GaAs, GaP, GaSb, InAs, InP, InSb

Vol. 2: Ternary and Quaternary A_3B_5 Semiconductors

Vol. 3: A_4B_4, A_4B_6 and A_3N Semiconductors

Vol. 4: A_2B_6 Semiconductors and Ternary A_2B_6 Compounds

Vol. 5: Amorphous Semiconductors and SiO_2, Si_3N_4

VOLUME 1 Si, Ge, C (Diamond), GaAs, GaP, GaSb, InAs, InP, InSb

HANDBOOK SERIES ON

SEMICONDUCTOR PARAMETERS

Editors

M LEVINSHTEIN
S RUMYANTSEV
Ioffe Institute

M SHUR
Rensselaer Polytechnic Institute

World Scientific
Singapore • New Jersey • London • Hong Kong

Published by

World Scientific Publishing Co. Pte. Ltd.

P O Box 128, Farrer Road, Singapore 912805

USA office: Suite 1B, 1060 Main Street, River Edge, NJ 07661

UK office: 57 Shelton Street, Covent Garden, London WC2H 9HE

British Library Cataloguing-in-Publication Data
A catalogue record for this book is available from the British Library.

First published 1996
Reprinted 2000

HANDBOOK SERIES ON SEMICONDUCTOR PARAMETERS
VOLUME 1: Si, Ge, C (Diamond), GaAs, GaP, GaSb, InAs, InP, InSb

ISBN 981-02-1420-0 (Set)
ISBN 981-02-2934-8

This book is printed on acid-free paper.

Printed in Singapore by Uto-Print

To our children,
Alexandra, Dina, Ira, Natasha, Vladimir, and Luba,
their mothers, and our wives.

This page is intentionally left blank

PREFACE

This handbook contains frequently needed information for the most important semiconductor materials. We have also included basic references where one can find additional information if required.

The data for each material is organized in the same way in order to facilitate searching for information. We have tried to come up with a handbook which will be useful for every semiconductor student, researcher, or engineer.

For almost every parameter given in this handbook, different sources give somewhat different values. Often, these differences are larger than the stated accuracy. In such cases, we chose the values which we believe to be more reliable.

In compiling this handbook, we took advantage of generous help from many colleagues at the A. F. Ioffe Institute and the University of Virginia who made many excellent suggestions, and, in some cases, provided us with more accurate values of material parameters.

The Editors

This page is intentionally left blank

CONTENTS

CHAPTER 1

SILICON (Si)

M. E. Levinshtein and **S. L. Rumyantsev**
Ioffe Institute, St. Petersburg, Russia

1.1. Basic Parameters at 300 K

Crystal structure		Diamond
Group of symmetry		O_h^7–Fd3m
Number of atoms in 1 cm^3		5×10^{22}
Auger recombination coefficient	($cm^6\ s^{-1}$)	
	C_n	1.1×10^{-30}
	C_p	3×10^{-31}
Debye temperature	(K)	640
Density	($g\,cm^{-3}$)	2.329
Dielectric constant		11.7
Effective electron masses (in units of m_o)		
longitudinal m_l/m_o		0.98
transverse m_t/m_o		0.19
Effective hole masses	(in units of m_o)	
heavy m_h/m_o		0.49
light m_{lp}/m_o		0.16
Electron affinity	(eV)	4.05
Lattice constant	(Å)	5.431
Optical phonon energy	(eV)	0.063

Band structure and carrier concentration

Energy gap	(eV)	1.12
Energy separation ($E_{\Gamma 2}$)	(eV)	4.2
Energy spin-orbital splitting	(eV)	0.044
Intrinsic carrier concentration	(cm^{-3})	1×10^{10}
Intrinsic resistivity	($\Omega \times cm$)	3.2×10^{5}
Effective conduction band density of states	(cm^{-3})	3.2×10^{19}
Effective valence band density of states	(cm^{-3})	1.8×10^{19}

Electrical properties

Breakdown field	($V\,cm^{-1}$)	$\simeq 3 \times 10^{5}$
Mobility	($cm^2\ V^{-1}\ s^{-1}$)	
	electrons	≤ 1400
	holes	≤ 450
Diffusion coefficient	($cm^2\ s^{-1}$)	
	electrons	≤ 36
	holes	≤ 12
Electron thermal velocity	($m\ s^{-1}$)	2.3×10^{5}
Hole thermal velocity	($m\ s^{-1}$)	1.65×10^{5}

Optical properties

Index of refraction	3.42
Radiative recombination coefficient ($cm^3\ s^{-1}$)	1.1×10^{-14}

Thermal and mechanical properties

Bulk modulus	($dyn\,cm^{-2}$)	9.8×10^{11}
Melting point	(°C)	1412
Specific heat	($J\ g^{-1}\ °C^{-1}$)	0.7
Thermal conductivity	($W\ cm^{-1}\ °C^{-1}$)	1.3
Thermal diffusivity	($cm^2\,s^{-1}$)	0.8
Thermal expansion, linear	($°C^{-1}$)	2.6×10^{-6}

1.2. Band Structure and Carrier Concentration

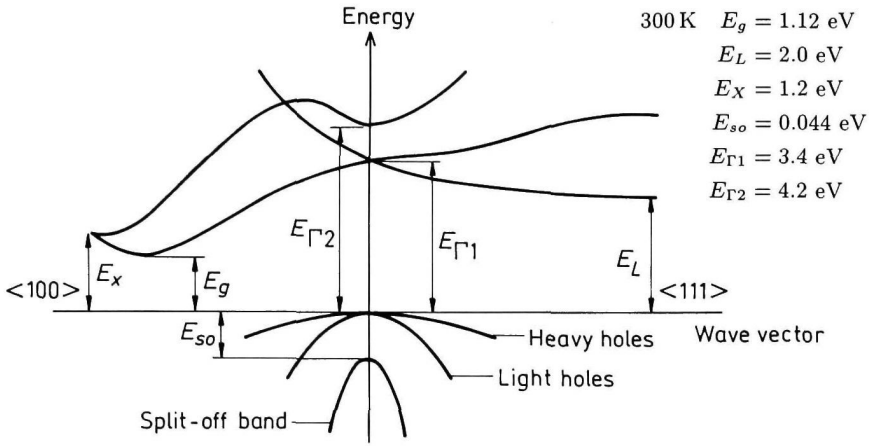

Fig. 1.2.1. Band structure of Si. Important minima of the conduction band and maxima of the valence band.

1.2.1. *Temperature Dependences*

Temperature dependence of the energy gap

$$E_g = 1.17 - 4.73 \times 10^{-4} \frac{T^2}{T + 636} \text{ (eV)} , \tag{1.2.1}$$

where T is temperature in degrees K.

Temperature dependence of the direct band gap $E_{\Gamma 2}$

$$E_{\Gamma 2} = 4.34 - 3.91 \times 10^{-4} \frac{T^2}{T + 125} \text{ (eV)} . \tag{1.2.2}$$

Intrinsic carrier concentration

$$n_i = (N_c \cdot N_v)^{1/2} \exp\left[-\frac{E_g}{2k_B T}\right] . \tag{1.2.3}$$

Effective density of states in the conduction band

$$N_c = 4.82 \times 10^{15} M \left(\frac{m_c}{m_o}\right)^{3/2} \times T^{3/2}$$

$$= 4.82 \times 10^{15} \left(\frac{m_{cd}}{m_o}\right)^{3/2} \times T^{3/2} \ (\mathrm{cm}^{-3}) \qquad (1.2.4)$$

or

$$N_c = 6.2 \times 10^{15} \times T^{3/2} \ (\mathrm{cm}^{-3}) \ ,$$

$M = 6$ is the number of equivalent valleys in the conduction band.
$m_c = 0.36\ m_o$ is the effective mass of the density of states in one valley of conduction band.
$m_{cd} = 1.18\ m_o$ is the effective mass of density of states.

Effective density of states in the valence band

$$N_v = 3.5 \times 10^{15} \times T^{3/2} \ (\mathrm{cm}^{-3}) \qquad (1.2.5)$$

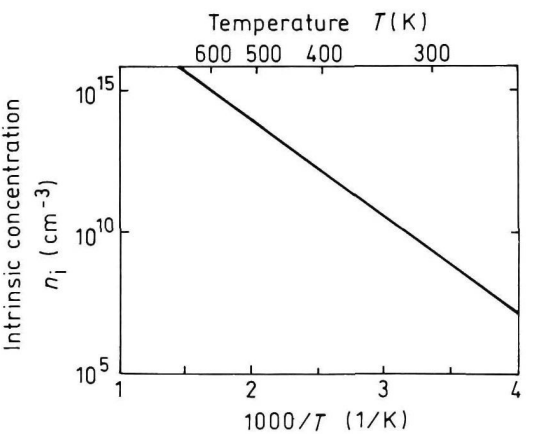

Fig. 1.2.2. The temperature dependence of the intrinsic carrier concentration (Shur [1990]). (Figure reprinted with permission of Prentice Hall, Inc.)

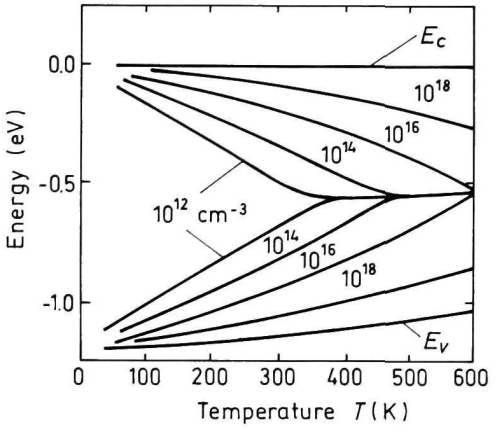

Fig. 1.2.3. Fermi level versus temperature for different concentrations of shallow donors and acceptors (Grove [1967]). (Figure reprinted by permission of John Wiley and Sons, Inc.)

1.2.2. *Dependence of the Energy Gap on Hydrostatic Pressure*

$$E_g = E_g(0) - 1.4 \times 10^{-3}\ P\ \text{(eV)} \tag{1.2.6}$$

where P is pressure in kbar.

1.2.3. *Energy Gap Narrowing at High Doping Levels*

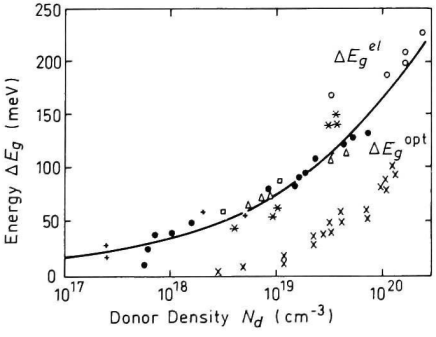

Fig. 1.2.4. Electrical and optical energy gap narrowing versus donor doping density (Van Overstraeten and Mertens [1987]). (Figure reprinted with kind permission from Elsevier Science Ltd.)

For $10^{17} \leq N_d \leq 3 \times 10^{20}$ cm^{-3}, $\Delta E_g^{el} \simeq 3.5 \times 10^{-8} \cdot N_d^{1/3}$ (eV) (N_d in cm^{-3}).

1.2.4. *Effective Masses*

Electrons

The surfaces of equal energy are ellipsoids. $m_l = 0.98\ m_0$
$m_t = 0.19\ m_0$

Effective mass of density of states $m_c = 0.36\ m_0$.

There are 6 equivalent valleys in the conduction band.
Effective mass of conductivity $m_{cc} = 0.26\ m_0$

Holes

heavy	$m_h = 0.49\ m_0$
light	$m_{lp} = 0.16\ m_0$
split-off band	$m_{so} = 0.24\ m_0$

Effective mass of density of states $m_v = 0.81\ m_0$ (300 K)

1.2.5. *Donors and Acceptors*

Ionization energies of shallow donors (eV)

As	0.054
P	0.045
Sb	0.043

Ionization energies of shallow acceptors (eV)

Al	0.072
B	0.045
Ga	0.074
In	0.157

The most important deep levels with impurities

Impurity	Type	Position in the forbidden gap	$\sigma_n(\mathrm{cm}^2)$	$\sigma_p(\mathrm{cm}^2)$
Au	d	$E_v + 0.35$ eV	10^{-15}	3.5×10^{-15}
	a	$E_c - 0.55$ eV	8×10^{-17}	9.0×10^{-15}
Cu	d	$E_v + 0.24$ eV		3.5×10^{-20}
	a	$E_v + 0.37$ eV		
	a	$E_v + 0.52$ eV		
Fe	d	$E_v + 0.39$ eV		2.0×10^{-17}
Ni	a	$E_c - 0.35$ eV	7×10^{-12}	
	a	$E_v + 0.23$ eV		
Pt	d	$E_v + 0.32$ eV		$\sim 10^{-15}$
	a	$E_v + 0.36$ eV		
	a	$E_c - 0.25$ eV	5×10^{-14}	
Zn	a	$E_v + 0.32$ eV	10^{-15}	10^{-13}
	a	$E_c - 0.5$ eV	10^{-19}	10^{-13}

a – acceptor, d – donor

The most important deep levels with radiation defects

Defect	Type	Position in the forbidden gap	$\sigma_n(\mathrm{cm}^2)$	$\sigma_p(\mathrm{cm}^2)$
A-center	a	$E_c - 0.17$ eV	10^{-14}	$> 5 \times 10^{-14}$
E-center	a	$E_c - 0.45$ eV	5×10^{-15}	$> 10^{-13}$
K-center	d	$E_v + 0.35$ eV	$\ll 10^{-15}$	$(0.1 \div 1) \times 10^{-15}$
Vac–Vac	d	$E_v + 0.20$ eV	4×10^{-14}	5×10^{-16}
	a	$E_c - 0.23$ eV	5×10^{-16}	4×10^{-14}
	a	$E_c - 0.41$ eV	$\sim 10^{-14}$	3×10^{-15}

a – acceptor, d – donor

1.3. Electrical Properties

1.3.1. *Mobility and Hall Effect*

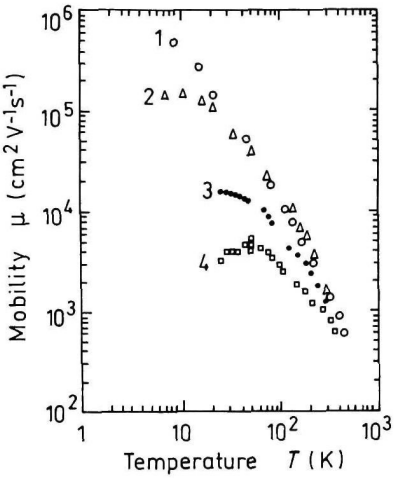

Fig. 1.3.1. Electron mobility versus temperature for different doping levels.

1. High purity Si($N_d < 10^{12}$cm^{-3}); time-of-flight technique (Canali *et al.* [1975]).
2. High purity Si($N_d = 4 \times 10^{13}$cm^{-3}); photo-Hall effect (Norton *et al.* [1973]).
3. $N_d = 1.75 \times 10^{16}$ cm^{-3}; $N_a = 1.48 \times 10^{15}$ cm^{-3}; Hall-effect (Morin and Maita [1954]).
4. $N_d = 1.3 \times 10^{17}$ cm^{-3}; $N_a = 2.2 \times 10^{15}$ cm^{-3}; Hall-effect (Morin and Maita [1954]).

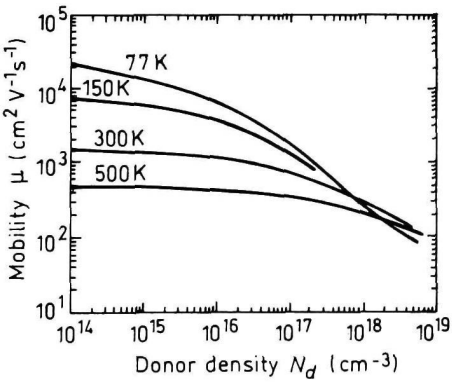

Fig. 1.3.2. Electron drift mobility versus donor density at different temperatures (Li and Thurber [1977]). (Figure reprinted with kind permission from Elsevier Science Ltd.)

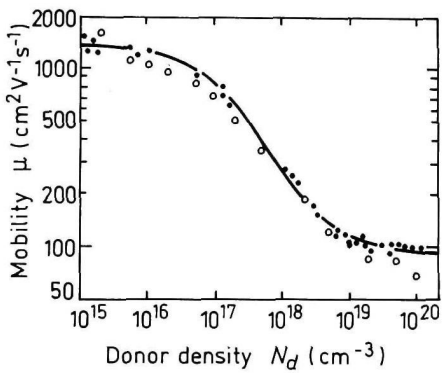

Fig. 1.3.3. Electron drift mobility versus donor density, 300 K (Jacoboni *et al.* [1977]). (Figure reprinted with kind permission from Elsevier Science Ltd.)

At 300 K for 10^{15} cm$^{-3} \leq N_d \leq 10^{20}$ cm^{-3} electron drift mobility μ_n

$$\mu_n \simeq \mu_{\min} + \frac{\mu_{\max} - \mu_{\min}}{1 + (N_d/N_{\text{ref}})^{\alpha}} , \tag{1.3.1}$$

where $\mu_{\min} = 92$ cm^2 V^{-1} s^{-1}, $\mu_{\max} = 1360$ cm^2 V^{-1} s^{-1}, $\alpha = 0.91$, $N_{\text{ref}} = 1.3 \times 10^{17}$ cm^{-3} (Baccarani and Ostoja [1975]).

For $N_d \leq 10^{15}$ cm^{-3} and $250 \leq T \leq 600$ K,

$$\mu_n \simeq 1430 \times \left(\frac{300}{T}\right)^{2.2} \text{(cm}^2 \text{ V}^{-1} \text{ s}^{-1}\text{)} \tag{1.3.2}$$

(Dorkel and Leturcq [1981]).

For $N_d \leq 10^{18}$ cm^{-3} and 200 K $\leq T \leq 600$ K,

$$\mu_n \simeq \frac{\mu_L \times \mu_I}{\mu_L + \mu_I} , \tag{1.3.3}$$

where

$$\mu_L = 1430 \left(\frac{300}{T}\right)^{2.2} \quad \text{(cm}^2 \text{ V}^{-1} \text{ s}^{-1}\text{)}$$

$$\mu_I = \frac{A \times T^{3/2}}{N_d} \times \left[\ln\left(1 + \frac{B \times T^2}{N_d}\right) - \frac{B \times T^2}{N_d + B \times T^2}\right]^{-1} ,$$

where $A = 4.61 \times 10^{17}$ cm^{-1} V^{-1} s^{-1} K$^{-3/2}$, $B = 1.52 \times 10^{15}$ cm^{-3} K^{-2} (Dorkel and Leturcq [1981]).

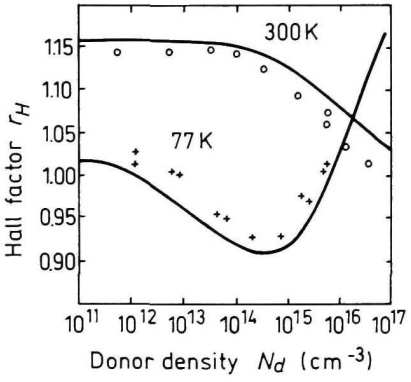

Fig. 1.3.4. The electron Hall factor versus donor density for 77 K and 300 K. Solid lines show the results of calculations. Symbols represent experimental data (Kirnas *et al.* [1974]).

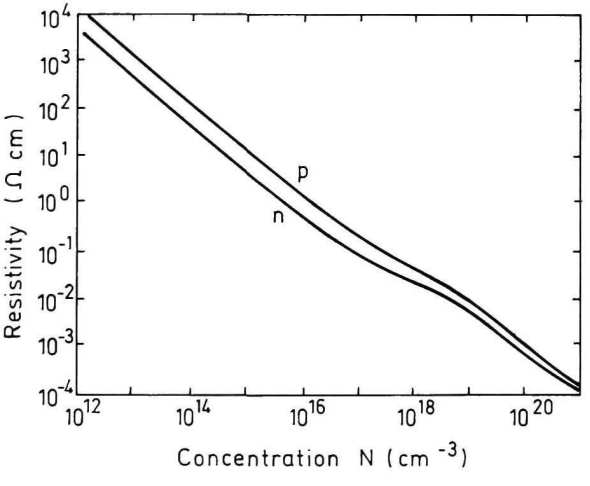

Fig. 1.3.5. Resistivity versus impurity concentration for Si at 300 K (Sze [1980]). (Figure reprinted by permission of John Wiley and Sons, Inc.)

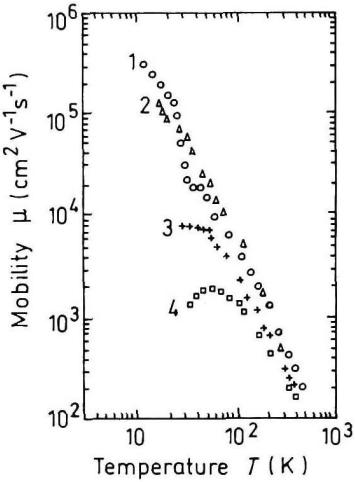

Fig. 1.3.6. Temperature dependences of hole mobility for different doping levels.

1. High purity Si($N_a \leq 10^{12}$ cm^{-3}); time-of-flight technique (Ottaviani *et al.* [1975]).
2. High purity Si($N_a \simeq 10^{14}$ cm^{-3}); Hall-effect (Logan and Peters [1960]).
3. $N_a = 2.4 \times 10^{16}$ cm^{-3}; $N_d = 2.3 \times 10^{15}$ cm^{-3}; Hall-effect (Morin and Maita [1954]).
4. $N_a = 2 \times 10^{17}$ cm^{-3}; $N_d = 4.9 \times 10^{15}$ cm^{-3}; Hall-effect (Morin and Maita [1954]).

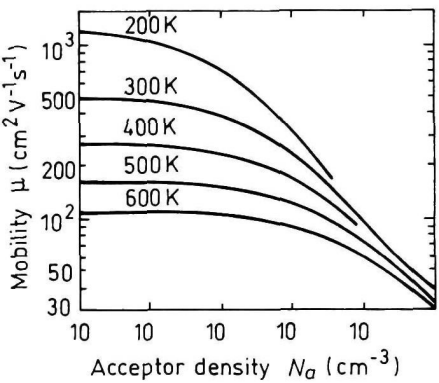

Fig. 1.3.7. Hole drift mobility versus acceptor density at different temperatures (Dorkel and Leturcq [1981]). (Figure reprinted with kind permission from Elsevier Science Ltd.)

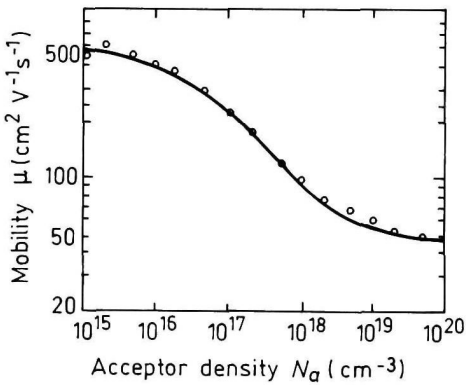

Fig. 1.3.8. Hole drift mobility versus acceptor density, 300 K (Jacoboni *et al.* [1977]). (Figure reprinted with kind permission from Elsevier Science Ltd.)

At 300 K for $10^{15}\text{cm}^{-3} \leq N_a \leq 10^{20}\text{cm}^{-3}$ hole drift mobility μ_p

$$\mu_p \simeq \mu_{\min} + \frac{\mu_{\max} - \mu_{\min}}{1 + (N_a/N_{\text{ref}})^{\alpha}} , \tag{1.3.4}$$

where $\mu_{\min} = 48\ \text{cm}^2\text{V}^{-1}\text{s}^{-1}$, $\mu_{\max} = 450\ \text{cm}^2\text{V}^{-1}\text{s}^{-1}$, $\alpha = 0.76$, $N_{\text{ref}} = 6.3 \times 10^{16}\,\text{cm}^{-3}$.

For $N_a \leq 10^{18}\,\text{cm}^{-3}$ and $200\,\text{K} \leq T \leq 600\,\text{K}$,

$$\mu_p \simeq \frac{\mu_L \times \mu_I}{\mu_L + \mu_I} , \tag{1.3.5}$$

where

$$\mu_L = 495 \left(\frac{300}{T}\right)^{2.2} \quad (\text{cm}^2\text{V}^{-1}\text{s}^{-1})$$

$$\mu_I = \frac{A \times T^{3/2}}{N_a} \times \left[\ln\left(1 + \frac{B \times T^2}{N_a}\right) - \frac{B \times T^2}{N_a + B \times T^2}\right]^{-1} ,$$

where $A = 1 \times 10^{17}\text{cm}^{-1}\text{V}^{-1}\text{s}^{-1}\text{K}^{-3/2}$, $B = 6.25 \times 10^{14}\text{cm}^{-3}\text{K}^{-2}$ (Dorkel and Leturcq [1981]).

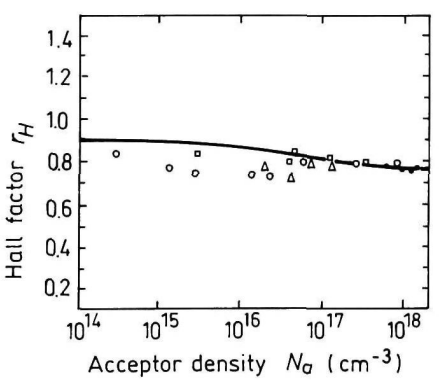

Fig. 1.3.9. The hole Hall factor versus acceptor density, 300 K (Lin *et al.* [1981]). (Figure reprinted with kind permission from Elsevier Science Ltd.)

1.3.2. *Transport Properties in High Electric Field*

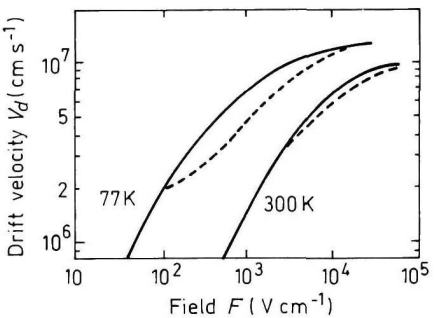

Fig. 1.3.10. Field dependences of the electron drift velocity. Solid lines: $F\|(111)$; Dashed lines: $F\|(100)$ (Jacoboni *et al.* [1977]). (Figure reprinted with kind permission from Elsevier Science Ltd.)

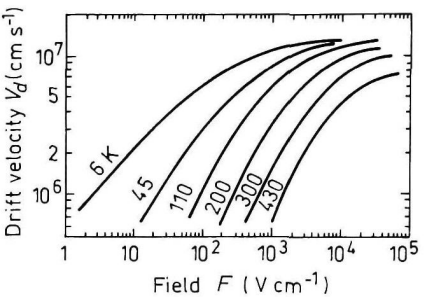

Fig. 1.3.11. Field dependences of the electron drift velocity at different temperatures. $F\|(111)$ (Jacoboni *et al.* [1977]). (Figure reprinted with kind permission from Elsevier Science Ltd.)

For $F\|(111)$, $N_d \leq 10^{16}$ cm^{-3} and $T > 250$ K electron drift velocity v_d can be fitted by the equation

$$v_d \simeq v_s \times \frac{F}{F_c} \times \left[1 + (F/F_c)^\beta\right]^{-1/\beta} , \tag{1.3.6}$$

where $v_s = 1.53 \times 10^9 \times T^{-0.87}$cm s^{-1}; $F_c = 1.01 \times T^{1.55}$V cm^{-1}, $\beta = 2.57 \times 10^{-2} \times T^{0.66}$ (Jacoboni *et al.* [1977]).

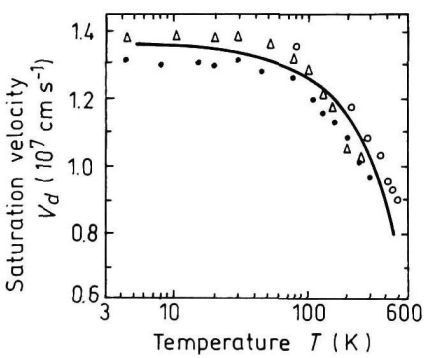

Fig. 1.3.12. Temperature dependence of the saturation electron drift velocity (Jacoboni *et al.* [1977]).
Solid line is calculated according to equation

$$v_s = v_{so} \times [1 + C \times \exp(T/\theta)]^{-1} ,$$

where $v_s = 2.4 \times 10^7$cm s^{-1}, $C = 0.8$, $\theta = 600$ K. (Figure reprinted with kind permission from Elsevier Science Ltd.)

At 300 K the dependence of the electron drift velocity versus field at different donor concentrations can be calculated as

$$v_d \simeq \frac{\mu_0 \times F}{\left[1 + \frac{N_d}{N_d/C_n + N_{\text{ref}}} + \frac{(F/A_n)^2}{F/A_n + G_n} + \left(\frac{F}{B_n}\right)^2\right]^{1/2}} \tag{1.3.7}$$

where $\mu_o = 1400\,\text{cm}^2\text{V}^{-1}\text{s}^{-1}$, $N_{\text{ref}} = 3 \times 10^{16}\,\text{cm}^{-3}$, $C_n = 350$, $A_n = 3.5 \times 10^3\ \text{V cm}^{-1}$, $B_n = 7.4 \times 10^3\ \text{V cm}^{-1}$, $G_n = 8.8$ (Scharfetter and Gummel [1969]).

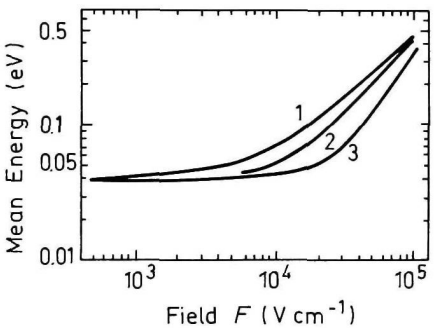

Fig. 1.3.13. Mean energy of electrons as a function of electric field F at different donor densities, $F\|(111)$, 300 K (Jacoboni *et al.* [1977]).

1. $N_d = 0$,
2. $N_d = 4 \times 10^{18}\ \text{cm}^{-3}$;
3. $N_d = 4 \times 10^{19}\ \text{cm}^{-3}$. (Reprinted with kind permission from Elsevier Science Ltd.)

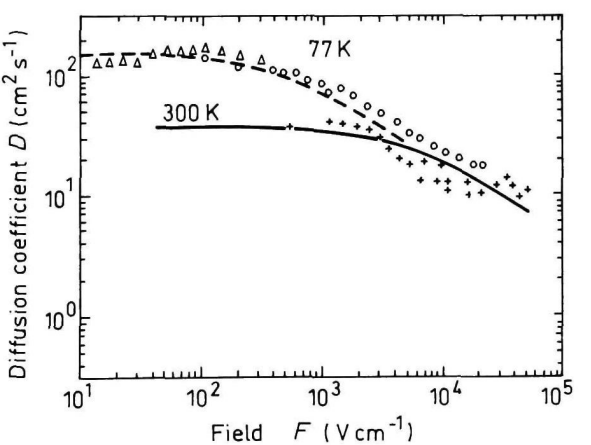

Fig. 1.3.14. The field dependence of longitudinal electron diffusion coefficient D for 77 K and 300 K, $F\|(111)$. Dashed and solid lines show the results of the Monte-Carlo simulation. Symbols represent measured data (Canali *et al.* [1985]).

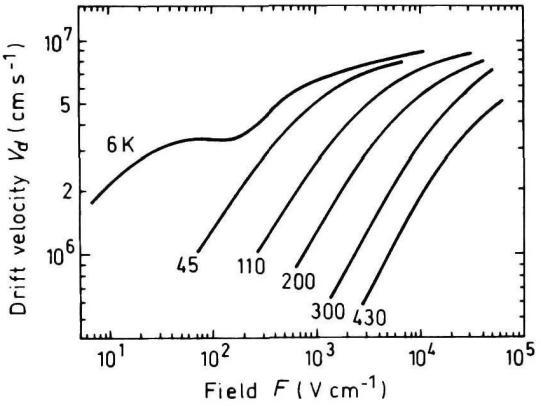

Fig. 1.3.15. Field dependences of the hole drift velocity at different temperatures, $F\|(100)$ (Jacoboni *et al.* [1977]). (Reprinted with kind permission from Elsevier Science Ltd.)

For $N_a \leq 10^{16}$ cm^{-3} and $T > 250$ K hole drift velocity v_d can be fitted by the equation

$$v_d \simeq v_s \times \frac{F}{F_c} \times \left[1 + (F/F_c)^{\beta}\right]^{-1/\beta} , \tag{1.3.8}$$

where

$$v_s \simeq 1.62 \times 10^8 \times T^{-0.52} \ (\mathrm{cm\,s^{-1}}) , \tag{1.3.9}$$

$F_c = 1.24 \times T^{1.68}$ V cm^{-1}, $\beta = 0.46 \times T^{0.17}$ (Jacoboni *et al.* [1977]).

At 300 K the dependence of the hole drift velocity versus field at different acceptor concentrations can be calculated as

$$v_d \simeq \frac{\mu_0 \times F}{\left[1 + \dfrac{N_a}{N_a/C_p + N_{\mathrm{ref}}} + \dfrac{(F/A_p)^2}{F/A_p + G_p} + \left(\dfrac{F}{B_p}\right)^2\right]^{1/2}} \tag{1.3.10}$$

where $\mu_o = 480\,\mathrm{cm^2\ V^{-1}\ s^{-1}}$, $N_{\mathrm{ref}} = 4 \times 10^{16}\,\mathrm{cm^{-3}}$, $C_p = 81$, $A_p = 6.1 \times 10^3$ V cm^{-1}, $B_p = 2.5 \times 10^3$ V cm^{-1}, $G_p = 1.6$ (Scharfetter and Gummel [1969]).

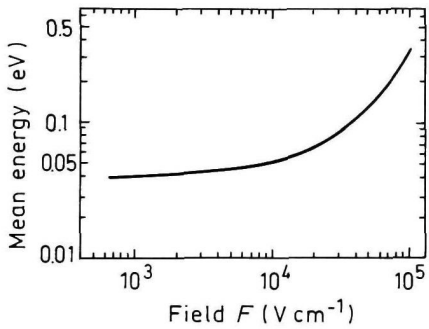

Fig. 1.3.16. Mean energy of holes as a function of electric field F. $N_a = 0$, 300 K (Jacoboni *et al.* [1977]). (Reprinted with kind permission from Elsevier Science Ltd.)

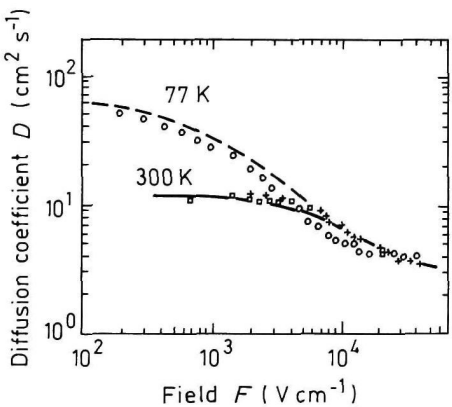

Fig. 1.3.17. The field dependence of longitudinal hole diffusion coefficient D for 77 K and 300 K, $F\|(111)$. Dashed and solid lines show the results of the Monte-Carlo simulation. Symbols represent measured data (Canali *et al.* [1985]).

1.3.3. *Impact Ionization*

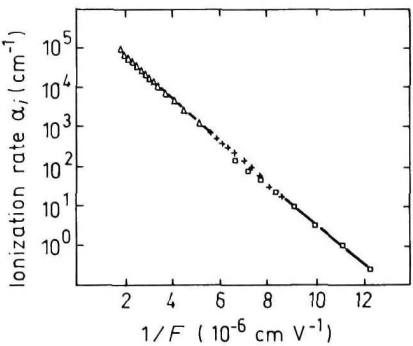

Fig. 1.3.18. The dependence of ionization rate α_i for electrons versus $1/F$, 300 K (Maes *et al.* [1990]). (Reprinted with kind permission from Elsevier Science Ltd.)

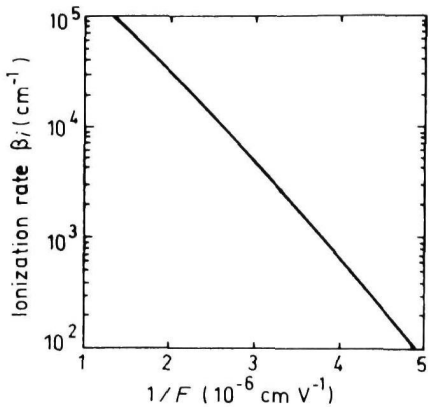

Fig. 1.3.19. The dependence of ionization rate β_i for holes versus $1/F$, 300 K (Grant [1973]). (Reprinted with kind permission from Elsevier Science Ltd.)

For electrons

$$\alpha_i = \alpha_0 \times \exp[-F_{no}/F] \tag{1.3.11}$$

For 300 K, $\alpha_o = 3.318 \times 10^5$ cm^{-1}, $F_{no} = 1.174 \times 10^6$ V cm^{-1} (Maes *et al.* [1990]).

For holes

$$\beta_i = \beta_0 \times \exp[-F_{po}/F] \tag{1.3.12}$$

For 300 K (Grant [1973])

2×10^5 V cm^{-1} $< F <$ 5.3×10^5 V cm^{-1}, $\beta_0 = 2\times10^6$cm^{-1}, $F_{po} = 1.97\times10^6$ V cm^{-1}
$F > 5.3 \times 10^5$V cm^{-1}, $\beta_0 = 5.6 \times 10^5$cm^{-1}, $F_{po} = 1.32 \times 10^6$ V cm^{-1}

The dependence of ionization rates α_i and β_i on crystal orientation has not been found.

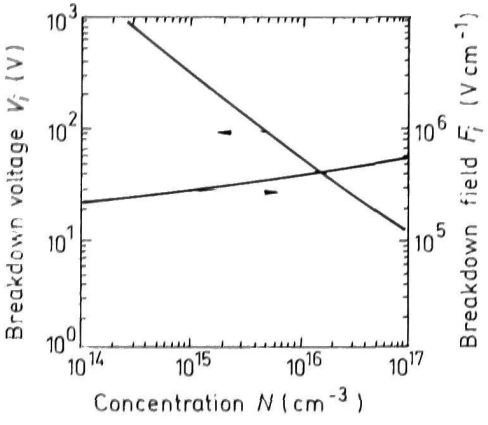

Fig. 1.3.20. Breakdown voltage and breakdown field versus doping density for an abrupt *p-n* junction, 300 K (Sze [1981]). (Figure reprinted by permission of John Wiley and Sons, Inc.)

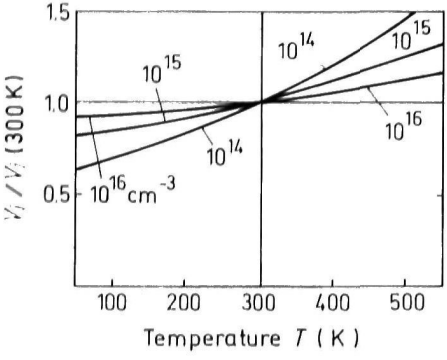

Fig. 1.3.21. Normalized breakdown voltage versus temperature for an abrupt *p-n* junction at different doping levels (Crowell and Sze [1966]).

1.3.4. *Recombination Parameters*

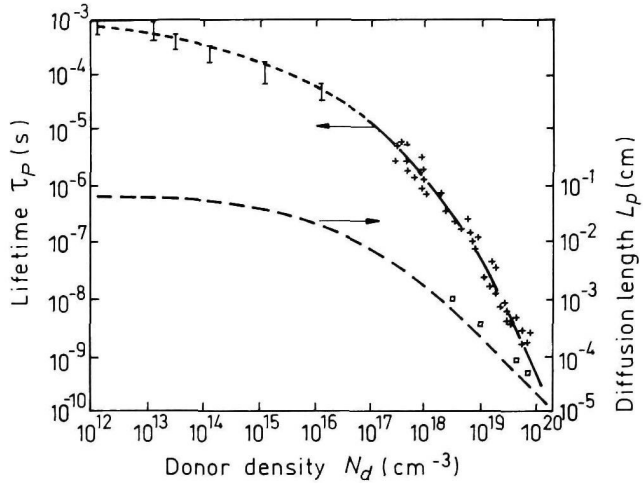

Fig. 1.3.22. Lifetime τ_p and diffusion length L_p of holes in n-type Si versus donor density, 300 K.

$\tau_p(N_d)$ dependence:

For $10^{12}\text{cm}^{-3} < N_d \leq 10^{17}\text{cm}^{-3}$ from numerous experimental data for good quality industrial produced n-Si.

For $N_d \geq 10^{17}\text{cm}^{-3}$ – (Alamo and Swanson [1987]).

$L_p(N_d)$ dependence (dashed line) is calculated as

$$L_p(N_d) = [D_p(N) \times \tau_p(N)]^{1/2}$$

where

$$D_p = \frac{k_B \times T}{q} \times \mu_p \ .$$

The dependence of μ_p versus N is taken from Fig. 1.3.8. The dependence of τ_p versus N is taken from this figure. Squares indicate experimental results of Wang *et al.* [1989].

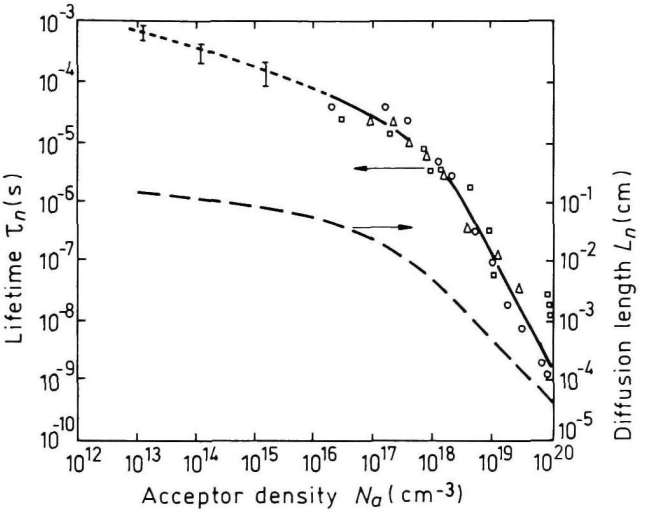

Fig. 1.3.23. Lifetime τ_n and diffusion length L_n of electrons in p-type Si versus acceptor density, 300 K.

$\tau_n(N_a)$ dependence:

For $10^{13}\text{cm} < N_a \leq 10^{16}\text{cm}^{-3}$ — from numerous experimental data for good quality industrial produced p-Si.

For $N_a \geq 10^{16}\text{cm}^{-3}$ — (Tyagi and Van Overstraeten [1983]).

$L_n(N_a)$ dependence (dashed line) is calculated as

$$L_n(N_a) = [D_n(N) \times \tau_n(N)]^{1/2}$$

where

$$D_n = \frac{k_B \times T}{q} \times \mu_n \ .$$

The dependence of μ_n versus N is taken from Fig. 1.3.3. The dependence of τ_n versus N is taken from this figure.

Surface recombination

Surface recombination rate depending on treatment of Si surface lies in the range between $10^2 \div (6\text{–}8) \times 10^4$ cm s^{-1}. Surface recombination rate on the Si–SiO_2 interface can be as small as ≤ 0.5 cm s^{-1}.

Radiative recombination coefficient at 300 K (Gerlach *et al.* [1972])

$$1.1 \times 10^{-14} \text{ cm}^3 \text{ s}^{-1}$$

Auger coefficient at 300 K

C_n	1.1×10^{-30} cm^6 s^{-1}
C_p	0.3×10^{-30} cm^6 s^{-1}
$C = C_n + C_p$	1.4×10^{-30} cm^6 s^{-1}

for $180\,\text{K} \leq T \leq 400\,\text{K}$

$$C \simeq 1.4 \times 10^{-30} \left(\frac{T}{300}\right)^{0.5} \quad (\text{cm}^6\,\text{s}^{-1}) \,. \tag{1.3.13}$$

1.4. Optical Properties

Infrared refractive index $n_\infty = (k_\infty)^{1/2}$

for $77\,\mathrm{K} < T < 400\,\mathrm{K}$.

$$n_\infty = 3.38 \times (1 + 3.9 \times 10^{-5} \times T) \qquad (1.4.1))$$

for $T = 300\,\mathrm{K}$ $\qquad n_\infty = 3.42$

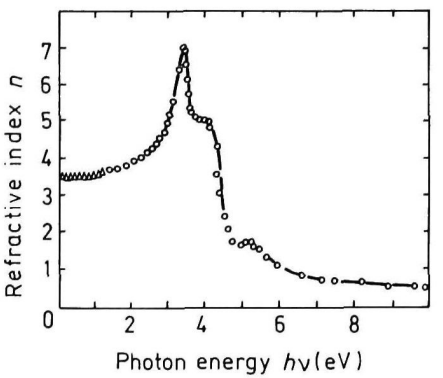

Fig. 1.4.1. Refractive index n versus photon energy, 300 K (Philipp and Taft [1960]).

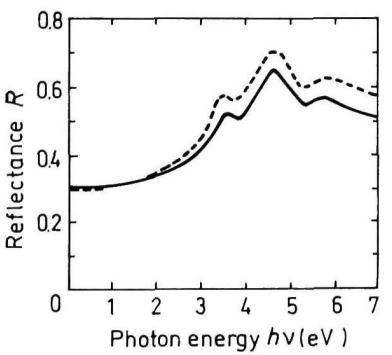

Fig. 1.4.2. Experimental (dashed line) and theoretical (solid line) values of reflectance versus photon energy for Si (Chelikowsky and Cohen [1976]).

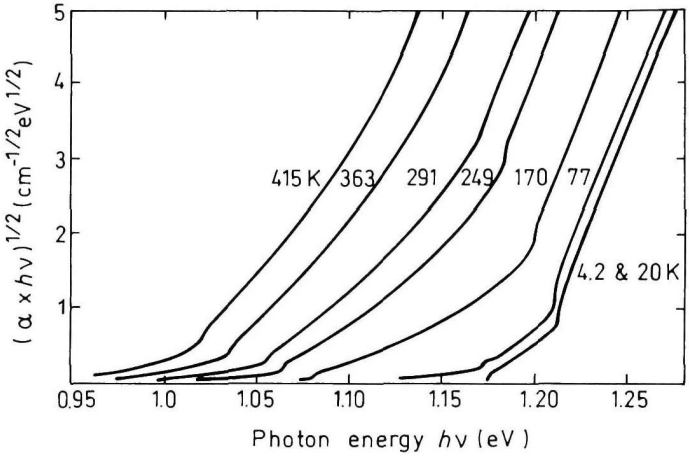

Fig. 1.4.3. Low-level absorption spectrum of high purity Si at various temperatures (Macfarlane *et al.* [1959]). (Reprinted with kind permission from Elsevier Science Ltd.)

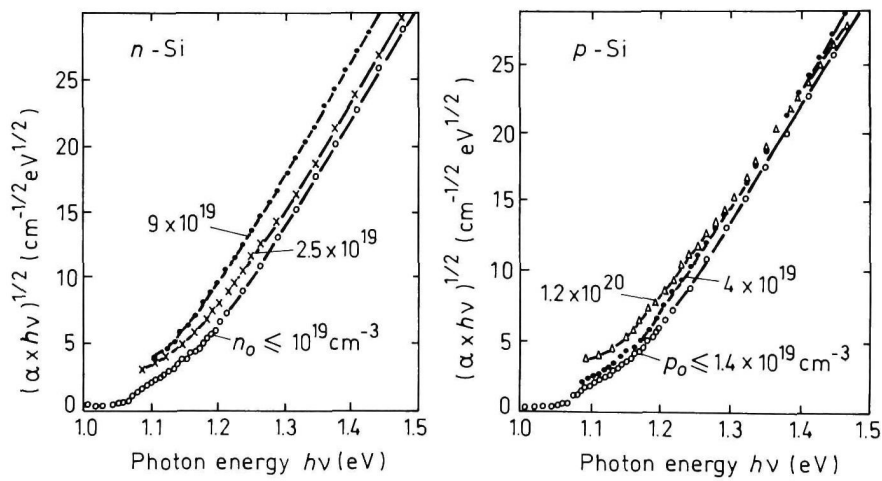

Fig. 1.4.4. Intrinsic absorption edge at different doping levels, 300 K (Wolfson and Subashiev [1967]).

A ground state Rydberg energy $R_0 = 14.7$ meV.

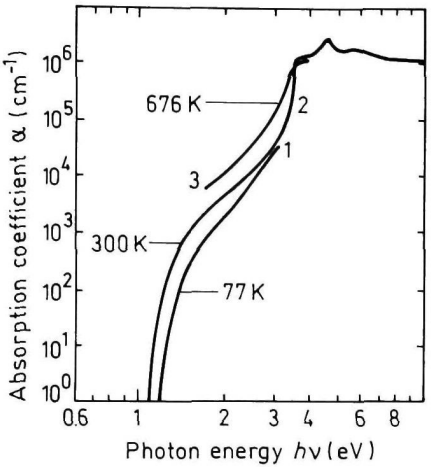

Fig. 1.4.5. The absorption coefficient versus photon energy at different temperatures.
Curves 1 and 2 – Sze [1981],
Curve 3 – Jellison and Modine [1982].

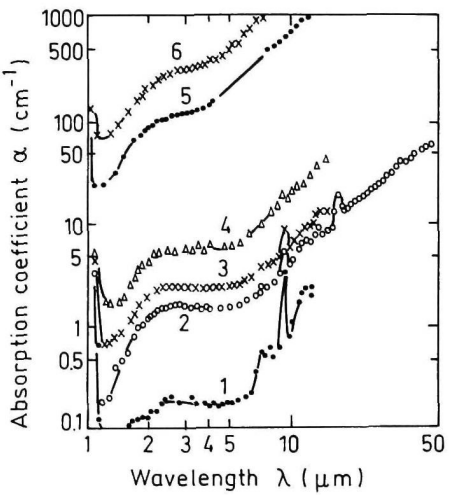

Fig. 1.4.6. Free carrier absorption versus wavelength at different doping levels, n-Si, 300 K (Spitzer and Fan [1957]). Conduction electron concentrations are:

1. $1.4 \times 10^{16}\,\mathrm{cm}^{-3}$, 2. $8 \times 10^{16}\,\mathrm{cm}^{-3}$
3. $1.7 \times 10^{17}\,\mathrm{cm}^{-3}$, 4. $3.2 \times 10^{17}\,\mathrm{cm}^{-3}$
5. $6.1 \times 10^{18}\,\mathrm{cm}^{-3}$, 6. $1 \times 10^{19}\,\mathrm{cm}^{-3}$

At 300 K for $\lambda \geq 5\,\mu$m, $\alpha_n \simeq 10^{-18} \times n_0 \lambda^2$ (Schroeder *et al.* [1978]).

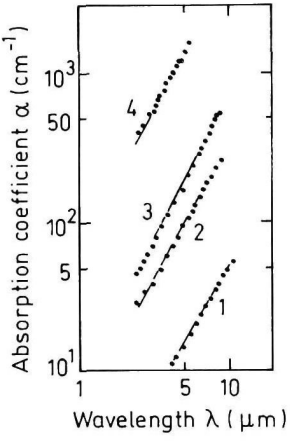

Fig. 1.4.7. Free carrier absorption versus wavelength at different doping levels (p-Si), 300 K (Hara and Nishi [1966]).
Hole concentrations are
1. $4.6 \times 10^{17}\,cm^{-3}$, 2. $1.4 \times 10^{18}\,cm^{-3}$
3. $2.5 \times 10^{18}\,cm^{-3}$, 4. $1.68 \times 10^{19}\,cm^{-3}$

At 300 K for $\lambda \geq 5\,\mu m$, $\alpha_p \simeq 2.7 \times 10^{-18} \times p_0 \lambda^2$ (Schroeder *et al.* [1978]).

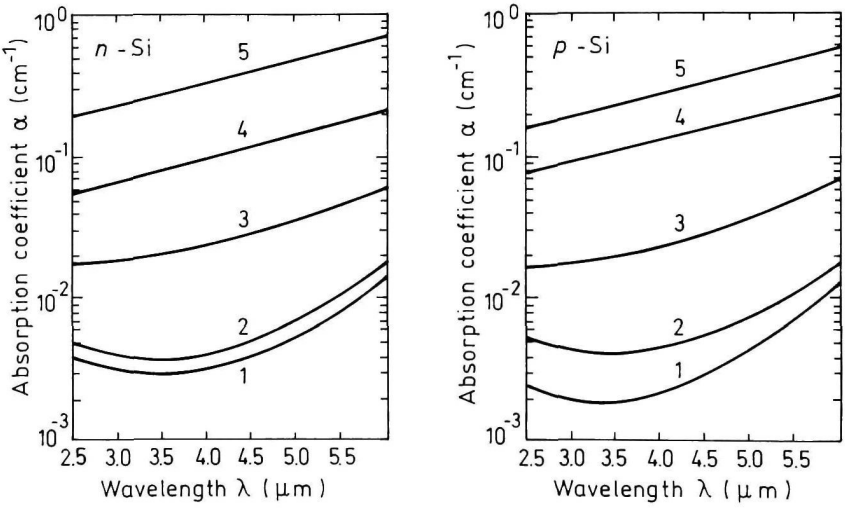

Fig. 1.4.8. Free carrier absorption versus wavelength for high purity Si at different temperatures (Runyan [1966]).
Temperatures are 1. 300 K, 2. 473 K, 3. 573 K, 4. 623 K, 5. 673 K (Figure reprinted with permission of McGraw-Hill Book Co.).

1.5. Thermal Properties

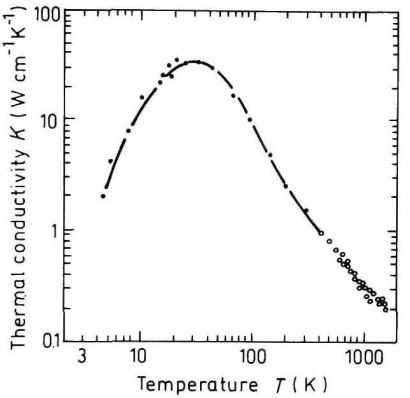

Fig. 1.5.1. Temperature dependence of thermal conductivity for high purity Si (Glassbrenner and Slack [1964]).

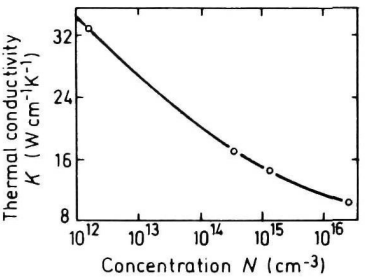

Fig. 1.5.2. The dependence of thermal conductivity K versus doping level N at 20 K, p-Si (Thompson and Younglove [1961]). (Reprinted with kind permission from Elsevier Science Ltd.)

For $T > 100$ K thermal conductivity is practically independent on doping level N.

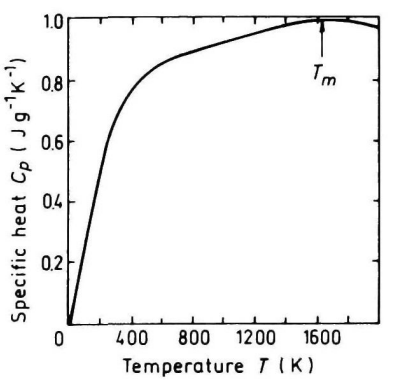

Fig. 1.5.3. Temperature dependence of specific heat at constant pressure. T_m is the melting point (Okhotin *et al.* [1972]).

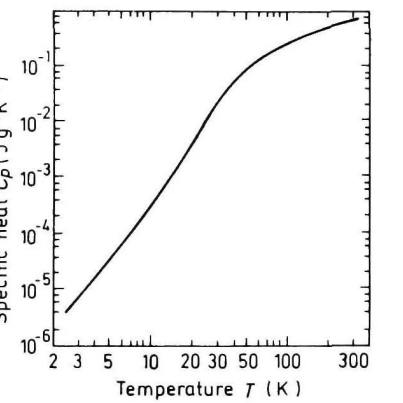

Fig. 1.5.4. Temperature dependence of specific heat at low temperatures (Flubacher *et al.* [1959]).

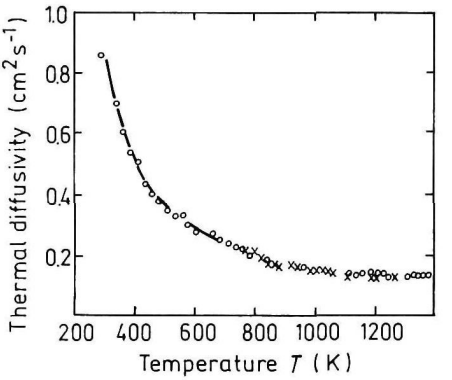

Fig. 1.5.5. Temperature dependence of thermal diffusivity (Shanks *et al.* [1963]).

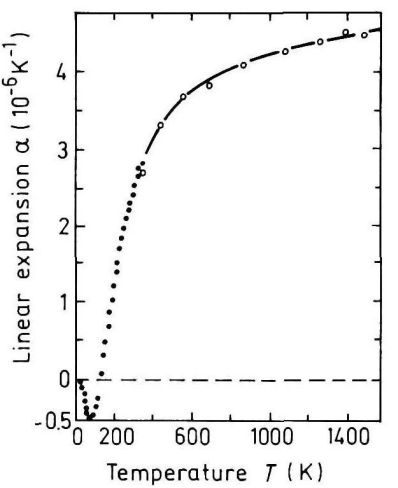

Fig. 1.5.6. Temperature dependence of linear expansion coefficient α (Okada and Tokumaru [1984]).

Melting point $T_m = 1685\,\mathrm{K}$

$$T_m \simeq 1685 - 3.8\,P \quad (P \text{ in kbar})$$

Saturated vapor pressure (in Pascals)

for 850°C	2×10^{-9}
for 1100°C	2×10^{-5}
for 1300°C	5×10^{-3}

1.6. Mechanical Properties, Elastic Constants, Lattice Vibrations, Other Properties

Density	$2.329\,\mathrm{g\,cm^{-3}}$
Hardness	7 on the Mohs scale
Surface microhardness (using Knoop's pyramid test)	$1150\,\mathrm{kg\,mm^{-2}}$
Cleavage plane	{111}
Elastic constants at 300 K	
C_{11}	$16.60 \times 10^{11}\,\mathrm{dyn\,cm^{-2}}$
C_{12}	$6.40 \times 10^{11}\,\mathrm{dyn\,cm^{-2}}$
C_{44}	$7.96 \times 10^{11}\,\mathrm{dyn\,cm^{-2}}$

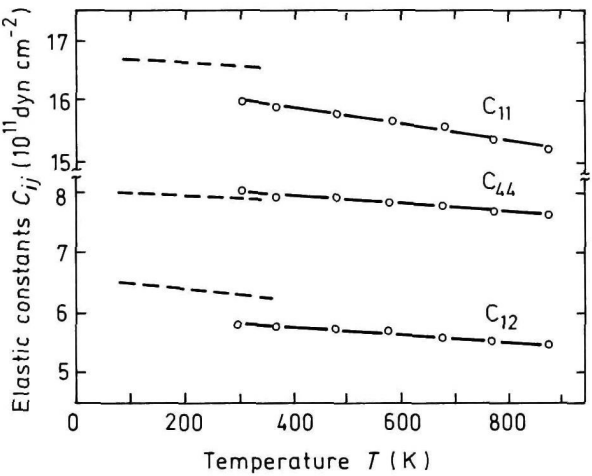

Fig. 1.6.1. Temperature dependences of elastic constants. Dashed lines (McSkimin [1953]). Circles (Nikanorov *et al.* [1971]).

For $400\,\mathrm{K} < T < 873\,\mathrm{K}$ (in units of $10^{11}\,\mathrm{dyn\,cm^{-2}}$)

$$C_{11} \simeq 16.38\text{–}1.28 \times 10^{-3}\,T$$
$$C_{12} \simeq 5.92\text{–}0.48 \times 10^{-3}\,T$$
$$C_{44} \simeq 8.17\text{–}0.59 \times 10^{-3}\,T$$

For 300 K

Bulk modulus (compressibility^{-1})	$B_s = 9.8 \times 10^{11}$ dyn cm^{-2}
Shear modulus	$C' = 5.2 \times 10^{11}$ dyn cm^{-2}
[111] Young's modulus	$Y_{111} = 18.5 \times 10^{11}$ dyn cm^{-2}
[110] Young's modulus	$Y_{110} = 17.0 \times 10^{11}$ dyn cm^{-2}
[100] Young's modulus	$Y_{100} = 13.0 \times 10^{11}$ dyn cm^{-2}
[100] Poisson ratio	$\sigma_{100} = 0.28$
[111] Poisson ratio	$\sigma_{111} = 0.26$

Acoustic Wave Speeds

Wave propagation direction	Wave character	Expression for wave speed	Wave speed (in units of 10^5 cm s^{-1})
[100]	V_L	$(C_{11}/\rho)^{1/2}$	8.43
	V_T	$(C_{44}/\rho)^{1/2}$	5.84
[110]	V_l	$[(C_{11} + C_{12} + 2C_{44})/2\rho]^{1/2}$	9.13
	$V_{t\parallel}$	$V_t = V_T = (C_{44}/\rho)^{1/2}$	5.84
	$V_{t\perp}$	$[(C_{11} - C_{12})/2\rho]^{1/2}$	4.67
[111]	V_l'	$[(C_{11} + 2C_{12} + 4C_{44})/3\rho]^{1/2}$	9.36
	V_t'	$[(C_{11} - C_{12} + C_{44})/3\rho]^{1/2}$	5.10

Phonon frequencies (in units of 10^{12} Hz)

$\nu_{LTO}(\Gamma_{25'})$	15.5	$\nu_{TA}(L_3)$	3.45
$\nu_{TA}(X_3)$	4.5	$\nu_{LA}(L_{2'})$	11.3
$\nu_{LAO}(X_1)$	12.3	$\nu_{LO}(L_1)$	12.6
$\nu_{TO}(X_4)$	13.9	$\nu_{TO}(L_{3'})$	14.7

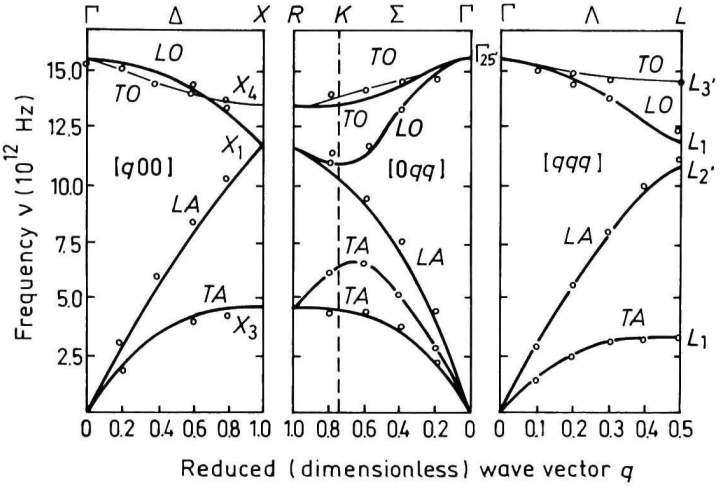

Fig. 1.6.2. Room temperature dispersion curves for acoustic and optical branch phonons. Solid lines are theoretical calculations. Symbols are experimental data (Dolling [1963] and Tubino *et al.* [1972]).

References

Baccarani, G. and P. Ostoja, *Solid State Electron.* **18**, 6 (1975) 579–580.

Canali, C., C. Jacoboni, F. Nava, G. Ottaviani, and A. A. Quaranta, *Phys. Rev.* **B12**, 4 (1975) 2265–2284.

Canali, C., F. Nava, and L. Reggiani, "Hot electron transport in semiconductors" *Topics in Physics*, L. Reggiani, ed., vol. 58, Springer-Verlag, Berlin, 1985.

Chelikowsky, J. R. and M. L. Cohen, *Phys. Rev.* **B14**, 2 (1976) 556–582.

Crowell, C. R. and S. M. Sze, *Appl. Phys. Lett.* **9**, 6 (1966) 242–244.

del Alamo, J. A. and R. M. Swanson, *Solid State Electron.* **30**, 11 (1987) 1127–1136.

Dolling, G., *Proc. Symp. Inelastic Scattering Neutrons in Solids and Liquids*, Chalk River, IAEA, Vienna, vol. 2, 1963, p. 37.

Dorkel, J. M. and Ph. Leturcq, *Solid State Electron.* **24**, 9 (1981) 821–825.

Flubacher, P., A. J. Leadbetter, and J. A. Morrison, *Phil. Mag.* **4**, 39 (1959) 273–294.

Gerlach, W., H. Schlangenotto, and H. Maeder, *Phys. Status Solidi (A)* **13**, 1 (1972) 277–283.

Glassbrenner, C. J. and G. A. Slack, *Phys. Rev.* **134**, 4A (1964) A1058–A1069.

Grant, W. N., *Solid State Electron.* **16**, 10 (1973) 1189–1203.

Grove, A. S., *Physics and Technology of Semiconductor Devices*, Wiley, N.Y., 1967.

Hara, H. and Y. Nishi, *J. Phys. Soc. Jpn* **21**, 6 (1966) 1222.

Jacoboni, C., C. Canali, G. Ottaviani, and A. A. Quaranta, *Solid State Electron.* **20**, 2 (1977) 77–89.
Jellison, Jr., G. E. and F. A. Modine, *Appl. Phys. Lett.* **41**, 2 (1982) 180–182.
Kirnas, I. G., P. M. Kurilo, P. G. Litovchenko, V. S. Lutsyak, and V. M. Nitsovich, *Phys. Status Solidi (A)* **23**, 2 (1974) K123-K127.
Li, S. S. and W. R. Thurber, *Solid State Electron.* **20**, 7 (1977) 609–616.
Lin, J. F., S. S. Li, L. C. Linaress, and K. W. Teng, *Solid State Electron.* **24**, 9 (1981) 827–833.
Logan, R. A. and A. J. Peters, *J. Appl. Phys.* **31**, 1 (1960) 122–124.
Macfarlane, G. G., T. P. McLean, J. E. Quarrington, and V. Roberts, *J. Phys. Chem. Solids* **8**, (1959) 388–392.
Maes, W., K. De Meyer, and R. Van Overstraeten, *Solid State Electron.* **33**, 6 (1990) 705–718.
McSkimin, H. J., *J. Appl. Phys.* **24**, 8 (1953) 988–997.
Morin, F. J. and J. P. Maita, *Phys. Rev.* **96**, 1 (1954) 28–35.
Nikanorov, S. P., Yu. A. Burenkov, and A. V. Stepanov, *Sov. Phys. Solid State* **13**, 10 (1971) 2516–2519.
Norton, P., T. Braggins, and H. Levinstein, *Phys. Rev.* **B8**, 12 (1973) 5632–5653.
Okada, Y. and Y. Tokumaru, *J. Appl. Phys.* **56**, 2 (1984) 314–320.
Okhotin, A. S., A. S. Pushkarskii, and V. V. Gorbachev, *Thermophysical Properties of Semiconductors*, Moscow, "Atom" Publ. House, 1972, (in Russian).
Ottaviani, G., L. Reggiani, C. Canali, F. Nava, and A. A. Quaranta, *Phys. Rev.* **B12**, 8 (1975) 3315–3322.
Phillipp, H. R. and E. A. Taft, *Phys. Rev.* **120**, 1 (1960) 37–38.
Runyan, W. R., *Technology Semiconductor Silicon*, McGraw-Hill Book Company, 1966.
Scharfetter, D. L. and H. K. Gummel, *IEEE Trans. Electron. Dev.* **ED-16**, 1 (1969) 64–77.
Schroder, D. K., R. N. Thomos, and J. C. Swartz, *IEEE Trans. Electron. Dev.* **ED-25**, 2 (1978) 254- -261.
Shanks, H. R., P. D. Maycock, P. H. Sidles, and G. C. Danielson, *Phys. Rev.* **130**, 5 (1963) 1743–1748.
Shur, M., *Physics of Semiconductor Devices*, Prentice Hall, 1990.
Spitzer, W. and H. Y. Fan, *Phys. Rev.* **108**, 2 (1957) 268–271.
Sze, S. M., *Physics of Semiconductor Devices*, John Wiley and Sons, N.Y., 1981.
Thompson, J. C. and B. A. Younglove, *J. Phys. Chem. Solids* **20**, 112 (1961) 146–149.
Tubino, R., L. Piseri, and G. Zerbi, *J. Chem. Phys.* **56**, 3 (1972) 1022–1039.
Tyagi, M. S. and R. Van Overstraeten, *Solid State Electron.* **26**, 6 (1983) 577–598.
Van Overstraeten, R. J. and R. P. Mertens, *Solid State Electron.* **30**, 11 (1987) 1077– 1087.
Wang, C. H., K. Misiakos, and A. Neugroschel, *Appl. Phys. Lett.* **54**, 20 (1989) 2233–2234.
Wolfson, A. A. and V. K. Subashiev, *Fiz. Tekh. Poluprovodn.* **1**, 3 (1967) 397–404 (in Russian).

CHAPTER 2

GERMANIUM (Ge)

L. E. Vorobyev
St. Petersburg State Technical University
Russia

2.1. Basic Parameters at 300 K

Crystal structure		Diamond
Group of symmetry		O_h^7–Fd3m
Number of atoms in 1 cm^3		4.4×10^{22}
Auger recombination coefficient	($cm^6\,s^{-1}$)	10^{-30}
Debye temperature	(K)	374
Density	($g\,cm^{-3}$)	5.3234
Dielectric constant		16.2
Effective electron masses	(in units of m_o)	
longitudinal m_l/m_o		1.6
transverse m_t/m_o		0.08
Effective hole masses	(in units of m_o)	
heavy m_h/m_o		0.33
light m_{lp}/m_o		0.043
Electron affinity	(eV)	4.0
Lattice constant	(Å)	5.658
Optical phonon energy	(eV)	0.037

Band structure and carrier concentration

Energy gap	(eV)	0.661
Energy separation ($E_{\Gamma 1}$)	(eV)	0.8
Energy separation (ΔE)	(eV)	0.85
Energy spin-orbital splitting	(eV)	0.29
Intrinsic carrier concentration	(cm^{-3})	2.0×10^{13}
Intrinsic resistivity	($\Omega \times cm$)	46
Effective conduction band density of states	(cm^{-3})	1.0×10^{19}
Effective valence band density of states	(cm^{-3})	5.0×10^{18}

Electrical properties

Breakdown field	($V\,cm^{-1}$)	$\simeq 10^5$
Mobility	($cm^2\ V^{-1}\ s^{-1}$)	
	electrons	≤ 3900
	holes	≤ 1900
Diffusion coefficient	($cm^2\ s^{-1}$)	
	electrons	≤ 100
	holes	≤ 50
Electron thermal velocity	($m\,s^{-1}$)	3.1×10^5
Hole thermal velocity	($m\,s^{-1}$)	1.9×10^5

Optical properties

Index of refraction	4.0
Radiative recombination coefficient ($cm^3\ s^{-1}$)	6.4×10^{-14}

Thermal and mechanical properties

Bulk modulus	($dyn\,cm^{-2}$)	7.5×10^{11}
Melting point	(°C)	937
Specific heat	($J\,g^{-1}\ °C^{-1}$)	0.31
Thermal conductivity	($W\,cm^{-1}\ °C^{-1}$)	0.58
Thermal diffusivity	($cm^2\,s^{-1}$)	0.36
Thermal expansion, linear	($°C^{-1}$)	5.9×10^{-6}

2.2. Band Structure and Carrier Concentration

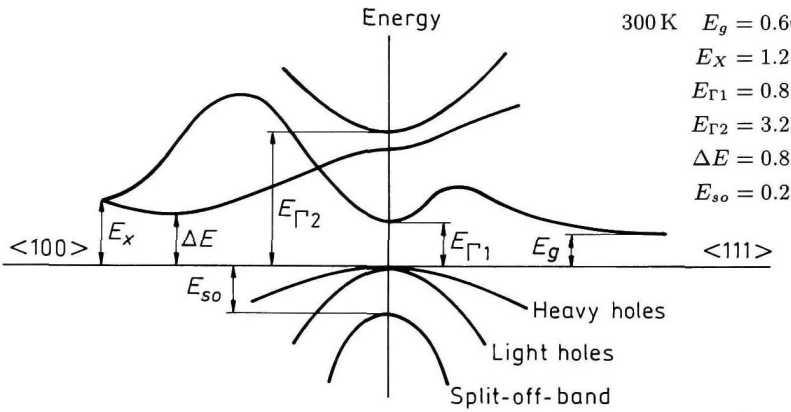

Fig. 2.2.1. Band structure of Ge. Important minima of the conduction band and maxima of the valence band.

2.2.1. *Temperature Dependences*

Temperature dependence of the energy gap

$$E_g = 0.742 - 4.8 \times 10^{-4} \frac{T^2}{T + 235} \text{ (eV)} , \tag{2.2.1}$$

where T is temperature in degrees K.

Temperature dependence of the direct band gap $E_{\Gamma 1}$

$$E_{\Gamma 1} = 0.89 - 5.82 \times 10^{-4} \frac{T^2}{T + 296} \text{ (eV)} . \tag{2.2.2}$$

Effective density of states in the conduction band

$$N_c = 4.82 \times 10^{15} M \left(\frac{m_c}{m_o}\right)^{3/2} \times T^{3/2} \ (\mathrm{cm}^{-3}), \tag{2.2.3}$$

or

$$N_c = 1.98 \times 10^{15} \times T^{3/2} \ (\mathrm{cm}^{-3}) \ ,$$

$M = 4$ is the number of equivalent valleys in the conduction band. $m_c = 0.22 m_o$ is the effective mass of the density of states in one valley of the conduction band.

Effective density of states in the valence band

$$N_v = 9.6 \times 10^{14} \times T^{3/2} \ (\mathrm{cm}^{-3}) \ . \tag{2.2.4}$$

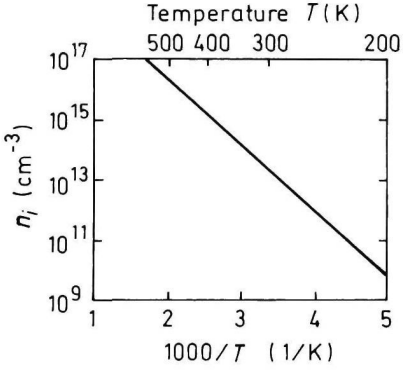

Fig. 2.2.2. The temperature dependence of the intrinsic carrier concentration n_i.

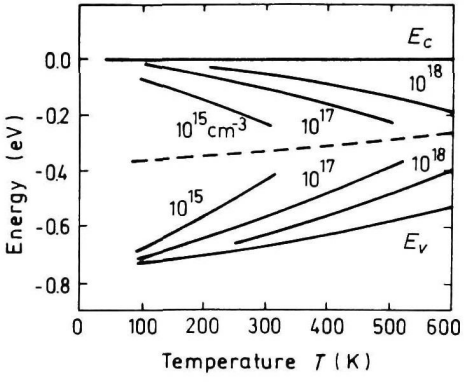

Fig. 2.2.3. Fermi level versus temperature for different concentrations of shallow donors and acceptors. Dashed line shows Fermi level dependence versus temperature for intrinsic Ge.

2.2.2. *Dependences on Hydrostatic Pressure*

$$E_g = E_g(0) + 5.1 \times 10^{-3}\ P \text{ (eV)}$$
$$E_{\Gamma 1} = E_{\Gamma 1}(0) + 1.53 \times 10^{-2}\ P \text{ (eV)} \tag{2.2.5}$$

where P is pressure in kbar.

2.2.3. *Energy Gap Narrowing at High Doping Levels*

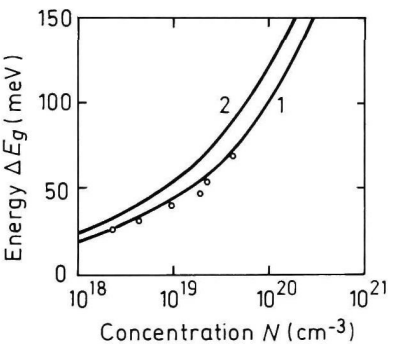

Fig. 2.2.4. Energy gap narrowing versus donor (Curve 1) and acceptor (Curve 2) doping density. Open curves are experimental values (Jain and Roulston [1991]). (Reprinted with kind permission from Elsevier Science Ltd.)

For n-type Ge

$$\Delta E_g = 8.67 \times \left(\frac{N_d}{10^{18}}\right)^{1/3} + 8.14 \times \left(\frac{N_d}{10^{18}}\right)^{1/4} + 4.31 \times \left(\frac{N_d}{10^{18}}\right)^{1/2} \text{ (eV)}$$

For p-type Ge (2.2.6)

$$\Delta E_g = 8.21 \times \left(\frac{N_a}{10^{18}}\right)^{1/3} + 9.18 \times \left(\frac{N_a}{10^{18}}\right)^{1/4} + 5.77 \times \left(\frac{N_a}{10^{18}}\right)^{1/2} \text{ (eV)}$$

(Jain and Roulston [1991]).

2.2.4. *Effective Masses*

Electrons

The surfaces of equal energy are ellipsoids.

$$m_l = 1.59m_0$$
$$m_t = 0.0815m_0$$

Effective mass of density of states $m_c = 0.22m_0$

There are 4 equivalent valleys in the conduction band.
Effective mass of conductivity $m_{cc} = 0.12m_0$

Holes

heavy	$m_h = 0.33m_0$
light	$m_{lp} = 0.043m_0$
split-off band	$m_{so} = 0.084m_0$

Effective mass of density of states $m_v = 0.34m_0$

2.2.5. *Donors and Acceptors*

Ionization energies of shallow donors (eV)

As	0.014
P	0.013
Sb	0.010
Bi	0.013
Li	0.093

Ionization energies of shallow acceptors (eV)

Al	0.011
B	0.011
Ga	0.011
In	0.012
Tl	0.013

2.3. Electrical Properties

2.3.1. *Mobility and Hall Effect*

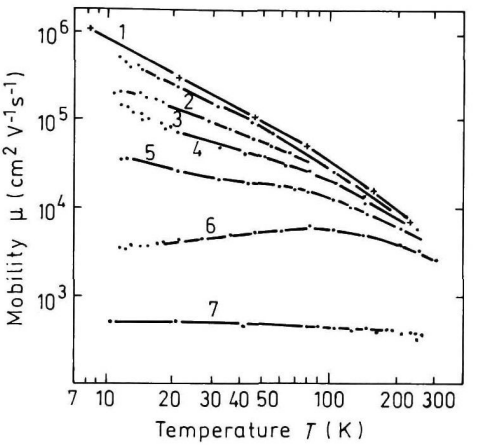

Fig. 2.3.1. Electron mobility versus temperature for different doping levels. 1. High purity Ge; time-of-flight technique (Jacoboni *et al.* [1981]). 2.–6. Hall effect (Debye and Conwell [1954]). $N_d - N_a$ (cm^{-3}). 2. 1×10^{13}; 3. 1.4×10^{14}; 4. 1.7×10^{15}; 5. 7.5×10^{15}; 6. 5.5×10^{16}; 7. $N_d - N_a = 1.2 \times 10^{19}\,cm^{-3}$; Hall-effect (Fistul *et al.* [1962]).

For weakly doped Ge in the range $77 \div 300$ K electron mobility $\mu_n \simeq 4.9 \times 10^7 \times T^{-1.66}$ ($cm^2\ V^{-1}\ s^{-1}$).

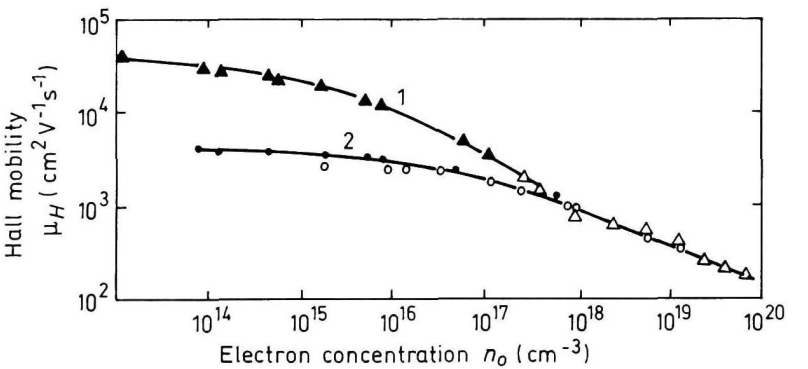

Fig. 2.3.2. Electron Hall mobility versus electron concentration (Fistul *et al.* [1962]). 1. 77 K 2. 300 K.

Approximate formula for the Hall mobility. 300 K. (Hilsum [1974]), $\mu = \mu_{OH}/[1 + (N_d/10^{17})^{1/2}]$, where $\mu_{OH} \simeq 3900\,cm^2\ V^{-1}\ s^{-1}$, N_d – in cm^{-3}.

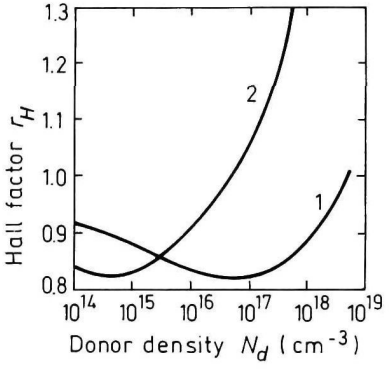

Fig. 2.3.3. The electron Hall factor versus donor density for 300 K (Curve 1) and 77 K (Curve 2) (Babich *et al.* [1969]).

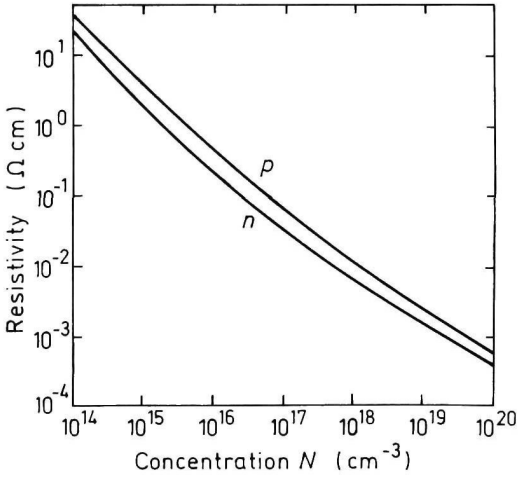

Fig. 2.3.4. Resistivity versus impurity concentration for Ge at 300 K (Cuttris [1961]).

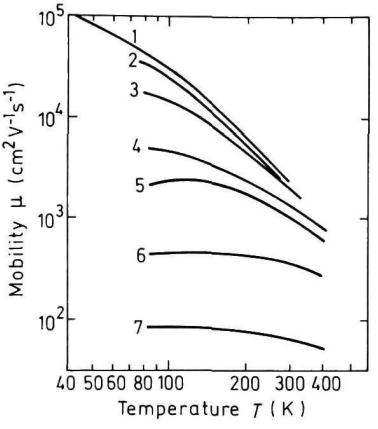

Fig. 2.3.5. Temperature dependences of hole mobility for different doping levels. 1. High purity Ge; time-of-flight technique (Ottaviani *et al.* [1973]). 2.–7. Hall effect (Golikova *et al.* [1961]). $N_a - N_d$ (cm^{-3}): 2. 4.9×10^{13}, 3. 3.2×10^{15}, 4. 2.7×10^{16}, 5. 1.2×10^{17}, 6. 4.9×10^{18}, 7. 2.0×10^{20}.

For weakly doped Ge in the range $100 \div 300$ K hole mobility $\mu_p \simeq 1.05 \times 10^9 \times T^{-2.33}$ ($cm^2\ V^{-1}\ s^{-1}$).

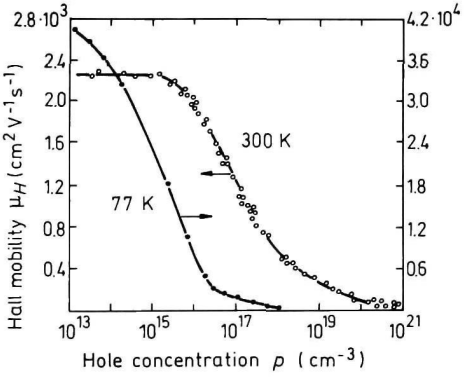

Fig. 2.3.6. The hole Hall mobility versus hole concentration. Experimental points: data from three References (Golikova *et al.* [1961]).

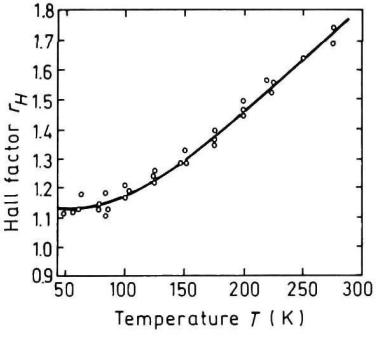

Fig. 2.3.7. The hole Hall factor versus temperature for high purity *p*-Ge (Morin [1954]).

2.3.2. *Transport Properties in High Electric Field*

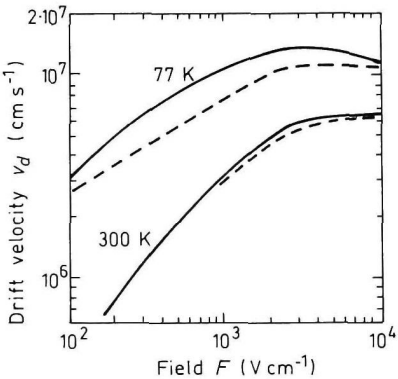

Fig. 2.3.8. Field dependences of the electron drift velocity. Solid lines: $F\|(100)$. Dashed lines: $F\|(111)$ (Jacoboni *et al.* [1981]).

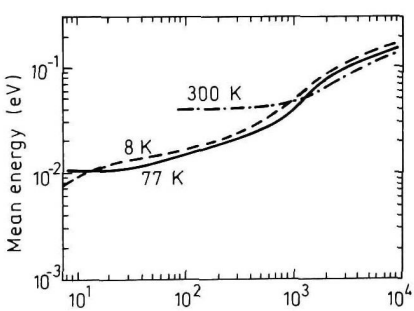

Fig. 2.3.9. Mean energy of electrons in lower valleys as a function of electric field for three lattice temperatures. $F\|(100)$ (Jacoboni *et al.* [1981]).

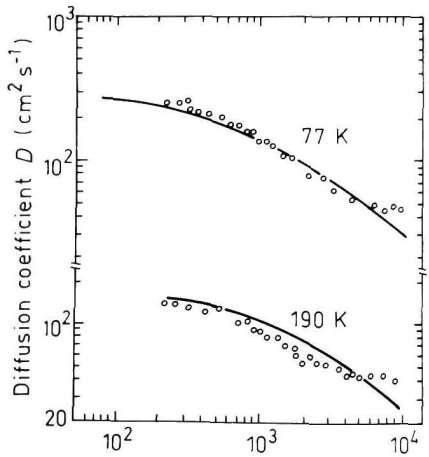

Fig. 2.3.10. The field dependences of longitudinal electron diffusion coefficient D for 77 K and 190 K. $F\|(100)$. Solid lines shows the result of calculation. Symbols represent measured data (Jacoboni *et al.* [1981]).

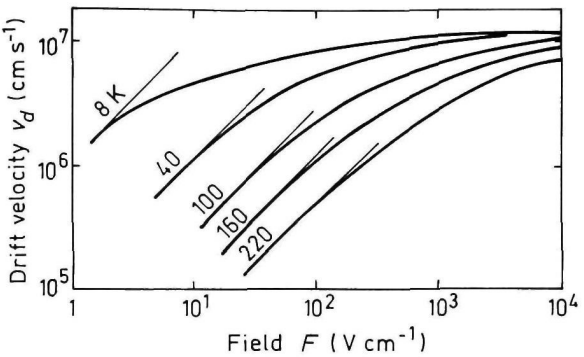

Fig. 2.3.11. Field dependences of the hole drift velocity at different temperatures. $F\|(100)$ (Ottaviani *et al.* [1973]).

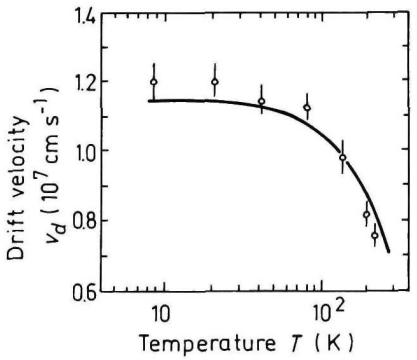

Fig. 2.3.12. Drift velocity v_d as a function of temperature for an electric field $F = 10^4\,\mathrm{V\,cm^{-1}}$. $F\|(100)$. Solid line shows the results of calculation in the case where non-parabolic effects are taken into account (Reggiani *et al.* [1977]).

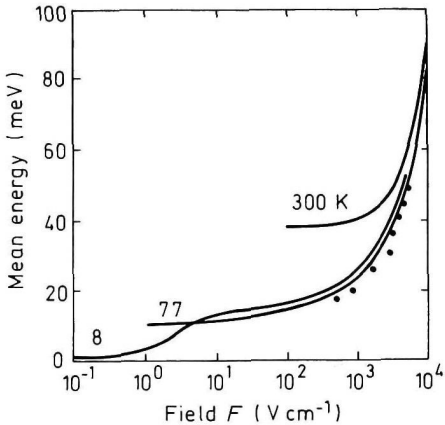

Fig. 2.3.13. Mean energy of holes versus electric field at different lattice temperatures. Solid lines are Monte-Carlo calculations for $F\|(111)$ (Reggiani *et al.* [1977]). Points show experimental results for 82 K (Vorob'ev *et al.* [1978]).

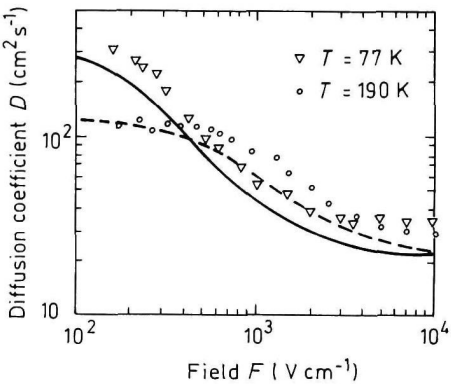

Fig. 2.3.14. The field dependence of longitudinal hole diffusion coefficient D for 77 K and 190 K. $F\|(111)$. Dashed and solid lines show the results of the calculations. Symbols represent measured data (Reggiani *et al.* [1978]).

2.3.3. *Impact Ionization*

The are two schools of thought regarding the impact ionization in Ge. The first one states that impact ionization rates α_i and β_i for electrons and holes in Ge are known accurately enough to distinguish such subtle details as the anisothropy of α_i and β_i for different crystallographic directions.

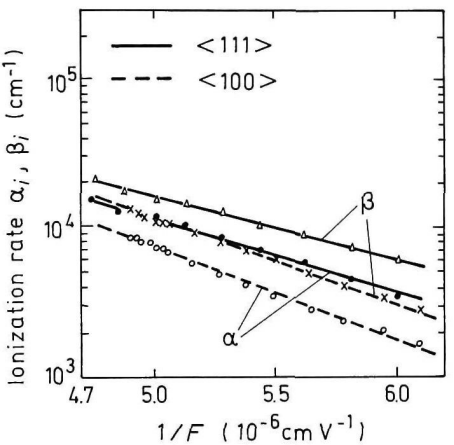

Fig. 2.3.15. Ionization rates in (111) and (100) directions versus $1/F$ for Ge, 300 K (Mikawa *et al.* [1980]).

For electrons

$$\alpha_i = \alpha_0 \times \exp[-F_{no}/F] \tag{2.3.1}$$

(111) direction: $\alpha_o = 2.72 \times 10^6\,\mathrm{cm}^{-1}$, $F_{no} = 1.1 \times 10^6\,\mathrm{V\,cm}^{-1}$
(100) direction: $\alpha_o = 8.04 \times 10^6\,\mathrm{cm}^{-1}$, $F_{no} = 1.4 \times 10^6\,\mathrm{V\,cm}^{-1}$

For holes

$$\beta_i = \beta_0 \times \exp[-F_{po}/F] \tag{2.3.2}$$

(111) direction: $\beta_o = 1.72 \times 10^6\,\mathrm{cm}^{-1}$, $F_{po} = 9.37 \times 10^5\,\mathrm{V\,cm}^{-1}$
(100) direction: $\beta_o = 6.39 \times 10^6\,\mathrm{cm}^{-1}$, $F_{po} = 1.27 \times 10^6\,\mathrm{V\,cm}^{-1}$

(Mikawa *et al.* [1980]).

The second school contends that the values of α_i and β_i for the same electric field reported by different researches differ by an order of magnitude. This point of view is explained by Kyuregyan and Yurkov [1989]. In accordance with this approach we can assume that

For electrons

$$\alpha_i = \alpha_0 \times \exp[-F_{no}/F] \tag{2.3.3}$$

where $\alpha_o = 2.84 \times 10^6\,\mathrm{cm}^{-1}$, $F_{no} = 1.14 \times 10^6\,\mathrm{V\,cm}^{-1}$

For holes

$$\beta_i = \beta_0 \times \exp[-F_{po}/F] \tag{2.3.4}$$

where $\beta_o = 4.21 \times 10^6\,\mathrm{cm}^{-1}$, $F_{po} = 1.11 \times 10^6\,\mathrm{V\,cm}^{-1}$

for all crystallographic directions.

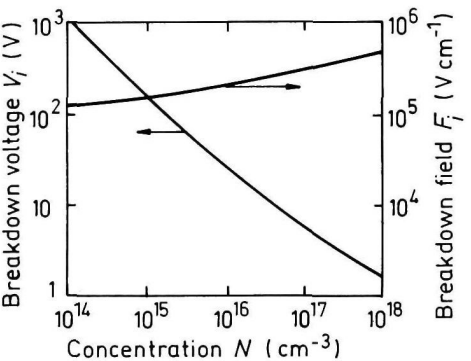

Fig. 2.3.16. Breakdown voltage and breakdown field versus doping density for an abrupt p-n junction (Kyuregyan and Yurkov [1989]).

2.3.4. *Recombination Parameters*

Pure *n*-type material

300 K

The longest lifetime of holes		$\tau_p \geq 10^{-3}\,\mathrm{s}$
Diffusion length	$L_p = (D_p \times \tau_p)^{1/2}$	$L_p \geq 0.2\,\mathrm{cm}$

77 K

The longest lifetime of holes		$\tau_p \geq 10^{-4}\,\mathrm{s}$
Diffusion length	$L_p = (D_p \times \tau_p)^{1/2}$	$L_p \geq 0.15\,\mathrm{cm}$

Pure *p*-type material

300 K

The longest lifetime of electrons		$\tau_n \geq 10^{-3}\,\mathrm{s}$
Diffusion length	$L_n = (D_n \times \tau_n)^{1/2}$	$L_n \geq 0.3\,\mathrm{cm}$

77 K

The longest lifetime of electrons		$\tau_n \geq 10^{-4}\,\mathrm{s}$
Diffusion length	$L_n = (D_n \times \tau_n)^{1/2}$	$L_n \geq 0.15\,\mathrm{cm}$

Surface recombination

Surface recombination rate depending on the treatment of Ge surface lies in the range between $10 \div 10^6\,\mathrm{cm\,s^{-1}}$.

Radiative recombination coefficient at 300 K	$6.4 \times 10^{-14}\mathrm{cm^3\,s^{-1}}$
Auger coefficient at 300 K	$\sim 10^{-30}\mathrm{cm^6\,s^{-1}}$

2.4. Optical Properties

Infrared refractive index $n_\infty = 4.00$ (300 K)

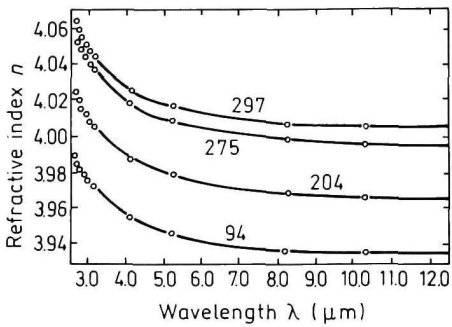

Fig. 2.4.1. Refractive index n versus wavelength at four different temperatures (Icenogle *et al.* [1976]).

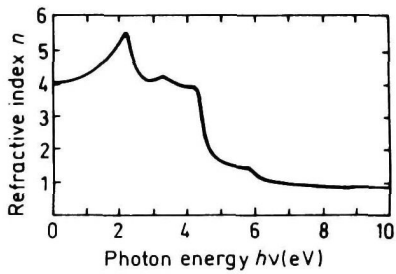

Fig. 2.4.2. Refractive index n versus photon energy, 300 K (Philipp and Taft [1959]).

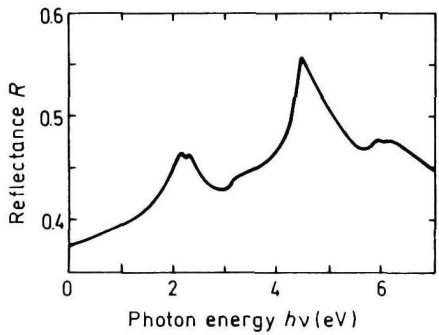

Fig. 2.4.3. Reflectance versus photon energy, 300 K (Cordona *et al.* [1967]).

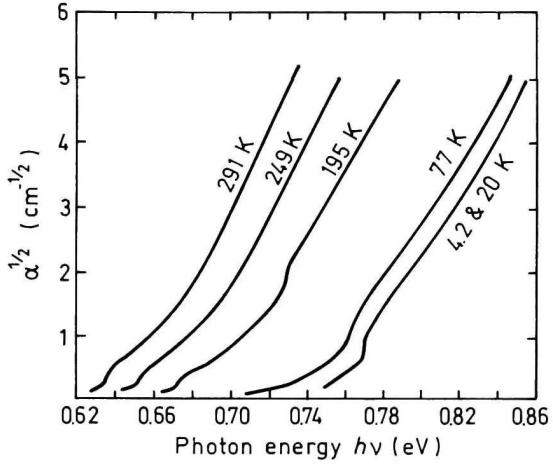

Fig. 2.4.4. Low-level absorption spectrum of high purity Ge at various temperatures (Macfarlane *et al.* [1957]).

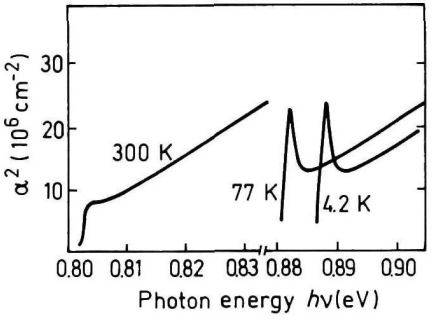

Fig. 2.4.5. The absorption edge at three different temperatures (Seysyan *et al.* [1968]).

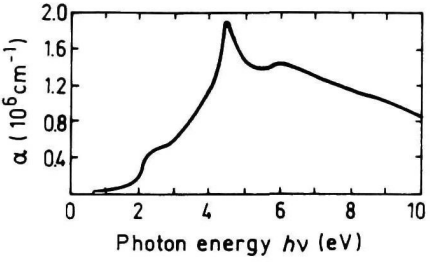

Fig. 2.4.6. The absorption coefficient versus photon energy, 300 K (Phillipp and Taft [1959]).

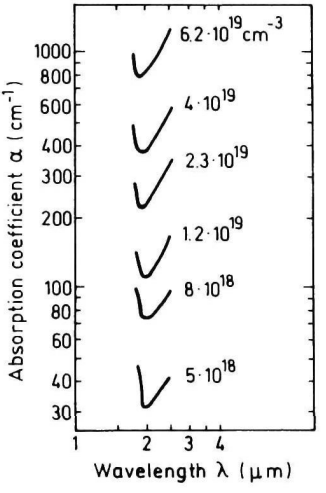

Fig. 2.4.7. The absorption coefficient at different donor (As) concentrations, 300 K (Pankove and Aigrain [1962]).

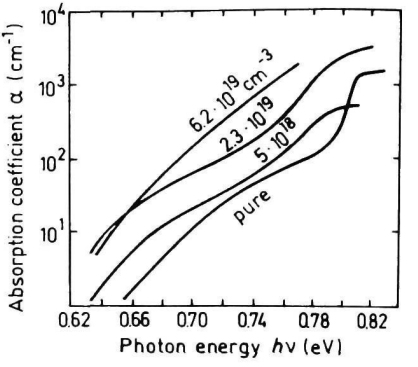

Fig. 2.4.8. Intrinsic absorption edges at different donor (As) concentrations at 300 K obtained after substracting the free carrier absorption from the measured values (Pankove and Aigrain [1962]).

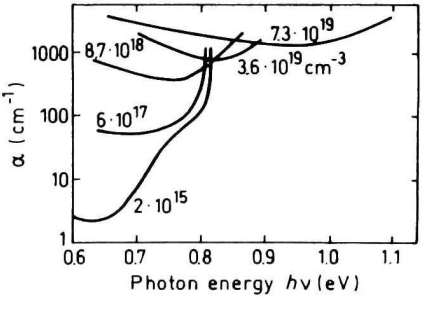

Fig. 2.4.9. The absorption coefficient at different acceptor (Ga) concentrations, 293 K (Bagaev *et al.* [1962]).

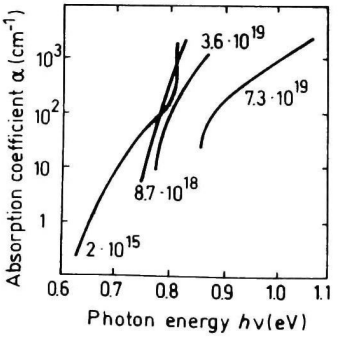

Fig. 2.4.10. Intrinsic absorption edge at different doping (Ga) level at 293 K obtained from Fig. 2.4.9 by substracting the free carrier absorption (Bagaev *et al.* [1962]).

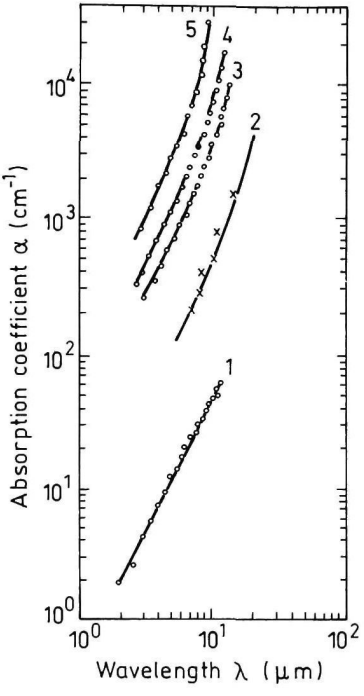

Fig. 2.4.11. Free carrier absorption versus wavelength at different doping levels. n-Ge, 300 K (Fistul [1967]). Conduction electron concentration n_0 (cm^{-3}):
1. 8×10^{17}, 2. 4.8×10^{18}, 3. 1.35×10^{19}, 4. 1.8×10^{19}, 5. 3.6×10^{19}.

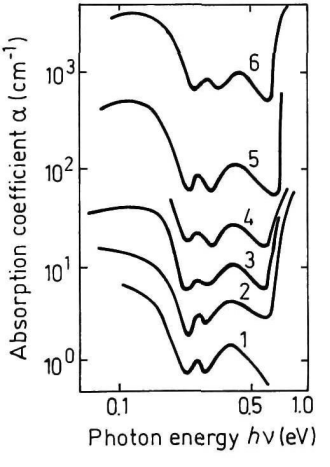

Fig. 2.4.12. Free carrier absorption versus photon energy at different doping levels. p-Ge, 300 K (Ukhanov [1977] and Vasilyeva *et al.* [1967]). Free hole concentration p_0 (cm^{-3}):
1. 7.3×10^{15}, 2. 1.6×10^{16}, 3. 6.0×10^{16}, 4. 1.9×10^{17}, 5. 1.2×10^{18}, 6. 1.0×10^{19}.

2.5. Thermal Properties

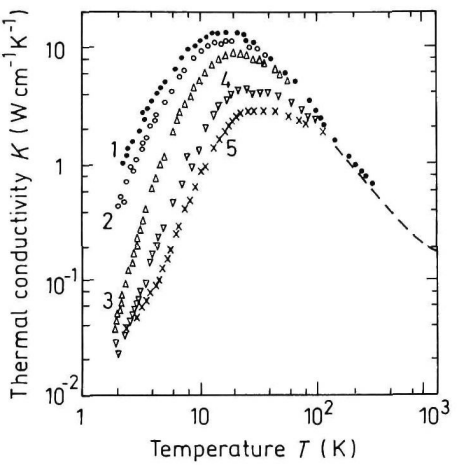

Fig. 2.5.1. Temperature dependences of thermal conductivity at different doping levels. (Carruthes *et al.* [1957]). Dashed line (Glassbrenner and Slack [1964]). p-Ge, N_a (cm^{-3}):
1. $\sim 10^{13}$, 2. 10^{15}, 3. 2.3×10^{16}, 4. 2.0×10^{18}, 5. 10^{19}.

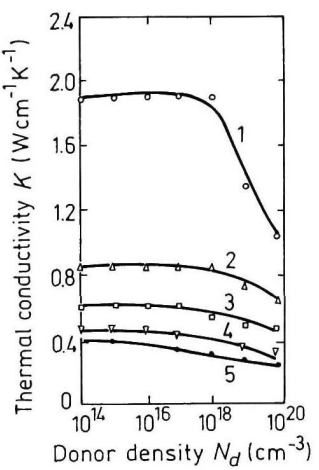

Fig. 2.5.2. The dependences of thermal conductivity versus doping level (Okhotin *et al.* [1972]) n-Ge, $T°$(K):
1. 100, 2. 200, 3. 300, 4. 400, 5. 500.

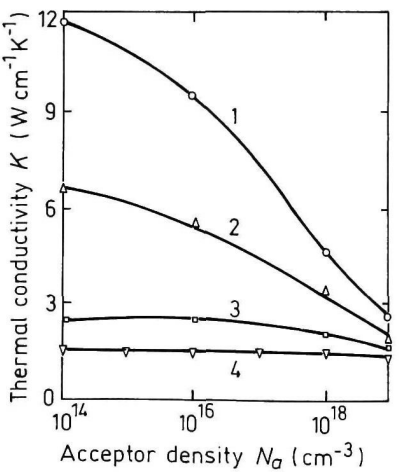

Fig. 2.5.3. The dependences of thermal conductivity versus doping level (Okhotin *et al.* [1972]) p-Ge, $T°$(K):
1. 20, 2. 50, 3. 100, 4. 200.

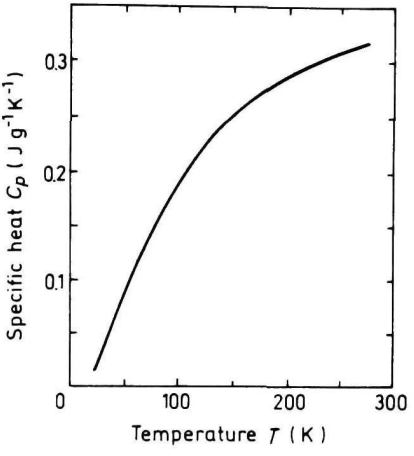

Fig. 2.5.4. Temperature dependence of specific heat at constant pressure (Piesbergen [1963]).

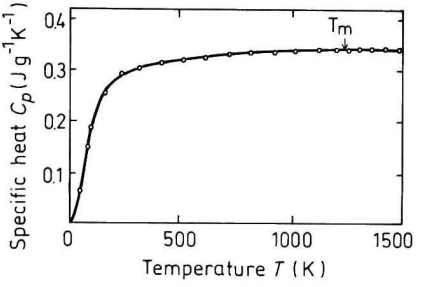

Fig. 2.5.5. Temperature dependence of specific heat (high temperatures) (Okhotin *et al.* [1972]).

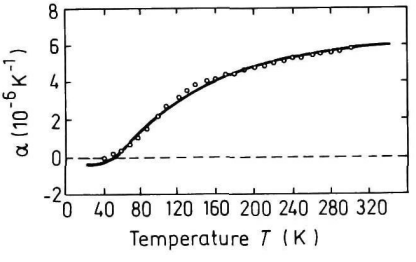

Fig. 2.5.6. Temperature dependence of linear expansion coefficient α (Novikova [1960]).

Melting point $T_m = 1210\,\mathrm{K}$

$$T_m \simeq 1210 - 2.0 \times P \quad (P \text{ in kbar}).$$

Saturated vapor pressure (in Pascals)

For 760°C 10^{-6}
For 1330°C 1

2.6. Mechanical Properties, Elastic Constants, Lattice Vibrations, Other Properties

Density	$5.323\,\mathrm{g\,cm^{-3}}$
Hardness on the Mohs scale	6
Surface microhardness (using Knoop's pyramid test)	$780\,\mathrm{kg\,mm^{-2}}$
Cleavage plane	{001}
Elastic constants at 300 K	
C_{11}	$12.60 \times 10^{11}\,\mathrm{dyn\,cm^{-2}}$
C_{12}	$4.40 \times 10^{11}\,\mathrm{dyn\,cm^{-2}}$
C_{44}	$6.77 \times 10^{11}\,\mathrm{dyn\,cm^{-2}}$

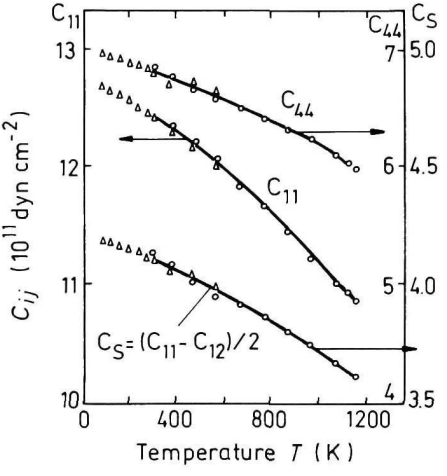

Fig. 2.6.1. Temperature dependences of elastic constants (Nikanorov and Kardashev [1985]).

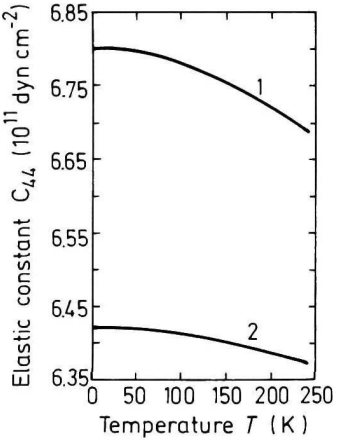

Fig. 2.6.2. Elastic constant C_{44} versus temperature for pure (Curve 1) and doped (Curve 2, $N_d = 3.5 \times 10^{19}\,\mathrm{cm^{-3}}$) samples (Bruner and Keyes [1961]).

For $T = 300\,\mathrm{K}$
Bulk modulus (compressibility^{-1})

$$B_s = \frac{C_{11} + 2C_{12}}{3} \qquad B_s = 7.13 \times 10^{11}\,\mathrm{dyn\,cm^{-2}}$$

Shear modulus

$$C' = (C_{11} - C_{12})/2 \qquad C' = 4.1 \times 10^{11}\,\mathrm{dyn\,cm^{-2}}$$

[100] Young's modulus

$$Y_o = \frac{(C_{11} + 2C_{12})(C_{11} - C_{12})}{(C_{11} + C_{12})} \qquad Y_o = 10.3 \times 10^{11}\,\mathrm{dyn\,cm^{-2}}$$

[100] Poisson ratio

$$\sigma_0 = \frac{C_{12}}{C_{11} + C_{12}} \qquad \sigma_0 = 0.26$$

Acoustic Wave Speeds

Wave propagation direction	Wave character	Expression for wave speed	Wave speed (in units of $10^5\,\mathrm{cm\,s^{-1}}$)
[100]	V_L	$(C_{11}/\rho)^{1/2}$	4.87
	V_T	$(C_{44}/\rho)^{1/2}$	3.57
[110]	V_l	$[(C_{11} + C_{12} + 2C_{44})/2\rho]^{1/2}$	5.36
	$V_{t\parallel}$	$V_{t\parallel} = V_T = (C_{44}/\rho)^{1/2}$	3.57
	$V_{t\perp}$	$[(C_{11} - C_{12})/2\rho]^{1/2}$	2.77
[111]	V_l'	$[(C_{11} + 2C_{12} + 4C_{44})/3\rho]^{1/2}$	5.51
	V_t'	$[(C_{11} - C_{12} + C_{44})/3\rho]^{1/2}$	3.06

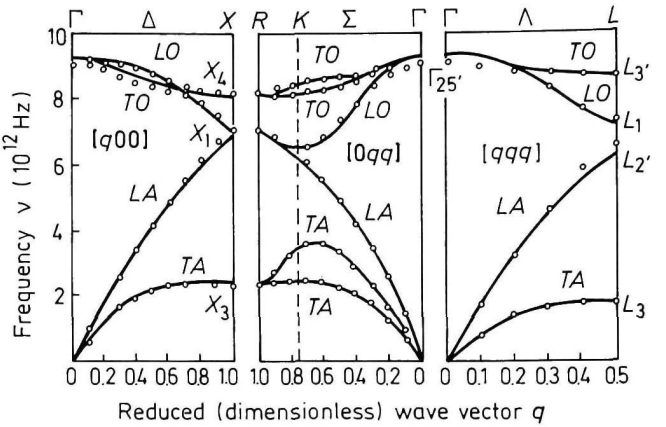

Fig. 2.6.3. Room temperature dispersion curves for acoustic and optical branch phonons. Solid lines are theoretical calculations. Symbols are experimental data (Weber [1977]).

Phonon frequencies (in units of 10^{12} Hz) (Nilsson and Nelin [1972]).

$\nu_{LTO}(\Gamma_{25'})$	9.02
$\nu_{TO}(X_4)$	8.17
$\nu_{LAO}(X_1)$	7.14
$\nu_{TA}(X_3)$	2.38
$\nu_{TO}(L_{3'})$	8.55
$\nu_{LO}(L_1)$	7.27
$\nu_{LA}(L_{2'})$	6.63
$\nu_{TA}(L_3)$	1.87

References

Babich, V. M., P. I. Baranskii, I. V. Dakhovskii, and A. G. Samoylovich, *Ukrain Fiz. Zhurnal* **14**, 3 (1969) 418–422.

Bagaev, V. S., G. P. Proshko, and A. P. Shotov, *Sov. Phys. Solid State* **4**, 11 (1963) 2363–2368.

Bruner, L. J. and R. W. Keyes, *Phys. Rev. Lett.* **7**, 2 (1961) 55–56.

Carruthers, J. A., T. H. Geballe, H. M. Rosenberg, and J. M. Ziman, *Proc. Royal Soc.* **238**, 1215 (1957) 502–514.

Cardona, M., K. L. Shaklee, and F. H. Pollak, *Phys. Rev.* **154**, 3 (1967) 696–720.

Cuttris, D. B., *Bell Syst. Techn. J.* **40**, 2 (1961) 509–523.

Debye, P. P. and E. M. Conwell, *Phys. Rev.* **93**, 4 (1954) 693–706.

Fistul, V. I., M. I. Iglitsyn, and E. M. Omelyanovskii, *Sov. Phys. Solid State* **4**, 4 (1962) 784–785.
Fistul, V. I., *Heavy Doped Semiconductors*, "Nauka", Moscow, 1967 (in Russian).
Glassbrenner, J. and G. A. Slack, *Phys. Rev.* **164**, 4A (1964) 1058–1069.
Golikova, O. A., B. Ya Moizhez, and L. S. Stilbans, *Sov. Phys. Solid State* **3**, 10 (1962) 2259–2265.
Hilsum, C., *Electron. Lett.* **10**, 13 (1974) 259–260.
Hutchinson, C. J., C. Lewis, J. A. Savage, and A. Pitt, *Appl. Optics* **21**, 8 (1982) 1490–1495.
Icenogle, H. W., B. C. Platt, and W. L. Wolfe, *Appl. Optics* **15**, 10 (1976) 2348–2351.
Jacoboni, C., F. Nava, C. Canali, and G. Ottaviani, *Phys. Rev.* **B24**, 2 (1981) 1014–1026.
Jain, S. C. and D. A. Roulston, *Solid State Electron.* **34**, 5 (1991) 453–465.
Kyuregyan, A. S. and S. N. Yurkov, *Sov. Phys. Semicond.* **23**, 10 (1989) 1126–1132.
Macfarlane, G. G., T. P. McLean, J. E. Quarrington, and V. Roberts, *Phys. Rev.* **108**, 6 (1957) 1377–1383.
Mikawa, T., S. Kagawa, T. Kaneda, Y. Toyama, and O. Mikami, *Appl. Phys. Lett.* **37**, 4 (1980) 387–389.
Morin, F. J., *Phys. Rev.* **93**, 1 (1954) 62–63.
Nikanorov, S. P. and B. K. Kardashev, *Elasticity and Dislocation Inelasticity of Crystals*, Moscow, "Nauka" Publ. House, 1985 (in Russian).
Nilsson, G. and G. Nelin, *Phys. Rev.* **B6**, 10 (1972) 3777–3786.
Novikova, S. I., *Sov. Phys. Solid State* **2**, 1 (1960) 37–38.
Okhotin, A. S., A. S. Pushkarskii, and V. V. Gorbachev, *Thermophysical Properties of Semiconductors*, Moscow, "Atom" Publ. House, 1972, (in Russian).
Ottaviani, G., C. Canali, F. Nava, and J. W. Mayer, *J. Appl. Phys.* **44**, 6 (1973) 2917–2918.
Pankove, J. I. and P. Aigrain, *Phys. Rev.* **126**, 3 (1962) 956–962.
Philipp, H. P. and E. A. Taft, *Phys. Rev.* **113**, 4 (1959) 1002–1005.
Piesbergen, U., *Z. Naturforshung,* **18a**, 2 (1963) 141–147.
Reggiani, L., C. Canali, F. Nava, and G. Ottaviani, *Phys. Rev.* **B16**, 6 (1977) 2786–2791.
Reggiani, L., C. Canali, F. Nava, and A. A. Quaranta, *J. Appl. Phys.* **49**, 8 (1978) 4446–4452.
Seysyan, R. P., A. V. Varfolomeev, and B. P. Zaharchenya, *Fiz. i Tekhn. Polupr.* **2**, 9 (1968) 1276–1280 (in Russian).
Ukhanov, Ju. I., *Optical Properties of Semiconductors*, "Nauka", 1977 (in Russian).
Vasiljeva, M. A., L. E. Vorobyev, and V. I. Stafeev, *Fiz. i Tekhn. Polupr.* **1**, 1 (1967) 29–33 (in Russian).
Vorobev, L. E., Yu. K. Pozhela, A. S. Reklaitis, E. S. Smirnitskaya, V. I. Stafeev, and A. B. Fedortsov, *Sov. Phys. Semicond.* **12**, 4 (1978) 433–436.
Weber, W., *Phys. Rev.* **B15**, 10 (1977) 4789–4803.

CHAPTER 3

DIAMOND (C)

G. Sh. Gildenblat
Department of Electrical Engineering and Electronic Material and Processing Research Laboratory, The Pennsylvania State University, USA

and

P. E. Schmidt
Department of Electrical and Computer Engineering, Florida International University, USA

3.1. Basic Parameters at 300 K (Field [1992])

Crystal structure		Diamond
Group of symmetry		O_h^7–Fd3m
Number of atoms in 1 cm^3		1.764×10^{23}
Debye temperature	(K)	1860
Density	($g\,cm^{-3}$)	3.515
Dielectric constant	($10^2 \div 10^4$ Hz)	5.7
Effective electron masses at 85 K (in units of m_o)		
longitudinal m_l/m_o		1.4
transverse m_t/m_o		0.36
Effective hole masses at 1.2 K (in units of m_o)		
heavy m_h/m_o		2.12
light m_{lp}/m_o		0.70
split-off m_{so}/m_o		1.06
Lattice constant	(Å)	3.567
Optical phonon energy	(eV)	0.16

Band structure and carrier concentration

Energy gap	(eV)	5.46–5.6
Energy separation ($E_{\Gamma 1}$)	(eV)	7.3–7.4
Energy of spin-orbital splitting E_{so}	(eV)	0.006
Intrinsic carrier concentration	(cm^{-3})	$\sim 10^{-27}$
Intrinsic resistivity	($\Omega \times$ cm)	$\gtrsim 10^{42}$
Resistivity of natural diamonds	($\Omega \times$ cm)	
	Types I and IIa (usually)	$\sim 10^{16}$
	Type IIb	~ 1–10^{3}
Effective conduction band density of states	(cm^{-3})	$\sim 10^{20}$
Effective valence band density of states	(cm^{-3})	$\sim 10^{19}$

Electrical properties

Breakdown field	($V\,cm^{-1}$)	10^{6}–10^{7}
Mobility	($cm^2\,V^{-1}\,s^{-1}$)	
	electrons	≤ 2200
	holes	≤ 1800
Diffusion coefficient	($cm^2\,s^{-1}$)	
	electrons	≤ 57
	holes	≤ 46
Electron thermal velocity	($m\,s^{-1}$)	$\sim 10^{5}$
Hole thermal velocity	($m\,s^{-1}$)	$\sim 10^{5}$

Optical properties

Index of refraction	2.4
Radiative recombination coefficient ($cm^3\,s^{-1}$)	9×10^{-12}

Thermal and mechanical properties

Bulk modulus	($dyn\,cm^{-2}$)	44.2×10^{11}
Melting point (°C) (at pressure $p = 125$ kbar)		4373
Specific heat	($J\,g^{-1}\,°C^{-1}$)	0.52
Thermal conductivity	($W\,cm^{-1}\,°C^{-1}$)	6–20
Thermal diffusivity	($cm^2\,s^{-1}$)	3–11
Thermal expansion, linear	($°C^{-1}$)	0.8×10^{-6}

3.2. Band Structure and Carrier Concentration

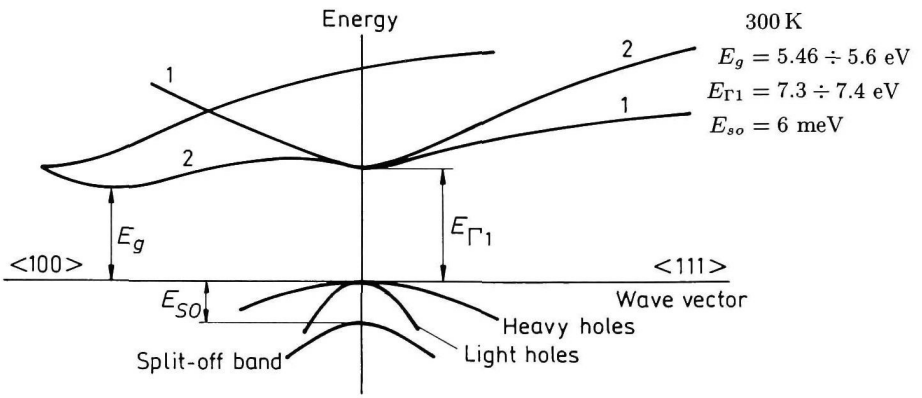

Fig. 3.2.1. Schematic representation of major extrema in the conduction and valence bands of C (diamond).

3.2.1. *Temperature Dependences*

Temperature dependence of the energy gap

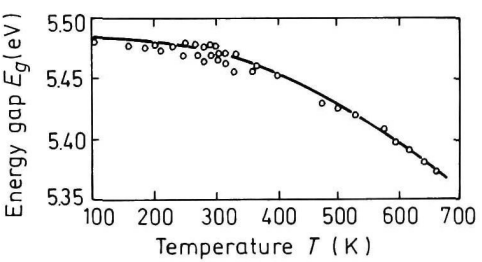

Fig. 3.2.2. Energy gap E_g versus temperature (Clark *et al.* [1964]).

At 300 K: $dE_g/dT = -(5.4 \pm 0.5) \times 10^{-5}\,\mathrm{eV\,K^{-1}}$ (Vavilov and Konorova [1976])

Temperature dependence of the direct band gap $E_{\Gamma 1}$ at 300 K:

$$dE_{\Gamma 1}/dT \simeq -6 \cdot 10^{-4}\,\mathrm{eV\,K^{-1}} \qquad \text{(Clark } et\ al. \text{ [1964])}$$

3.2.2. *Effective Masses and Density of States*

Electrons

The surfaces of equal energy are ellipsoids.

$$m_l = 1.4m_0$$
$$m_t = 0.36m_0$$

Effective mass of density of states
in one valley of conduction band

$$m_c = (m_l \times m_t^2)^{1/3} = 0.57m_0$$

There are 6 equivalent valleys in the "Si-like" conduction band of diamond.

Effective mass of density of states
for all valleys of conduction band $m_{cd} \simeq 1.9m_0$

Effective mass of conductivity

$$m_{cc} = 3 \times \left(\frac{1}{m_l} + \frac{2}{m_t}\right)^{-1} = 0.48m_0$$

Holes

Cyclotron resonance measurement date (Rauch [1962]):

heavy	$m_h = 2.12m_0$
light	$m_{lp} = 0.7m_0$
split-off band	$m_{so} = 1.06m_0$

Effective mass of density of states $m_v = 0.8m_0$

There is a considerable uncertainty regarding the density of states effective mass. The values as low as $m_v = 0.16m_0$ (Kemmey and Wederpohl [1965]) and as high as $m_v = 1.1m_0$ (Dean [1965]) have been reported. For estimations, one can use the value of $m_v = 0.8m_0$ which is close to $m_v = 0.75m_0$ (Collins and Williams [1971]) and $m_v = 0.88m_0$ (Prosser [1964]).

3.2.3. *Donors and Acceptors*

B (boron):

Boron is a deep acceptor level with an activation energy of 0.37 eV. So far semiconductor applications of diamond have been based almost exclusively on boron-doped p-type samples (Gildenblat *et al.* [1991]).

N (nitrogen):

Nitrogen is a most common impurity (donor) in diamond. It is difficult to specify the activation energy since nitrogen can appear as isolated substitutional impurity, simple aggregates or platelets (Stoneham [1992]). In particular, the energy levels of 1.7 eV and 4 eV below the bottom of the conduction band are often ascribed to nitrogen impurities (Davies [1977]; Vermeulen and Farer [1975]; Novikov [1987]).

P (phosphorus):

There are indications that doping with phosphorus results in donor states with activation energies $0.84 \div 1.16$ eV (Okano *et al.* [1990]). Further details are reviewed in Gildenblat *et al.* [1991] and Stoneham [1992]).

3.3. Electrical Properties

3.3.1. *Mobility and Hall Effect*

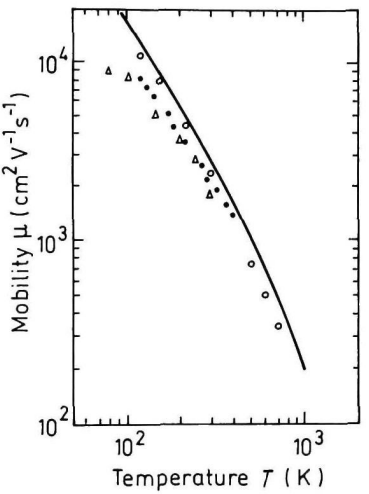

Fig. 3.3.1. Electron mobility as a function of temperature in natural diamond. The continuous curve refers to theoretical calculation. Open circles are experimental data for drift mobility. Triangles and closed circles are experimental data for Hall mobility (Nava *et al.* [1980]).

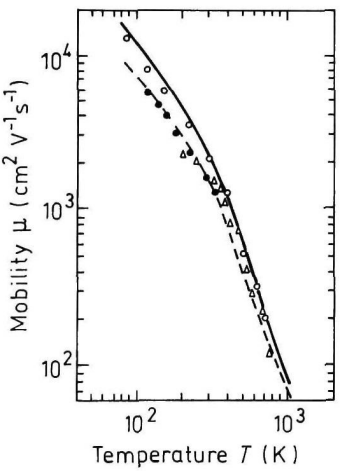

Fig. 3.3.2. Hole mobility as a function of temperature in natural diamond. Curves show the results of calculations of drift mobility (solid line) and Hall mobility (dashed line). Open circles are experimental data for drift mobility. Triangles and closed circles are experimental data for Hall mobility (Reggiani *et al.* [1983]).

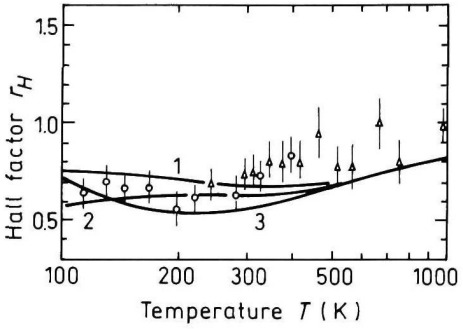

Fig. 3.3.3. The hole Hall factor versus temperature at different impurity concentrations. N_a (cm^{-3}): 1. 10^{11}, 2. 10^{13}, 3. 10^{15}. Points show experimental data from Konorova and Shevchenko [1967] and Dean *et al.* [1965] (Reggiani *et al.* [1983]).

3.3.2. *Transport Properties in High Electric Field*

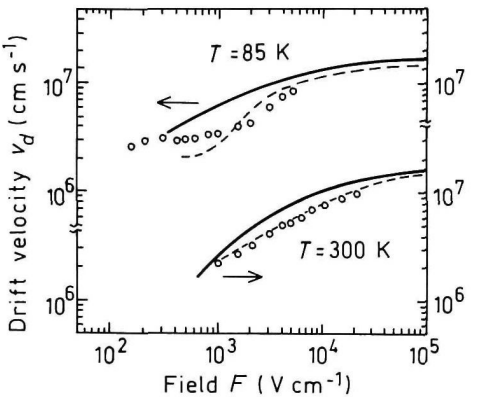

Fig. 3.3.4. Field dependences of the electron drift velocity. Solid lines: $F\|(111)$. Dashed lines: $F\|(100)$ (Nava *et al.* [1980]).

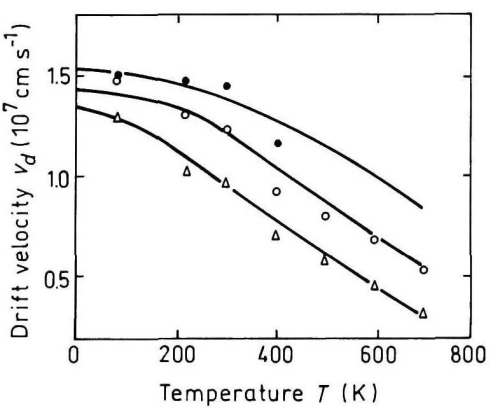

Fig. 3.3.5. Temperature dependences of the electron drift velocity at different fields. $F\|(111) \pm 15°$. Field (kV cm^{-1}): closed circles – 40, open circles – 20, triangles – 10. Lines refer to theoretical calculations (Nava *et al.* [1980]).

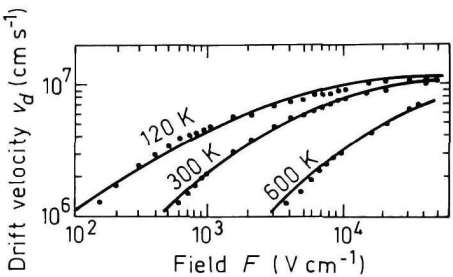

Fig. 3.3.6. Field dependences of the hole drift velocity $F\|(100)$ (Reggiani *et al.* [1981]).

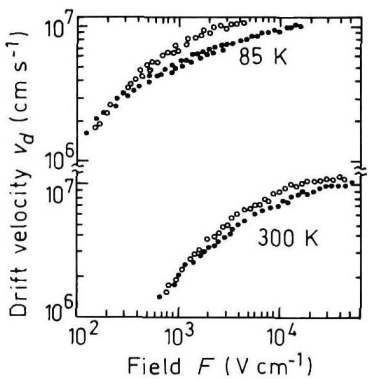

Fig. 3.3.7. Field dependences of the hole drift velocity for $F\|(110)$ (filled circles) and $F\|(100)$ (open circles). (Reggiani *et al.* [1981]).

3.3.3. *Impact Ionization*

Breakdown fields in the $10^6 \div 10^7$ V cm^{-1} range have been reported in several papers for natural diamonds (Bogdanov *et al.* [1982]; Konorova *et al.* [1983]). Breakdown fields in excess of $2 \cdot 10^7$ V cm^{-1} have been reported by Landstrass *et al.* [1993] for homoepitaxial diamond films.

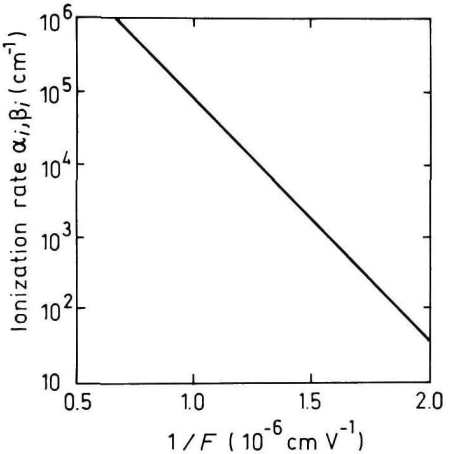

Fig. 3.3.8. Ionization rates for electrons and holes ($\alpha_i = \beta_i$) versus $1/F$ (Trew *et al.* [1991]). $\alpha_i = \beta_i = 1.935 \times 10^8 \exp(-7.749 \cdot 10^6/F)$, where F is electric field in V cm^{-1}.

3.4. Optical Properties

Infrared refractive index $n_\infty = 2.375$.

At 300 K

$$\frac{1}{n}\frac{dn}{dT} = 4.04 \times 10^{-6}\ \mathrm{K}^{-1}$$

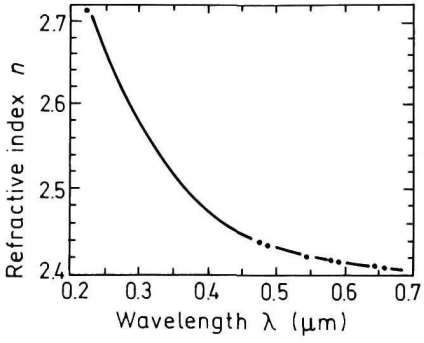

Fig. 3.4.1. Type IIa diamond refractive index versus wavelength. Experimental points: data from four references (Edwards and Ochoa [1981]).

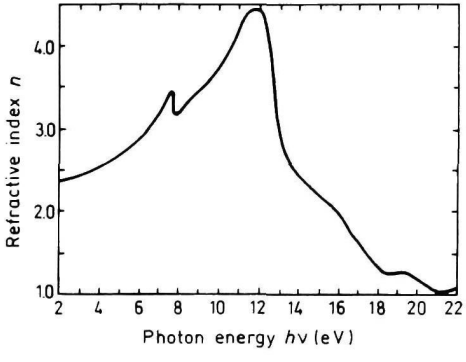

Fig. 3.4.2. Type IIa diamond refractive index versus photon energy at 300 K (Walker and Osantowski [1964]).

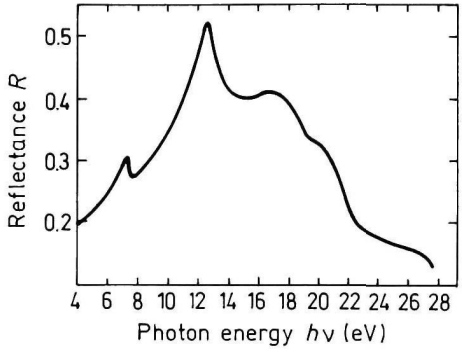

Fig. 3.4.3. Reflectance versus photon energy, 300 K (Walker and Osantowski [1964]).

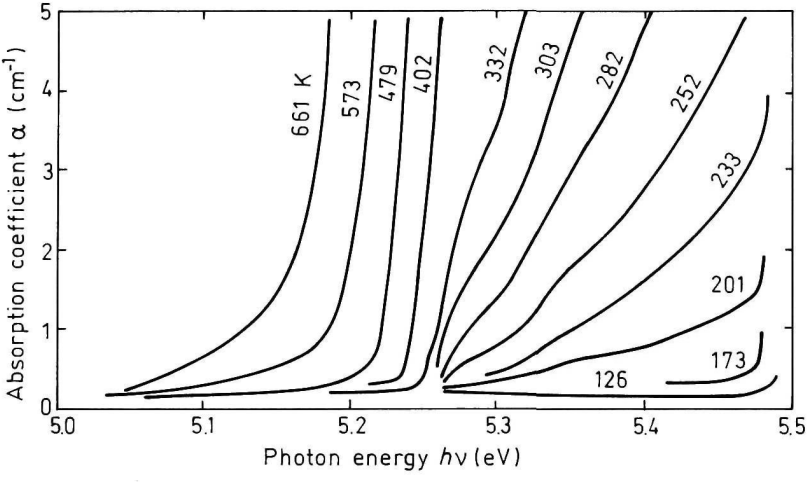

Fig. 3.4.4. Absorption edge spectrum of diamond at various temperatures (Clark *et al.* [1964]).

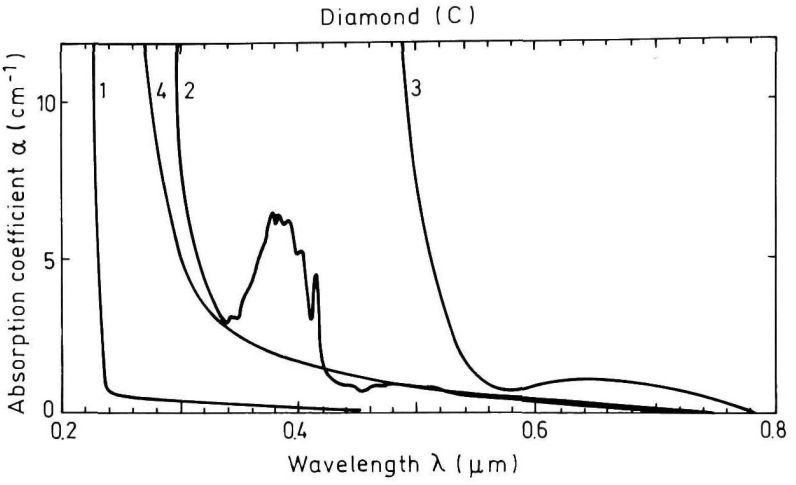

Fig. 3.4.5. Visible and ultraviolet absorption spectra of a diamond with different types of impurities. Predominant type of impurity is: 1. boron atoms, 2. N3 centers, 3. single nitrogen atoms, 4. absorption spectra of a brown diamond (Wilks and Wilks [1991]).

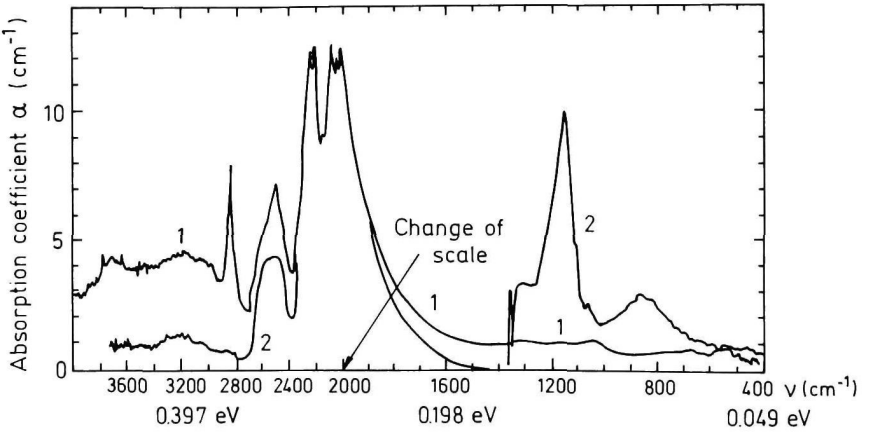

Fig. 3.4.6. Infrared absorption spectra of a diamond in which 1. boron atoms are predominant impurities, 2. single nitrogen atoms are predominant impurities (Wilks and Wilks [1991]).

3.5. Thermal Properties

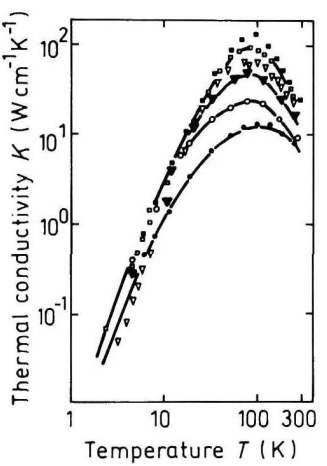

Fig. 3.5.1. Thermal conductivity versus temperature for different diamond types (low temperatures) ▼, ○, ● – Type Ia (three different specimens), ▽ – Type Ib, □, ■ – Type IIb (Berman *et al.* [1975]).

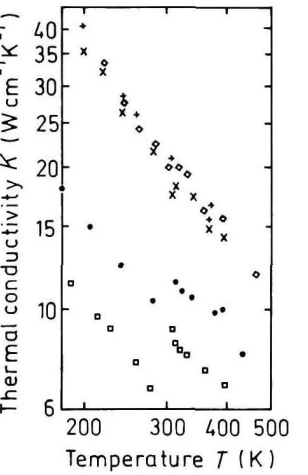

Fig. 3.5.2. Thermal conductivity versus temperature (high temperatures). ●, □ – Type Ia, × – Type Ib, ◇ – Type IIa, + – Type IIb (Burgemeister [1978]).

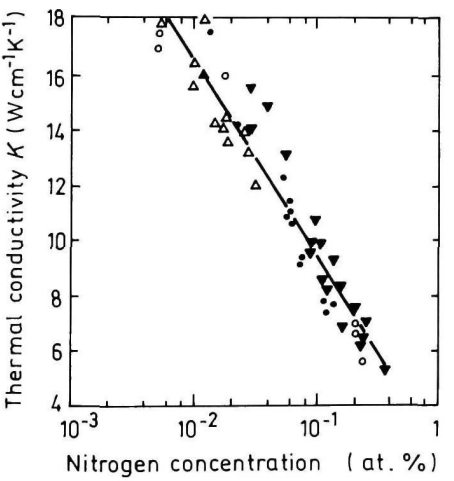

Fig. 3.5.3. Thermal conductivity versus nitrogen concentration, 320 K. Measurements of various authors (Burgemeister [1978]).

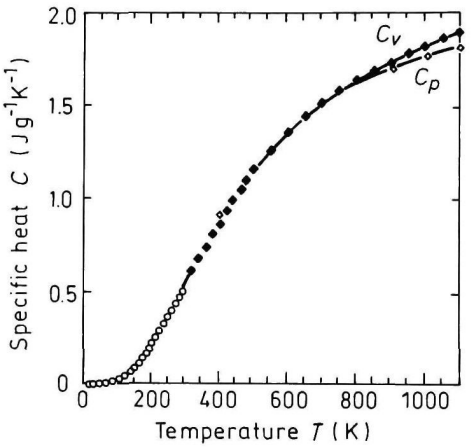

Fig. 3.5.4. Specific heat C_p versus temperature from 20 K to 300 K (DeSorbo [1953]) and C_p (◊) and C_v (♦) from 273 K to 1073 K (Viktor [1962]).

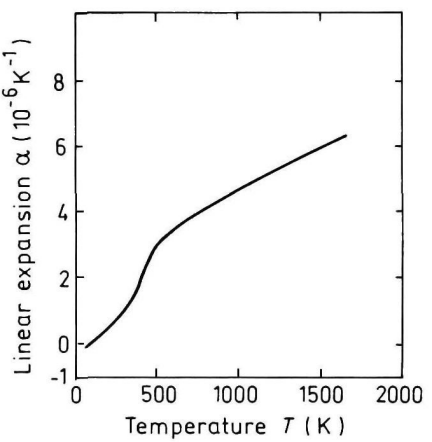

Fig. 3.5.5. Temperature dependence of linear expansion coefficient α (Slack and Batram [1975]).

Melting point $T_m = 4100$ K (for $P = 125$ kbar).

3.6. Mechanical Properties, Elastic Constants, Lattice Vibrations, Other Properties (Field [1979]; Field [1992])

Density	$3.515\,\mathrm{g\,cm^{-3}}$
Hardness on the Mohs scale	10
Surface microhardness (using Knoop's pyramid test)	$(8 \div 10) \times 10^3\,\mathrm{kg\,mm^{-2}}$
Cleavage plane	{111}

Elastic constants at 300 K (McSkimin and Andreatch, Jr. [1972]).

C_{11}	$107.9 \times 10^{11}\,\mathrm{dyn\,cm^{-2}}$
C_{12}	$12.4 \times 10^{11}\,\mathrm{dyn\,cm^{-2}}$
C_{44}	$57.8 \times 10^{11}\,\mathrm{dyn\,cm^{-2}}$

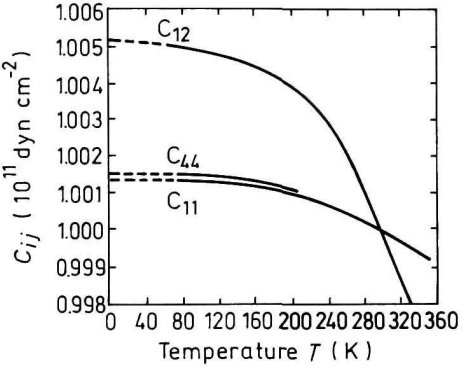

Fig. 3.6.1. Ratio of modulus at temperature T to modulus at 25°C (McSkimin and Andreatch, Jr. [1972]).

Bulk modulus (compressibility^{-1}) For $T = 300\,\mathrm{K}$

$$B_s = \frac{C_{11} + 2C_{12}}{3} \qquad B_s = 44.2 \times 10^{11}\,\mathrm{dyn\,cm^{-2}}$$

Shear modulus

$$C' = (C_{11} - C_{12})/2 \qquad C' = 47.8 \times 10^{11}\,\mathrm{dyn\,cm^{-2}}$$

[100] Young's modulus

$$Y_0 = \frac{(C_{11} + 2C_{12})(C_{11} - C_{12})}{C_{11} + C_{12}} \qquad Y_0 = 105 \times 10^{11}\,\mathrm{dyn\,cm^{-2}}$$

[100] Poisson ratio

$$\sigma_0 = \frac{C_{12}}{C_{11} + C_{12}} \qquad \sigma_0 = 0.1$$

Acoustic Wave Speeds

Wave propagation direction	Wave character	Expression for wave speed	Wave speed (in units of $10^5\,\mathrm{cm\,s^{-1}}$)
[100]	V_L	$(C_{11}/\rho)^{1/2}$	17.52
	V_T	$(C_{44}/\rho)^{1/2}$	12.82
[110]	V_l	$[(C_{11}+C_{12}+2C_{44})/2\rho]^{1/2}$	18.32
	$V_{t\parallel}$	$V_{t\parallel}=V_T=(C_{44}/\rho)^{1/2}$	12.82
	$V_{t\perp}$	$[(C_{11}-C_{12})/2\rho]^{1/2}$	11.66
[111]	V_l'	$[(C_{11}+2C_{12}+4C_{44})/3\rho]^{1/2}$	18.58
	V_t'	$[(C_{11}-C_{12}+C_{44})/3\rho]^{1/2}$	12.06

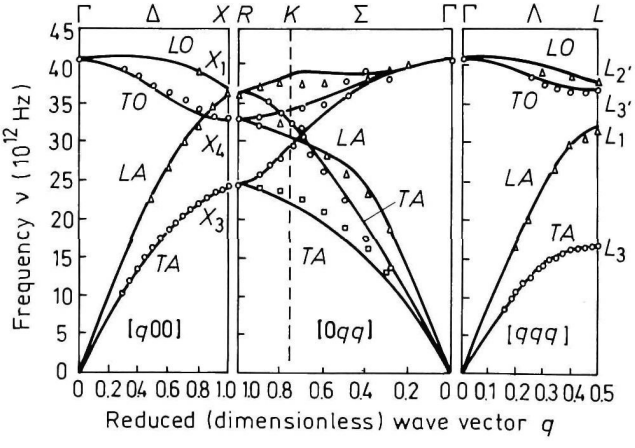

Fig. 3.6.2. Room temperature dispersion curves for acoustic and optical branch phonons. Solid lines are theoretical calculations. Symbols are experimental data (Warren *et al.* [1967]).

Phonon frequencies (in units of 10^{12} Hz) (Solin and Ramdas [1970]).

$\nu_{LTO}(\Gamma_{25'})$	39.9
$\nu_{LAO}(X_1)$	35.5
$\nu_{TA}(X_3)$	24.2
$\nu_{TO}(X_4)$	32.1
$\nu_{LA}(L_1)$	30.2
$\nu_{LO}(L_{2'})$	37.6
$\nu_{TO}(L_{3'})$	36.2
$\nu_{TA}(L_3)$	16.9

References

Berman, R., P. R. W. Hudson, and M. Martinez, *J. Phys. C.* **8**, 21 (1975) L430–L434.

Bogdanov, A. V., I. M. Vikulin, and T. V. Bogdanova, *Sov. Phys. Semicond.* **16**, (1982) 720–721.

Burgemeister, E. A., *Physica* **B93** (1978) 165–179.

Clark, C. D., P. J. Dean, and P. V. Harris, *Proc. Roy. Soc. (London)* **A277** (1964) 312–329.

Collins, A. T. and A. W. S. Wiliams, *J. Phys. C.: Solid State Phys.* **4** (1971) 1789–1800.

Davies, J., in *Chemistry and Physics of Carbon*, R. L. Walker, Jr. and P. A. Thrower, eds., vol. 13, 1977, pp. 1–143.

Dean, P. J., E. C. Lightowlers, and D. R. Wight, *Phys. Rev.* **140**, 1A (1965) 352–368.

Dean, P. J., *Phys. Rev.* **139** (1965) A588–A602.

De Sorbo, W., *J. Chem. Phys.* **21** (1953) 876–880.

Edwards, D. F. and E. Ochoa, *J. Opt. Soc. Amer.* **71** (1981) 607–608.

Field, J. E., in *The Properties of Diamond*, Academic Press, London, 1979.

Field, J. E., in *The Properties of Natural and Synthetic Diamonds*, J. E. Field, ed., Academic Press, London, 1992.

Gildenblat, G. Sh., S. A. Grot, and A. Badzian, *Proc. IEEE* **79**, 5 (1991) 647–668.

Kemmey, P. J. and P. T. Wedepohl, in *Physical Properties of Diamonds*, R. Berman, ed., Clarendon Press, Oxford, 1965.

Konorova, E. A. and S. A. Shevchenko, *Sov. Phys. Semicond.* **1** (1967) 299.

Konorova, E. A., Yu. A. Kuznetsov, V. F. Sergienko, S. D. Tkachenko, A. V. Tsikunov, A. V. Spitsyn, and Yu. Z. Danyushevskii, *Sov. Phys. Semicond.* **17**, (1983) 146–149.

Landstrass, M. I., M. A. Plano, M. A. Moreno, S. McWilliams, L. S. Pan, D. R. Kania, and S. Han, *Diamond and Related Materials* **2** (1993) 1033–1037.

McSkimin, H. J. and P. Andreatch, *J. Appl. Phys.* **43**, (1972) 2944–2948.

Nava, F., C. Canali, C. Jacoboni, L. Reggiani, and S. F. Kozlov, *Solid State Commun.* **33**, (1980) 475–477.

Okano, K., H. Kiyota, T. Iwasaki, T. Kurosu, M. Ida, and T. Nakamura, *Proc. Second Int. Conf. on the New Diamond Science and Technology*, Washington D.C., 1990, pp. 917–922.

Prosser, V., *Czech. J. Phys.* **B15**, (1964) 128–134.

Rauch, C. J., *Proc. of Int. Conf. on the Physics of Semiconductors*, Exeter, UK, A. C. Stickland, ed., Institute of Physics and the Physical Society of London, pp. 276–280, 1962.

Reggiani, L., S. Bosi, C. Canali, F. Nava, and S. F. Kozlov, *Phys. Rev.* **B23**, 6 (1981) 3050–3057.

Reggiani, L., D. Waechter, and S. Zukotynskii, *Phys. Rev.* **B28**, 6 (1983) 3550–3555.

Setako, N., *Extended Abstracts of Technology Update on Diamond Films, Spring MRS Meeting*, 1989, pp. 3–8.

Slack, G. A. and J. Bartram, *J. Appl. Phys.* **46**, 1 (1975) 89–98.

Solin, S. A. and A. K. Ramdas, *Phys. Rev.* **B1**, 4 (1970) 1687–1698.

Stoneham, A. M., *The Properties of Natural and Synthetic Diamond*, J. E. Field, ed., Academic Press, London, 1992, pp. 3–34.

Trew, R. J., J.-B. Yan, and P. M. Mock, *Proc. IEEE* **79**, 5 (1991) 598–620.

Vavilov, V. S. and E. A. Konorova, *Sov. Phys. Usp.* **19**, 4 (1976) 301–316.

Vermeulen, L. A. and R. J. Farrer, *Diamond Research 1975, Suppl. Ind. Diam. Rev.* (1975) 18–23.

Victor, A. C., *J. Chem. Phys.* **36**, 7 (1962) 1903–1911.

Walker, W. C. and J. Osantowski, *Phys. Rev.* **134**, 1A (1964) A153–A157.

Warren, J. L., J. L. Yarnell, G. Dolling, and R. A. Cowley, *Phys. Rev.* **B158**, 3 (1967) 805–808.

Wilks, J. and E. Wilks, *Properties and Applications of Diamond*, Butterworth-Heinemann Ltd., Oxford, 1991.

CHAPTER 4

GALLIUM ARSENIDE (GaAs)

M. E. Levinshtein and **S. L. Rumyantsev**
Ioffe Institute,
St. Petersburg, Russia

4.1. Basic Parameters at 300 K

Crystal structure		Zinc Blende
Group of symmetry		T_d^2–F$\bar{4}$3m
Number of atoms in 1 cm^3		4.42×10^{22}
de Broglie electron wavelength	(Å)	240
Debye temperature	(K)	360
Density	(g cm^{-3})	5.32
Dielectric constant	static	12.9
Dielectric constant	high frequency	10.89
Effective electron mass	(in units of m_o)	0.063
Effective hole masses	(in units of m_o)	
heavy m_h/m_o		0.51
light m_{lp}/m_o		0.082
Electron affinity	(eV)	4.07
Lattice constant	(Å)	5.65325
Optical phonon energy	(eV)	0.035

Band structure and carrier concentration

Energy gap	(eV)	1.424
Energy separation ($E_{\Gamma L}$) between Γ and L valleys	(eV)	0.29

Energy separation ($E_{\Gamma X}$) between Γ and X valleys	(eV)	0.48
Energy spin-orbital splitting	(eV)	0.34
Intrinsic carrier concentration	(cm^{-3})	2.1×10^6
Intrinsic resistivity	($\Omega \times cm$)	3.3×10^8
Effective conduction band density of states	(cm^{-3})	4.7×10^{17}
Effective valence band density of states	(cm^{-3})	9.0×10^{-18}

Electrical properties

Breakdown field	($V\,cm^{-1}$)	$\simeq 4 \times 10^5$
Mobility	($cm^2\ V^{-1}\,s^{-1}$)	
	electrons	≤ 8500
	holes	≤ 400
Diffusion coefficient	($cm^2\,s^{-1}$)	
	electrons	≤ 200
	holes	≤ 10
Electron thermal velocity	($m\,s^{-1}$)	4.4×10^5
Hole thermal velocity	($m\,s^{-1}$)	1.8×10^5

Optical properties

Infrared refractive index	3.3
Radiative recombination coefficient ($cm^3\ s^{-1}$)	7×10^{-10}

Thermal and mechanical properties

Bulk modulus	($dyn\,cm^{-2}$)	7.53×10^{11}
Melting point	(°C)	1240
Specific heat	($J\,g^{-1}\,°C^{-1}$)	0.33
Thermal conductivity	($W\,cm^{-1}\,°C^{-1}$)	0.55
Thermal diffusivity	($cm^2\,s^{-1}$)	0.31
Thermal expansion, linear	($°C^{-1}$)	5.73×10^{-6}

4.2. Band Structure and Carrier Concentration

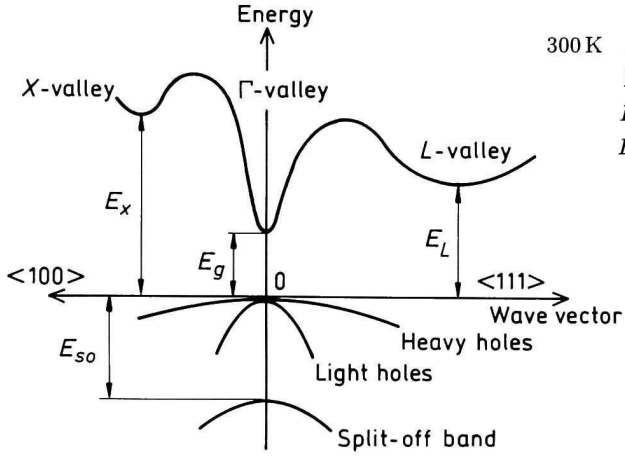

Fig. 4.2.1. Band structure of GaAs. Important minima of the conduction band and maxima of the valence band.

4.2.1. *Temperature Dependences*

Temperature dependence of the energy gap

$$E_g = 1.519 - 5.405 \times 10^{-4} \frac{T^2}{T + 204} \text{ (eV)} , \tag{4.2.1}$$

where T is temperatures in degrees K ($0 < T < 10^3$).

Temperature dependence of the energy difference between the top of the valence band and the bottom of the L-valley of the conduction band

$$E_L = 1.815 - 6.05 \times 10^{-4} \frac{T^2}{T + 204} \text{ (eV)} . \tag{4.2.2}$$

Temperature dependence of the energy difference between the top of the valence band and the bottom of the X-valley of the conduction band

$$E_X = 1.981 - 4.60 \times 10^{-4} \frac{T^2}{T + 204} \text{ (eV)} . \tag{4.2.3}$$

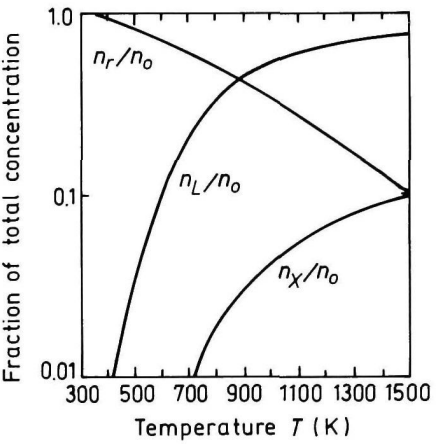

Fig. 4.2.2. The temperature dependences of the relative populations of the Γ, L and X valleys (Blakemore [1982]).

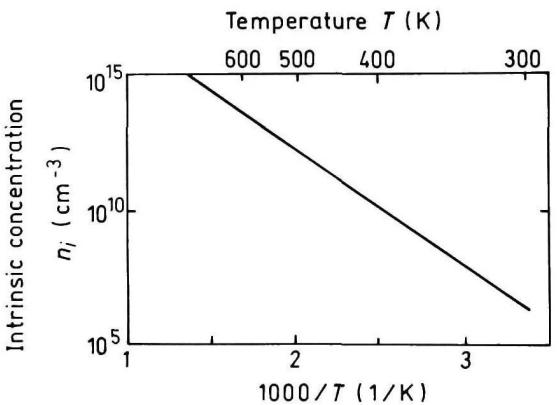

Fig. 4.2.3. The temperature dependence of the intrinsic carrier concentration (Shur [1990]). (Figure reprinted with permission of Prentice Hall Inc.)

Intrinsic carrier concentration

$$n_i = (N_c \cdot N_v)^{1/2} \exp\left[-\frac{E_g}{2k_B T}\right] . \tag{4.2.4}$$

Effective density of states in the conduction band taking into account the non-parabolicity of the Γ-valley and contributions from the X and L-valleys

$$N_c = 8.63 \times 10^{13} T^{3/2} \left[1 - 1.93 \times 10^{-4} T - 4.19 \times 10^{-8} T^2 + 21 \exp\left(-\frac{E_{\Gamma L}}{k_B T}\right) + 44 \exp\left(-\frac{E_{\Gamma X}}{k_B T}\right)\right] \quad (\mathrm{cm}^{-3}) \tag{4.2.5}$$

Effective density of states in the valence band

$$N_v = 1.83 \times 10^{15} \times T^{3/2} \ (\mathrm{cm}^{-3}) . \tag{4.2.6}$$

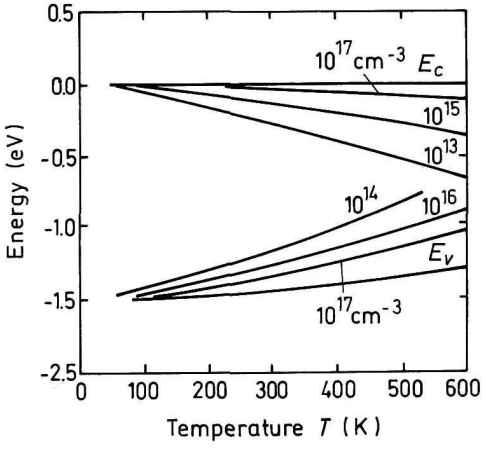

Fig. 4.2.4. Fermi level versus temperature for different concentrations of shallow donors and acceptors.

4.2.2. *Dependences on Hydrostatic Pressure*

$$\begin{aligned} E_g &= E_g(0) + 0.0126P - 3.77 \times 10^{-5}\ P^2\ \text{(eV)} \\ E_L &= E_L(0) + 5.5 \times 10^{-3}\ P\ \text{(eV)} \\ E_X &= E_X(0) - 1.5 \times 10^{-3}\ P\ \text{(eV)} \end{aligned} \tag{4.2.7}$$

where P is pressure in kbar.

4.2.3. *Energy Gap Narrowing at High Doping Levels*

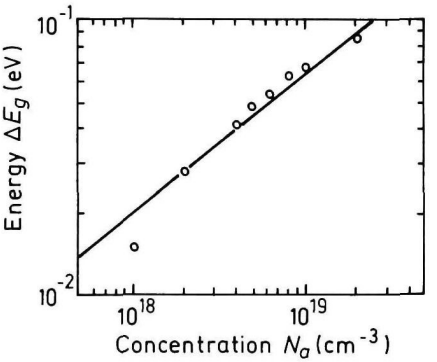

Fig. 4.2.5. Energy gap narrowing at high doping levels (Tiwari and Wright [1990]).

$$\Delta E_g \simeq 2 \times 10^{-11} N_a^{1/2}\ \text{(eV)}\ (N_a - \text{in cm}^{-3})$$

4.2.4. *Effective Masses*

Electrons

For Γ-valley $m_\Gamma = 0.063m_0$

In the L-valley the surfaces of equal energy are ellipsoids

$$m_l = 1.9m_0$$
$$m_t = 0.075m_0$$

Effective mass of density of states

$$m_L = (16m_l m_t^2)^{1/3} = 0.56m_0$$

In the X-valley surfaces of equal energy are ellipsoids

$$m_l = 1.9m_0$$
$$m_t = 0.19m_0$$

Effective mass of density of states

$$m_X = (9m_l m_t^2)^{1/3} = 0.85m_0$$

Holes

heavy	$m_h = 0.51m_0$
light	$m_{lp} = 0.082m_0$
split-off band	$m_{so} = 0.15m_0$
Effective mass of density of states	$m_v = 0.53m_0$

4.2.5. *Donors and Acceptors*

Ionization energies of shallow donors (Milnes [1973]) (eV)

S	~ 0.006
Se	~ 0.006
Si	~ 0.006
Ge	~ 0.006
Sn	~ 0.006
Te	~ 0.03

Ionization energies of shallow acceptors (Milnes [1973]) (eV)

C	~ 0.02
Si three acceptor levels	~ 0.03, 0.1 and 0.22
Ge	~ 0.03
Zn	~ 0.025
Sn	~ 0.2

4.3. Electrical Properties

4.3.1. *Mobility and Hall Effect*

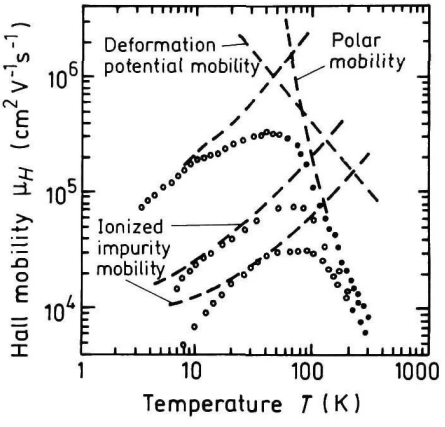

Fig. 4.3.1. Electron Hall mobility versus temperature for different doping levels.

1. Bottom curve: $N_d = 5 \times 10^{15}\ cm^{-3}$,
2. Middle curve: $N_d = 10^{15}\ cm^{-3}$,
3. Top curve: $N_d = 5 \times 10^{13}\ cm^{-3}$.

(Stillman *et al.* [1970]). (Figure reprinted with kind permission from Elsevier Science Ltd.).

For weakly doped GaAs at temperature close to 300 K, electron Hall mobility $\mu_H \simeq 9400(300/T)^{2/3}$ ($cm^2\ V^{-1}\ s^{-1}$).

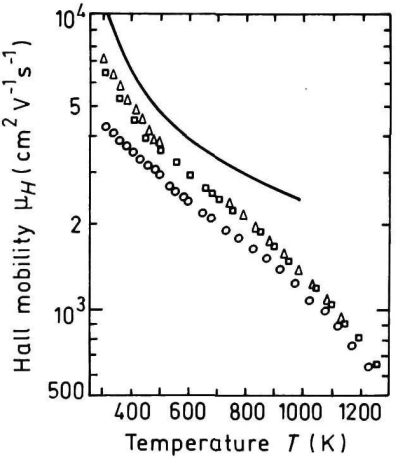

Fig. 4.3.2. Electron Hall mobility versus temperature for different doping levels and degrees of compensation (high temperatures):

Open circles $N_d = 4N_a = 1.2 \times 10^{17}\ cm^{-3}$
Open squares $N_d = 4N_a = 10^{16}\ cm^{-3}$
Open triangles $N_d = 3N_a = 2 \times 10^{15}\ cm^{-3}$.

Solid curve represents the calculation for pure GaAs (Blakemore [1982]).

For weakly doped GaAs at temperatures, close to 300 K, electron drift mobility $\mu_n \simeq 8000(300/T)^{2/3}$ ($cm^2\ V^{-1}\ s^{-1}$).

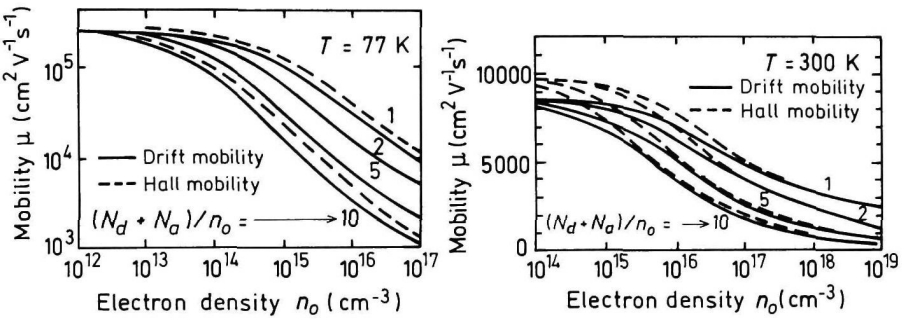

Fig. 4.3.3. Drift and Hall mobilities versus electron concentration for different degrees of compensation (Rode [1975]).

Approximate formula for the Hall mobility $\mu = \mu_{OH}/[1 + (N_d/10^{17})^{1/2}]$, where $\mu_{OH} \simeq 9400\,\mathrm{cm^2\,V^{-1}\,s^{-1}}$, N_d – in $\mathrm{cm^{-3}}$ (Hilsum [1974]).

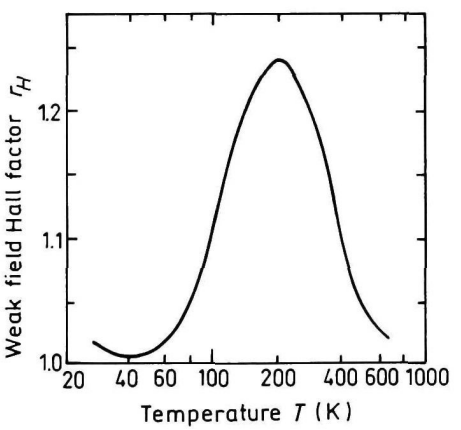

Fig. 4.3.4. Temperature dependence of the Hall factor for pure n-type GaAs in a weak magnetic field (Rode [1975]).

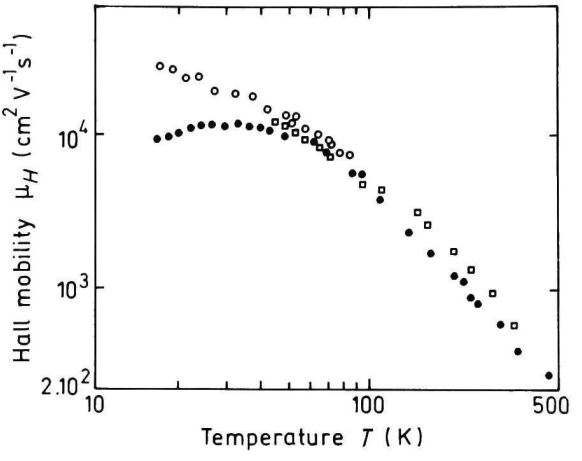

Fig. 4.3.5. Temperature dependences of hole Hall mobility for three high-purity samples (Wiley [(1975)].

For GaAs at temperatures close to 300 K, hole Hall mobility

$$\mu_{pH} = \left[0.0025\left(\frac{T}{300}\right)^{2.3} + 4 \times 10^{-21} p \left(\frac{T}{300}\right)^{1.5}\right]^{-1} \quad (\mathrm{cm^2\,V^{-1}\,s^{-1}})$$

(p – in $\mathrm{cm^{-3}}$).

For weakly doped GaAs at temperatures close to 300 K, hole Hall mobility

$$\mu_{pH} = 400(300/T)^{2.3} \quad (\mathrm{cm^2\,V^{-1}\,s^{-1}})$$

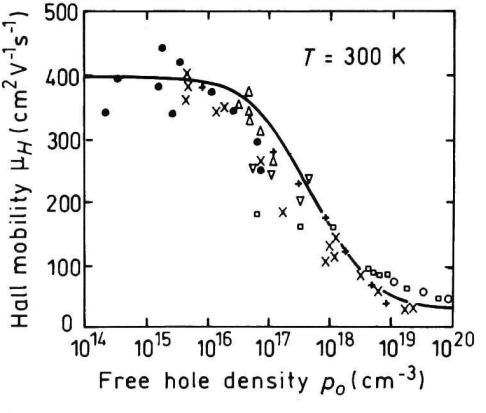

Fig. 4.3.6. Hall hole mobility versus hole density (Wiley [1975]).

At $T = 300$ K, the hole Hall factor in pure GaAs $r_H = 1.25$.

4.3.2. *Transport Properties in High Electric Field*

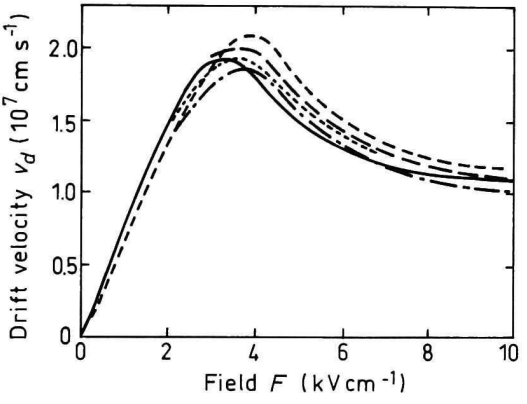

Fig. 4.3.7. Field dependences of the electron drift velocity (Blakemore [1982]). Solid curve was calculated by Pozhela and Reklaitis [1980]. Dashed and dotted curves are measured data, 300 K.

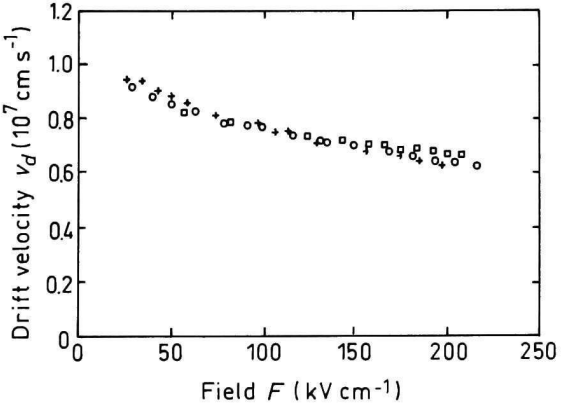

Fig. 4.3.8. The field dependence of the electron drift velocity for high electric fields, 300 K (Blakemore [1982]).

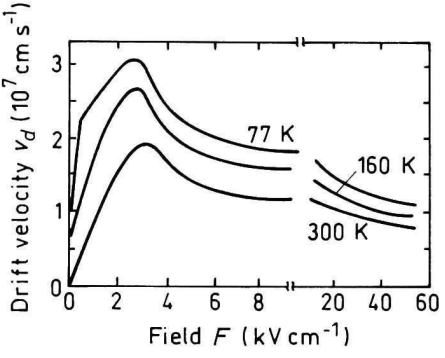

Fig. 4.3.9. Field dependences of the electron drift velocity at different temperatures (Pozhela and Reklaitis [1980]). (Figure reprinted with kind permission from Elsevier Science Ltd.)

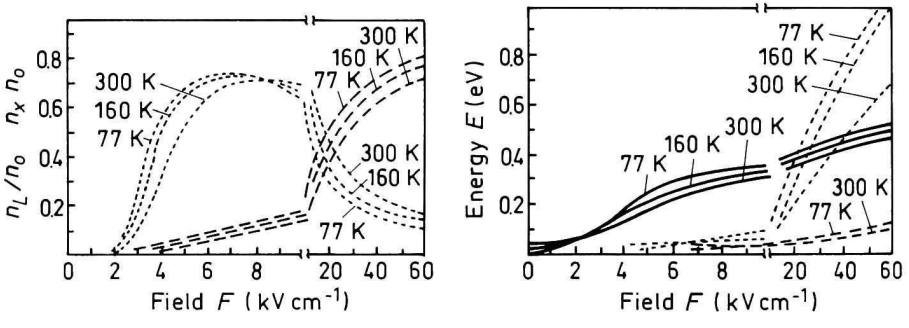

(a) (b)

Fig. 4.3.10. Fraction of electrons in L and X valleys. n_L and n_X (a) and mean energy E in Γ, L, and X valleys (b) as a function of electric field F at 77, 160, and 300 K, $N_d = 0$ (Pozhela and Reklaitis [1980]). Solid curves – Γ valley, dotted curves – L valleys, dashed curves – X valleys. (Figure reprinted with kind permission from Elsevier Science Ltd.)

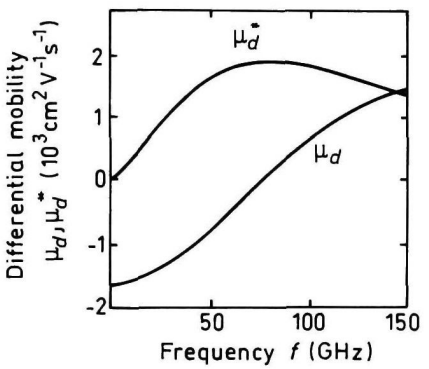

Fig. 4.3.11. Frequency dependences of electron differential mobility in GaAs. μ_d is a real part of the differential mobility; μ_d^* is an imaginary part of differential mobility. $F = 5.5\,\mathrm{kV\,cm^{-1}}$ (Rees [1969]). (Figure reprinted with kind permission from Elsevier Science Ltd.)

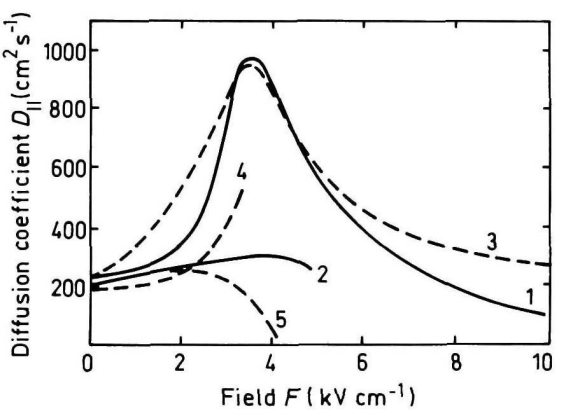

Fig. 4.3.12. The field dependences of longitudinal electron diffusion coefficient $D\|F$. Solid curves 1 and 2 are theoretical calculations. Dashed curves 3, 4, and 5 are experimental data. Curve 1 – from Pozhela and Reklaitis [1980]. Curve 2 – from Fauquembergue *et al.* [1980]. Curve 3 – from Ruch and Kino [1968]. Curve 4 – from Bareikis *et al.* [1978]. Curve 5 – from de Murcia [1991].

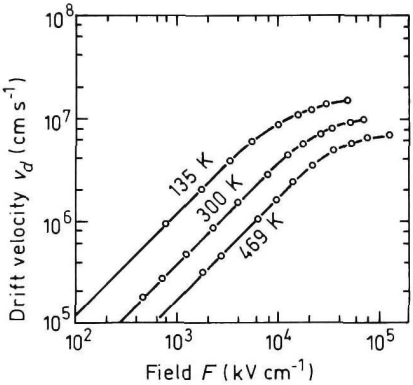

Fig. 4.3.13. Field dependences of the hole drift velocity at different temperatures (Dalal *et al.* [1971]).

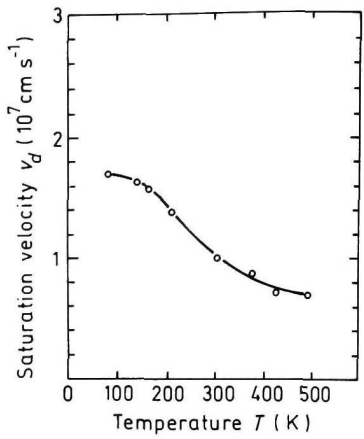

Fig. 4.3.14. Temperature dependence of the saturation hole velocity in high electric fields (Dalal *et al.* [1971]).

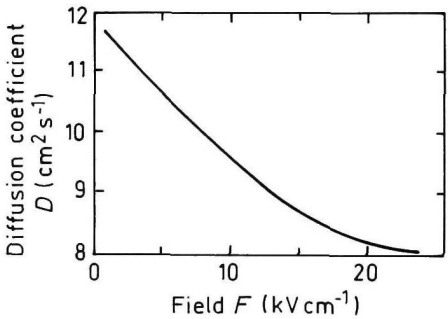

Fig. 4.3.15. The field dependence of the hole diffusion coefficient (Joshi and Crendin [1989]).

4.3.3. *Impact Ionization*

The are two schools of thought regarding the impact ionization in GaAs. The first one states that impact ionization rates α_i and β_i, for electrons and holes in GaAs are known accurately enough to distinguish subtle details such as the anisothropy of α_i and β_i for different crystallographic directions. This approach is described in detail in the work by Dmitriev *et al.* [1987].

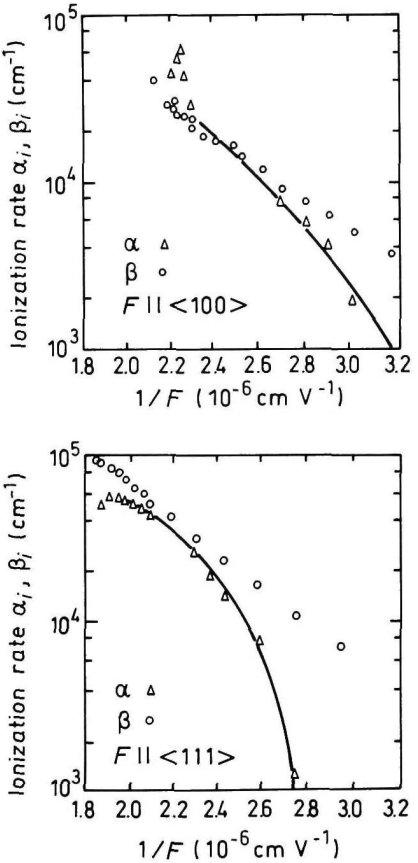

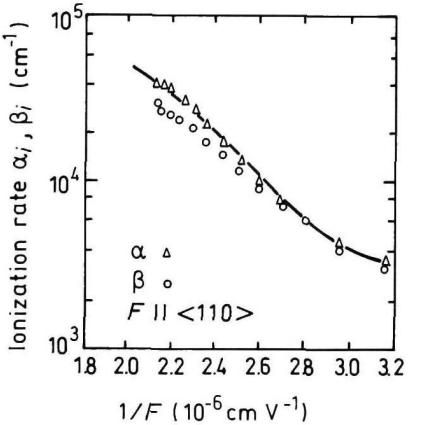

Fig. 4.3.16. Experimental curves α_i and β_i versus $1/F$ for GaAs for three orientations of the electric field (Pearsall *et al.* [1978]). (Figure reprinted with kind permission from Elsevier Science Ltd.)

The second school focuses on the values α_i and β_i for the same electric field reported by different researchers differ by an order of magnitude or more. This point of view is explained by Kyuregyan and Yurkov [1989]. According to this approach we can assume that $\alpha_i \simeq \beta_i$. Approximate formula for the field dependence of ionization rates

$$\alpha_i = \beta_i = \alpha_0 \exp\left[\delta - \sqrt{\delta^2 + (F_o/F)^2}\right] \tag{4.3.1}$$

where $\alpha_o = 0.245 \times 10^6\,\mathrm{cm}^{-1}$, $\delta = 57.6$, $F_o = 6.65 \times 10^6\ \mathrm{V\,cm}^{-1}$ (Kyuregyan and Yurkov [1989]).

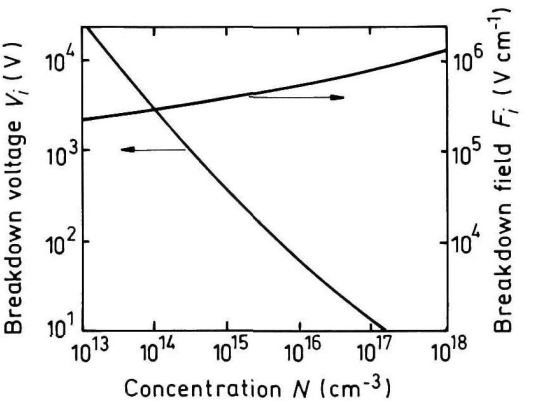

Fig. 4.3.17. Breakdown voltage and breakdown field versus doping density for an abrupt p-n junction (Kyuregyan and Yurkov [1989]).

4.3.4. *Recombination Parameters*

Pure *n*-type material ($n_0 \sim 10^{14}\,\mathrm{cm}^{-3}$)

The longest lifetime of holes		$\tau_p \sim 3 \times 10^{-6}\,\mathrm{s}$
Diffusion length	$L_p = (D_p \times \tau_p)^{1/2}$	$L_p \sim 30\text{–}50\,\mu\mathrm{m}$

Pure *p*-type material

(a) low injection level

The longest lifetime of electrons		$\tau_n \sim 5 \times 10^{-9}\,\mathrm{s}$
Diffusion length	$L_n = (D_n \times \tau_n)^{1/2}$	$L_n \sim 10\,\mu\mathrm{m}$

(b) high injection level (filled traps)

The longest lifetime of electrons	$\tau_n \sim 2.5 \times 10^{-7}\,\mathrm{s}$
Diffusion length L_n	$L_n \sim 70\,\mu\mathrm{m}$

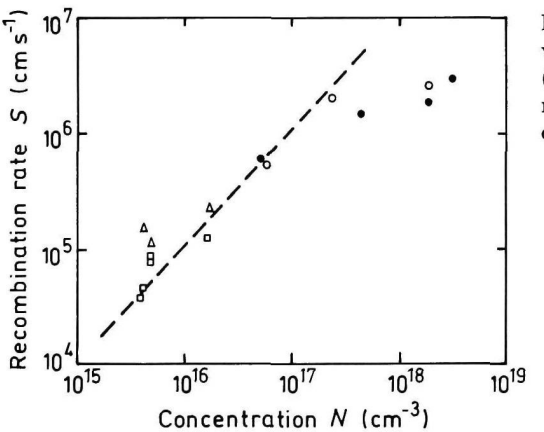

Fig. 4.3.18. Surface recombination velocity versus doping density (Aspnes [1983]). Different experimental points correspond to different surface treatment methods.

Radiative recombination coefficient (Varshni [1967])

$90\,\mathrm{K} - 1.8 \times 10^{-8}\ \mathrm{cm}^3\,\mathrm{s}^{-1}$
$185\,\mathrm{K} - 1.9 \times 10^{-9}\ \mathrm{cm}^3\,\mathrm{s}^{-1}$
$300\,\mathrm{K} - 7.2 \times 10^{-10}\ \mathrm{cm}^3\,\mathrm{s}^{-1}$

Auger coefficient

$300\,\mathrm{K} - \sim 10^{-30}\ \mathrm{cm}^6\,\mathrm{s}^{-1}$
$500\,\mathrm{K} - \sim 10^{-29}\ \mathrm{cm}^6\,\mathrm{s}^{-1}$

4.4. Optical Properties

Infrared refractive index

$$n_\infty = (k_\infty)^{1/2} = 3.255 \times (1 + 4.5 \times 10^{-5} T) \tag{4.4.1}$$

for 300 K $\qquad n_\infty = 3.299$

Long-wave *TO* phonon energy

$$h\nu_{TO} = 33.81 \times (1 - 5.5 \times 10^{-5} T) \quad \text{(meV)} \tag{4.4.2}$$

for 300 K $\qquad h\nu_{TO} = 33.2\,\text{meV}$

Long-wave *LO* phonon energy

$$h\nu_{LO} = 36.57 \times (1 - 4 \times 10^{-5} T) \quad \text{(meV)} \tag{4.4.3}$$

for 300 K $\qquad h\nu_{LO} = 36.1\,\text{meV}$

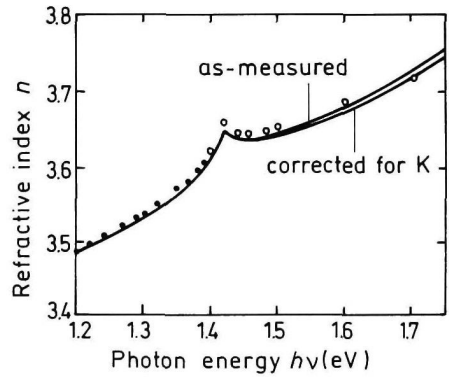

Fig. 4.4.1. Refractive index n versus photon energy for a high-purity GaAs ($n_0 \simeq 5 \times 10^{13}\,\text{cm}^{-3}$). Solid curve is deduced from two-beam reflectance measurements at 279 K. Dark circles are obtained from refraction measurements. Light circles are calculated from Kramers–Krönig analysis (Blakemore [1982]).

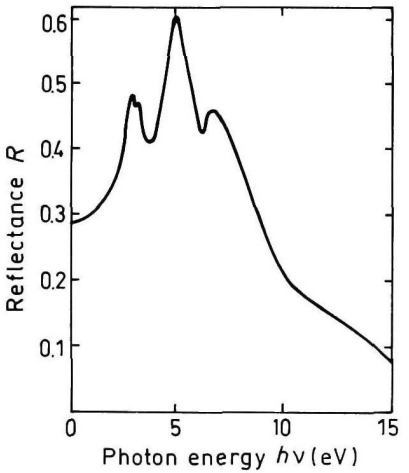

Fig. 4.4.2. Normal incidence reflectivity versus photon energy (Phillip and Ehrenreich [1963]).

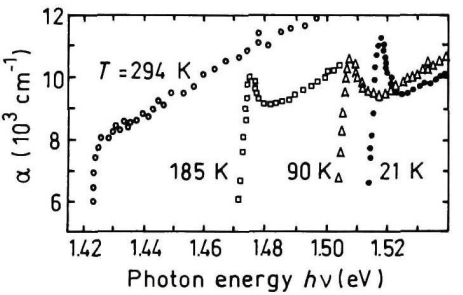

Fig. 4.4.3. Intrinsic absorption coefficient near the intrinsic absorption edge for different temperatures (Sturge [1962]).

A ground state Rydberg energy $R_{X1} = 4.2\,\text{meV}$

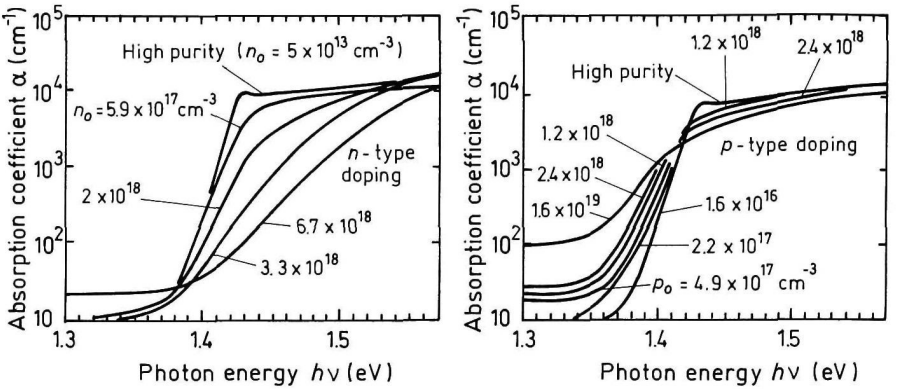

Fig. 4.4.4. Intrinsic absorption edge at 297 K at different doping levels (Casey *et al.* [1975]).

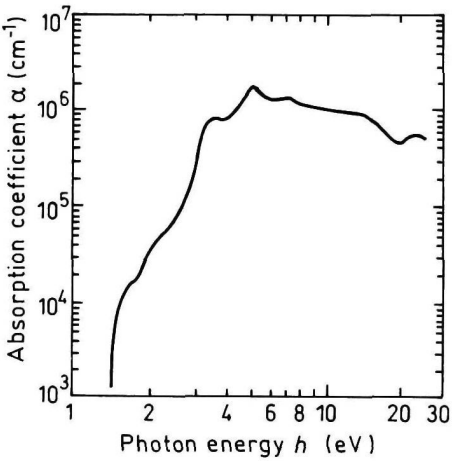

Fig. 4.4.5. The absorption coefficient versus photon energy from intrinsic edge to 25 eV (Casey *et al.* [1975]).

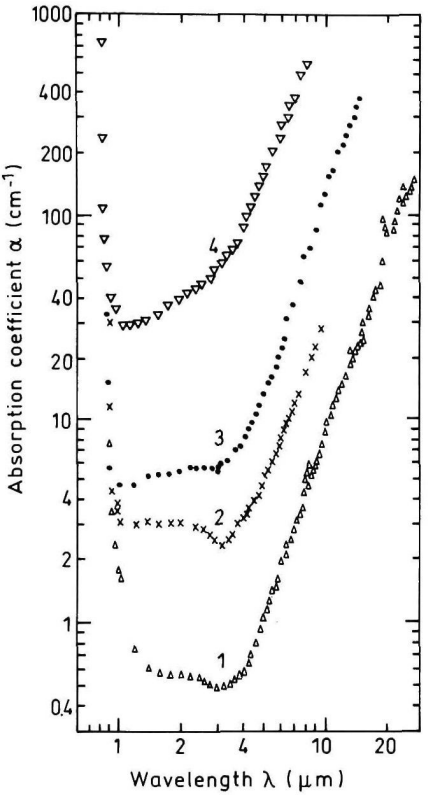

Fig. 4.4.6. Free carrier absorption versus wavelength at different doping levels, 296 K (Spitzer and Whelan [1959]). Conduction electron concentrations are:

1. $1.3 \times 10^{17}\,\mathrm{cm}^{-3}$, 2. $4.9 \times 10^{17}\,\mathrm{cm}^{-3}$, 3. $10^{18}\,\mathrm{cm}^{-3}$, 4. $5.4 \times 10^{18}\,\mathrm{cm}^{-3}$.

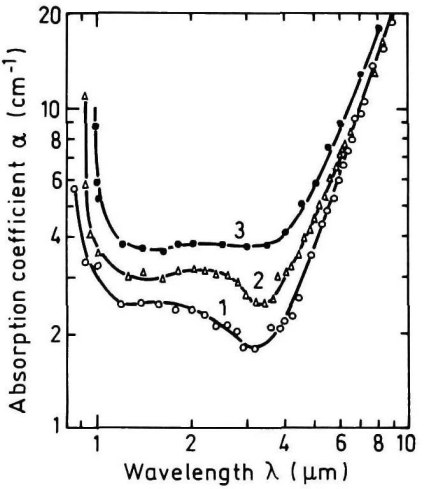

Fig. 4.4.7. Free carrier absorption versus wavelength at different temperatures. $n_0 = 4.9 \times 10^{17}\,\mathrm{cm}^{-3}$ (Spitzer and Whelan [1959]) Temperatures are:

1. 100 K, 2. 297 K, 3. 443 K.

At 300 K
For $\lambda \simeq 2\,\mu\mathrm{m}$

$$\alpha = 6 \times 10^{-18} n_0\,(\mathrm{cm}^{-1})$$

(n_0 – in cm^{-3})
For $\lambda > 4\,\mu\mathrm{m}$ and
$10^{17} < n_0 < 10^{18}\,\mathrm{cm}^{-3}$

$$\alpha \simeq 7.5 \times 10^{-20} n_0 \lambda^3\,(\mathrm{cm}^{-1})$$

(n_0 – in cm^{-3}, λ – in $\mu\mathrm{m}$)

4.5. Thermal Properties

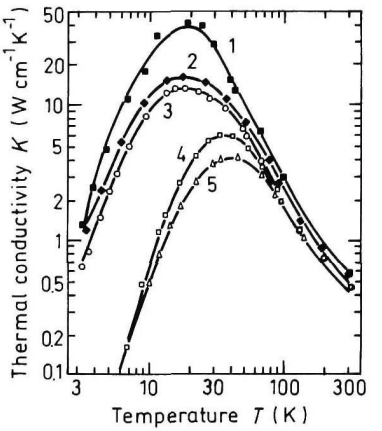

Fig. 4.5.1. Temperature dependences of thermal conductivity (Carlson *et al.* [1965]). n-type sample, n_0 =: 1. 10^{16} cm^{-3}, 2. 1.4×10^{16} cm^{-3}, 3. 10^{18} cm^{-3}. p-type samples, p_0 =: 4. 3×10^{18} cm^{-3}, 5. 1.2×10^{19} cm^{-3}.

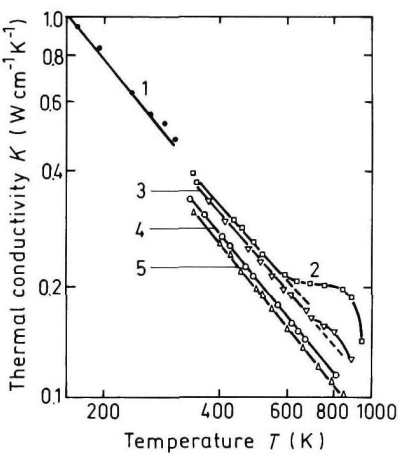

Fig. 4.5.2. Temperature dependences of thermal conductivity (for high temperatures) (Blakemore [1982]). n-type samples, n_0 =: 1. 7×10^{15} cm^{-3}, 2. 5×10^{16} cm^{-3}, 3. 4×10^{17} cm^{-3}, 4. 8×10^{18} cm^{-3}. p-type sample, p_0 =: 5. 6×10^{19} cm^{-3}.

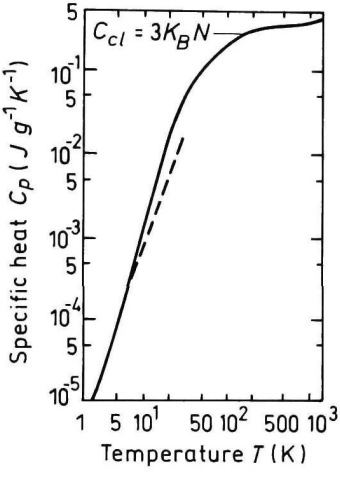

Fig. 4.5.3. Temperature dependence of specific heat at constant pressure (Blakemore [1982]).

$C_{cl} = 3k_B N = 0.345$ Jg^{-1} K^{-1}.
N is the number of atoms in 1 g of GaAs.
Dashed line:
$C_p = (4\pi^4 C_{cl}/5\theta_0^3) \times T^3$ for $\theta_0 = 345$ K.

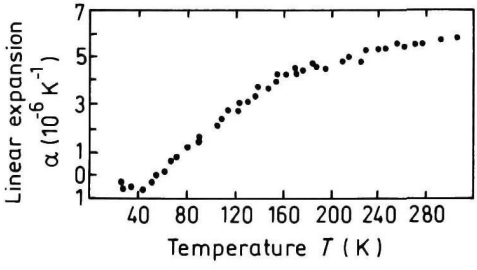

Fig. 4.5.4. Temperature dependence of linear expansion coefficient α (Novikova [1961]).

Melting point
for $0 < P < 45$ kbar

$T_m = 1513$ K
$T_m = 1513 - 3.5\,P$ (P in kbar)

Saturated vapor pressure (Sze [1981])

(in Pascals)
for 1173 K – 1
for 1323 K – 100

4.6. Mechanical Properties, Elastic Constants, Lattice Vibrations, Other Properties

Density		$5.317\,\mathrm{g\,cm^{-3}}$
Hardness on the Mohs scale		between 4 and 5
Surface microhardness (using Knoop's pyramid test)		$750\,\mathrm{kg\,mm^{-2}}$
Cleavage plane		{110}
Elastic constants at 300 K	C_{11}	$11.90 \times 10^{11}\,\mathrm{dyn\,cm^{-2}}$
	C_{12}	$5.34 \times 10^{11}\,\mathrm{dyn\,cm^{-2}}$
	C_{44}	$5.96 \times 10^{11}\,\mathrm{dyn\,cm^{-2}}$

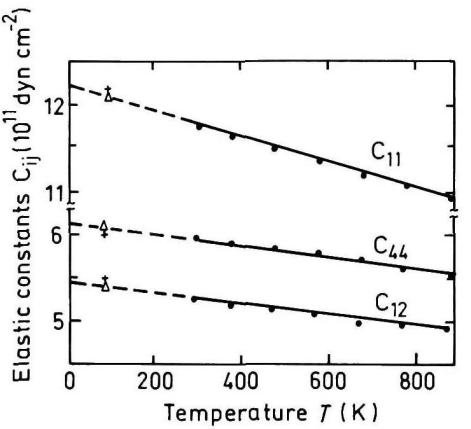

Fig. 4.6.1. Temperature dependences of elastic constants for $0 < T < T_m = 1513$ K (in units of $10^{11}\,\mathrm{dyn\,cm^{-2}}$)

$C_{11} \simeq 12.17\text{–}1.44 \times 10^{-3}\,T$
$C_{12} \simeq 5.46\text{–}0.64 \times 10^{-3}\,T$
$C_{44} \simeq 6.16\text{–}0.70 \times 10^{-3}\,T$
(Burenkov *et al.* [1973]).

For $T = 300$ K

Bulk modulus (compressibility^{-1})

$$B_s = \frac{C_{11} + 2C_{12}}{3} \qquad B_s = 7.53 \times 10^{11}\,\mathrm{dyn\,cm^{-2}}$$

Shear modulus $C' = (C_{11} - C_{12})/2$ $\qquad C' = 3.28 \times 10^{11}\,\mathrm{dyn\,cm^{-2}}$

[100] Young's modulus

$$Y_0 = \frac{(C_{11} + 2C_{12})(C_{11} - C_{12})}{(C_{11} + C_{12})} \qquad Y_0 = 8.59 \times 10^{11}\,\mathrm{dyn\,cm^{-2}}$$

[100] Poisson ratio $\sigma_0 = \dfrac{C_{12}}{C_{11} + C_{12}}$ $\qquad \sigma_0 = 0.31$

Acoustic Wave Speeds

Wave propagation direction	Wave character	Expression for wave speed	Wave speed (in units of $10^5\,\mathrm{cm\,s^{-1}}$)
[100]	V_L	$(C_{11}/\rho)^{1/2}$	4.73
	V_T	$(C_{44}/\rho)^{1/2}$	3.35
[110]	V_l	$[(C_{11}+C_{12}+2C_{44})/2\rho]^{1/2}$	5.24
	$V_{t\parallel}$	$V_{t\parallel}=V_T=(C_{44}/\rho)^{1/2}$	3.35
	$V_{t\perp}$	$[(C_{11}-C_{12})/2\rho]^{1/2}$	2.48
[111]	V_l'	$[(C_{11}+2C_{12}+4C_{44})/3\rho]^{1/2}$	5.4
	V_t'	$[(C_{11}-C_{12}+C_{44})/3\rho]^{1/2}$	2.8

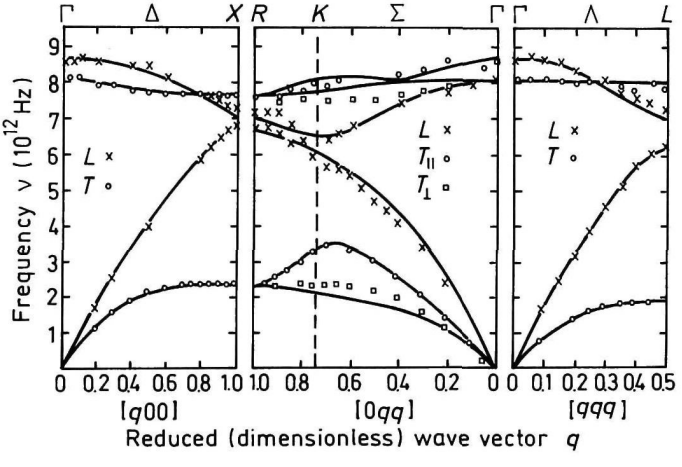

Fig. 4.6.2. Room temperature dispersion curves for acoustic and optical branch phonons. Solid lines are calculated according to dipole approximation force constant model (Waugh and Dolling [1963]).

Phonon frequencies (in units of 10^{12} Hz) (Waugh and Dolling [1963])

$\nu_{TO}(\Gamma)$	8.02	$\nu_{LO}(X)$	7.22
$\nu_{LO}(\Gamma)$	8.55	$\nu_{TA}(L)$	1.86
$\nu_{TA}(X)$	2.36	$\nu_{LA}(L)$	6.26
$\nu_{LA}(X)$	6.80	$\nu_{TO}(L)$	7.84
$\nu_{TO}(X)$	7.56	$\nu_{LO}(L)$	7.15

Piezoelectric constant e_{14} $\quad -0.16\,\mathrm{C\,m^{-2}}$

References

Aspnes, D. E., *Surface Sci.* **132**, 1–3 (1983) 406–421.

Bareikis, V., F. Galdikas, R. Milisyte, and V. Viktoravicius, *Proc. 5th Conf. on Noise in Physical Systems*, Bad Nauheim, West Germany, Mar. 1978, p. 212.

Blakemore, J. S., *J. Appl. Phys.* **53**, 10 (1982) R123–R181.

Burenkov, Yu. A., Yu. M. Burdukov, S. Yu. Davidov, and S. P. Nikanorov, *Sov. Phys. Solid State* **15**, 6 (1973) 1175–1177.

Carlson, R. O., G. A. Slack, and S. J. Silverman, *J. Appl. Phys.* **36**, 2 (1965) 505.

Casey, H. C., D. D. Sell, and K. W. Wecht, *J. Appl. Phys.* **46**, 1 (1975) 250.

Dalal, V. L., A. B. Dreeben, and A. Triano, *J. Appl. Phys.* **42**, 7 (1971) 2864–2867.

de Murcia, M., D. Gasquet, A. Elamri, J. P. Nougier, and J. Vanbremeerch, *IEEE Trans. Electron. Dev.* **ED-38**, 11 (1991) 2531–2539.

Dmitriev, A. P., M. P. Mikhailova, and I. N. Yassievich, *Phys. Status Solidi (B)* **140**, 1 (1987) 9–137.

Fauquembergue, R., J. Zimmermann, A. Kaszynski, and E. Constant, *J. Appl. Phys.* **51**, 2 (1980) 1065–1071.

Hilsum, C., *Electron. Lett.* **10**, 13 (1974) 259–260.

Joshi, R. and R. O. Grendin, *Appl. Phys. Lett.* **54**, 24 (1989) 2438–2439.

Kyuregyan, A. S. and S. N. Yurkov, *Sov. Phys. Semicond.* **23**, 10 (1989) 1126–1132.

Milnes, A. G., *Deep Impurities in Semiconductors*, John Wiley and Sons, N.Y., 1973.

Novikova, S. I., *Sov. Phys. Solid State* **3**, 1 (1961) 129.

Pearsall, T. P., F. Capasso, R. E. Nahory, M. A. Pallack, and J. Chelikowsky, *Solid State Electron.* **21**, 1 (1978) 297–302.

Phillip, H. R. and H. Ehrenreich, *Phys. Rev.* **129**, 4 (1963) 1550–1560.

Pozhela, J. and A. Reklaitis, *Solid State Electron.* **23**, 9 (1980) 927–933.

Rees, H. D., *Solid State Commun.* **7**, 2 (1969) 267–269.

Rode, D. L., *Semiconductors and Semimetals*, R. K. Willardson and A. C. Beer, eds., Academic Press, N.Y., vol. 10, 1975, p. 1.

Ruch, J. G. and G. S. Kino, *Phys. Rev.* **174**, 3 (1968) 921–931.

Shur, M., *Physics of Semiconductor Devices*, Prentice Hall, 1990.

Spitzer, W. G. and J. M. Whelan, *Phys. Rev.* **114**, 1 (1959) 59–63.

Stillman, G. E., C. M. Walfe, and J. O. Dimmock, *J. Phys. Chem. Solids* **31**, 6 (1970) 1199–1204.

Sturge, M. D., *Phys. Rev.* **127**, 3 (1962) 768.

Sze, S. M., *Physics of Semiconductor Devices*, John Wiley and Sons, N.Y., 1981.

Tiwari, S. and S. L. Wright, *Appl. Phys. Lett.* **56**, 6 (1990) 563–565.

Varshni, V. P., *Phys. Status Solidi* **19**, 2 (1967) 459–514; **20**, 1 (1967) 9–36.

Waugh, J. L. T. and G. Dolling, *Phys. Rev.* **132**, 6 (1963) 2410.

Wiley, J. D., *Semiconductor and Semimetals*, R. K. Willardson and A. C. Beer, eds., Academic Press, N.Y., vol. 10, 1975, p. 91.

CHAPTER 5

GALLIUM PHOSPHIDE (GaP)

Yu. A. Goldberg
Ioffe Institute, St. Petersburg, Russia

5.1. Basic Parameters at 300 K

Crystal structure		Zinc Blende
Group of symmetry		T_d^2–F$\bar{4}$3m
Number of atoms in 1 cm^3		4.94×10^{22}
Auger recombination coefficient	(cm^6 s^{-1})	10^{-30}
Debye temperature	(K)	445
Density	(g cm^{-3})	4.14
Dielectric constant		
static		11.1
high frequency		9.11
Effective electron masses	(in units of m_o)	
longitudinal m_l/m_o		1.12
transverse m_t/m_o		0.22
Effective hole masses	(in units of m_o)	
heavy m_h/m_o		0.79
light m_{lp}/m_o		0.14
Electron affinity	(eV)	3.8
Lattice constant	(Å)	5.4505
Optical phonon energy	(eV)	0.051

Band structure and carrier concentration

Energy gap	(eV)	2.26
Energy separation E_0 ($\Gamma_{1c} - \Gamma_{15v}$)	(eV)	2.78
Energy spin-orbital splitting	(eV)	0.08
Intrinsic carrier concentration	(cm^{-3})	2
Effective conduction band density of states	(cm^{-3})	1.8×10^{19}
Effective valence band density of states	(cm^{-3})	1.9×10^{19}

Electrical properties

Breakdown field	($V\,cm^{-1}$)	$\simeq 1 \times 10^6$
Mobility	($cm^2\,V^{-1}\,s^{-1}$)	
	electrons	≤ 250
	holes	≤ 150
Diffusion coefficient	($cm^2\,s^{-1}$)	
	electrons	≤ 6.5
	holes	≤ 4
Electron thermal velocity	($m\,s^{-1}$)	2×10^5
Hole thermal velocity	($m\,s^{-1}$)	1.3×10^5

Optical properties

Infrared refractive index	3.02
Radiative recombination coefficient ($cm^3\,s^{-1}$)	10^{-13}

Thermal and mechanical properties

Bulk modulus	($dyn\,cm^{-2}$)	8.8×10^{11}
Melting point	(°C)	1457
Specific heat	($J\,g^{-1}\,°C^{-1}$)	0.43
Thermal conductivity	($W\,cm^{-1}\,°C^{-1}$)	1.1
Thermal diffusivity	($cm^2\,s^{-1}$)	0.62
Thermal expansion, linear	($°C^{-1}$)	4.65×10^{-6}

5.2. Band Structure and Carrier Concentration

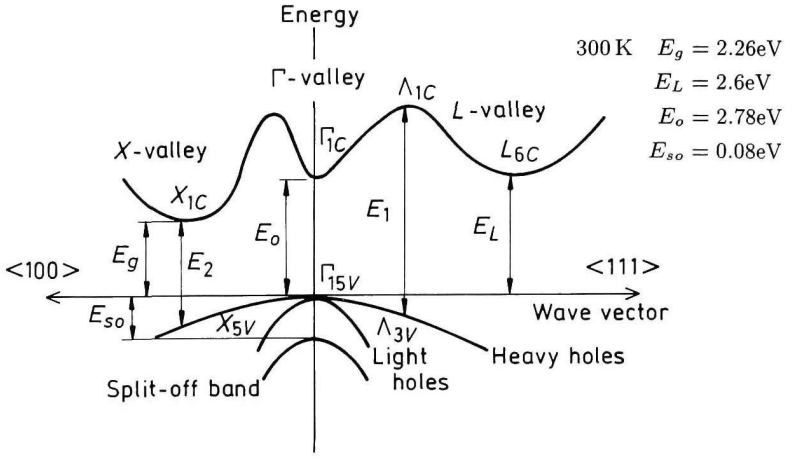

Fig. 5.2.1. Band structure of GaP. Important minima of the conduction band and maxima of the valence band.

5.2.1. *Temperature Dependences*

Temperature dependence of the energy gap (Panish and Casey [1969])

$$E_g = 2.34 - 6.2 \times 10^{-4} \frac{T^2}{T + 460} \text{ (eV)} , \tag{5.2.1}$$

where T is temperature in degrees K ($0 < T < 1200$).

Temperature dependence of the direct band gap E_o (Takizawa [1983])

$$E_o = 2.866 - 0.108[\coth(164/T) - 1] \text{ (eV)} , \tag{5.2.2}$$

($100 < T < 300$ K).

Effective density of states in the conduction band

$$N_c \simeq 3.4 \times 10^{15} \times T^{3/2} \quad (\mathrm{cm}^{-3}) \tag{5.2.3}$$

Effective density of states in the valence band

$$N_v \simeq 3.6 \times 10^{15} \times T^{3/2} \ (\mathrm{cm}^{-3}) \ . \tag{5.2.4}$$

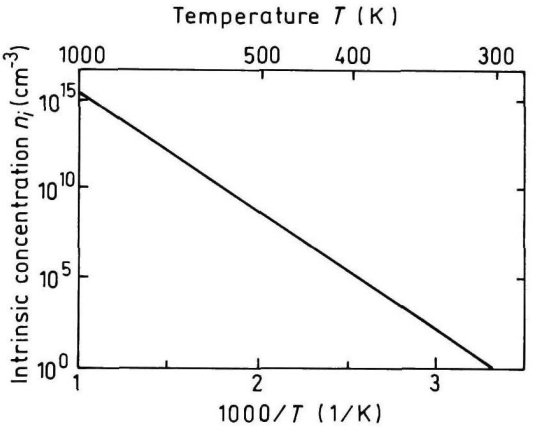

Fig. 5.2.2. The temperature dependence of the intrinsic carrier concentration.

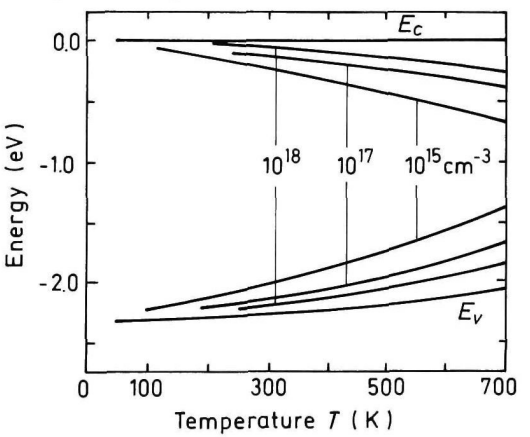

Fig. 5.2.3. Fermi level versus temperature for different concentrations of shallow donors and acceptors.

5.2.2. *Dependences on Hydrostatic Pressure* (Ves *et al.* [1985])

$$E_g = E_g(0) - 2.4 \times 10^{-3}\ P - 4.6 \times 10^{-6}\ P^2 \text{ (eV)}$$
$$E_o = E_o(0) + 9.5 \times 10^{-3}\ P - 3.4 \times 10^{-5}\ P^2 \text{ (eV)}, \tag{5.2.5}$$

where P is pressure in kbar.

5.2.3. *Energy Gap Narrowing at High Doping Levels*

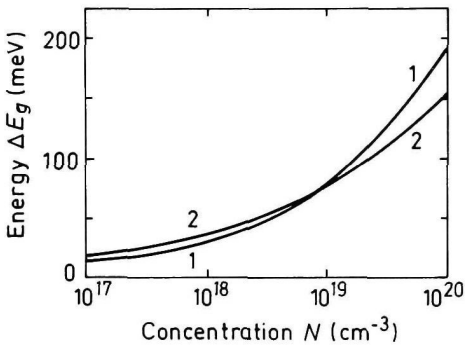

Fig. 5.2.4. Energy gap narrowing versus donor (Curve 1) and acceptor (Curve 2) doping density 300 K (Calculated according Jain *et al.* [1990]).

For n-type GaP

$$\Delta E_g = 10.7 \times 10^{-9} \times N_d^{1/3} + 3.45 \times 10^{-7} \times N_d^{1/4} + 9.97 \times 10^{-12} \times N_d^{1/2} \quad \text{(eV)}$$

For p-type GaP

$$\Delta E_g = 12.7 \times 10^{-9} \times N_a^{1/3} + 5.85 \times 10^{-7} \times N_a^{1/4} + 3.90 \times 10^{-12} \times N_a^{1/2} \quad \text{(eV)}$$

(Jain *et al.* [1990]). (5.2.6)

5.2.4. *Effective Masses*

Electrons

The surfaces of equal energy are ellipsoids (X-valley):

$$m_l = 1.12m_0$$
$$m_t = 0.22m_0$$

Effective mass of density of states

$$m_c = (9m_l m_t^2)^{1/3} = 0.79m_0$$

Effective mass of conductivity $m_{cc} = 0.35m_0$

For Γ-valley $m_\Gamma = 0.09m_0$

For L-valley $m_l = 1.2m_0$

$m_t = 0.15m_0$

Holes

heavy	$m_h = 0.79m_0$
light	$m_{lp} = 0.14m_0$
Effective mass of density of states	$m_v = 0.83m_0$

5.2.5. *Donors and Acceptors*

Ionization energies of shallow donors (eV) (Dean [1973], Kopylov and Pikhtin [1978])

S_p	0.107
Se_p	0.105
Te_p	0.093
Li_p	0.091
Ge_{Ga}	0.204
Si_{Ga}	0.085
Sn_{Ga}	0.072
Li_{Ga}	0.061

Ionization energies of shallow acceptors (eV) (Dean [1973])

Ge_p	0.265
C_p	0.0543
Si_p	0.210
Be_{Ga}	0.0566
Cd_{Ga}	0.1022
Mg_{Ga}	0.0599
Zn_{Ga}	0.0697

Most important deep levels (Dean and Henry [1968], Clerjaud *et al.* [1981])

Impurity		Position in the forbidden gap
O_p	(donor)	$E_c - 0.89$ eV
Cr	(acceptor)	$E_c - 1.2$ eV
		$E_c - 0.5$ eV

Radiative centers (Bergh and Dean [1976])

N	$E_v + 0.008$ eV
Zn_{Ga}–O_p	$E_c - 0.30$ eV

Capture cross section for electrons to neutral Zn – O complex	(at 300 K)	$\sigma_n \sim (1.5 \div 4.5) \times 10^{-16}\,\mathrm{cm}^2$
Capture cross section for holes to negative Zn – O complex	(at 77 K)	$\sigma_p \sim 5 \times 10^{-17}\,\mathrm{cm}^2$
Cd_{Ga}–O_p		$E_c - 0.40$ eV
Mg–O		$E_c - 0.14$ eV

5.3. Electrical Properties

5.3.1. *Mobility and Hall Effect*

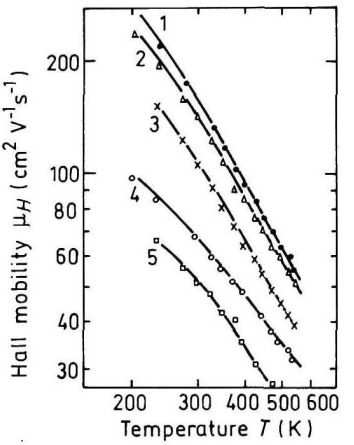

Fig. 5.3.1. Electron Hall mobility versus temperature for different donor (Sn) densities (Kao and Eknoyan [1983]). N_d (cm^{-3}):
1. 5×10^{16}, 2. 2×10^{17}, 3. 2.5×10^{18}, 4. 7.5×10^{18}, 5. 1.2×10^{19}.

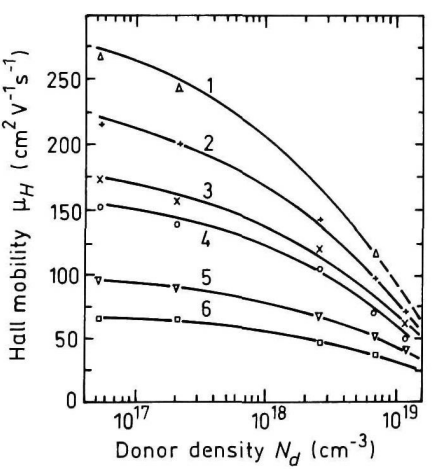

Fig. 5.3.2. Electron Hall mobility versus donor (Sn) density at different temperatures (Kao and Eknoyan [1983]). T (K): 1. 203, 2. 233, 3. 273, 4. 300, 5. 400, 6. 500.

For $T > 200$ K electron Hall mobility $\mu_{nH} \sim T^{-1.7}$

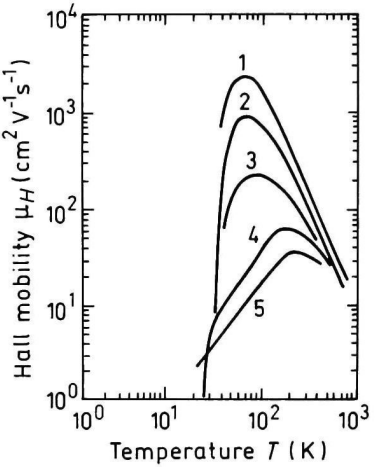

Fig. 5.3.3. Hole Hall mobility versus temperature for different acceptor (Zn) densities (Casey *et al.* [1969]). N_a (cm^{-3}):
1. 6.7×10^{16}, 2. 1.9×10^{17}, 3. 6.7×10^{17}, 4. 3.8×10^{18}, 5. 1.2×10^{19}

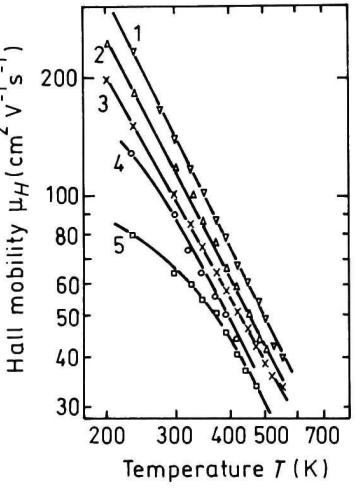

Fig. 5.3.4. Hole Hall mobility versus temperature for different acceptor (Mg) densities (Kao and Eknoyan [1983]). N_a (cm^{-3}):
1. 5×10^{16}, 2. 3×10^{17}, 3. 6×10^{17}, 4. 1×10^{18}, 5. 2×10^{18}.

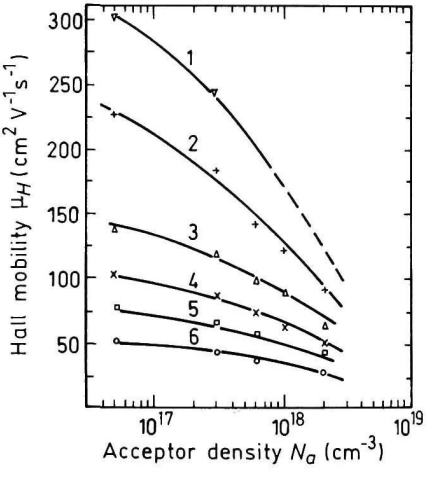

Fig. 5.3.5. Hole Hall mobility versus acceptor (Mg) density at different temperatures (Kao and Eknoyan [1983]). T (K):
1. 203, 2. 233, 3. 300, 4. 350, 5. 400, 6. 500.

For $T > 200$ K hole Hall mobility $\mu_{pH} \sim T^{-2.3}$.

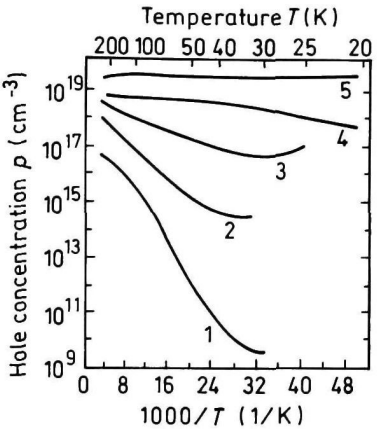

Fig. 5.3.6. Hole concentration versus temperature for different acceptor (Zn) densities (Casey *et al.* [1969]). N_a (cm^{-3}): 1. 6.7×10^{16}, 2. 6.7×10^{17}, 3. 3.8×10^{18}, 4. 1.2×10^{19}, 5. 2.1×10^{19}.

5.3.2. *Transport Properties in High Electric Field*

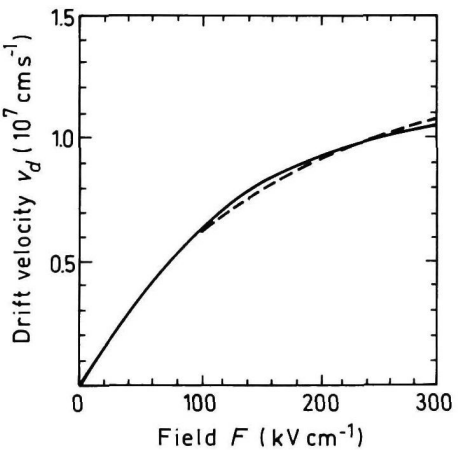

Fig. 5.3.7. Field dependences of the electron drift velocity 300 K. Solid line shows the results of the calculation. Dashed line shows the experimental results (Arora *et al.* [1987]).

Saturation electron drift velocity $v_s = 1.25 \times 10^7\,\mathrm{cm\,s^{-1}}$ (300 K) (Johnson and Eknoyan [1985]).

5.3.3. *Impact Ionization*

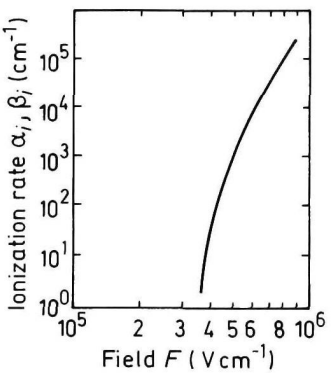

Fig. 5.3.8. The dependence of ionization rates for electrons α_i and holes β_i versus electric field, 300 K. $\alpha_i = \beta_i$ (Sze [1969]).

At 300 K for 5×10^5 V cm$^{-1} < F < 1.3 \times 10^6$ V cm^{-1}

$$\alpha_i = \beta_i = \alpha_0 \exp\left[\delta - (\delta^2 + (F_0/F)^2)^{1/2}\right] , \tag{5.3.1}$$

where $\alpha_0 = 0.39 \times 10^6$ cm^{-1}, $\delta = 19.1$, $F_o = 7.51 \times 10^6$ V cm $^{-1}$. (Kyuregyan and Yurkov [1989]).

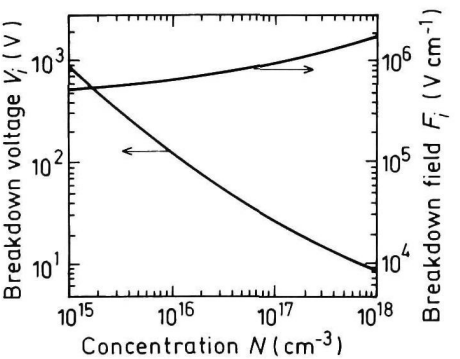

Fig. 5.3.9. Breakdown voltage and breakdown field versus doping density for an abrupt p-n junction, 300 K (Sze and Gibbons [1966]).

5.3.4. *Recombination Parameters*

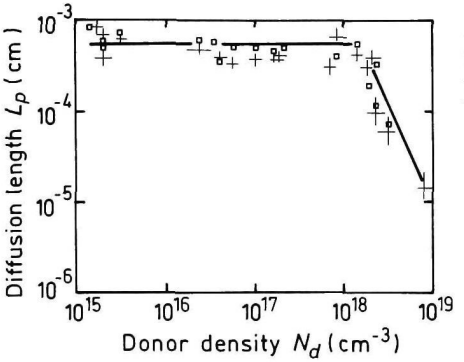

Fig. 5.3.10. Hole diffusion length L_p in n-type GaP (undoped or doped with S) versus donor density, 300 K (Young and Wight [1974]).

The longest lifetime of holes (undoped GaP)	$\tau_p \sim 1 \times 10^{-6}$ s
Diffusion length $L_p = (D_p \times \tau_p)^{1/2}$	$L \sim 20\ \mu$m

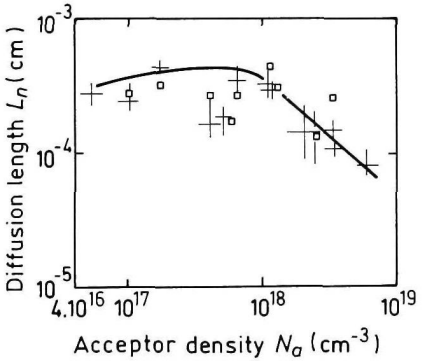

Fig. 5.3.11. Electron diffusion length L_n in p-type GaP versus acceptor (Zn) density, 300 K (Young and Wight [1974]).

The longest lifetime of electrons	$\tau_n \sim 1 \times 10^{-7}$ s
Diffusion length $L_n = (D_n \times \tau_n)^{1/2}$	$L_n \sim 7\ \mu$m

Surface recombination (Gershenzon and Mikulyak [1966]).

20 K	$(0.1 \div 3.4) \times 10^2$ cm s^{-1}
77 K	$(1.1 \div 90) \times 10^4$ cm s^{-1}
300 K	$(0.4 \div 2) \times 10^6$ cm s^{-1}

Radiative recombination

Band to band radiative
recombination coefficient $\sim 10^{-13}\text{cm}^3\,\text{s}^{-1}$

Impurity recombination (Yunovich [1972], Bergh and Dean [1976]) at 300 K

Zn–O complex (red LED, $h\nu \simeq 1.8\,\text{eV}$, $\lambda \simeq 0.7\,\mu\text{m}$)

Radiative exciton lifetime	$\sim 10^{-7}\text{s}^{-1}$
Oscillator force for exciton recombination	0.07
Non-radiative exciton lifetime	
$\tau_{xn} = 1/B \times p$	$B \simeq 10^{-10} \div 10^{-11}\,\text{cm}^{-3}\,\text{s}^{-1}$
Non-radiative single electron lifetime	
$\tau_{cn} = 1/C \times p^2$	$C \simeq 10^{-30}\,\text{cm}^6\,\text{s}^{-1}$

N–isoelectron impurity (green LED, $h\nu \simeq 2.22\,\text{eV}$, $\lambda \simeq 0.56\,\mu\text{m}$)

Radiative exiton lifetime	$\sim 3 \times 10^{-8}\text{s}$
Oscillator force for exciton recombination	0.09
Bond energy of exciton in GaP doped with N:	
free exciton	0.021 eV
NN bound exciton	0.143 eV
(Zwang *et al.* [1990])	

Auger recombination coefficient $\sim 10^{-30}\text{cm}^6\,\text{s}^{-1}$

5.4. Optical Properties

Infrared refractive index

$$n_\infty = (k_\infty)^{1/2} = 2.932 \times (1 + 10^{-4} \times T) \qquad (80 < T < 300\,\mathrm{K}) \qquad (5.4.1)$$

for 300 K, $n_\infty = 3.02$

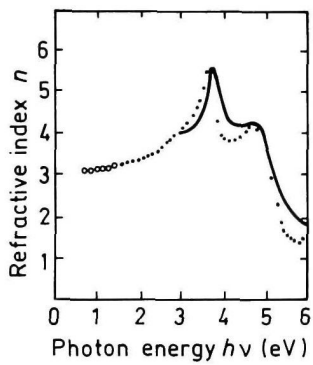

Fig. 5.4.1. Refractive index n versus photon energy. Solid curve is the theoretical calculation. Points represent experimental data, 300 K (Adachi [1989]).

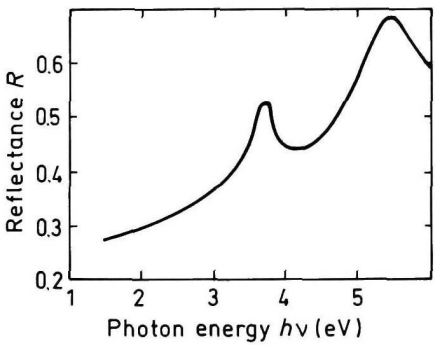

Fig. 5.4.2. Normal incidence reflectivity versus photon energy, 300 K (Aspnes and Studna [1983]).

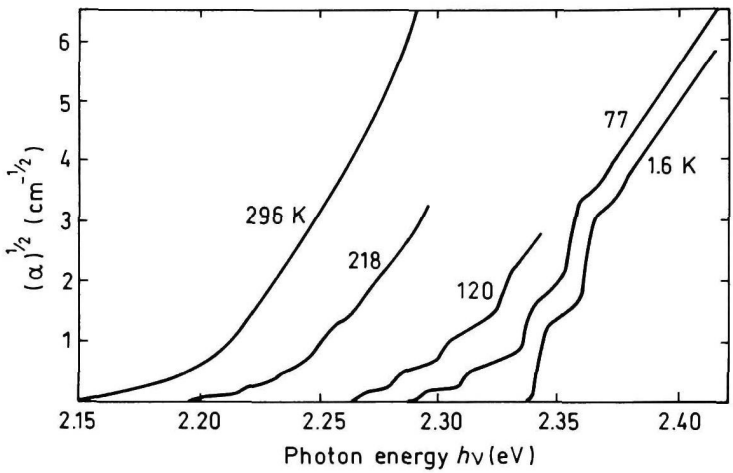

Fig. 5.4.3. Low-level absorption spectrum of n-type GaP ($n_0 = 1 \times 10^{16}\,cm^{-3}$) at different temperatures (Dean and Thomas [1966]).

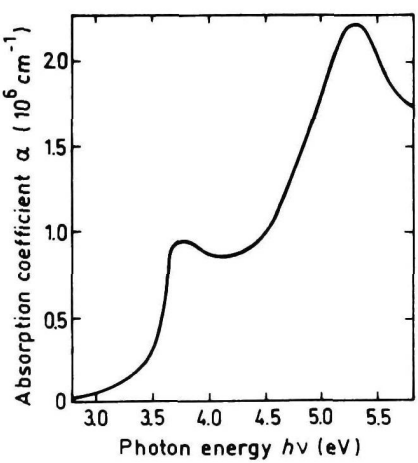

Fig. 5.4.4. The absorption coefficient versus photon energy. 300 K (Aspnes and Studna [1983]).

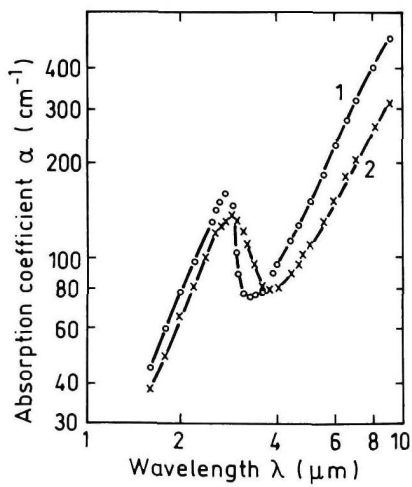

Fig. 5.4.5. Free carrier absorption coefficient versus wavelength at different temperatures. $n_0 = 1 \times 10^{18}\,cm^{-3}$ T (K): 1. 80, 2. 295. (Spitzer *et al.* [1959]). (Figure reprinted with kind permission from Elsevier Science Ltd.)

5.5. Thermal Properties

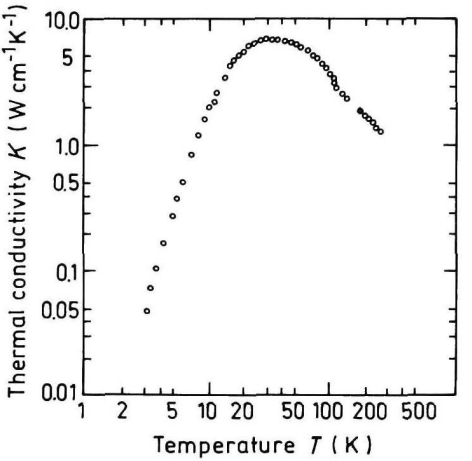

Fig. 5.5.1. Temperature dependence of thermal conductivity (Muzhdaba *et al.* [1968]).

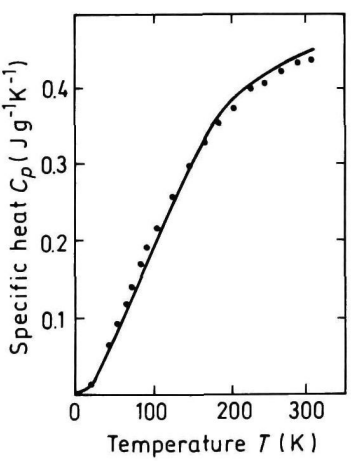

Fig. 5.5.2. Temperature dependence of specific heat (Sirota and Sidorov [1988]).

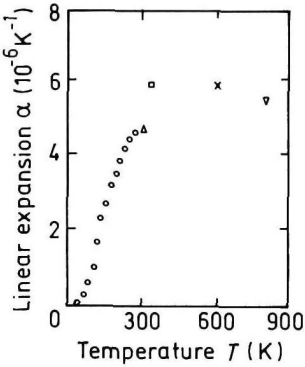

Fig. 5.5.3. Temperature dependence of linear expansion coefficient α (Deus *et al.* [1983]).

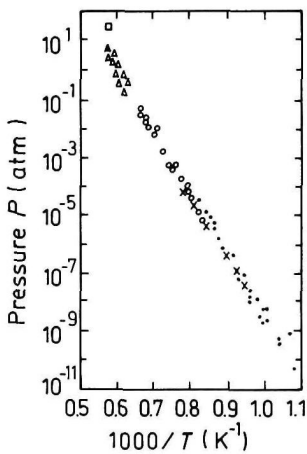

Fig. 5.5.4. Temperature dependence of equilibrium pressure of P_2 along the liquidus curve (Ilegems *et al.* [1974]).

Melting point $T_m = 1730\,\mathrm{K}$
Saturated vapor pressure at melting point 32 atm.

5.6. Mechanical Properties, Elastic Constants, Lattice Vibrations, Other Properties

Density	$4.138\ \mathrm{g\,cm^{-3}}$
Hardness on the Mohs scale	5
Surface microhardness (using Knoop's pyramid test)	$850\ \mathrm{kg\,mm^{-2}}$
Cleavage plane	{110}
Elastic constants at 300 K	
C_{11}	$14.05 \times 10^{11}\ \mathrm{dyn\,cm^{-2}}$
C_{12}	$6.20 \times 10^{11}\ \mathrm{dyn\,cm^{-2}}$
C_{44}	$7.03 \times 10^{11}\ \mathrm{dyn\,cm^{-2}}$ (Yogurtcu *et al.* [1981])

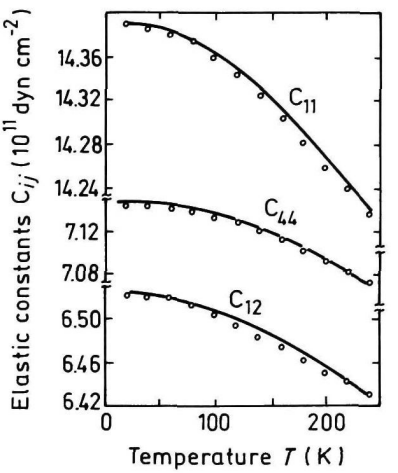

Fig. 5.6.1. Temperature dependences of elastic constants (Boyle and Sladek [1975]).

For $T = 300\ \mathrm{K}$

Bulk modulus (compressibility^{-1}) $B_s = \dfrac{C_{11} + 2C_{12}}{3}$	$B_s = 8.82 \times 10^{11}\ \mathrm{dyn\,cm^{-2}}$
Shear modulus $C' = (C_{11} - C_{12})/2$	$C' = 3.92 \times 10^{11}\ \mathrm{dyn\,cm^{-2}}$
[100] Young's modulus $Y_0 = \dfrac{(C_{11} + 2C_{12})(C_{11} - C_{12})}{(C_{11} + C_{12})}$	$Y_0 = 10.3 \times 10^{11}\ \mathrm{dyn\,cm^{-2}}$
[100] Poisson ratio $\sigma_0 = \dfrac{C_{12}}{C_{11} + C_{12}}$	$\sigma_0 = 0.31$

Acoustic Wave Speeds

Wave propagation direction	Wave character	Expression for wave speed	Wave speed (in units of $10^5\,\mathrm{cm\,s^{-1}}$)
[100]	V_L	$(C_{11}/\rho)^{1/2}$	5.83
	V_T	$(C_{44}/\rho)^{1/2}$	4.12
[110]	V_l	$[(C_{11}+C_{12}+2C_{44})/2\rho]^{1/2}$	6.43
	$V_{t\parallel}$	$V_{t\parallel}=V_T=(C_{44}/\rho)^{1/2}$	4.12
	$V_{t\perp}$	$[(C_{11}-C_{12})/2\rho]^{1/2}$	3.08
[111]	V_l'	$[(C_{11}+2C_{12}+4C_{44})/3\rho]^{1/2}$	6.63
	V_t'	$[(C_{11}-C_{12}+C_{44})/3\rho]^{1/2}$	3.46

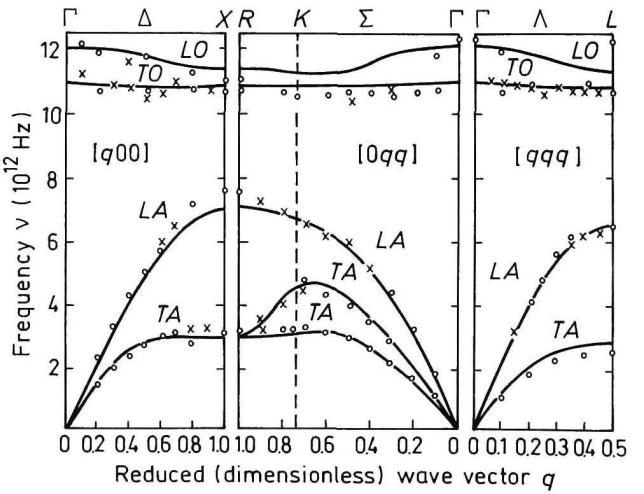

Fig. 5.6.2. Room temperature dispersion curves for acoustic and optical branch phonons. Solid lines are calculated according to overlap shell model (Borcherds *et al.* [1979]).

Phonon frequencies (in units of 10^{12} Hz). 4.2 K (Suto and Nashizawa [1990]).

$\nu_{LO}(X)$	11.3
$\nu_{TO}(X)$	10.96
$\nu_{LA}(X)$	7.65
$\nu_{TA}(X)$	3.16

Piezoelectric constant e_{14} $-0.1\,\mathrm{C\,m^{-2}}$

References

Adachi, S., *J. Appl. Phys.* **66**, 12 (1989) 6030–6040.

Arora, V. K., D. S. L. Mui, and H. Morkoc, *J. Appl. Phys.* **61**, 9 (1987) 4703–4704.

Aspnes, D. E. and A. A. Studna, *Phys. Rev.* **B27**, 2 (1983) 985–1009.

Bergh, A. A. and P. J. Dean, *Light-Emitting Diodes*, Clarendon Press, Oxford, 1976.

Borcherds, P. H., K. Kunc, G. F. Alfrey, and R. L. Hall, *J. Phys.* **C12**, 22 (1979) 4699–4706.

Boyle, W. F. and R. J. Sladek, *Phys. Rev.* **B11**, 8 (1975) 2933–2940.

Casey Jr., H. C., F. Ermanis, and K. B. Wolfstirn, *J. Appl. Phys.* **40**, 7 (1969) 2945–2958.

Clerjaud, B., F. Gendron, and C. Porte, *Appl. Phys. Lett.* **38**, 4 (1981) 212–214.

Dean, P. J., *Progress in Solid-State Chemistry*, J. O. McCaldin and G. Somorjaj, eds., vol. 8, part 1, New York, 1973.

Dean, P. J. and C. H. Henry, *Phys. Rev.* **176**, 3 (1968) 928–937.

Dean, P. J. and D. G. Thomas, *Phys. Rev.* **150**, 2 (1966) 690–703.

Deus, P., U. Voland, and H. A. Schneider, *Phys. Status Solidi (A)* **80**, 1 (1983) K29–K32.

Gershenzon, M. and R. M. Mikulyak, *Appl. Phys. Lett.* **8**, 10 (1966) 245–247.

Ilegems, M., M. B. Panish, and J. R. Arthur, *J. Chem. Thermodyn.* **6** (1974) 157.

Jain, S. C., J. M. McGregor, and D. J. Roulston, *J. Appl. Phys.* **68**, 7 (1990) 3747–3749.

Johnson, R. H. and O. Eknoyan, *J. Appl. Phys.* **58**, 3 (1985) 1402–1403.

Kao, Y. C. and O. Eknoyan, *J. Appl. Phys.* **54**, 5 (1983) 2468–2471.

Kopylov, A. A. and A. N. Pikhtin, *Solid State Commun.* **26**, 11 (1978) 735–740.

Kyuregyan, A. S. and S. N. Yurkov, *Sov. Phys. Semicond.* **23**, 10 (1989) 1126–1132.

Muzhdaba, V. M., A. Ya. Nashelskii, P. V. Tamarin, and S. S. Shalyt, *Sov. Phys. Solid State* **10**, 9 (1968) 2265–2267.

Panish, H. B. and H. C. Casey, *J. Appl. Phys.* **40**, 1 (1969) 163–167.

Sirota, N. N. and A. A. Sidorov, *Doklady Akademii Nauk SSSR* (*Soviet Physics Doklady*) **303**, 5 (1988) 1123–1126.

Spitzer, W. G., M. Gershenzon, C. J. Frosch, and D. F. Gibbs, *J. Phys. Chem. Solids* **11**, 3/4 (1959) 339–341.

Suto, K. and J. Nishizawa, *J. Appl. Phys.* **67**, 1 (1990) 459–464.

Sze, S. M. and G. Gibbons, *Appl. Phys. Lett.* **8**, 5 (1966) 111-113.

Sze, S. M., *Physics of Semiconductor Devices*, Wiley-Interscience, N.Y., 1969.

Takizawa, T., *J. Phys. Soc. Jpn.* **52**, 3 (1983) 1057–1063.

Ves, S., K. Strossner, C. K. Kim, and M. Cardona, *Solid State Commun.* **55**, 4 (1985) 327–331.

Yogurtcu, Y. K., A. J. Miller, and G. A. Saunders, *J. Phys. Chem. Solids* **42**, 1 (1981) 49–56.

Young, M. L. and D. R. Wight, *J. Phys.* **D7**, 13 (1974) 1824–1837.

Yunovich, A. E., Radiative recombination and optical properties of GaP, in *Radiative Recombination in Semiconductors*, ed., Ya. E., Pokrovskii, Moscow, 1972, (in Russian).

Zhang, X., K. Dou, Q. Hong, and M. Balkanski, *Phys. Rev.* **B41**, 3 (1990) 1376–1385.

CHAPTER 6

GALLIUM ANTIMONIDE (GaSb)

A. Ya. Vul'
Ioffe Institute,
St. Petersburg, Russia

6.1. Basic Parameters at 300 K

Crystal structure		Zinc Blende
Group of symmetry		T_d^2–F$\bar{4}$3m
Number of atoms in 1 cm^3		3.53×10^{22}
Debye temperature	(K)	266
Density	(g cm^{-3})	5.61
Dielectric constant		
static		15.7
high frequency		14.4
Effective electron mass	(in units of m_o)	0.041
Effective hole masses	(in units of m_o)	
heavy		0.4
light		0.05
Electron affinity	(eV)	4.06
Lattice constant	(Å)	6.09593
Optical phonon energy	(eV)	0.0297

Band structure and carrier concentration

Energy gap	(eV)	0.726
Energy separation ($E_{\Gamma L}$)		
between Γ and L valleys	(eV)	0.084

Energy separation ($E_{\Gamma X}$) between Γ and X valleys	(eV)	0.31
Energy spin-orbital splitting	(eV)	0.80
Intrinsic carrier concentration	(cm^{-3})	1.5×10^{12}
Intrinsic resistivity	($\Omega \times cm$)	10^3
Effective conduction band density of states	(cm^{-3})	2.1×10^{17}
Effective valence band density of states	(cm^{-3})	1.8×10^{19}

Electrical properties

Breakdown field	($V\,cm^{-1}$)	$\sim 5 \times 10^4$
Mobility	($cm^2\,V^{-1}\,s^{-1}$)	
electrons		≤ 3000
holes		≤ 1000
Diffusion coefficient	($cm^2\,s^{-1}$)	
electrons		≤ 75
holes		≤ 25
Electron thermal velocity	($m\,s^{-1}$)	5.8×10^5
Hole thermal velocity	($m\,s^{-1}$)	2.1×10^5

Optical properties

Index of refraction	3.8
Radiative recombination coefficient ($cm^3\,s^{-1}$)	$\sim 10^{-10}$

Thermal and mechanical properties

Bulk modulus	($dyn\,cm^{-2}$)	5.63×10^{11}
Melting point	(°C)	712
Specific heat	($J\,g^{-1}\,°C^{-1}$)	0.25
Thermal conductivity	($W\,cm^{-1}\,°C^{-1}$)	0.32
Thermal diffusivity	($cm^2\,s^{-1}$)	0.23
Thermal expansion, linear	($°C^{-1}$)	7.75×10^{-6}

6.2. Band Structure and Carrier Concentration

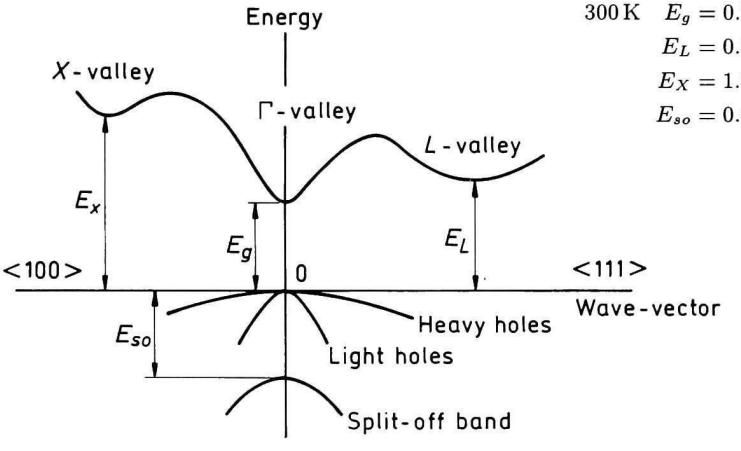

Fig. 6.2.1. Band structure of GaSb. Important minima of the conduction band and maxima of the valence band.

6.2.1. *Temperature Dependences*

Temperature dependence of the energy gap (Wu and Chen [1992])

$$E_g = 0.813 - 3.78 \times 10^{-4} \frac{T^2}{T + 94} \text{ (eV)} , \tag{6.2.1}$$

where T is temperature in degrees K ($0 < T < 300$).

Temperature dependence of energy E_L

$$E_L = 0.902 - 3.97 \times 10^{-4} \frac{T^2}{T + 94} \text{ (eV)} . \tag{6.2.2}$$

Temperature dependence of energy E_X

$$E_X = 1.142 - 4.75 \times 10^{-4} \frac{T^2}{T + 94} \text{ (eV)} \tag{6.2.3}$$

where T is temperature in degrees K (Lee and Woolley [1981]).

Effective density of states in the conduction band

$$N_c = 4.0 \times 10^{13} \times T^{3/2} \ (\mathrm{cm}^{-3}) \tag{6.2.4}$$

Effective density of states in the valence band

$$N_v = 3.5 \times 10^{15} \times T^{3/2} \ (\mathrm{cm}^{-3}) \ . \tag{6.2.5}$$

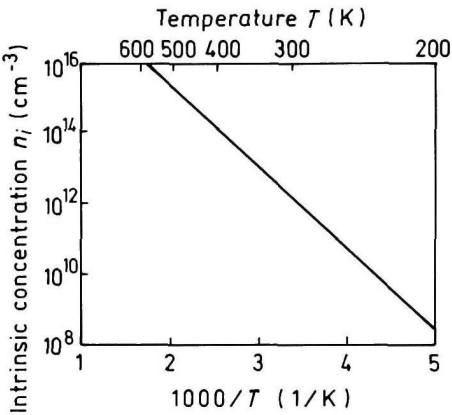

Fig. 6.2.2. The temperature dependence of the intrinsic carrier concentration.

6.2.2. *Dependences on Hydrostatic Pressure*

$$\begin{aligned} E_g &= E_g(0) + 14.5 \times 10^{-3} \ P \ (\mathrm{eV}) \\ E_L &= E_L(0) + 5.0 \times 10^{-3} \ P \ (\mathrm{eV}) \\ E_X &= E_X(0) - 1.5 \times 10^{-3} \ P \ (\mathrm{eV}) \end{aligned} \tag{6.2.6}$$

where P is pressure in kbar.

6.2.3. *Energy Gap Narrowing at High Doping Levels*

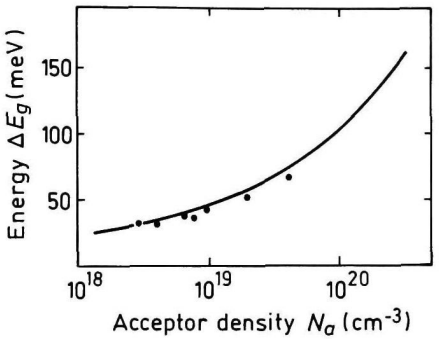

Fig. 6.2.3. Energy gap narrowing versus acceptor doping density. Curve is calculated for p-GaSb according to Eq. (6.2.7). Experimental points are taken from Titkov *et al.* [1981] (Jain *et al.* [1990]).

For n-type GaSb

$$\Delta E_g = 13.6 \times 10^{-9} \times N_d^{1/3} + 1.66 \times 10^{-7} \times N_d^{1/4} + 119 \times 10^{-12} \times N_d^{1/2} \text{ (eV)}$$

For p-type GaSb

$$\Delta E_g = 8.07 \times 10^{-9} \times N_a^{1/3} + 2.80 \times 10^{-7} \times N_a^{1/4} + 4.12 \times 10^{-12} \times N_a^{1/2} \text{ (eV)}$$

(Jain *et al.* [1990]). (6.2.7)

6.2.4. *Effective Masses*

Electrons

For Γ-valley $m_\Gamma = 0.041 m_0$

In the L-valley the surfaces of equal energy are ellipsoids.

$$m_l = 0.95 m_0$$
$$m_t = 0.11 m_0$$

Effective mass of density of states

$$m_L = (16 m_l m_t^2)^{1/3} = 0.57 m_0$$

In the X-valley the surfaces of equal energy are ellipsoids.

$$m_l = 1.51m_0$$
$$m_t = 0.22m_0$$

Effective mass of density of states

$$m_x = (9m_l m_t^2)^{1/3} = 0.87m_0$$

Holes

heavy	$m_h = 0.4m_0$
light	$m_l = 0.05m_0$
Split-off band	$m_{so} = 0.14m_0$
Effective mass of density of states	$m_v = 0.8m_0$
Effective mass of conductivity (Heller and Hamerly [1985])	$m_{vc} = 0.3m_0$

6.2.5. *Donors and Acceptors*

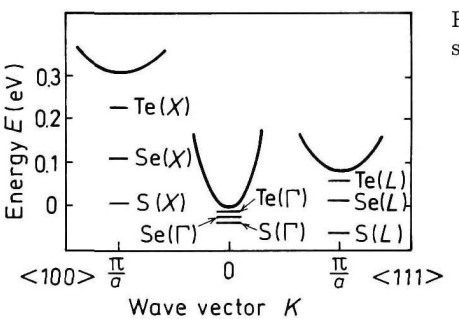

Fig. 6.2.4. The diagram of VI group donor states (Vul' *et al.* [1970]).

Ionization energies of shallow donors (eV)

Te(L)	~ 0.02
Te(X)	≤ 0.08
Se(L)	~ 0.05
Se(X)	~ 0.23
S(L)	~ 0.15
S(X)	~ 0.30

For typical donor concentrations $N_d \geq 10^{17}\,\mathrm{cm}^{-3}$ the shallow donor states connected with Γ-valley did not appear.

Ionization energies of shallow acceptors (eV).
The dominant acceptor of undoped GaSb seems to be a native defect. This acceptor is doubly ionizable

E_{a1}	0.03 eV
E_{a2}	0.1 eV
Si	~ 0.01
Ge	~ 0.009
Zn	~ 0.037

6.3. Electrical Properties

6.3.1. *Mobility and Hall Effect*

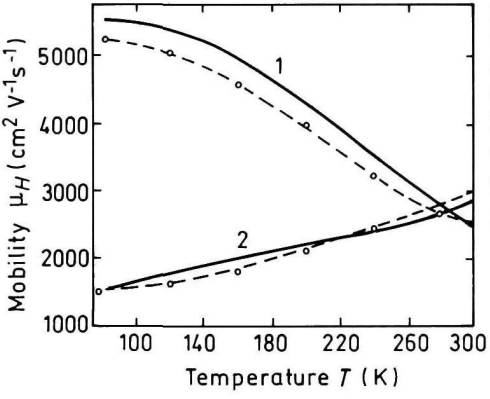

Fig. 6.3.1. Electron Hall mobility versus temperature for different doping levels. Curves 1. $N_d = 1.7 \times 10^{18}$ cm^{-3}, Curves 2. $N_d = 2.8 \times 10^{17}$ cm^{-3}. Broken curves represent the experimental data. Continuous curves represent theoretical calculations. (Mathur and Jain [1979]).

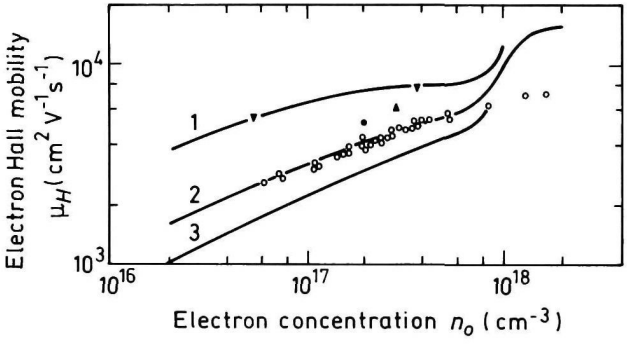

Fig. 6.3.2. Electron Hall mobility versus electron concentration. 77 K. Open circles represent measurements with a group of samples having approximately the same residual acceptor concentrations N_a. Full symbols: specimens with lower residual acceptor concentrations. Solid lines represent the theoretical calculations for different values of compensating acceptor densities — either singly (N_a^-) or doubly (N_a^{--}) ionized.

1. $N_a^- = 1.2 \times 10^{17}$ or $N_a^{--} = 0.4 \times 10^{17}$ cm^{-3}
2. $N_a^- = 2.85 \times 10^{17}$ or $N_a^{--} = 0.95 \times 10^{17}$ cm^{-3}
3. $N_a^- = 4.5 \times 10^{17}$ or $N_a^{--} = 1.5 \times 10^{17}$ cm^{-3} (Baxter *et al.* [1967]).

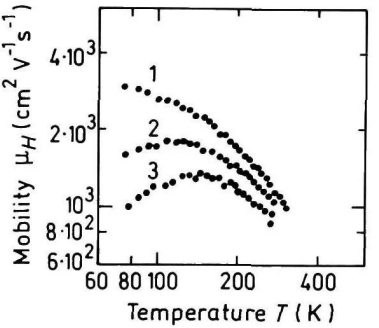

Fig. 6.3.3. Hole Hall mobility versus temperature at different compensation levels. 1. $N_a = 1.39 \times 10^{17}\,\mathrm{cm}^{-3}$; $N_d = 9 \times 10^{15}\,\mathrm{cm}^{-3}$, 2. $N_a = 1.3 \times 10^{17}\,\mathrm{cm}^{-3}$; $N_d = 9.5 \times 10^{16}\,\mathrm{cm}^{-3}$, 3. $N_a = 1.1 \times 10^{17}\,\mathrm{cm}^{-3}$; $N_d = 9.5 \times 10^{16}\,\mathrm{cm}^{-3}$ (Nakashima [1981]).

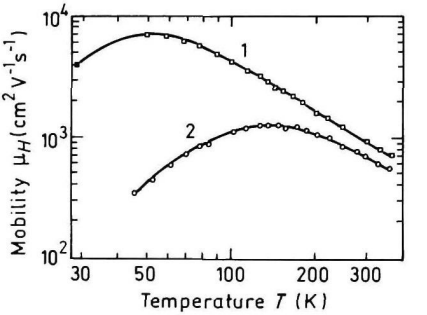

Fig. 6.3.4. Hole Hall mobility versus temperature. MBE technique. Carrier concentration p_0 at 300 K: 1. $2.28 \times 10^{16}\,\mathrm{cm}^{-3}$, 2. $1.9 \times 10^{16}\,\mathrm{cm}^{-3}$ (Johnson *et al.* [1988]).

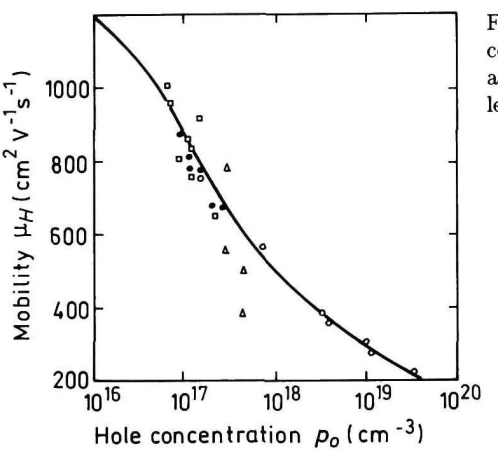

Fig. 6.3.5. Hole Hall mobility versus hole concentration. 300 K. Experimental data are taken from five different papers (Wiley [1975]).

6.3.2. *Transport Properties in High Electric Field*

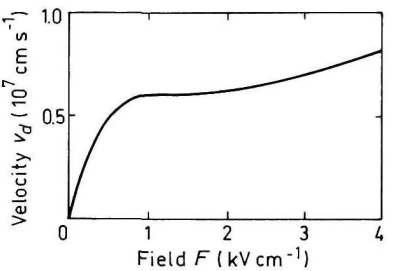

Fig. 6.3.6. Calculated field dependence of the electron drift velocity, 300 K (Ikoma *et al.* [1977]).

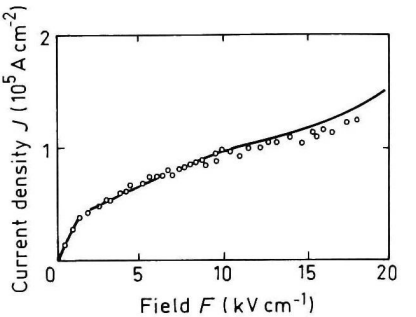

Fig. 6.3.7. Calculated (solid) and experimental (points) current density dependencies versus the electric field, 300 K (Jantsch and Heinrich [1971]).

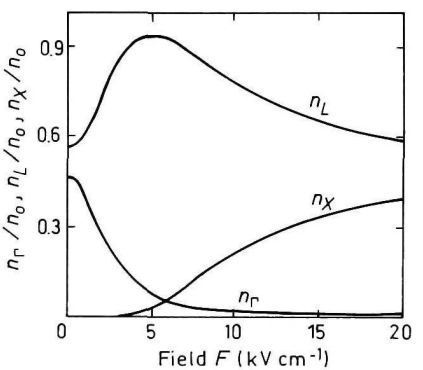

Fig. 6.3.8. Fraction of electrons in Γ, L, X valleys n_Γ, n_L, n_X as a function of electric field, 300 K. $n = 6.8 \times 10^{16}$ cm^{-3} (Jantsch and Heinrich [1971]).

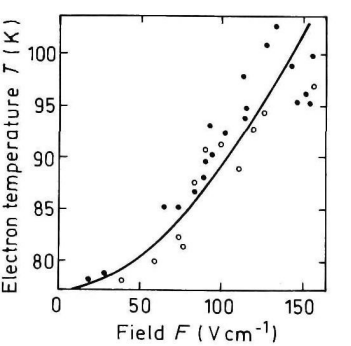

Fig. 6.3.9. Experimental (full and open circles) and calculated results of the electron temperature as a function of the electric field, 77 K (Jantsch and Heinrich [1971]).

6.3.3. *Impact Ionization*

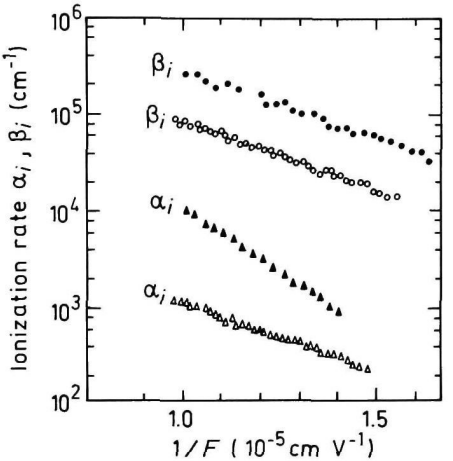

Fig. 6.3.10. Dependences of ionization rates for electrons α_i and holes β_i versus $1/F$ for two orientations of electric field, 77 K. Open symbols: $F||(111)$; Filled symbols: $F||(100)$ (Zhingarev *et al.* [1981]).

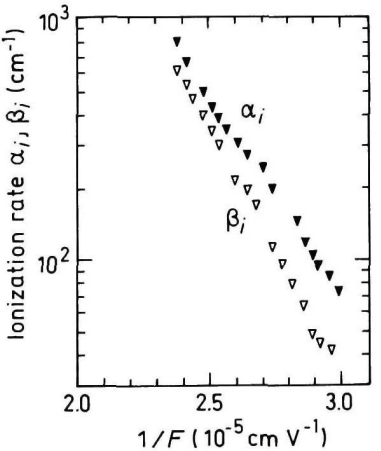

Fig. 6.3.11. Experimental curves α_i and β_i versus $1/F$ 300 K, $F||(100)$ (Hildebrand *et al.* [1980]).

6.3.4. *Recombination Parameters*

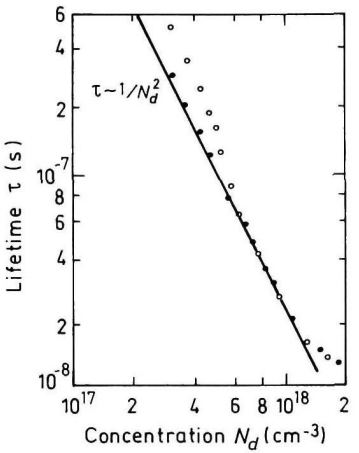

Fig. 6.3.12. Radiative lifetime versus donor concentration, 77 K, GaSb(Te). To extract these dependences from experimental data the values of internal quantum efficiency η were taken: open circles $\eta = 0.8$, filled circles $\eta = 1$ (Agaev *et al.* [1984]).

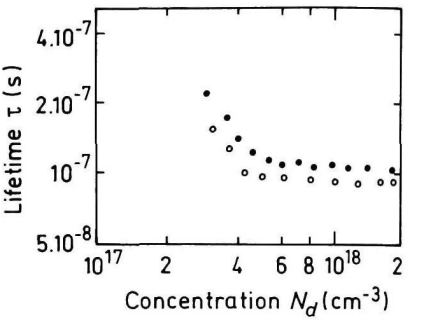

Fig. 6.3.13. Nonradiative lifetime versus donor concentrations, 77 K, GaSb(Te). Open circles: $\eta = 0.8$, filled circles $\eta = 1$ (Agaev *et al.* [1984]).

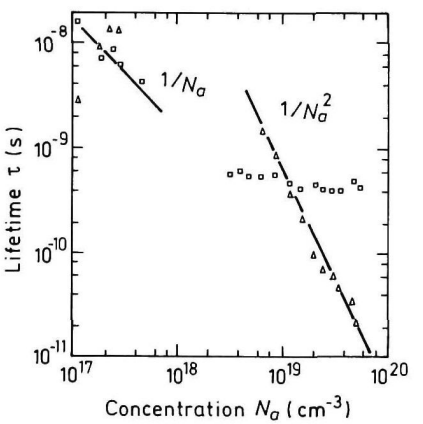

Fig. 6.3.14. Electron radiative (triangles) and nonradiative (squares) lifetime versus acceptor concentration, *p*-GaSb, 77 K, (Titkov *et al.* [1986]).

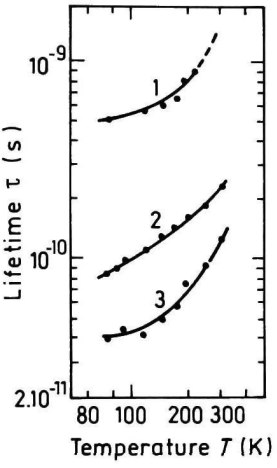

Fig. 6.3.15. Electron lifetime versus temperature at different acceptor concentrations, N_a cm^{-3}: 1. 5×10^{18}, 2. 2.2×10^{19}, 3. 3.5×10^{19} (Titkov *et al.* [1986]).

Radiative recombination coefficient	$\sim 10^{-10}$ cm^3 s^{-1}
Auger coefficient	
77 K	2×10^{-29} cm^6 s^{-1}
300 K	5×10^{-30} cm^6 s^{-1}

6.4. Optical Properties

Infrared refractive index

$$n_\infty = (k_\infty)^{1/2} \simeq 3.71 \times (1 + 8.25 \times 10^{-5} T) \tag{6.4.1}$$

For 300 K: $n_\infty \simeq 3.8$.

Long-wave TO phonon energy $h\nu_{TO} = 27.78$ meV (300 K).
Long-wave LO phonon energy $h\nu_{LO} = 28.89$ meV (300 K).

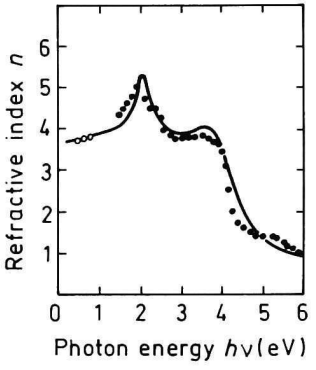

Fig. 6.4.1. Refractive index n versus photon energy, 300 K (Adachi [1989]).

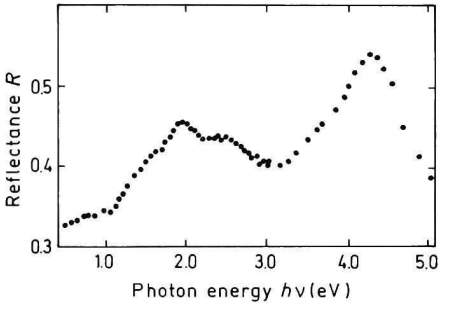

Fig. 6.4.2. Reflectivity versus photon energy, 300 K (Cardona [1961]).

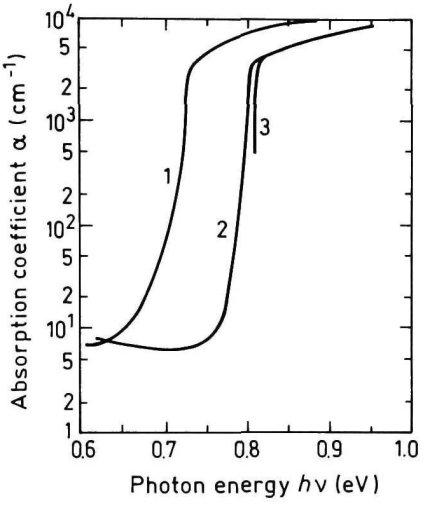

Fig. 6.4.3. Intrinsic absorption coefficient near the intrinsic absorption edge in pure p-type samples. T(K): 1. 300, 2. 77, 3. 4.2 (Becker *et al.* [1961]).

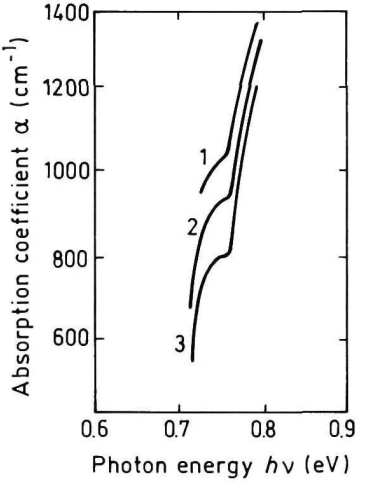

Fig. 6.4.4. Intrinsic absorption edge in p-type GaSb. $N_a = 3 \times 10^{19}\,\mathrm{cm}^{-3}$, T(K): 1. 215, 2. 140, 3. 77 (Iluridze *et al.* [1987]).

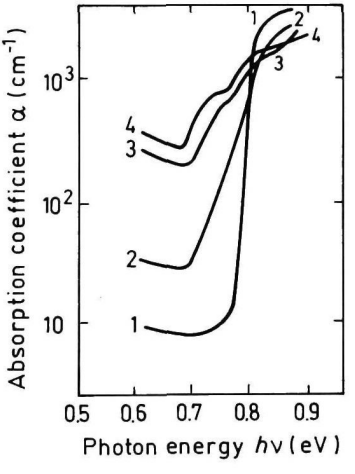

Fig. 6.4.5. Intrinsic absorption edge at 77 K for different doping levels, p-GaSb. $N_a(\mathrm{cm}^{-3})$:, 1. 2.9×10^{17}, 2. 5×10^{18}, 3. 1.8×10^{19}, 4. 3×10^{19} (Iluridze *et al.* [1987]).

A ground state Rydberg energy $R_{X1} = 2.8\,\mathrm{meV}$.

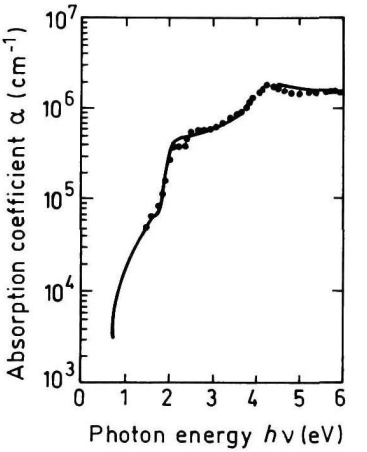

Fig. 6.4.6. The absorption coefficient versus photon energy, 300 K (Adachi [1989]).

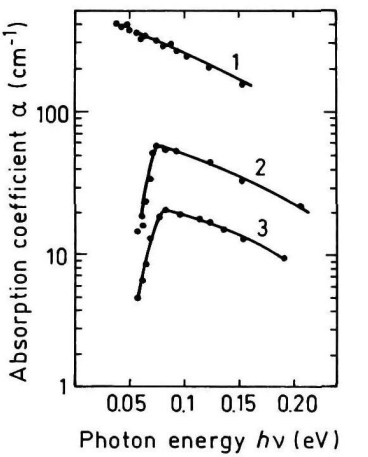

Fig. 6.4.7. The impurity absorption at low photon energies, 80 K
1. Undoped sample ($p = 2.4 \times 10^{17}\,\mathrm{cm}^{-3}$ at 300 K),
2. Te added ($p = 7.5 \times 10^{16}\,\mathrm{cm}^{-3}$),
3. Se added ($p = 4.1 \times 10^{16}\,\mathrm{cm}^{-3}$) (Johnson and Fan [1965]).

6.5. Thermal Properties

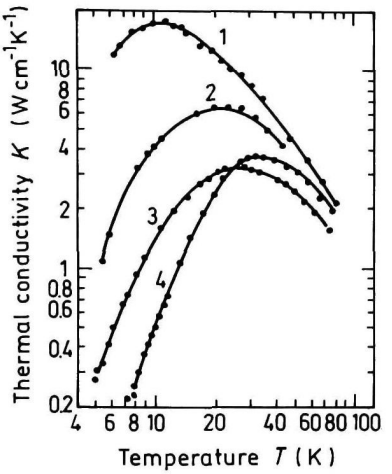

Fig. 6.5.1. Temperature dependences of thermal conductivity.
1, 2, 3 – are n-type samples,
n (300 K) cm^{-3}:
1. 1.6×10^{17}, 2. 8.6×10^{17}, 3. 1.8×10^{18},
4. p-type sample. Undoped GaSb,
p (300 K), cm^{-3} – 1.4×10^{17} (Poujade and Albany [1969]).

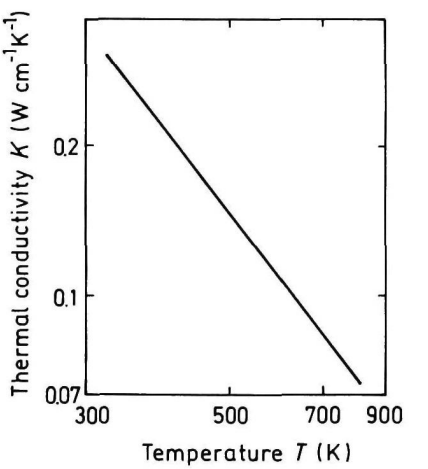

Fig. 6.5.2. Temperature dependence of thermal conductivity (for high temperatures) (Okhotin *et al.* [1972]).

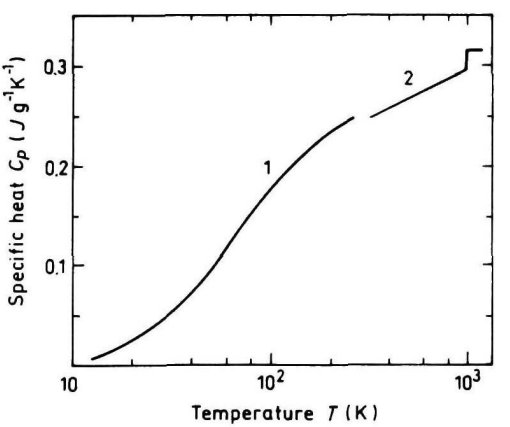

Fig. 6.5.3. Temperature dependence of specific heat
1. Piesbergen [1963],
2. Okhotin *et al.* [1972].

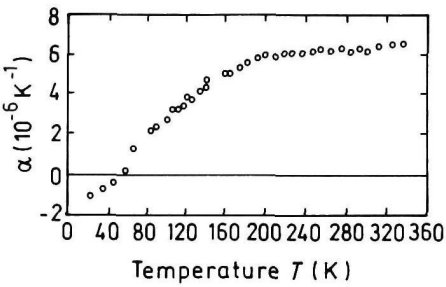

Fig. 6.5.4. Temperature dependence of linear expansion coefficient α (Novikova and Abrikosov [1963]).

Melting point $T_m = 985\,\mathrm{K}$.

6.6. Mechanical Properties, Elastic Constants, Lattice Vibrations, Other Properties

Density		$5.614\ \mathrm{g\,cm^{-3}}$
Hardness		4.5 on the Mohs scale
Surface microhardness (using Knoop's pyramid test)		$450\ \mathrm{kg\,mm^{-2}}$
Cleavage plane		{110}
Elastic constants at 300 K	C_{11}	$8.83 \times 10^{11}\ \mathrm{dyn\,cm^{-2}}$
	C_{12}	$4.02 \times 10^{11}\ \mathrm{dyn\,cm^{-2}}$
	C_{44}	$4.32 \times 10^{11}\ \mathrm{dyn\,cm^{-2}}$

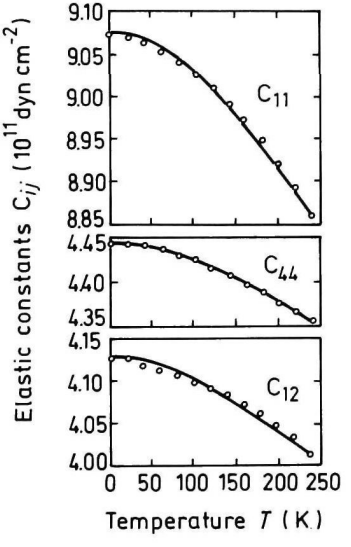

Fig. 6.6.1. Temperature dependences of elastic constants (Boyle and Sladek [1975]).

For $T = 300\,\mathrm{K}$
Bulk modulus (compressibility^{-1})

$$B_s = \frac{C_{11} + 2C_{12}}{3} \qquad B_s = 5.62 \times 10^{11}\,\mathrm{dyn\,cm^{-2}}$$

Shear modulus

$$C' = (C_{11} - C_{12})/2 \qquad C' = 2.4 \times 10^{11}\,\mathrm{dyn\,cm^{-2}}$$

[100] Young's modulus

$$Y_0 = \frac{(C_{11} + 2C_{12})(C_{11} - C_{12})}{(C_{11} + C_{12})} \qquad Y_0 = 6.31 \times 10^{11}\,\mathrm{dyn\,cm^{-2}}$$

[100] Poisson ratio

$$\sigma_0 = \frac{C_{12}}{C_{11} + C_{12}} \qquad \sigma_0 = 0.31$$

Acoustic Wave Speeds

Wave propagation direction	Wave character	Expression for wave speed	Wave speed (in units of $10^5\,\mathrm{cm\,s^{-1}}$)
[100]	V_L	$(C_{11}/\rho)^{1/2}$	3.97
	V_T	$(C_{44}/\rho)^{1/2}$	2.77
[110]	V_l	$[(C_{11} + C_{12} + 2C_{44})/2\rho]^{1/2}$	4.38
	$V_{t\parallel}$	$V_{t\parallel} = V_T = (C_{44}/\rho)^{1/2}$	2.77
	$V_{t\perp}$	$[(C_{11} - C_{12})/2\rho]^{1/2}$	2.07
[111]	V_l'	$[(C_{11} + 2C_{12} + 4C_{44})/3\rho]^{1/2}$	4.50
	V_t'	$[(C_{11} - C_{12} + C_{44})/3\rho]^{1/2}$	2.33

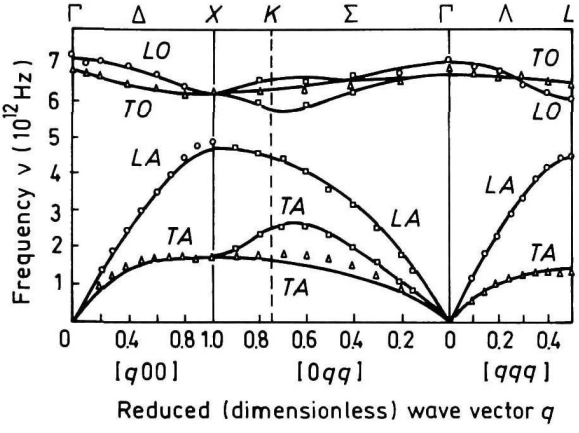

Fig. 6.6.2. Room temperature dispersion curves for acoustic and optical branch phonons. Solid lines are calculated according to 14 parameter shell model. Symbols: Experimental results from inelastic neutron scattering (Farr *et al.* [1975]).

Phonon frequencies (in units of 10^{12} Hz)

$\nu_{TO}(\Gamma_{15})$	6.87	$\nu_{TA}(L_3)$	1.37
$\nu_{TA}(X_5)$	1.70	$\nu_{LA}(L_1)$	4.60
$\nu_{LA}(X_3)$	4.99	$\nu_{LO}(L_1)$	6.15
$\nu_{TO}(X_5)$	6.36	$\nu_{TO}(L_3)$	6.48
$\nu_{LO}(X_1)$	6.35		

Piezoelectric constant e_{14} $-0.13\,\mathrm{C\,m^{-2}}$.

References

Adachi, S., *J. Appl. Phys.* **66**, 12 (1989) 6030–6040.

Agaev, V. V., A. N. Titkov, and E. I. Chaykina, *Sov. Phys. Semicond.* **18**, 4 (1984) 468.

Baxter, R. D., F. J. Reid, and A. C. Reer, *Phys. Rev.* **162**, 3 (1967) 718–727.

Becker, W. M., A. K. Randas, and H. Y. Fan, *J. Appl. Phys.* **32** (Suppl.), 10 (1961) 2094–2102.

Boyle, W. F. and R. J. Sladek, *Phys. Rev.* **B11**, 8 (1975) 2933–2940.

Cardona, M., *Zeitschrift fur Physik* **161**, 1 (1961) 99–102.

Farr, M. K., J. G. Taylor, and S. K. Sinha, *Phys. Rev.* **B11**, 4 (1975) 1587–1594.

Heinrich, H. and W. Jantsch, *Phys. Rev.* **B4**, 8 (1971) 2504–2508.

Heller, M. W. and R. G. Hamerly, *J. Appl. Phys.* **57**, 10 (1985) 4626–4632.

Hildebrand, O., W. Kuebart, and M. H. Pilkuhn, *Appl. Phys. Lett.* **37**, 9 (1980) 801–803.

Ikoma, T., K. Sasaki, Y. Adachi, and H. Yanai, *Jpn. J. Appl. Phys.* **16**, 8 (1977) 1379–1387.

Iluridze, G. N., A. N. Titkov, and E. I. Chaykina, *Sov. Phys. Semicond.* **21**, 1 (1987) 47–50.

Jain, S. L., J. M. McGregor, and D. J. Roulston, *J. Appl. Phys.* **68**, 7 (1990) 3747–3749.

Jantsch, W. and H. Heinrich, *Phys. Rev.* **B3**, 2 (1971) 420–426.

Johnson, E. J. and H. Y. Fan, *Phys. Rev.* **139**, 6A (1965) A1991–A2001.

Johnson, G. R., B. C. Cavenett, and T. M. Kerr, *Semicond. Sci. Technol.* **3**, (1988) 1157–1165.

Lee, H. J. and J. C. Woolley, *Can. J. Phys.* **59**, 12 (1981) 1844–1850.

Mathur, P. C. and S. Jain, *Phys. Rev.* **B19**, 6 (1979) 3159–3166.

Nakashima, K., *Jpn. J. Appl. Phys.* **20**, 6 (1981) 1085–1094.

Novikova, S. I. and N. Kh. Abrikosov, *Sov. Phys. Solid State* **5** (1963) 1558.

Okhotin, A. S., A. S. Pushkarskii, and V. V. Gorbachev, *Thermophysical Properties of Semiconductors*, "Atom" Publ. House, Moscow, 1972, (in Russian).

Piesbergen, V., *Zeitschrift fur Naturforschung* **18a**, 2 (1963) 141–147.

Poudjade, A. M. and H. J. Albany, *Phys. Rev.* **182**, 3 (1969) 802–807.

Titkov, A. N., E. I. Chaykina, E. M. Komova, and N. G. Ermakova, *Sov. Phys. Semicond.* **15**, 2 (1981) 198–202.

Titkov, A. N., E. N. Iluridze, I. F. Mironov, and V. A. Chaban, *Sov. Phys. Semicond.* **20**, 1 (1986) 16–21.

Vul', A. Ya., G. I. Bir, and Yu. V. Shmartsev, *Sov. Phys. Semicond.* **4**, 12 (1970) 2005–2016.

Wiley, J. D., *Semiconductors and Semimetals*, R. K. Willardson and A. C. Beer, eds., Academic Press, N.Y., vol. 10, 1975, p. 91.

Wu, M. C. and C. C. Chen, *J. Appl. Phys.* **72**, 9 (1992) 4275–4280.

Zhingarev, M. Z., V. I. Korolkov, M. P. Mikhailova, and V. V. Sazonov, *Sov. Tech. Phys. Lett.* **7**, 12 (1981) 637–638.

CHAPTER 7

INDIUM ARSENIDE (InAs)

Maya P. Mikhailova
Ioffe Institute,
St. Petersburg, Russia

7.1. Basic Parameters at 300 K

Crystal structure		Zinc Blende
Group of symmetry		T_d^2–F$\bar{4}$3m
Number of atoms in 1 cm^3		3.59×10^{22}
de Broglie electron wavelength (Å)		400
Debye temperature	(K)	280
Density	(g cm^{-3})	5.68
Dielectric constant		
static		15.15
high frequency		12.3
Effective electron mass	(in units of m_o)	0.023
Effective hole masses (in units of m_o)		
heavy	m_h/m_o	0.41
light	m_{lp}/m_o	0.026
Electron affinity	(eV)	4.9
Lattice constant	(Å)	6.0583
Optical phonon energy	(eV)	0.030

Band structure and carrier concentration

Energy gap	(eV)	0.354
Energy separation ($E_{\Gamma L}$) between Γ and L valleys	(eV)	0.73
Energy separation ($E_{\Gamma X}$) between Γ and X valleys	(eV)	1.02
Energy spin-orbital splitting	(eV)	0.41
Intrinsic carrier concentration	(cm^{-3})	1×10^{15}
Intrinsic resistivity	($\Omega \times cm$)	0.16
Effective conduction band density of states	(cm^{-3})	8.7×10^{16}
Effective valence band density of states	(cm^{-3})	6.6×10^{18}

Electrical properties

Breakdown field	($V\,cm^{-1}$)	$\simeq 4 \times 10^4$
Mobility	($cm^2\,V^{-1}\,s^{-1}$)	
electrons		$\leq 4 \times 10^4$
holes		$\leq 5 \times 10^2$
Diffusion coefficient	($cm^2\,s^{-1}$)	
electrons		$\leq 10^3$
holes		≤ 13
Electron thermal velocity	($m\,s^{-1}$)	7.7×10^5
Hole thermal velocity	($m\,s^{-1}$)	2×10^5

Optical properties

Infrared refractive index	3.51
Radiative recombination coefficient ($cm^3\,s^{-1}$)	1.1×10^{-10}

Thermal and mechanical properties

Bulk modulus	($dyn\,cm^{-2}$)	5.8×10^{11}
Melting point	(°C)	942
Specific heat	($J\,g^{-1}\,°C^{-1}$)	0.25
Thermal conductivity	($W\,cm^{-1}\,°C^{-1}$)	0.27
Thermal diffusivity	($cm^2\,s^{-1}$)	0.19
Thermal expansion, linear	($°C^{-1}$)	4.52×10^{-6}

7.2. Band Structure and Carrier Concentration

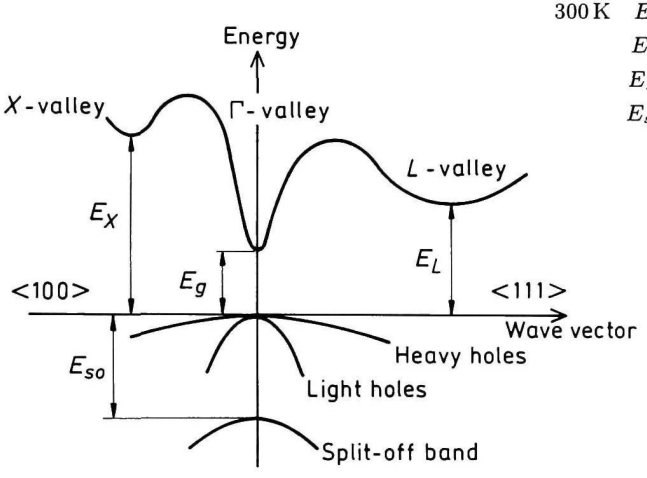

Fig. 7.2.1. Band structure of InAs. Important minima of the conduction band and maxima of the valence band.

7.2.1. *Temperature Dependences*

Temperature dependence of the energy gap (Fang *et al.* [1990])

$$E_g = 0.415 - 2.76 \times 10^{-4} \frac{T^2}{T + 83} \text{ (eV)} , \tag{7.2.1}$$

where T is temperature in degrees K ($0 < T < 300$).

Effective density of states in the conduction band

$$N_c \simeq 1.68 \times 10^{13} \times T^{3/2} \text{ (cm}^{-3}\text{)} \tag{7.2.2}$$

Effective density of states in the valence band

$$N_v \simeq 1.27 \times 10^{15} \times T^{3/2} \text{ (cm}^{-3}\text{)} . \tag{7.2.3}$$

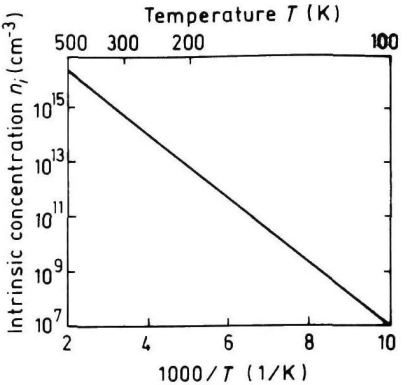

Fig. 7.2.2. The temperature dependence of the intrinsic carrier concentration.

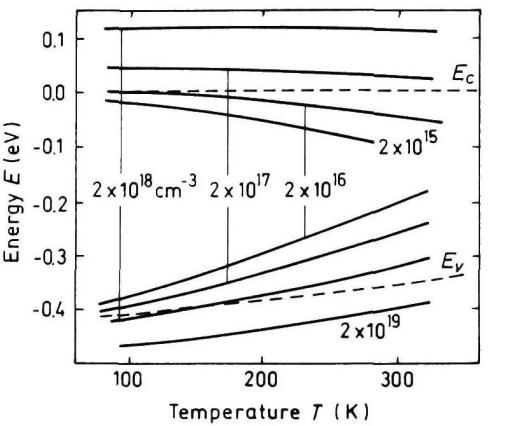

Fig. 7.2.3. Fermi level versus temperature for different concentrations of shallow donors and acceptors.

7.2.2. *Dependence on Hydrostatic Pressure*

$$E_g \simeq E_g(0) + 4.8 \times 10^{-3}\ P\ (\text{eV})$$
$$E_L \simeq E_L(0) + 3.2 \times 10^{-3}\ P\ (\text{eV}), \tag{7.2.4}$$

where P is pressure in kbar (Edwards and Drickamer [1961]).

7.2.3. *Energy Gap Narrowing at High Doping Levels*

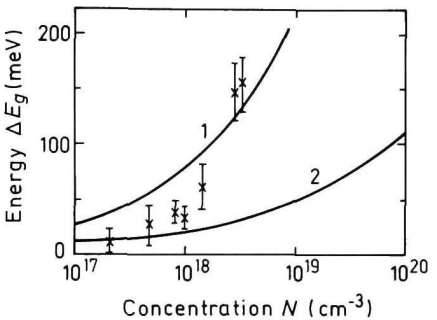

Fig. 7.2.4. Energy gap narrowing versus donor (Curve 1) and acceptor (Curve 2) doping density. Curves are calculated according Jain *et al.* [1990]. Points show experimental results for *n*-InAs (Semikolenova *et al.* [1978]).

For *n*-type InAs

$$\Delta E_g = 14.0 \times 10^{-9} \times N_d^{1/3} + 1.97 \times 10^{-7} \times N_d^{1/4} + 57.9 \times 10^{-12} \times N_d^{1/2} \text{ (eV)}$$

For *p*-type InAs (7.2.5)

$$\Delta E_g = 8.34 \times 10^{-9} \times N_a^{1/3} + 2.91 \times 10^{-7} \times N_a^{1/4} + 4.53 \times 10^{-12} \times N_a^{1/2} \text{ (eV)}$$

(Jain *et al.* [1990]).

7.2.4. *Effective Masses*

Electrons

For Γ-valley $m_\Gamma = 0.023 m_0$

Non-parabolicity: $E(1 + \alpha E) = \dfrac{h^2 k^2}{2 m_\Gamma}$ $\alpha = 1.4$ (eV^{-1})

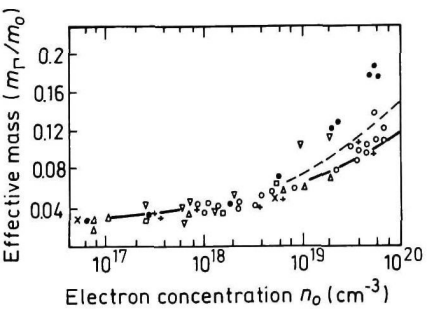

Fig. 7.2.5. Electron effective mass versus electron concentration (Kesamanly *et al.* [1969]).

In the L-valley effective mass of density of states

$$m_L = 0.29m_0$$

In the X-valley effective mass of density of states

$$m_X = 0.64m_0$$

Holes

heavy	$m_h = 0.41m_0$
light	$m_{lp} = 0.026m_0$
split-off band	$m_{so} = 0.16m_0$

Effective mass of density of states $m_v = 0.41m_0$

7.2.5. *Donors and Acceptors*

Ionization energies of shallow donors ≥ 0.001 (eV): Se, S, Te, Ge, Si, Sn, Cu

Ionization energies of shallow acceptors (eV) (from Guseva *et al.* [1974], Guseva *et al.* [1975])

Sn	0.01
Ge	0.014
Si	0.02
Cd	0.015
Zn	0.01

7.3. Electrical Properties

7.3.1. *Mobility and Hall Effect*

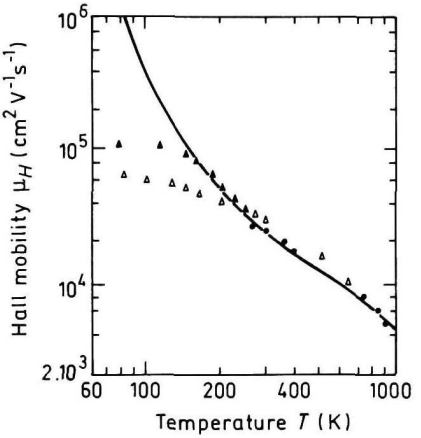

Fig. 7.3.1. Electron Hall mobility versus temperature for different electron concentration: full triangles – $n_0 = 4 \times 10^{15}\,cm^{-3}$, circles – $n_0 = 4 \times 10^{16}\,cm^{-3}$, open triangles – $n_0 = 1.7 \times 10^{16}\,cm^{-3}$. Solid curve – calculation for pure InAs (Rode [1975]).

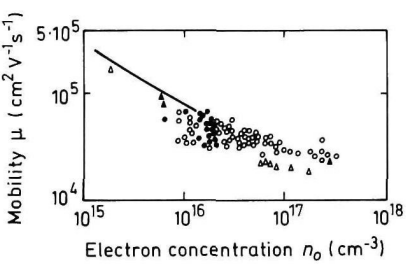

Fig. 7.3.2. Electron Hall mobility versus electron concentration (Karataev *et al.* [1977]), $T = 77\,K$.

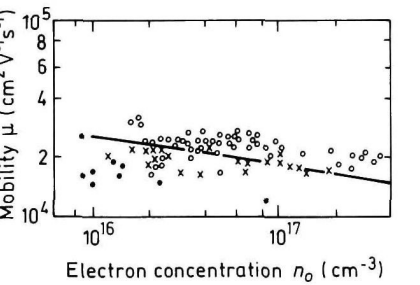

Fig. 7.3.3. Electron Hall mobility versus electron concentration (Karataev *et al.* [1977]), $T = 300\,K$.

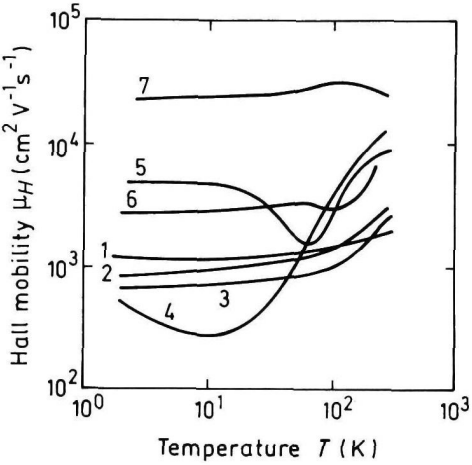

Fig. 7.3.4. Electron Hall mobility ($R \times \sigma$) in compensated material (Garyagdyev *et al.* [1974]).

Curve	n cm^{-3}	$N_a + N_d$ cm^{-3}	$\theta = \frac{N_a}{N_d}$
1	8.2×10^{16}	3×10^{17}	0.58
2	3.2×10^{17}	6.1×10^{18}	0.9
3	5.1×10^{16}	3.2×10^{18}	0.96
4	3.3×10^{16}	7.5×10^{17}	0.91
5	7.6×10^{15}	3.4×10^{17}	0.95
6	6.4×10^{15}	3.8×10^{17}	0.96
7	3.3×10^{15}	3.9×10^{17}	0.98

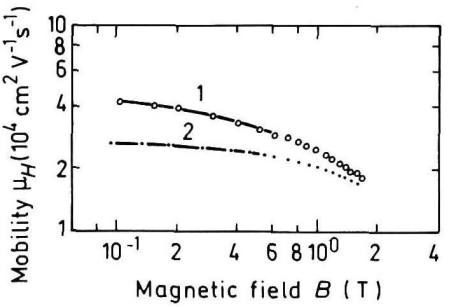

Fig. 7.3.5. Electron Hall mobility versus transverse magnetic field, $T = 77$ K (Kamakura *et al.* [1975]). N_d(cm^{-3}): 1. 1.7×10^{16}, 2. 5.8×10^{16}.

At $T = 300$ K the electron Hall factor in pure n-InAs $r_H \simeq 1.3$.

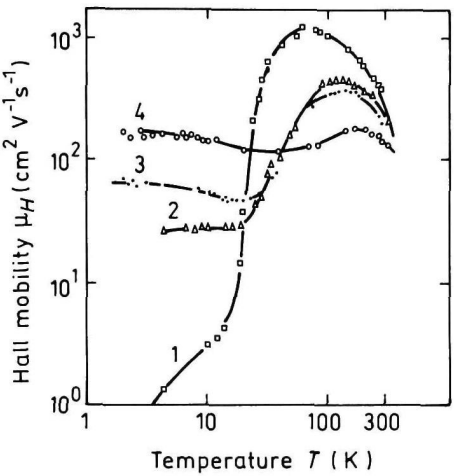

Fig. 7.3.6. Hole Hall mobility ($R \times \sigma$) versus temperature for different acceptor densities (Kesamanly *et al.* [1968]). Hole concentration at 300 K p_0 (cm^{-3}): 1. 5.7×10^{16}, 2. 2.6×10^{17}, 3. 4.2×10^{17}, 4. 1.3×10^{18}.

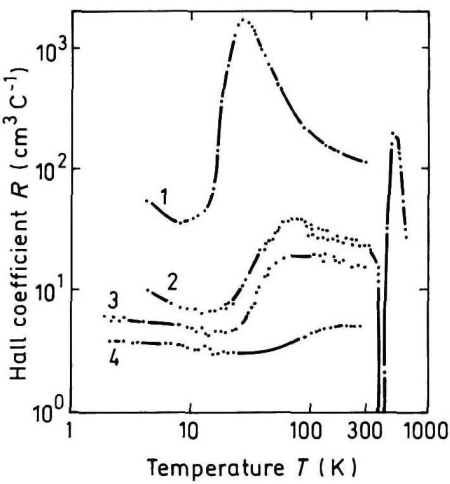

Fig. 7.3.7. Hall coefficient versus temperature for different acceptor densities (Kesamanly *et al.* [1968]). Hole concentration at 300 K. p_0 (cm^{-3}): 1. 5.7×10^{16}, 2. 2.6×10^{17}, 3. 4.2×10^{17}, 4. 1.3×10^{18}.

7.3.2. *Transport Properties in High Electric Field*

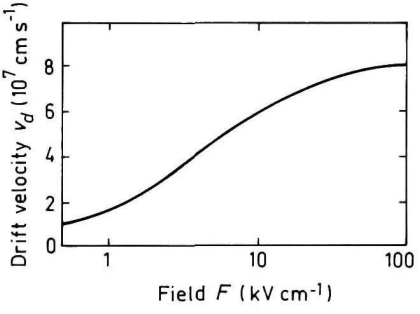

Fig. 7.3.8. Steady state field dependence of the electron drift velocity, 300 K, $F||(100)$. Theoretical calculation (Brennan and Hess [1984]).

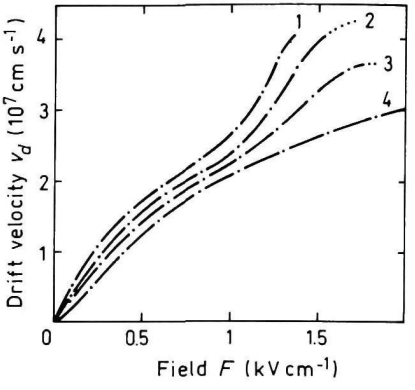

Fig. 7.3.9. Field dependences of the electron drift velocity at different transverse magnetic fields for long (microsecond) pulses. Experimental results, 77 K (Kamakura *et al.* [1975]). Magnetic field $B(T)$: 1. 0.0, 2. 0.3, 3. 0.9, 4. 1.5.

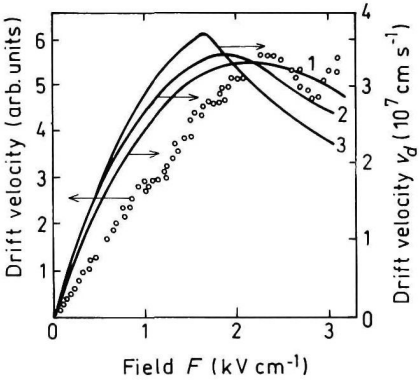

Fig. 7.3.10. Field dependences of the electron drift velocity, 77 K. Solid lines show results of theoretical calculation for different non-parabolicity $\alpha(\mathrm{eV})^{-1}$: 1. 2.85, 2. 2.0, 3. 1.5 (Kuchar *et al.* [1973]). Points show experimental results for very short (pico-second) pulses (Krotkus and Dobrovolskis [1988]).

7.3.3. *Impact Ionization*

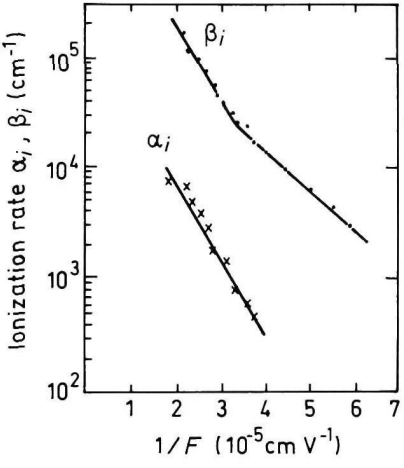

Fig. 7.3.11. The dependences of ionization rates for electrons – α_i and holes – β_i versus $1/F$, $T = 77$ K. (Mikhailova *et al.* [1976]).

For electrons

$$\alpha_i = \alpha_0 \times \exp[-F_{no}/F] \tag{7.3.1}$$

$\alpha_o = 1.8 \times 10^5$ cm^{-1}, $F_{no} = 1.6 \times 10^5$V cm^{-1} (77 K)

For holes

$$\beta_i = \beta_0 \times \exp[-F_{po}/F] \tag{7.3.2}$$

At 77 K

1.5×10^4 V cm^{-1} $< F < 3 \times 10^4$ V cm^{-1}

$\beta_0 = 4.7 \times 10^5$ cm^{-1}, $F_{po} = 0.85 \times 10^5$ V cm^{-1}

3×10^4 V cm^{-1} $< F < 6 \times 10^4$ V cm^{-1}

$\beta_0 = 4.5 \times 10^6$ cm^{-1}, $F_{po} = 1.54 \times 10^5$ V cm^{-1}

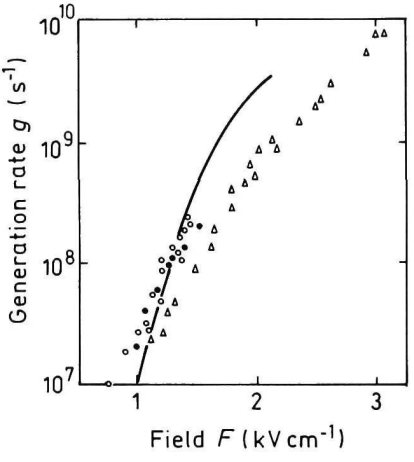

Fig. 7.3.12. Generation rate g versus electric field for relatively low fields, $T = 77$ K. Solid line shows the result of calculation. Experimental results: open and full circles – undoped InAs, open triangles – compensated InAs (Krotkus and Dobrovolskis [1988]).

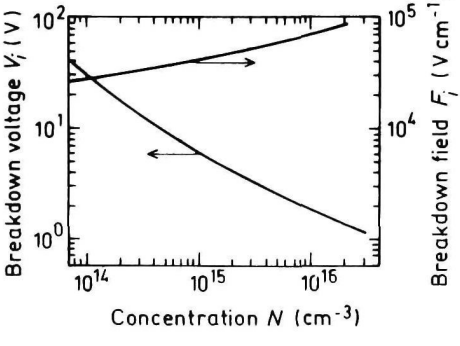

Fig. 7.3.13. Breakdown voltage and breakdown field versus doping density for abrupt p-n junction, $T = 77$ K.

7.3.4. *Recombination Parameters*

Pure n-type material ($n_0 = 2 \times 10^{15}\,\mathrm{cm}^{-3}$)

The longest lifetime of holes	$\tau_p \sim 3 \times 10^{-6}\,\mathrm{s}$
Diffusion length	$L_p \sim 10$–$20\,\mu\mathrm{m}$

Pure p-type material

The longest lifetime of electrons	$\tau_n \sim 3 \times 10^{-8}\,\mathrm{s}$
Diffusion length $L_n = (D_n \times \tau_n)^{1/2}$	$L_p = 30$–$60\,\mu\mathrm{m}$

Characteristic surface recombination rates ($\mathrm{cm\,s}^{-1}$) 10^2–10^4

Radiative recombination coefficient (Varshni [1967])

$77\,\mathrm{K} - 1.2 \times 10^{-9}\mathrm{cm}^3\,\mathrm{s}^{-1}$

$298\,\mathrm{K} - 1.1 \times 10^{-10}\mathrm{cm}^3\,\mathrm{s}^{-1}$

Auger coefficient

$300\,\mathrm{K} \sim 2.2 \times 10^{-27}\ \mathrm{cm}^6\,\mathrm{s}^{-1}$

(Gel'mont *et al.* [1982]).

7.4. Optical Properties

Infrared refractive index

$$n_\infty = (k_\infty)^{1/2} \simeq 3.51 \text{ (300 K)} \tag{7.4.1}$$

Long-wave TO phonon energy $h\nu_{TO} \simeq 27$ meV (300 K) (7.4.2)

Long-wave LO phonon energy $h\nu_{LO} \simeq 29$ meV (300 K) (7.4.3)

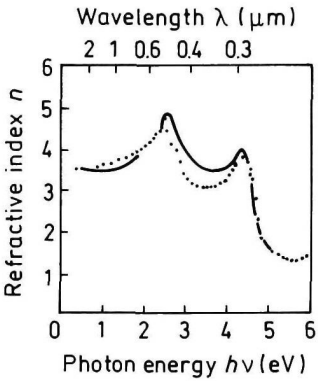

Fig. 7.4.1. Refractive index n versus photon energy. Solid curve is theoretical calculation. Points represent experimental data, 300 K (Adachi [1989]).

For $3.75\,\mu\text{m} < \lambda < 33\,\mu\text{m}$

$$n = \left[11.1 + \frac{0.71}{1 - 6.5 \times \lambda^{-2}} + \frac{2.75}{1 - 2085 \times \lambda^{-2}} - 6 \times 10^{-4} \times \lambda^2\right]^{1/2} \tag{7.4.4}$$

where λ is the wavelength in μm (300 K) (Lorimor and Spitzer [1965]).

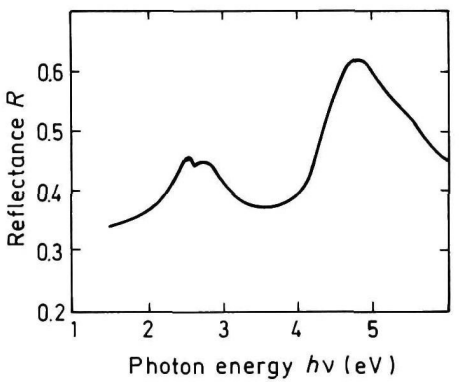

Fig. 7.4.2. Normal incidence reflectivity versus photon energy, 300 K (Aspnes and Studna [1983]).

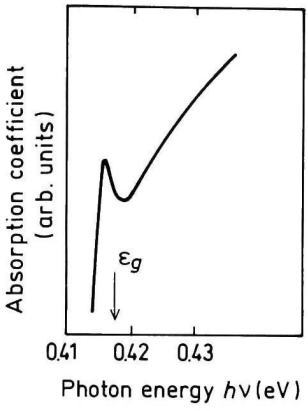

Fig. 7.4.3. Absorption coefficient near the intrinsic absorption edge for n-InAs. $T = 4.2\,\mathrm{K}$ (Varfolomeev *et al.* [1975]).

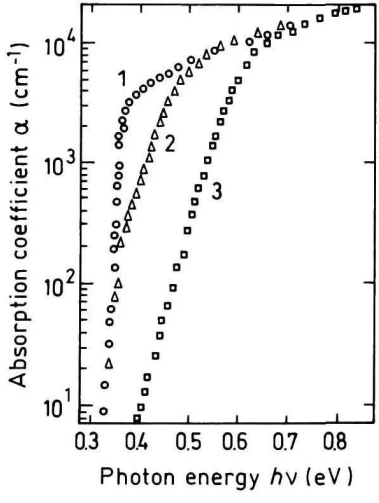

Fig. 7.4.4. Absorption coefficient versus photon energy for different donor concentration, 300 K (Dixon and Ellis [1961]). $n\,(\mathrm{cm}^{-3})$: 1. 3.6×10^{16}, 2. 6×10^{17}, 3. 3.8×10^{18}.

A ground state Rydberg energy $R_{X1} = 3.5$ meV.

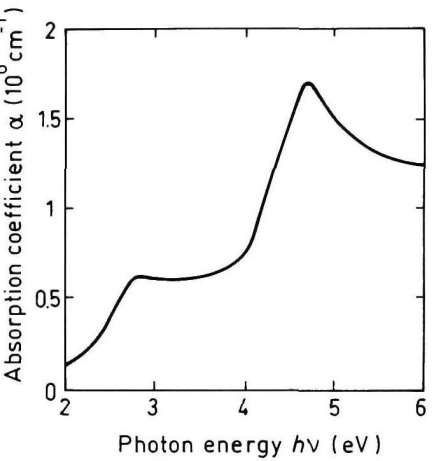

Fig. 7.4.5. Absorption coefficient versus photon energy, $T = 300\,\mathrm{K}$ (Aspnes and Studna [1983]).

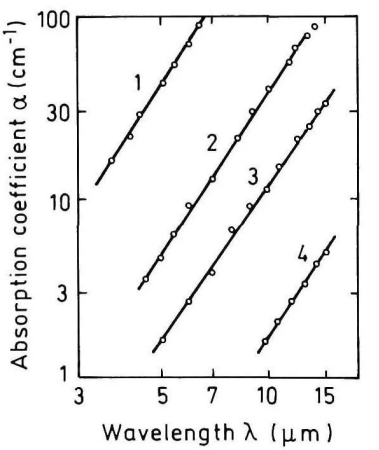

Fig. 7.4.6. Free carrier absorption versus wavelength at different electron concentrations (Dixon [1961]), 300 K. $n_0(\mathrm{cm}^{-3})$: 1. 3.9×10^{18}, 2. 7.8×10^{17}, 3. 2.5×10^{17}, 4. 2.8×10^{16}.

7.5. Thermal Properties

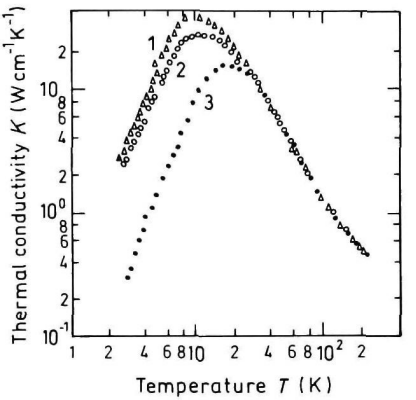

Fig. 7.5.1. Temperature dependences of thermal conductivity (Tamarin and Shalyt [1971]). 1, 2. – n-type samples, 1. $n_0 = 1.6 \times 10^{16}\,\mathrm{cm}^{-3}$, 2. $n_0 = 2.0 \times 10^{17}\,\mathrm{cm}^{-3}$, 3. p-type sample, $p_0 = 2.0 \times 10^{17}\,\mathrm{cm}^{-3}$.

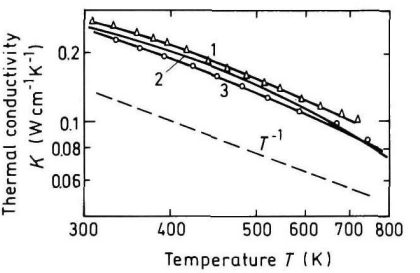

Fig. 7.5.2. Temperature dependences of thermal conductivity for high temperatures (Okhotin *et al.* [1972]). Electron concentration n_0(cm^{-3}): 1. 5×10^{16}, 2. 2×10^{16}, 3. 3×10^{16}.

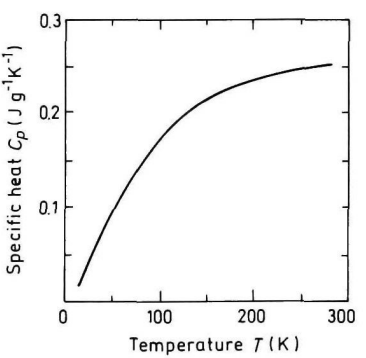

Fig. 7.5.3. Temperature dependence of specific heat at constant pressure (Piesbergen [1963]).

For $298 < T < 1215\,\mathrm{K}$

$$C_p = 0.240 + 3.97 \times 10^{-5}\,T\,(\mathrm{J\,g^{-1}\,K^{-1}})$$

(Barin *et al.* [1977]).

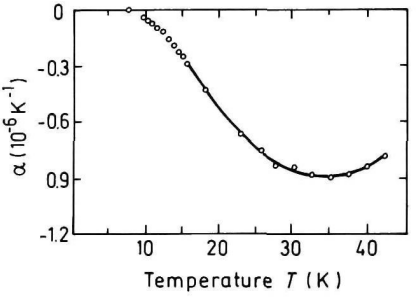

Fig. 7.5.4. Temperature dependence of linear expansion coefficient (low temperatures) (Sparks and Swenson [1967]).

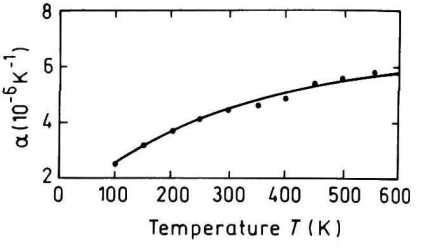

Fig. 7.5.5. Temperature dependence of linear expansion coefficient (high temperatures) (Sirota and Berger [1959]).

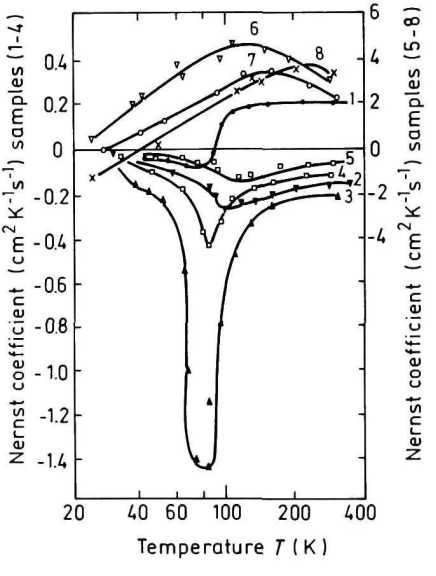

Fig. 7.5.6. Temperature dependences of Nernst coefficient (transverse Nernst–Ettinghausen effect) (Domanskaya *et al.* [1970]). Electron concentration at 77 K $n_0(\mathrm{cm}^{-3})$:

1. 2.96×10^{16}	2. 4.46×10^{16}
3. 8.43×10^{16}	4. 4.53×10^{17}
5. 1.56×10^{18}	6. 2.28×10^{18}
7. 5×10^{18}	8. 1.68×10^{19}

Melting point $T_m = 1215\,\mathrm{K}$

Saturated vapor pressure, (in Pascals)

For $950\,\mathrm{K} \sim 2 \times 10^{-3}$

For $1000\,\mathrm{K} \sim 10^{-2}$

For $1050\,\mathrm{K} \sim 10^{-1}$

7.6. Mechanical Properties, Elastic Constants, Lattice Vibrations, Other Properties

Density	$5.68\ \mathrm{g\,cm^{-3}}$
Hardness	3.8 (on the Mohs scale)
Surface microhardness (using Knoop's pyramid test)	$430\ \mathrm{kg\,mm^{-2}}$
Cleavage plane	{110}
Elastic constants at 293 K (Burenkov *et al.* [1975])	
C_{11}	$8.34 \times 10^{11}\ \mathrm{dyn\,cm^{-2}}$
C_{12}	$4.54 \times 10^{11}\ \mathrm{dyn\,cm^{-2}}$
C_{44}	$3.95 \times 10^{11}\ \mathrm{dyn\,cm^{-2}}$

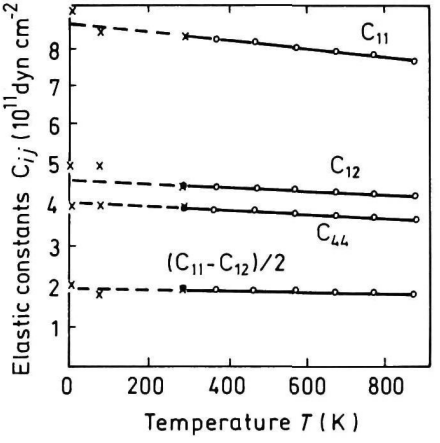

Fig. 7.6.1. Temperature dependences of elastic constants (Burenkov *et al.* [1975]).

For $T = 300$ K

Bulk modulus (compressibility^{-1}) $B_s = \dfrac{C_{11} + 2C_{12}}{3}$	$B_s = 5.81 \times 10^{11}\ \mathrm{dyn\,cm^{-2}}$
Shear modulus $C' = (C_{11} - C_{12})/2$	$C' = 1.90 \times 10^{11}\ \mathrm{dyn\,cm^{-2}}$
[100] Young's modulus $Y_0 = \dfrac{(C_{11} + 2C_{12})(C_{11} - C_{12})}{(C_{11} + C_{12})}$	$Y_0 = 5.14 \times 10^{11}\ \mathrm{dyn\,cm^{-2}}$
[100] Poisson ratio $\sigma_0 = \dfrac{C_{12}}{C_{11} + C_{11}}$	$\sigma_0 = 0.35$

Acoustic Wave Speeds

Wave propagation direction	Wave character	Expression for wave speed	Wave speed (in units of $10^5\,\mathrm{cm\,s^{-1}}$)
[100]	V_L	$(C_{11}/\rho)^{1/2}$	3.83
	V_T	$(C_{44}/\rho)^{1/2}$	2.64
[110]	V_l	$[(C_{11}+C_{12}+2C_{44})/2\rho]^{1/2}$	4.28
	$V_{t\parallel}$	$V_{t\parallel}=V_T=(C_{44}/\rho)^{1/2}$	2.64
	$V_{t\perp}$	$[(C_{11}-C_{12})/2\rho]^{1/2}$	1.83
[111]	V_l'	$[(C_{11}+2C_{12}+4C_{44})/3\rho]^{1/2}$	4.41
	V_t'	$[(C_{11}-C_{12}+C_{44})/3\rho]^{1/2}$	2.13

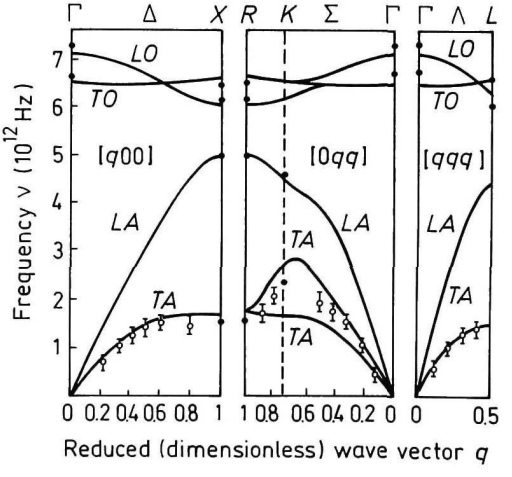

Fig. 7.6.2. Room temperature dispersion curves for acoustic and optical branch phonons. Solid lines are calculated according to overlap shell model (Carles *et al.* [1980]).

Phonon frequencies (in units of 10^{12} Hz)

$\nu_{TO}(\Gamma)$	6.44	$\nu_{LO}(X)$	6.20
$\nu_{LO}(\Gamma)$	7.01	$\nu_{TA}(L)$	1.50
$\nu_{TA}(X)$	1.70	$\nu_{LA}(L)$	4.46
$\nu_{LA}(X)$	4.94	$\nu_{TO}(L)$	6.44
$\nu_{TO}(X)$	6.47	$\nu_{LO}(L)$	6.26

Piezoelectric constant e_{14} $\quad -4.5 \cdot 10^{-2}\,\mathrm{C\,m^{-2}}$

Electron g-factor

298 K	−17.5
80 K	−15.4

References

Adachi, S., *J. Appl. Phys.* **66**, 12 (1989) 6030–6040.

Aspnes, D. E. and A. A. Studna, *Phys. Rev.* **B27**, 2 (1983) 985–1009.

Barin, I., O. Knacke, and O. Kubaschewski, *Thermochemical Properties of Inorganic Substances*, Springer, Berlin, 1977.

Blaut-Blachev, A. N., L. A. Balagurov, V. V. Karataev, and E. M. Omel'yanovskii, *Sov. Phys. Semicond.* **9**, 4 (1975) 515–516.

Brennan, K. and K. Hess, *Solid State Electron.* **27**, 4 (1984) 347–357.

Burenkov, Yu. A., S. Yu. Davydov, and S. P. Nikanorov, *Sov. Phys. Solid State* **17**, 7 (1975) 1446–1447.

Carles, R., N. Saint-Cricq, J. B. Renucci, M. A. Renucci, and A. Zwick, *Phys. Rev.* **B22**, 10 (1980) 4804–4815.

Dixon, J. R., *Proc. 5th Int. Conf. on Physics of Semiconductors*, Prague, 1961, p. 366.

Dixon, J. R. and J. M. Ellis, *Phys. Rev.* **123**, 5 (1961) 1560–1567.

Domanskaya, L. I., M. I. Iglitsyn, E. V. Soloveva, and I. M. Tsidilkovskii, *Sov. Phys. Semicond.* **3** (1970) 1548.

Edwards, A. L. and H. G. Drickamer, *Phys. Rev.* **122**, 4 (1960) 1149–1157.

Fang, Z. M., K. Y. Ma, D. H. Jaw, R. M. Cohen, and G. B. Stringfellow, *J. Appl. Phys.* **67**, 11 (1990) 7034–7039.

Garyagdyev, G., O. V. Emel'yanenko, N. V. Zotova, T. S. Lagunova, D. N. Nasledov, and A. V. Pentsov, *Sov. Phys. Semicond.* **8** (1974) 335.

Gel'mont, B. L., Z. N. Sokolova, and I. N. Yassievich, *Sov. Phys. Semicond.* **16**, 4 (1982) 592–600.

Guseva, M. I., N. V. Zotova, A. V. Koval, and D. N. Nasledov, *Sov. Phys. Semicond.* **8**, 10 (1975) 1323.

Guseva, M. I., N. V. Zotova, A. V. Koval, and D. N. Nasledov, *Sov. Phys. Semicond.* **8**, 1 (1974) 34–36.

Jain, S. L., J. M. McGregor, and D. J. Roulston, *J. Appl. Phys.* **68**, 7 (1990) 3747–3749.

Kamakura, K., T. Akashi, and M. Tsuzuki, *J. Phys. Soc. Jpn.* **38**, 5 (1975) 1383–1388.
Karataev, V. V., M. G. Mil'vidsky, N. S. Rytova, and V. I. Fistul, *Sov. Phys. Semicond.* **11**, 9 (1977) 1009–1011.
Kesamanly, F. P., T. S. Lagunova, D. N. Nasledov, L. A. Nikolaeva, and M. N. Pivovarov, *Fiz. i Tekhn. Polupr.* **2**, 1 (1968) 56–63 (in Russian).
Kesamanly, F. P., Yu. Mal'tsev, D. N. Nasledov, L. A. Nikolaeva, M. N. Pivovarov, V. A. Skripkin, and Yu. I. Uvanov, *Fiz. Tekhn. Polupr.* **3**, 8 (1969) 1182–1187 (in Russian).
Krotkus, A. and Z. Dobrovolskis, *Electrical Conductivity of Narrow-Gap Semiconductors*, Vilnus, Mokslas, 1988.
Kuchar, F., G. Bauer, and H. Hillbrand, *Phys. Status Solidi (A)* **17**, 2 (1973) 491–496.
Lorimor, O. G. and W. G. Spitzer, *J. Appl. Phys.* **36**, 6 (1965) 1841–1847.
Mikhailova, M. P., A. A. Rogachev, and I. N. Yassievich, *Sov. Phys. Semicond.* **10**, 8 (1976) 866–871.
Okhotin, A. S., A. S. Pushkarskii, and V. V. Gorbachev, *Thermophysical Properties of Semiconductors*, "Atom" Publ. House, Moscow, 1972, (in Russian).
Piesbergen, U., *Zeitschrift fur Naturforschung* **18a**, 2 (1963) 141–147.
Rode, D. L., *Semiconductors and Semimetals*, R. K. Willardson and A. C. Beer, eds., Academic Press, vol. 10, 1975, p. 1.
Semikolenova, N. A., I. M. Nesmelova, and E. N. Khabarov, *Sov. Phys. Semicond.* **12**, 10 (1978) 1139–1142.
Sirota, N. N. and L. I. Berger, *Inzh. Fiz. Zhurnal*, Akad. Nauk Beloruss. SSR, **2** (1959) 104 (in Russian).
Sparks, P. W. and C. A. Swenson, *Phys. Rev.* **163**, 3 (1967) 779–790.
Steigmeier, E. F. and I. Kudman, *Phys. Rev.* **132**, 2 (1963) 508–512.
Tamarin, P. V. and S. S. Shalyt, *Sov. Phys. Semicond.* **5**, 5 (1971) 1097–1098.
Varfolomeev, A. V., R. P. Seisyan, and R. N. Yakimova, *Sov. Phys. Semicond.* **9**, 4 (1975) 530.
Varshni, V. P., *Phys. Status Solidi* **19**, 2 (1967) 459–514; **20**, 1 (1967) 9–36.

CHAPTER 8

INDIUM PHOSPHIDE (InP)

Natalya M. Shmidt
Ioffe Institute,
St. Petersburg, Russia

8.1. Basic Parameters at 300 K

Crystal structure		Zinc Blende
Group of symmetry		T_d^2–F$\bar{4}$3m
Number of atoms in 1 cm^3		3.96×10^{22}
Debye temperature	(K)	425
Density	($g\,cm^{-3}$)	4.81
Dielectric constant		
static		12.5
high frequency		9.61
Effective electron mass	(in units of m_o)	0.08
Effective hole masses	(in units of m_o)	
heavy		0.6
light		0.089
Electron affinity	(eV)	4.38
Lattice constant	(Å)	5.8687
Optical phonon energy	(eV)	0.043

Band structure and carrier concentration

Energy gap	(eV)	1.344
Energy separation ($E_{\Gamma L}$) between Γ and L valleys	(eV)	0.59
Energy separation ($E_{\Gamma X}$) between Γ and X valleys	(eV)	0.85
Energy spin-orbital splitting	(eV)	0.11
Intrinsic carrier concentration	(cm^{-3})	1.3×10^7
Intrinsic resistivity	($\Omega \times cm$)	8.6×10^7
Effective conduction band density of states	(cm^{-3})	5.7×10^{17}
Effective valence band density of states	(cm^{-3})	1.1×10^{19}

Electrical properties

Breakdown field	($V\,cm^{-1}$)	$\sim 5 \times 10^5$
Mobility	($cm^2\,V^{-1}\,s^{-1}$)	
electrons		≤ 5400
holes		≤ 200
Diffusion coefficient	($cm^2\,s^{-1}$)	
electrons		≤ 130
holes		≤ 5
Electron thermal velocity	($m\,s^{-1}$)	3.9×10^5
Hole thermal velocity	($m\,s^{-1}$)	1.7×10^5

Optical properties

Infrared refractive index	3.1
Radiative recombination coefficient ($cm^3\,s^{-1}$)	1.2×10^{-10}

Thermal and mechanical properties

Bulk modulus	($dyn\,cm^{-2}$)	7.1×10^{11}
Melting point	(°C)	1060
Specific heat	($J\,g^{-1}\,°C^{-1}$)	0.31
Thermal conductivity	($W\,cm^{-1}\,°C^{-1}$)	0.68
Thermal diffusivity	($cm^2\,s^{-1}$)	0.372
Thermal expansion, linear	($°C^{-1}$)	4.60×10^{-6}

8.2. Band Structure and Carrier Concentration

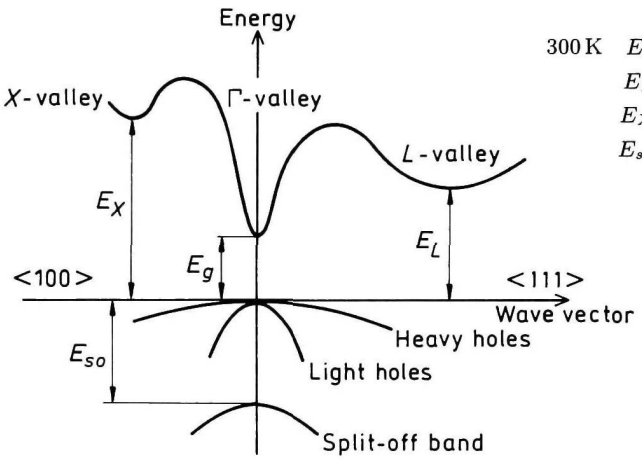

Fig. 8.2.1. Band structure of InP. Important minima of the conduction band and maxima of the valence band.

8.2.1. *Temperature Dependences*

Temperature dependence of the energy gap

$$E_g = 1.421 - 4.9 \times 10^{-4} \times \frac{T^2}{T + 327} \text{ (eV)} , \tag{8.2.1}$$

where T is temperature in degrees K ($0 < T < 800$).

Temperature dependence of the energy separation between Γ and X valleys

$$E_{\Gamma X} = 0.96 - 3.7 \times 10^{-4} \times T \text{ (eV)} , \tag{8.2.2}$$

where T is temperature in degrees K ($0 < T < 300$).

Effective density of states in the conduction band

$$N_c \simeq 1.1 \times 10^{14} \times T^{3/2} \ (\mathrm{cm}^{-3}) \tag{8.2.3}$$

Effective density of states in the valence band

$$N_v \simeq 2.2 \times 10^{15} \times T^{3/2} \ (\mathrm{cm}^{-3}) \ . \tag{8.2.4}$$

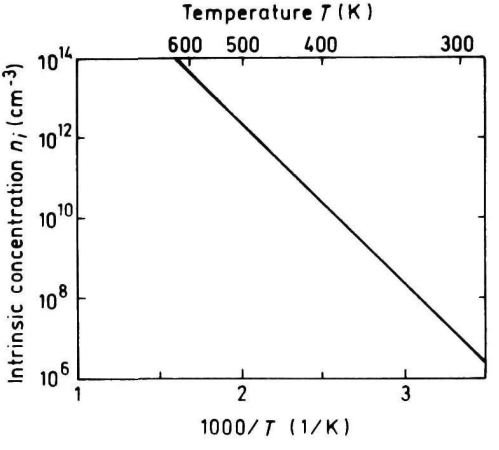

Fig. 8.2.2. The temperature dependence of the intrinsic carrier concentration.

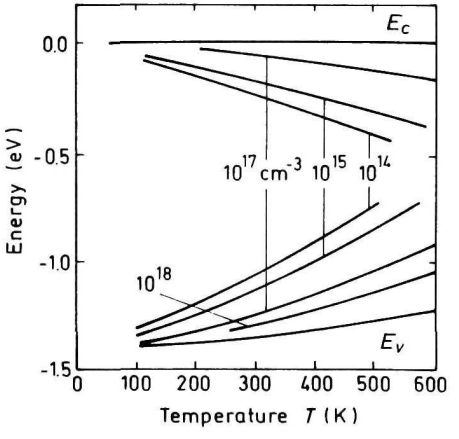

Fig. 8.2.3. Fermi level versus temperature for different concentrations of shallow donors and acceptors.

8.2.2. *Dependence on Hydrostatic Pressure*

$$
\begin{aligned}
E_g &= E_g(0) + 8.4 \times 10^{-3}\ P - 1.8 \times 10^{-5}\ P^2\ \text{(eV)},\\
E_L &= E_L(0) + 4.6 \times 10^{-3}\ P\ \text{(eV)},\\
E_X &= E_X(0) + 2 \times 10^{-3}\ P\ \text{(eV)},
\end{aligned}
\tag{8.2.5}
$$

where P is pressure in kbar.

8.2.3. *Energy Gap Narrowing at High Doping Levels*

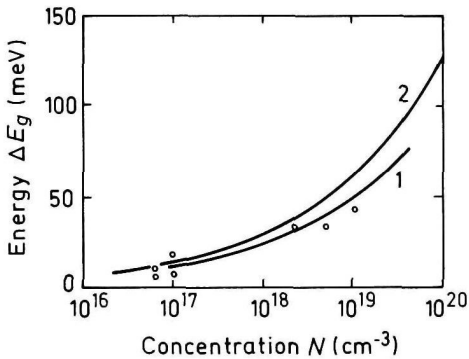

Fig. 8.2.4. Energy gap narrowing versus donor (Curve 1 and experimental points) and acceptor (Curve 2) doping density, 300 K. Curve 1 and experimental points (Bugajski and Lewandowski [1985]), Curve 2 (Jain *et al.* [1990]).

For n-type InP

$$\Delta E_g \simeq 22.5 \times 10^{-9}\ N_d^{1/3}\ \text{(eV)}$$

(Bugajski and Lewandowski [1985]).

For p-type InP

$$\Delta E_g = 10.3 \times 10^{-9} \times N_a^{1/3} + 4.43 \times 10^{-7} \times N_a^{1/4} + 3.38 \times 10^{-12} \times N_a^{1/2}\ \text{(eV)} \tag{8.2.6}$$

(Jain *et al.* [1990]).

8.2.4. *Effective Masses*

Electrons

For Γ-valley $m_\Gamma = 0.08m_0$

There are 4 equivalent L-valleys in the conduction band:

$m_L = 0.25m_0$ is the effective mass in one L-valley,
$m_{Ld} = 0.63m_0$ is the effective mass of density of states for all L-valleys.

There are 3 equivalent X-valleys in the conduction band:

$m_X = 0.32m_0$ is the effective mass in one X-valley.
$m_{Xd} = 0.66m_0$ is the effective mass of density of states for all X-valleys

Holes

heavy	$m_h = 0.6m_0$
light	$m_{lp} = 0.089m_0$
split-off band	$m_{so} = 0.17m_0$

Effective mass of density of states $m_v = 0.6m_0$

8.2.5. *Donors and Acceptors*

Ionization energies of shallow donors (eV) $\simeq 0.0057$: S, Si, Sn, Ge

Ionization energies of shallow acceptors (eV)

C	0.04
Hg	0.098
Zn	0.035
Cd	0.057
Si	0.03
Cu	0.06
Be	0.03 (MBE)
Mg	0.03 (MBE)
Ge	0.021
Mn	0.27

8.3. Electrical Properties

8.3.1. *Mobility and Hall Effect*

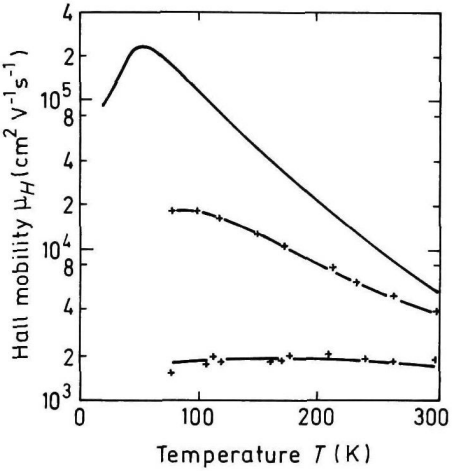

Fig. 8.3.1. Electron Hall mobility versus temperature for different doping levels. Bottom curve – $n_0 = N_d - N_a = 8 \times 10^{17}\,\mathrm{cm}^{-3}$, Middle curve – $n_0 = 2 \times 10^{15}\,\mathrm{cm}^{-3}$; Top curve – $n_0 = 3 \times 10^{13}\,\mathrm{cm}^{-3}$ (Razeghi *et al.* [1988] and Walukiewicz *et al.* [1980]).

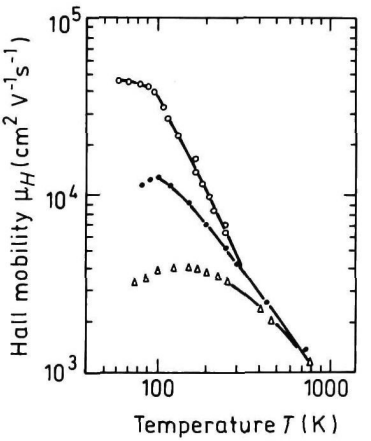

Fig. 8.3.2. Electron Hall mobility versus temperature (high temperatures). Bottom curve – $n_0 = N_d - N_a \simeq 3 \times 10^{17}\,\mathrm{cm}^{-3}$, Middle curve – $n_0 \simeq 1.5 \times 10^{16}\,\mathrm{cm}^{-3}$; Top curve – $n_0 \simeq 3 \times 10^{15}\,\mathrm{cm}^{-3}$ (Galavanov and Siukaev [1970]).

For weakly doped n-InP at temperatures close to 300 K electron drift mobility $\mu_n \simeq (4.2 \div 5.4) \times 10^3 \times \left(\frac{300}{T}\right)^2\ (\mathrm{cm}^2\,\mathrm{V}^{-1}\,\mathrm{s}^{-1})$.

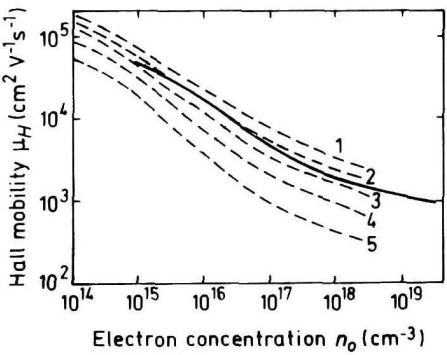

Fig. 8.3.3. Hall mobility versus electron concentration for different compensation ratios $\theta = N_a/N_d$, 77 K. Dashed curves are theoretical calculations: 1. $\theta = 0$, 2. $\theta = 0.2$, 3. $\theta = 0.4$, 4. $\theta = 0.6$, 5. $\theta = 0.8$ (Walukiewicz *et al.* [1980]). Solid line is mean observed values (Anderson *et al.* [1985]).

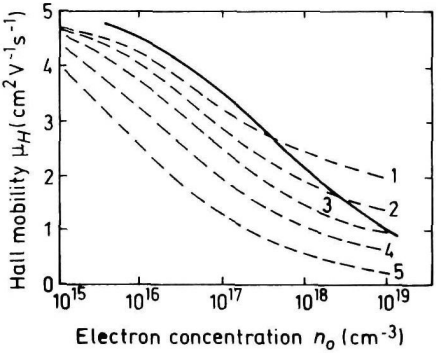

Fig. 8.3.4. Hall mobility versus electron concentration for different compensation ratios $\theta = N_a/N_d$, 300 K. Dashed curves are theoretical calculations: 1. $\theta = 0$, 2. $\theta = 0.2$, 3. $\theta = 0.4$, 4. $\theta = 0.6$, 5. $\theta = 0.8$ (Walukiewicz *et al.* [1980]). Solid line is mean observed values (Anderson *et al.* [1985]).

Approximate formula for electron Hall mobility

$$\mu = \mu_{OH}/[1 + (N_d/10^{17})^{1/2}] ,$$

where $\mu_{OH} \simeq 5000\,\mathrm{cm^2\,V^{-1}\,s^{-1}}$, N_d – in $\mathrm{cm^{-3}}$ (Hilsum [1974]).
At 300 K, the electron Hall factor r_n in n-InP for $N_d > 10^{15}\,\mathrm{cm^{-3}}$: $r_n \simeq 1$.

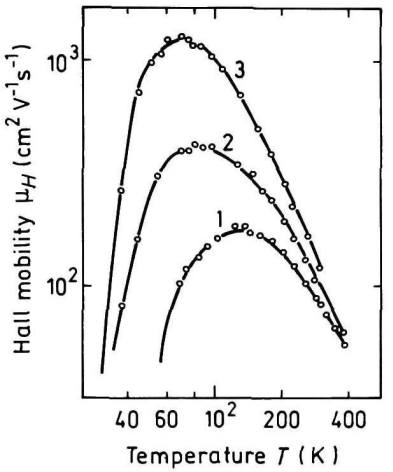

Fig. 8.3.5. Hole Hall mobility versus temperature for different doping (Zn) levels. Hole concentration at 300 K:
1. 1.75×10^{18} cm^{-3}, 2. 3.6×10^{17} cm^{-3}, 3. 4.4×10^{16} cm^{-3}.
$\theta = N_d/N_a \simeq 0.1$ for all samples (Kohanyuk *et al.* [1988]).

For weakly doped p-InP at temperatures close to 300 K the hole Hall mobility

$$\mu_{pH} \simeq 150 \times \left(\frac{300}{T}\right)^{2.2} (\mathrm{cm^2\,V^{-1}\,s^{-1}}).$$

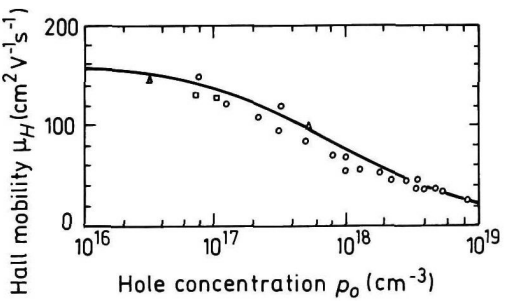

Fig. 8.3.6. Hole Hall mobility versus hole density, 300 K (Wiley [1975]).

The approximate formula for hole Hall mobility

$$\mu_p = \mu_{po}/[1 + (N_a/2 \times 10^{17})^{1/2}] ,$$

where $\mu_{po} \simeq 150\,\mathrm{cm^2\,V^{-1}\,s^{-1}}$, N_a in cm^{-3}

At 300 K, the hole Hall factor in pure p-InP: $r_p \simeq 1$.

8.3.2. *Transport Properties in High Electric Field*

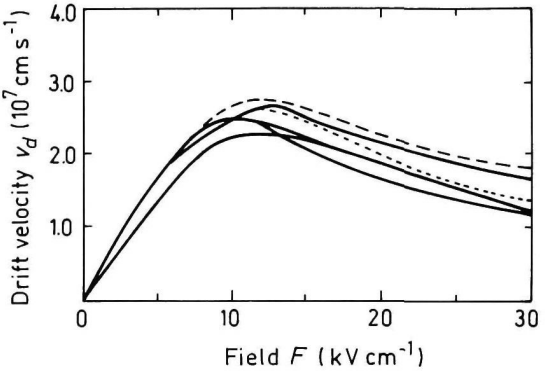

Fig. 8.3.7. Field dependences of the electron drift velocity in InP, 300 K. Solid curves are theoretical calculations. Dashed and dotted curves are measured data (Maloney and Frey [1977] and Gonzalez Sanchez *et al.* [1992]).

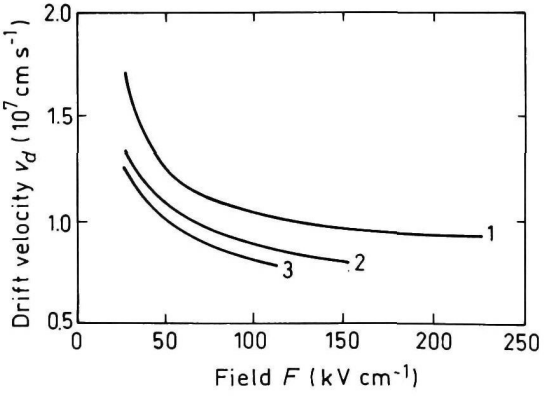

Fig. 8.3.8. The field dependences of the electron drift velocity for high electric fields $T(K)$: 1. 95, 2. 300, 3. 400 (Windhorn *et al.* [1983]).

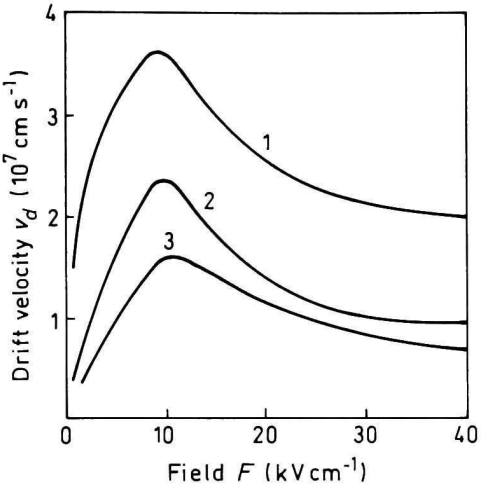

Fig. 8.3.9. Field dependences of the electron drift velocity at different temperatures. Curve 1 – 77 K (Gonzalez Sanchez *et al.* [1992]). Curve 2 – 300 K, Curve 3 – 500 K (Fawcett and Hill [1975]).

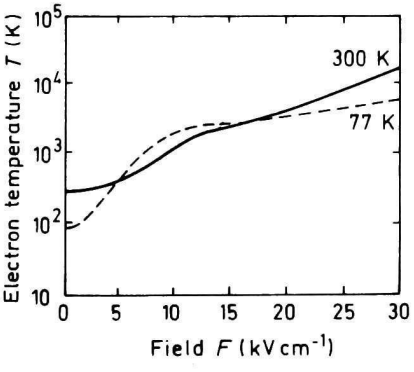

Fig. 8.3.10. Electron temperature versus electric field for 77 K and 300 K (Maloney and Frey [1977]).

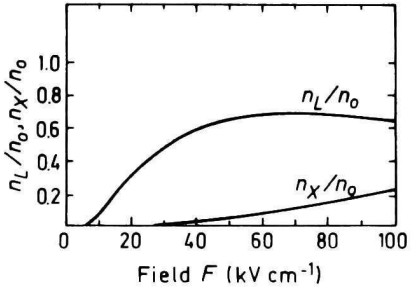

Fig. 8.3.11. Fraction of electrons in L and X valleys n_L/n_0 and n_X/n_0 as a function of electric field, 300 K (Borodovskii and Osadchii [1987]).

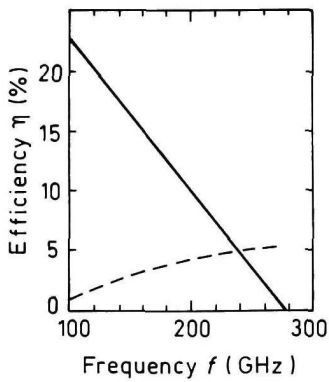

Fig. 8.3.12. Frequency dependence of the efficiency η at the first (solid line) and at the second (dashed line) harmonics in LSA mode. Monte Carlo simulation.

$$F = F_0 + F_1 \times \sin 2\pi f t + F_2 \left(\sin 4\pi f t + \frac{3\pi}{2} \right) .$$

$F_0 = F_1 = 35\,\mathrm{kV\,cm^{-1}}$, $F_2 = 10.5\,\mathrm{kV\,cm^{-1}}$ (Borodovskii and Osadchii [1987]).

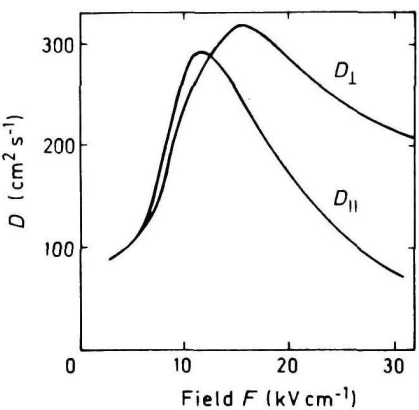

Fig. 8.3.13. Longitudinal ($D \parallel F$) and transverse ($D \perp F$) electron diffusion coefficients at 300 K. Ensemble Monte Carlo simulation (Aishima and Fukushima [1983]).

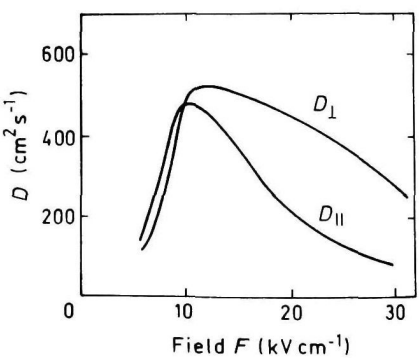

Fig. 8.3.14. Longitudinal ($D \parallel F$) and transverse ($D \perp F$) electron diffusion coefficients at 77 K. Ensemble Monte Carlo simulation (Aishima and Fukushima [1983]).

8.3.3. *Impact Ionization*

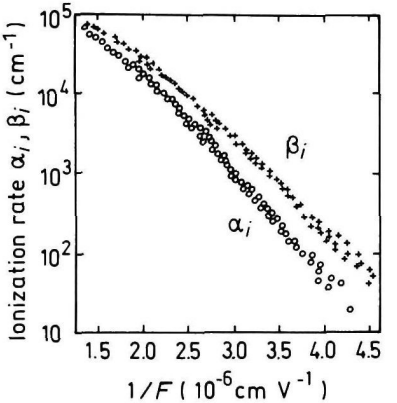

Fig. 8.3.15. The dependences of ionization rates for electrons α_i and holes β_i versus $1/F$, 300 K (Cook *et al.* [1982]).

The dependence of ionization rates α_i and β_i on crystal orientation has not been found.

At 300 K, and $2.2 \times 10^5\,\mathrm{V\,cm^{-1}} \leq F \leq 8 \times 10^5\,\mathrm{V\,cm^{-1}}$

For electrons

$$\alpha_i = \alpha_0 \times \exp[\delta_n - \sqrt{\delta_n^2 + (F_{no}/F)^2}\,] \tag{8.3.1}$$

where $\alpha_o = 5.5 \times 10^5\ \mathrm{cm^{-1}}$, $\delta_n = 2.88$, $F_{no} = 3.04 \times 10^6\,\mathrm{V\,cm^{-1}}$.

For holes

$$\beta_i = \beta_0 \times \exp[\delta_p - \sqrt{\delta_p^2 + (F_{po}/F)^2}\,] \tag{8.3.2}$$

where $\beta_o = 2.42 \times 10^5\ \mathrm{cm^{-1}}$, $\delta_p = 6.80$, $F_{po} = 3.14 \times 10^6\ \mathrm{V\ cm^{-1}}$ (Kyuregyan and Yurkov [1989]).

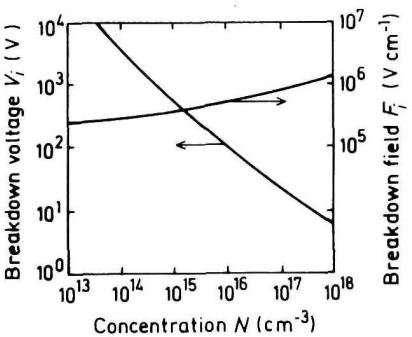

Fig. 8.3.16. Breakdown voltage and breakdown field versus doping density of an abrupt *p-n* junction, 300 K (Kyuregyan and Yurkov [1989]).

8.3.4. *Recombination Parameters*

Pure *n*-type material ($n_0 \simeq 10^{14}\,\mathrm{cm}^{-3}$)

The longest lifetime of holes	$\tau_p \sim 3 \times 10^{-6}\,\mathrm{s}$
Diffusion length $L_p = (D_p \times \tau_p)^{1/2}$	$L_p \sim 40\,\mu\mathrm{m}$

Pure *p*-type material ($p_0 \simeq 10^{15}\,\mathrm{cm}^{-3}$)

(a) Low injection level

The longest lifetime of electrons	$\tau_n \sim 2 \times 10^{-9}\,\mathrm{s}$
Diffusion length $L_n = (D_n \times \tau_n)^{1/2}$	$L_n \sim 8\,\mu\mathrm{m}$

(b) High injection level (filled traps)

The longest lifetime of electrons	$\tau \sim 10^{-8}\,\mathrm{s}$
Diffusion length L_n	$L_n \sim 25\,\mu\mathrm{m}$

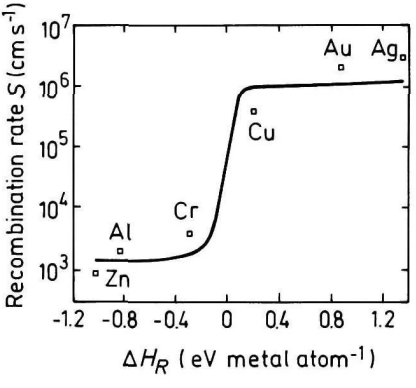

Fig. 8.3.17. Surface recombination velocity versus the heat of reaction per atom of each metal phosphide ΔH_R (*Rosenwaks et al.* [1990]).

If the surface Fermi level E_{FS} is pinned close to midgap ($E_{FS} \simeq E_g/2$) the surface recombination velocity increases from $\sim 5 \times 10^3\,\mathrm{cm\,s}^{-1}$ for doping level $n_0 \sim 3 \times 10^{15}\,\mathrm{cm}^{-3}$ to $\sim 10^6\,\mathrm{cm\,s}^{-1}$ for doping level $n_0 \sim 3 \times 10^{18}\,\mathrm{cm}^{-3}$ (Bothra *et al.* [1991]).

Radiative recombination coefficient	$300\,\mathrm{K} - 1.2 \times 10^{-10}\mathrm{cm}^3\,\mathrm{s}^{-1}$
Auger coefficient	$300\,\mathrm{K} - \sim 9 \times 10^{-31}\mathrm{cm}^6\,\mathrm{s}^{-1}$

8.4. Optical Properties

Infrared refractive index

$$n_\infty = (k_\infty)^{1/2} = 3.075 \times (1 + 2.7 \times 10^{-5}\ T) \tag{8.4.1}$$

For 300 K $n_\infty = 3.1$

Long-wave TO phonon energy at 300 K $\quad \hbar\nu_{TO} = 38.1$ meV

Long-wave LO phonon energy at 300 K $\quad \hbar\nu_{LO} = 42.6$ meV

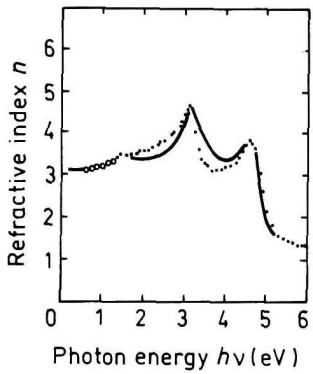

Fig. 8.4.1. Refractive index n versus photon energy. Solid curve is theoretical calculation. Points represent experimental data, 300 K (Adachi [1989]).

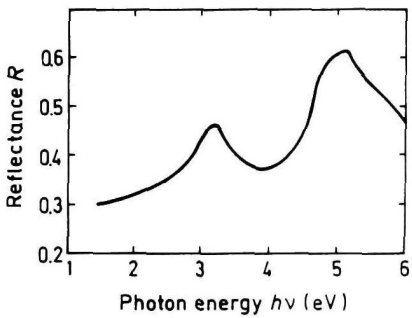

Fig. 8.4.2. Normal incidence reflectivity versus photon energy, 300 K (Aspnes and Studna [1983]).

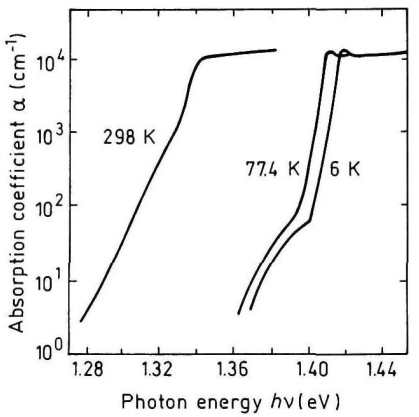

Fig. 8.4.3. Intrinsic absorption coefficient near the intrinsic absorption edge for different temperatures. n – InP. $n_0 = 5 \times 10^{15}\,\mathrm{cm}^{-3}$ (Turner *et al.* [1964]).

A ground state Rydberg energy $R_{X1} = 5.0$ meV.

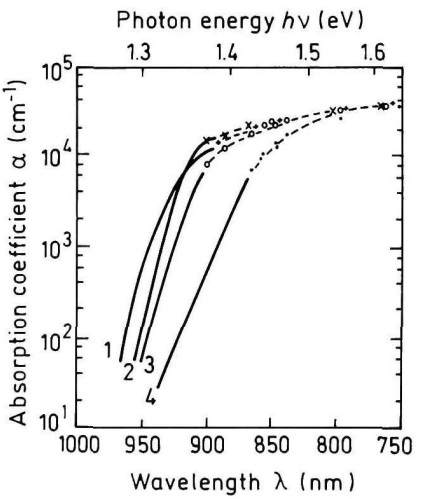

Fig. 8.4.4. Intrinsic absorption edge at 296 K at different doping levels (Burkhard *et al.* [1982]). 1. p-type sample, $p_0 = 1.1 \times 10^{18}\,\mathrm{cm}^{-3}$, $2 \div 4$. n-type samples, 2. $n_0 = 7.4 \times 10^{16}\,\mathrm{cm}^{-3}$, 3. $n_0 = 1.9 \times 10^{18}\,\mathrm{cm}^{-3}$, 4. $n_0 = 7 \times 10^{18}\,\mathrm{cm}^{-3}$.

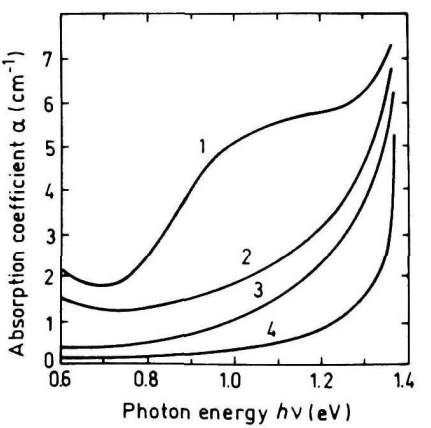

Fig. 8.4.5. Intrinsic absorption edge at 77 K for n-InP at different doping levels (Bugajski and Lewandowski [1985]). 1. $n_0 = 10^{19}\,\mathrm{cm}^{-3}$, 2. $n_0 = 5 \times 10^{18}\,\mathrm{cm}^{-3}$, 3. $n_0 = 2 \times 10^{18}\,\mathrm{cm}^{-3}$, 4. $n_0 = 9.6 \times 10^{16}\,\mathrm{cm}^{-3}$.

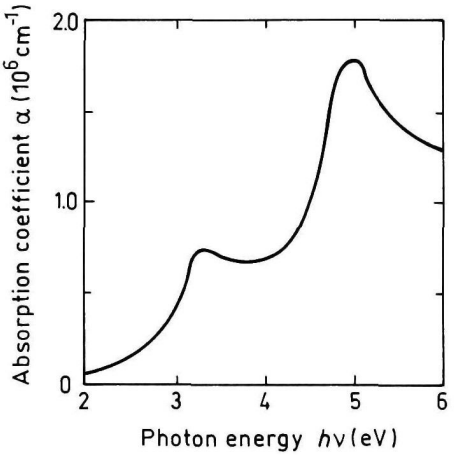

Fig. 8.4.6. The absorption coefficient versus photon energy, 300 K (Aspnes and Studna [1983]).

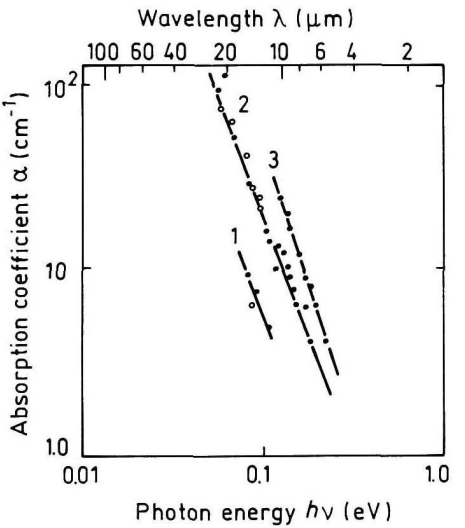

Fig. 8.4.7. Free carrier absorption versus photon energy at different doping levels, 300 K (Newman [1958]). Electron concentration n_0 (cm^{-3}): 1. 4×10^{16}, 2. 2×10^{17}, 3. 4×10^{17}.

8.5. Thermal Properties

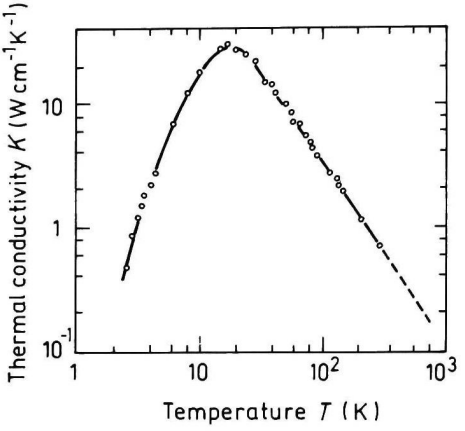

Fig. 8.5.1. Temperature dependence of thermal conductivity. n-type samples, $n_0 = 2 \times 10^{16}\,\mathrm{cm}^{-3}$ (Aliev *et al.* [1965]).

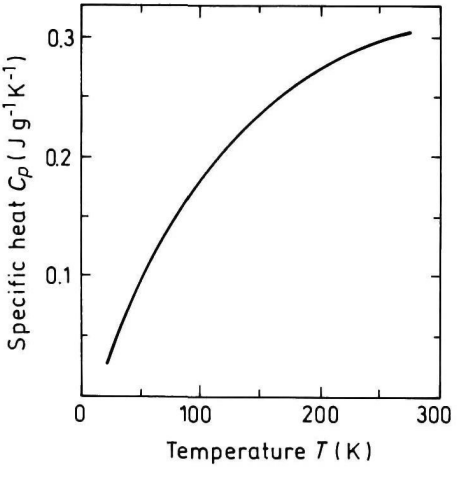

Fig. 8.5.2. Temperature dependence of specific heat at constant pressure (Piesbergen [1963]).

For $298 < T < 910$ K

$$C_p = 0.28 + 10^{-4} \times T \qquad (\mathrm{J\,g^{-1}\,K^{-1}})$$

(Barin *et al.* [1977]).

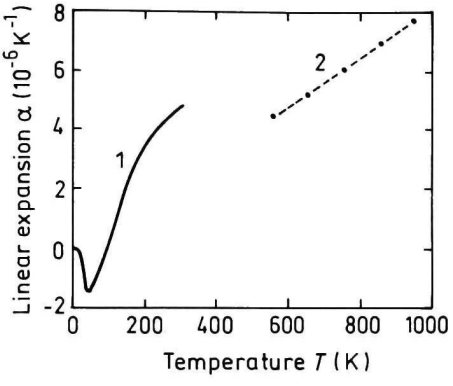

Fig. 8.5.3. Temperature dependence of linear expansion coefficient α. 1. Soma *et al.* [1982], 2. Glazov *et al.* [1977].

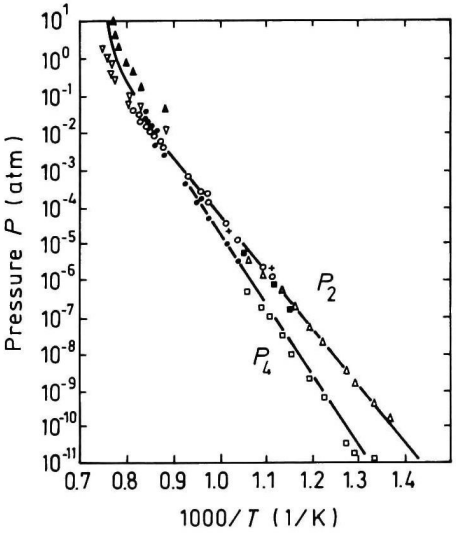

Fig. 8.5.4. Temperature dependences of saturation vapor pressure (Panish and Arthur [1970]).

Melting point $T_m = 1333\,\mathrm{K}$

For $0 < P < 40$ kbar

$$T_m = 1333 - 2.0 \times P \ (P \text{ in kbar}).$$

(Glazov *et al.* [1977]).

8.6. Mechanical Properties, Elastic Constants, Lattice Vibrations, Other Properties

Density	$4.81\ \mathrm{g\,cm^{-3}}$
Surface microhardness (using Knoop's pyramid test)	$\sim 460\ \mathrm{kg\,mm^{-2}}$
Cleavage plane	{100}

Elastic constants at 300 K (in units of $10^{11}\ \mathrm{dyn\,cm^{-2}}$):
$C_{11} = 10.11$; $C_{12} = 5.61$; $C_{44} = 4.56$ (Nichols *et al.* [1980]).

Bulk modulus	$B_s = 7.11 \times 10^{11}\ \mathrm{dyn\,cm^{-2}}$
Shear modulus	$C' = 2.25 \times 10^{11}\ \mathrm{dyn\,cm^{-2}}$
[100] Young's modulus	$Y_0 = 6.11 \times 10^{11}\ \mathrm{dyn\,cm^{-2}}$
[100] Poisson ratio	$\sigma_0 = 0.36$

Acoustic Wave Speeds

Wave propagation direction	Wave character	Expression for wave speed	Wave speed (in units of $10^5\ \mathrm{cm\,s^{-1}}$)
[100]	V_L	$(C_{11}/\rho)^{1/2}$	4.58
	V_T	$(C_{44}/\rho)^{1/2}$	3.08
[110]	V_l	$[(C_{11} + C_{12} + 2C_{44})/2\rho]^{1/2}$	5.08
	$V_{t\parallel}$	$V_{t\parallel} = V_T = (C_{44}/\rho)^{1/2}$	3.08
	$V_{t\perp}$	$[(C_{11} - C_{12})/2\rho]^{1/2}$	2.16
[111]	V_l'	$[(C_{11} + 2C_{12} + 4C_{44})/3\rho]^{1/2}$	5.23
	V_t'	$[(C_{11} - C_{12} + C_{44})/3\rho]^{1/2}$	2.51

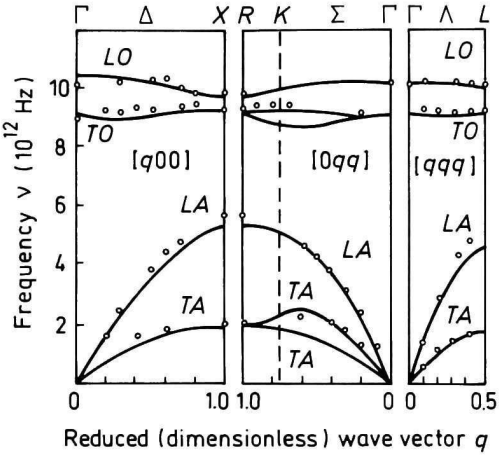

Fig. 8.6.1. Room temperature dispersion curves for acoustic and optical branch phonons. Solid lines are calculated according to overlap shell model (Borcherds *et al.* [1975]).

Phonon frequencies (in units of 10^{12} Hz) (Suto and Nashizawa [1990])

$\nu_{TO}(\Gamma)$	9.2	$\nu_{LO}(X)$	9.95
$\nu_{LO}(\Gamma)$	10.3	$\nu_{TA}(L)$	1.65
$\nu_{TA}(X)$	2.05	$\nu_{LA}(L)$	5.0
$\nu_{LA}(X)$	5.8	$\nu_{TO}(L)$	9.5
$\nu_{TO}(X)$	9.7	$\nu_{LO}(L)$	10.2

Piezoelectric constant: e_{14} $\quad -3.5 \times 10^{-2}\,\mathrm{C\,m^{-2}}$

References

Adachi, S., *J. Appl. Phys.* **66**, 12 (1989) 6030–6040.

Aliev, S. A., A. Ya. Nashelskii, and S. S. Shalyt, *Sov. Phys. Solid State* **7**, (1965) 1287.

Anderson, D. A., N. Apsley, P. Davies, and P. L. Giles, *J. Appl. Phys.* **58**, 8 (1985) 3059–3067.

Aishima, A. and Y. Fukushima, *Jpn. J. Appl. Phys.* **22**, 8 (1983) 1290–1293.

Aspnes, D. E. and A. A. Studna, *Phys. Rev.* **B27**, 2 (1983) 985–1009.

Barin, I., O. Knacke, and O. Kubaschewski, *Thermal Properties of Inorganic Substances*, Springer, Berlin, 1977.

Borcherds, P. H., G. F. Alfrey, D. H. Saunderson, and A. D. B. Woods, *J. Phys.* **C8**, 13 (1975) 2022–2030.

Borodovskii, P. A. and V. M. Osadchii, *Intervalley Transfer of Electrons in A_3B_5 Semiconductors*, Inst. of Semiconductor Physics, Novosibirsk, 1987, p. 170 (in Russian).

Bothra, S., S. Tyagi, S. K. Chandhi, and J. M. Borrego, *Solid State Electron.* **34**, 1 (1991) 47–50.

Bugajski, M. and W. Lewandowski, *J. Appl. Phys.* **57**, 2 (1985) 521–530.

Burkhard, H., H. W. Dinges, and E. Kuphal, *J. Appl. Phys.* **53**, 1 (1982) 655–662.

Cook, L. W., G. E. Bulman, and G. E. Stillman, *Appl. Phys. Lett.* **40**, 7 (1982) 589–591.

Fawcett, W. and G. Hill, *Electron. Lett.* **11**, 4 (1975) 80–81.

Galavanov, V. V. and N. V. Siukaev, *Phys. Status Solidi* **38**, 2 (1970) 523–530.

Glazov, V. M., K. Davletov, A. Ya. Nashelskii, and M. M. Mamedov, *Zh. Fiz. Khim.* **51**, 10 (1977) 2558–2561 (in Russian).

Gonzalez Sanchez, T., J. E. Velazquez Perez, P. M. Gutierrez Conde, and D. Pardo, *Semicond. Sci. Technol.* **7**, 1 (1992) 31–36.

Hilsum, C., *Electron. Lett.* **10**, 13 (1974) 259–260.

Jain, S. C., J. M. McGregor, and D. J. Roulston, *J. Appl. Phys.* **68**, 7 (1990) 3747–3749.

Kohanyuk, M. B., G. L. Lyakhu, I. P. Molodyan, and E. V. Russu, *Indium Phosphide in Semiconductor Electronics*, S. I. Radaucan, ed., Shtinca, Kishinev, 1988, pp. 200–222 (in Russian).

Kushwaha, M. S. and S. S. Kushwaha, *Can. J. Phys.* **58**, 3 (1980) 351–358.

Kyuregyan, A. S. and S. N. Yurkov, *Sov. Phys. Semicond.* **23**, 10 (1989) 1126–1132.

Maloney, T. J. and J. Frey, *J. Appl. Phys.* **48**, 2 (1977) 781–787.

Newman, R., *Phys. Rev.* **111**, 6 (1958) 1518–1521.

Nichols, D. N., D. S. Rimai, and R. J. Sladek, *Solid State Commun.* **36**, 8 (1980) 667–669.

Panish, M. B. and J. R. Arthur, *J. Chem. Thermodyn.* **2**, (1970) 299.

Piesbergen, U., *Z. Naturforschung* **18a**, 2 (1963) 141–147.

Razeghi, M., Ph. Maurel, M. Defour, F. Omnes, G. Neu, and A. Kozacki, *Appl. Phys. Lett.* **52**, 2 (1988) 117–119.

Rosenwaks, Y., Y. Shapira, and D. Huppert, *Appl. Phys. Lett.* **57**, 24 (1990) 2552–2554.

Soma, T., J. Satoh, and H. Matsuo, *Solid State Commun.* **42**, 12 (1982) 889–892.

Turner, W. J., W. E. Reese, and G. D. Pettit, *Phys. Rev.* **136**, 5A (1964) A1467–1470.

Walukiewicz, W., J. Lagowskii, L. Jastrzebski, P. Rava, M. Lichtensteiger, C. H. Gatos, and H. C. Gatos, *J. Appl. Phys.* **51**, 5 (1980) 2659–2668.

Wiley, J. D., *Semiconductor and Semimetals*, R. K. Willardson and A. C. Beer, eds., Academic Press, N.Y., vol. 10, 1975, p. 162.

Windhorn, T. H., L. W. Cook, M. A. Haase, and G. E. Stillman, *Appl. Phys. Lett.* **42**, 8 (1983) 725–727.

CHAPTER 9

INDIUM ANTIMONIDE (InSb)

Yu. A. Goldberg
Ioffe Institute,
St. Petersburg, Russia

9.1. Basic Parameters

9.1.1. *Basic Parameters at 300 K*

Crystal structure		Zinc Blende
Group of symmetry		T_d^2–F$\bar{4}$3m
Number of atoms in 1 cm^3		2.94×10^{22}
Debye temperature	(K)	160
Density	(g cm^{-3})	5.77
Dielectric constant		
static		16.8
high frequency		15.7
Effective electron masses	(in units of m_o)	0.014
Effective hole masses	(in units of m_o)	
heavy		0.43
light		0.015
Electron affinity	(eV)	4.59
Lattice constant	(Å)	6.479
Optical phonon energy	(eV)	0.025

Band structure and carrier concentration

Energy gap	(eV)	0.17
Energy separation ($E_{\Gamma L}$) between Γ and L valleys	(eV)	0.51
Energy separation ($E_{\Gamma X}$) between Γ and X valleys	(eV)	0.83
Energy spin-orbital splitting	(eV) ($\Gamma_{8V} - \Gamma_{7V}$)	0.80
Intrinsic carrier concentration	(cm^{-3})	2×10^{16}
Intrinsic resistivity	($\Omega \times cm$)	4×10^{-3}
Effective conduction band density of states	(cm^{-3})	4.2×10^{16}
Effective valence band density of states	(cm^{-3})	7.3×10^{18}

Electrical properties

Breakdown field	($V\,cm^{-1}$)	$\simeq 10^3$
Mobility	($cm^2\,V^{-1}\,s^{-1}$)	
electrons		$\leq 7.7 \times 10^4$
holes		≤ 850
Diffusion coefficient	($cm^2\,s^{-1}$)	
electrons		$\leq 2 \times 10^3$
holes		≤ 22
Electron thermal velocity	($m\,s^{-1}$)	9.8×10^5
Hole thermal velocity	($m\,s^{-1}$)	1.8×10^5

Optical properties

Infrared refractive index	4.0
Radiative recombination coefficient ($cm^3\,s^{-1}$)	5×10^{-11}

Thermal and mechanical properties

Bulk modulus	($dyn\,cm^{-2}$)	4.7×10^{11}
Melting point	(°C)	527
Specific heat	($J\,g^{-1}\,°C^{-1}$)	0.2
Thermal conductivity	($W\,cm^{-1}\,°C^{-1}$)	0.18
Thermal diffusivity	($cm^2\,s^{-1}$)	0.16
Thermal expansion, linear	($°C^{-1}$)	5.37×10^{-6}

9.1.2. *Basic Parameters at 77 K*

Debye temperature	(K)	220
Lattice constant	(Å)	6.472

Band structure and carrier concentration

Energy gap	(eV)	0.23
Intrinsic carrier concentration	(cm^{-3})	1×10^9
Intrinsic resistivity	($\Omega \times cm$)	5.2×10^3
Effective conduction band density of states	(cm^{-3})	5.4×10^{15}
Effective valence band density of states	(cm^{-3})	9.5×10^{17}

Electrical properties

Breakdown field	($V\,cm^{-1}$)	$\simeq 2.5 \times 10^2$
Mobility	($cm^2\,V^{-1}\,s^{-1}$)	
electrons		$\leq 1.2 \times 10^6$
holes		$\leq 10^4$
Diffusion coefficient	($cm^2\,s^{-1}$)	
electrons		$\leq 8 \times 10^3$
holes		≤ 65
Electron thermal velocity	($m\,s^{-1}$)	5×10^5
Hole thermal velocity	($m\,s^{-1}$)	0.9×10^5

Optical properties

Infrared refractive index	3.9
Radiative recombination coefficient ($cm^3\,s^{-1}$)	2.5×10^{-9}

Thermal and mechanical properties

Specific heat	($J\,g^{-1}\,°C^{-1}$)	0.14
Thermal conductivity	($W\,cm^{-1}\,°C^{-1}$)	1.0
Thermal diffusivity	($cm^2\,s^{-1}$)	1.24
Thermal expansion, linear	($°C^{-1}$)	1.6×10^{-6}

9.2. Band Structure and Carrier Concentration

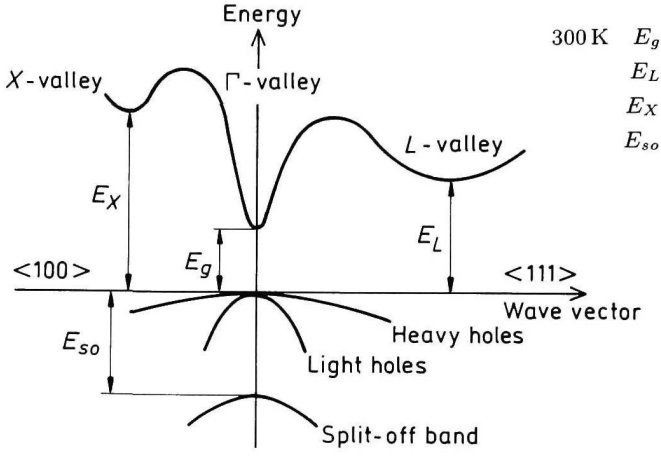

Fig. 9.2.1. Band structure of InSb. Important minima of the conduction band and maxima of the valence band.

9.2.1. *Temperature Dependences*

Temperature dependence of the energy gap (Littler and Seiger [1985])

$$E_g = 0.24 - 6 \times 10^{-4} \times \frac{T^2}{T + 500} \text{ (eV)} , \tag{9.2.1}$$

where T is temperature in degrees K ($0 < T < 300$).

Effective density of states in the conduction band

$$N_c \simeq 8 \times 10^{12} \times T^{3/2} \text{ (cm}^{-3}\text{)} \tag{9.2.2}$$

Effective density of states in the valence band

$$N_v \simeq 1.4 \times 10^{15} \times T^{3/2} \text{ (cm}^{-3}\text{)} . \tag{9.2.3}$$

Intrinsic carrier concentration

$$n_i = (N_c \times N_v)^{1/2} \times \exp\left(-\frac{E_g}{2k_B \times T}\right) . \tag{9.2.4}$$

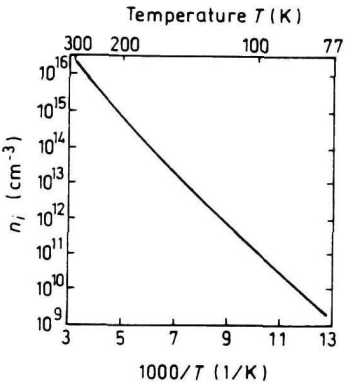

Fig. 9.2.2. The temperature dependence of the intrinsic carrier concentration.

For $200\,\mathrm{K} < T < 800\,\mathrm{K}$

$$n_i \simeq 2.9 \times 10^{11}(2400 - T)^{3/4} \times (1 + 2.7 \times 10^{-4} \times T) \times T^{1.5}$$
$$\times \exp\left(-\frac{0.129 - 1.5 \times 10^{-4}\,T}{k_B \times T}\right) \ (\mathrm{cm}^{-3}) \tag{9.2.5}$$

(Oszwaldowski and Zimpel [1988]).

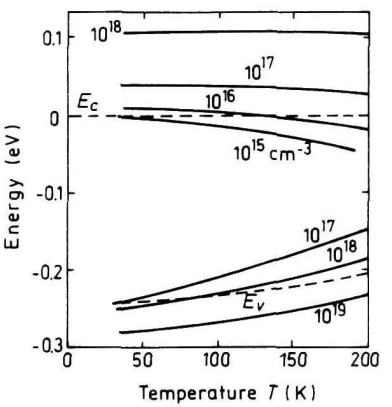

Fig. 9.2.3. Fermi level versus temperature for different concentrations of shallow donors and acceptors.

9.2.2. *Dependences on Hydrostatic Pressure*

$$E_g \simeq E_g(0) + 13.7 \times 10^{-3}\ P - 3.6 \times 10^{-5}\ P^2 \text{ (eV)},$$
$$E_L \simeq E_L(0) + 4.7 \times 10^{-3}\ P - 1.1 \times 10^{-5}\ P^2 \text{ (eV)}, \qquad (9.2.6)$$
$$E_X \simeq E_X(0) - 3.5 \times 10^{-3}\ P + 0.64 \times 10^{-5}\ P^2 \text{ (eV)},$$

where P is pressure in kbar (Van Camp *et al.* [1990]).

9.2.3. *Effective Masses*

Electrons

For Γ-valley $m_\Gamma = 0.014 m_0$

Non-parabolicity $E(1 + \alpha E) = \dfrac{h^2 k^2}{2 m_\Gamma}$; $\alpha = 4.1\ (\text{eV})^{-1}$

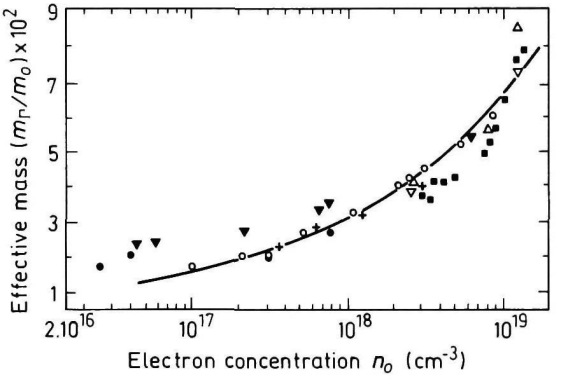

Fig. 9.2.4. Electron effective mass versus electron concentration (Zawadzki [1974]).

In the L-valley, effective mass of density of states $m_L = 0.25 m_0$

Holes

heavy	$m_h = 0.43 m_0$
light	$m_{lp} = 0.015 m_0$
split-off band	$m_{so} = 0.19 m_0$

Effective mass of density of states $m_v = 0.43 m_0$

9.2.4. *Donors and Acceptors*

Ionization energies of shallow donors ~ 0.0007 (eV): Se, S, Te.

Ionization energies of shallow acceptors (eV):

Cd	0.01
Zn	0.01
Cr	0.07
Cu°	0.028
Cu^{-}	0.056

9.3. Electrical Properties

9.3.1. *Mobility and Hall Effect*

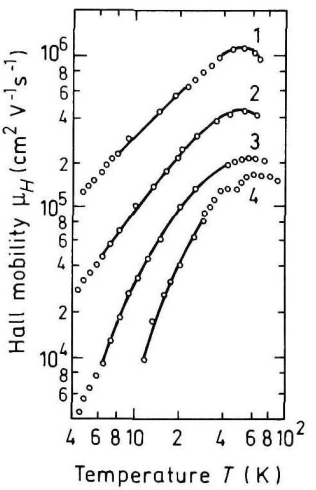

Fig. 9.3.1. Electron Hall mobility versus temperature for different doping levels and different compensation ratios $\theta = N_a/N_d$.
1. $N_d = 3.85 \times 10^{14}\,\mathrm{cm}^{-3}$, $\theta = 0.5$
2. $N_d = 8.5 \times 10^{14}\,\mathrm{cm}^{-3}$, $\theta = 0.88$
3. $N_d = 9.5 \times 10^{14}\,\mathrm{cm}^{-3}$, $\theta = 0.98$
4. $N_d = 1.35 \times 10^{15}\,\mathrm{cm}^{-3}$, $\theta = 0.99$
(Yaremenko *et al.* [1973]).

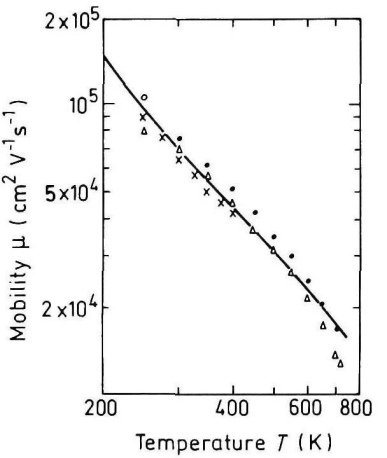

Fig. 9.3.2. Electron mobility versus temperature (high temperatures).
Solid line is theoretical calculation for electron drift mobility. Experimental data are Hall mobilities. (Rode [1971]).

For pure n-InSb at $T \geq 200\,\mathrm{K}$

$$\mu_{nH} \simeq 7.7 \times 10^4 \times \left(\frac{T}{300}\right)^{-1.66} \quad (\mathrm{cm}^2\,\mathrm{V}^{-1}\,\mathrm{s}^{-1}).$$

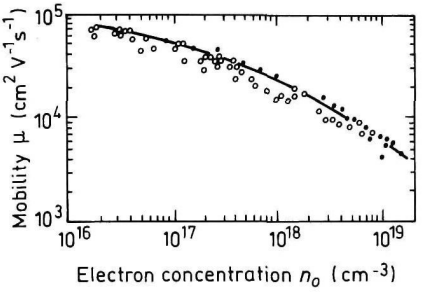

Fig. 9.3.3. Electron mobility versus electron concentration, 300 K (Litwin–Staszewska *et al.* [1981]).

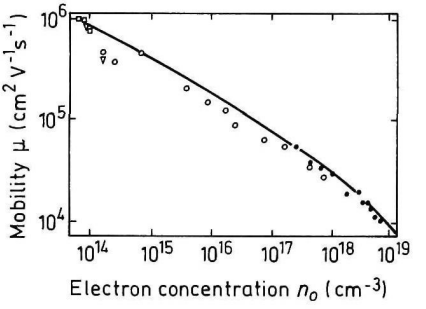

Fig. 9.3.4. Electron mobility versus electron concentration, 77 K (Litwin–Staszewska *et al.* [1981]).

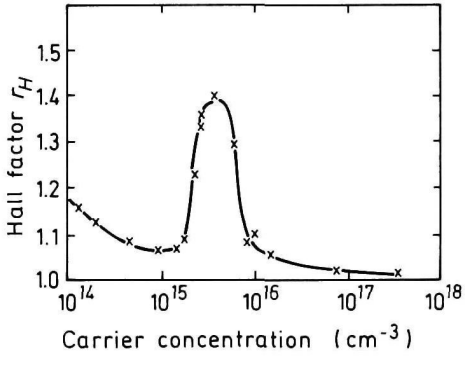

Fig. 9.3.5. The electron Hall factor versus carrier concentration, 77 K (Baranskii and Gorodnichii [1969]).

Maximal electron mobility for pure n-InSb
77 K – 1.2×10^6 cm^2 V^{-1} s^{-1}
300 K – 7.7×10^4 cm^2 V^{-1} s^{-1}

Maximal electron mobility for InSb grown on GaAs substrate
77 K – 1.5×10^5 cm^2 V^{-1} s^{-1} ($n_0 = 2.2 \times 10^{15}$ cm^{-3})
300 K – 7.0×10^4 cm^2 V^{-1} s^{-1} ($n_0 = 2.0 \times 10^{16}$ cm^{-3})

Maximal electron mobility for InSb grown on InP substrate
77 K – 1.1×10^5 cm^2 V^{-1} s^{-1}
300 K – 7.0×10^4 cm^2 V^{-1} s^{-1}

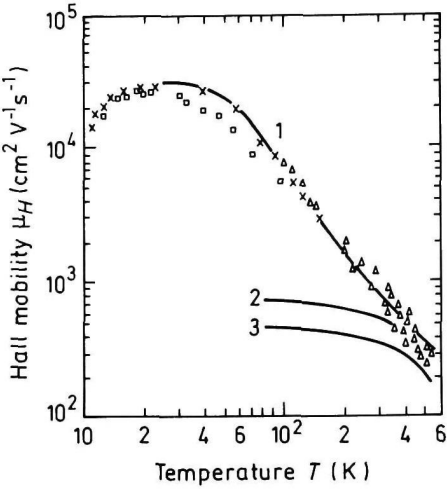

Fig. 9.3.6. Hole Hall mobility versus temperature for different hole concentrations. p_0 (cm^{-3}): 1. 8×10^{14}, 2. 3.15×10^{18}, 3. 2.5×10^{19} (Zimpel *et al.* [1989] and Filipchenko and Bolshakov [1976]).

For pure p-InSb at $T > 60\,\mathrm{K}$

$$\mu_{pH} \simeq 850 \times \left(\frac{T}{300}\right)^{-1.8} (\mathrm{cm^2\,V^{-1}\,s^{-1}}).$$

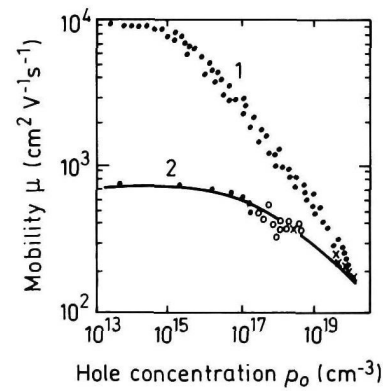

Fig. 9.3.7. Hall mobility versus hole concentration: 1. 77 K (Filipchenko and Bolshakov [1976]), 2. 290 K (Wiley [1975]).

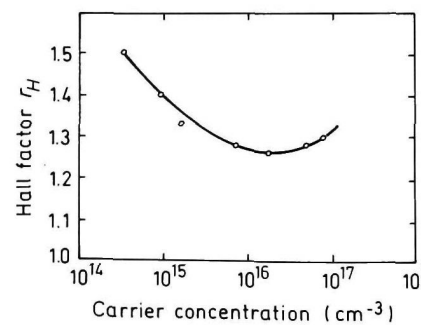

Fig. 9.3.8. The hole Hall factor versus carrier concentration, 77 K (Baranskii and Gorodnichii [1969]).

9.3.2. *Transport Properties in High Electric Field*

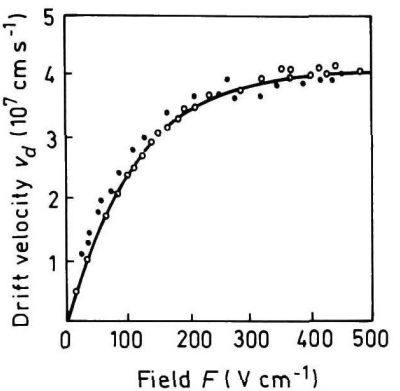

Fig. 9.3.9. Field dependence of the electron drift velocity, 77 K. The solid line is the Monte Carlo calculation. Points are experimental data (Asauskas *et al.* [1980]).

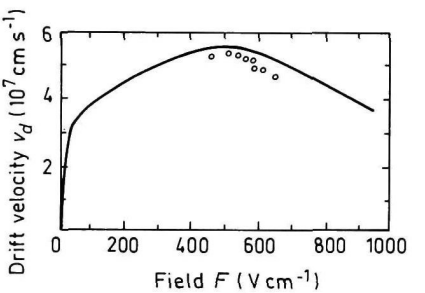

Fig. 9.3.10. Field dependence of the electron drift velocity, 77 K. The solid line is the Monte Carlo calculation. Points show the experimental results (Neukermans and Kino [1973]).

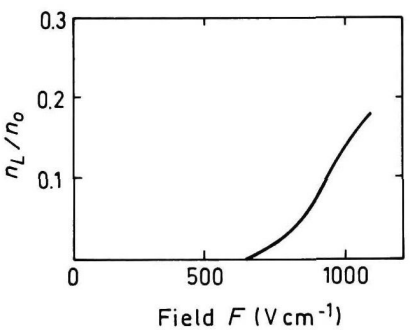

Fig. 9.3.11. Fraction of electrons in the L valley as a function of electric field F, 77 K (Asauskas *et al.* [1980]).

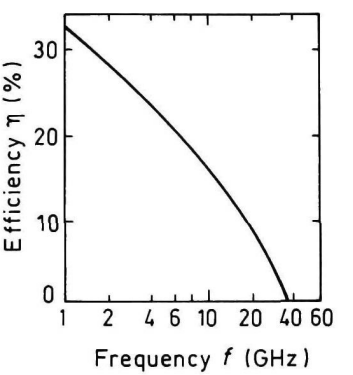

Fig. 9.3.12. Frequency dependence of the efficiency in LSA mode $F_0 = F + F_1 \sin 2\pi ft$: $F_0 = 2.5$ kV cm^{-1} (Prokhorov *et al.* [1977]).

9.3.3. *Impact Ionization*

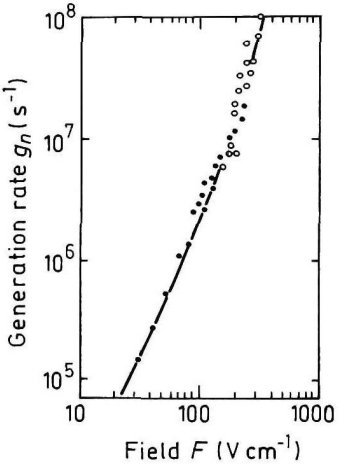

Fig. 9.3.13. The dependence of the generation rate for electrons g_n versus the electric field F, 300 K (Vorobyev *et al.* [1983]).

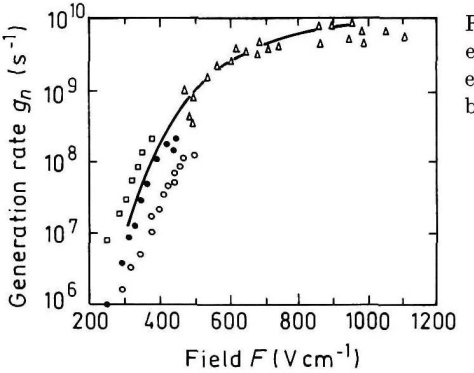

Fig. 9.3.14. The dependence of the generation rate for electrons g_n versus the electric field F, 77 K (Krotkus and Dobrovolskis [1988]).

For 300 K, for $30\,V\,cm^{-1} < F < 300\,V\,cm^{-1}$

$$g_n(F) = 126 \times F^2 \times \exp(F/160) \quad (s^{-1}), \tag{9.3.1}$$

where F is in $V\,cm^{-1}$.

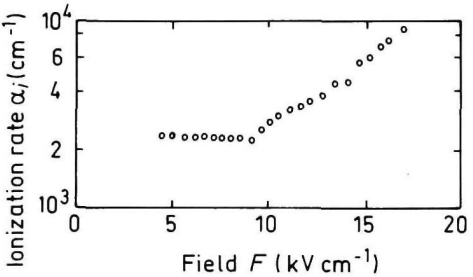

Fig. 9.3.15. The dependence of the ionization rate for electrons α_i versus the electric field F, 78 K (Gavrushko *et al.* [1978]).

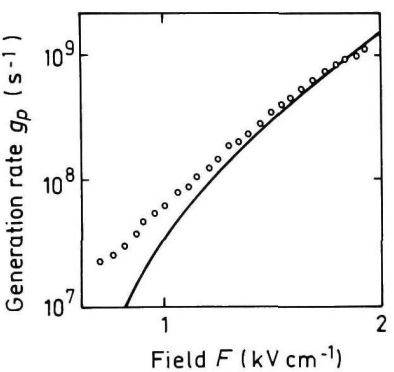

Fig. 9.3.16. The dependence of the generation rate for holes g_p versus the electric field F, 77 K (Adomaitis *et al.* [1985]).

9.3.4. *Recombination Parameters*

For pure InSb at $T \geq 250\,\mathrm{K}$ lifetime of carriers (electrons and holes) is determined by Auger recombination:

$$\tau_n = \tau_p \simeq 1/Cn_i^2 \,, \tag{9.3.2}$$

where $C \simeq 5 \times 10^{-26}\,\mathrm{cm^6\,s^{-1}}$ is the Auger coefficient. n_i is the intrinsic carrier concentration (see Eq. (9.2.5)).

For $T = 300\,\mathrm{K}$

$$\tau_n = \tau_p \simeq 5 \times 10^{-8}\ \mathrm{s}$$

At $T = 77\,\mathrm{K}$ for pure InSb

n-type:	the lifetime of holes	$\tau_p \sim 10^{-6}\,\mathrm{s}$
p-type:	the lifetime of electrons	$\tau_n \sim 10^{-10}\,\mathrm{s}$

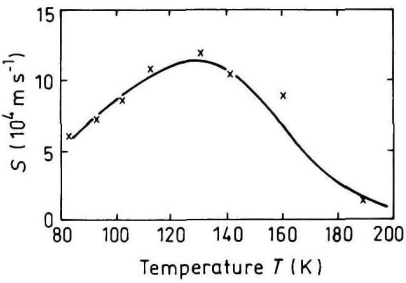

Fig. 9.3.17. Temperature dependence of surface recombination velocity for p-InSb (Euthymiou *et al.* [1981]).

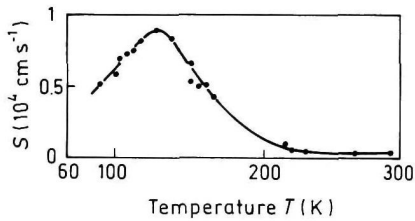

Fig. 9.3.18. Temperature dependence of surface recombination velocity for n-InSb (Skountzos and Euthymiou [1976]).

Radiative recombination coefficient	$B \sim 5 \times 10^{-11}\ \mathrm{cm^3\,s^{-1}}$
Auger coefficient	$C \sim 5 \times 10^{-26}\ \mathrm{cm^6\,s^{-1}}$

9.4. Optical Properties

Infrared refractive index

$$n_\infty = (k_\infty)^{1/2} \simeq 4.0 \quad \text{(for 300 K)} \tag{9.4.1}$$

For $120\,\mathrm{K} < T < 360\,\mathrm{K}$

$$\frac{1}{n_\infty}\frac{dn_\infty}{dT} = 1.6 \times 10^{-4}\ \mathrm{K}^{-1} \tag{9.4.2}$$

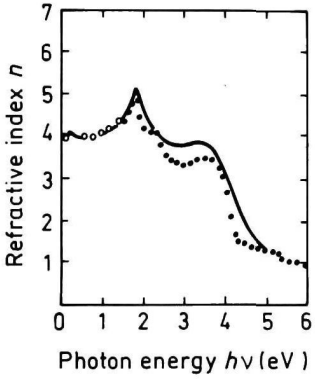

Fig. 9.4.1. Refractive index n versus photon energy, 300 K (Adachi [1989]).

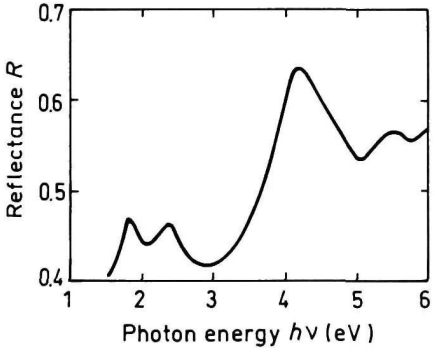

Fig. 9.4.2. Normal incidence reflectivity versus photon energy, 300 K (Aspnes and Studna [1983]).

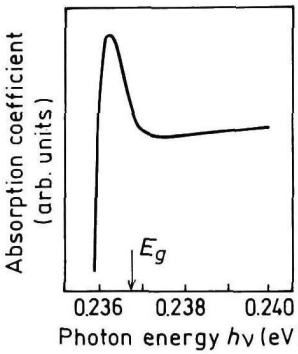

Fig. 9.4.3. Absorption coefficient near the intrinsic absorption edge, $T = 2\,\mathrm{K}$ (Kanskaya *et al.* [1979]).

A ground state Rydberg energy $R_{X1} = 0.5\,\mathrm{meV}$.

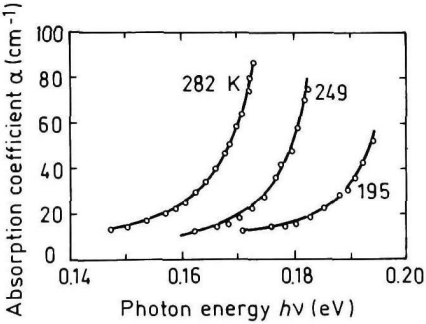

Fig. 9.4.4. Absorption coefficient near the intrinsic absorption edge for different temperatures (Dumke [1957]).

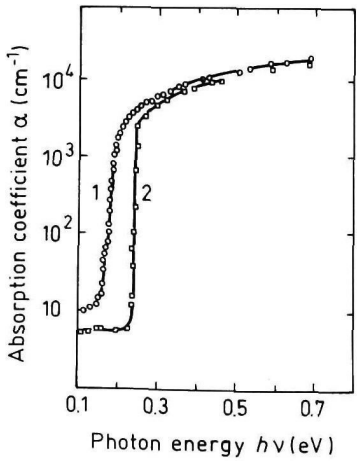

Fig. 9.4.5. Absorption edge of pure InSb. T (K): 1. 298, 2. 5 (Johnson [1967], Gobeli and Fan [1956]).

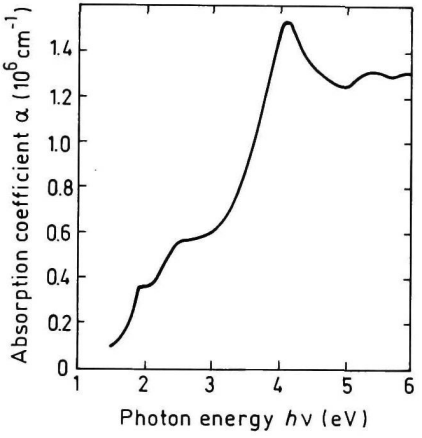

Fig. 9.4.6. Absorption coefficient versus photon energy, $T = 300\,\mathrm{K}$ (Aspnes and Studna [1983]).

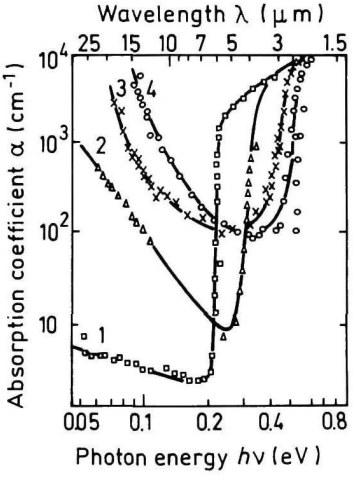

Fig. 9.4.7. Absorption coefficient versus photon energy at different doping levels, n-InSb, $T = 130$ K. $n_0(\mathrm{cm}^{-3})$: 1. 6.6×10^{13}, 2. 7.5×10^{17}, 3. 2.6×10^{18}, 4. 6×10^{18} (Ukhanov [1977]).

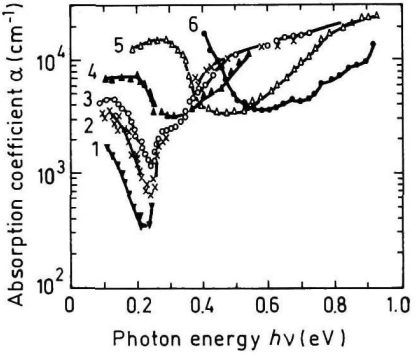

Fig. 9.4.8. Absorption coefficient versus photon energy at different doping levels, p-InSb, $T = 5$ K. $p_0(\mathrm{cm}^{-3})$: 1. 5.5×10^{17}, 2. 9×10^{17}, 3. 1.6×10^{18}, 4. 2.6×10^{18}, 5. 9.4×10^{18}, 6. 2×10^{19} (Gobeli and Fan [1960]).

9.5. Thermal Properties

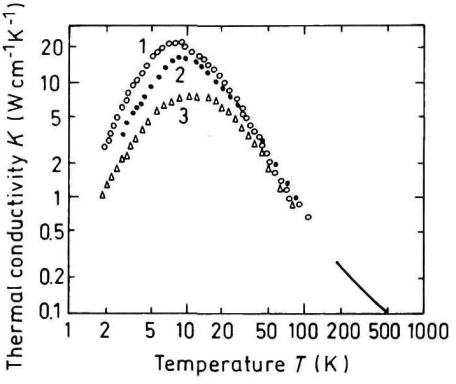

Fig. 9.5.1. Temperature dependences of thermal conductivity for n-InSb. Electron concentration at 78 K $n(cm^{-3})$: 1. 2×10^{14}, 2. 4.8×10^{16}, 3. 4×10^{18} (Kosarev *et al.* [1971]). Solid line shows the temperature dependence of thermal conductivity at high temperatures (Busch and Steigmeier [1961]).

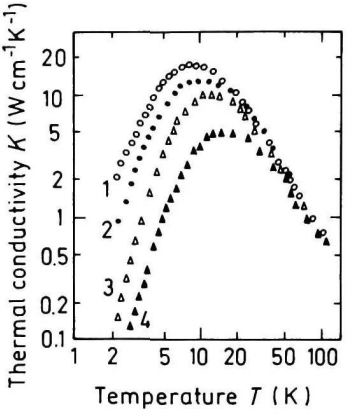

Fig. 9.5.2. Temperature dependences of thermal conductivity for p-InSb. Hole concentration at 78 K $p(cm^{-3})$: 1. 2.7×10^{14}, 2. 5.3×10^{15}, 3. 7.2×10^{17}, 4. 6×10^{18} (Kosarev *et al.* [1971]).

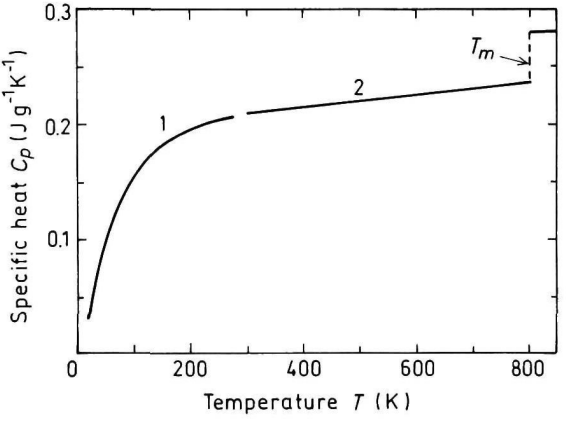

Fig. 9.5.3. Temperature dependences of specific heat at constant pressure. 1. Piesbergen [1963], 2. Okhotin *et al.* [1972].

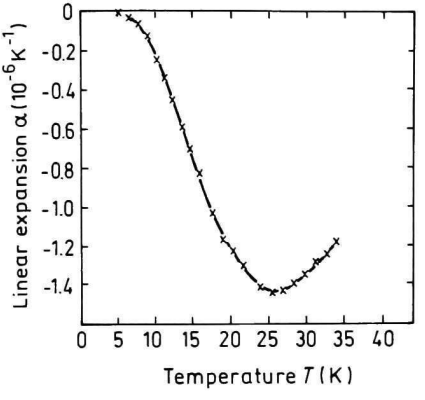

Fig. 9.5.4. Temperature dependence of linear expansion coefficient (low temperatures) (Sparks and Swenson [1967]).

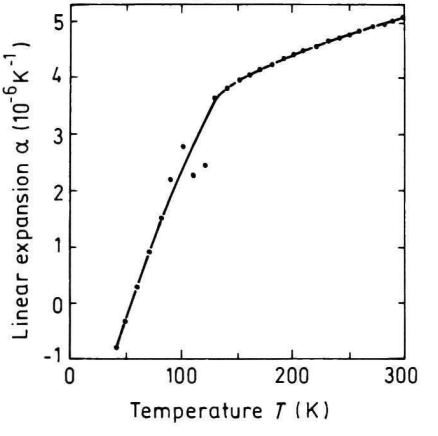

Fig. 9.5.5. Temperature dependence of linear expansion coefficient (high temperatures) (Gibbons [1958]).

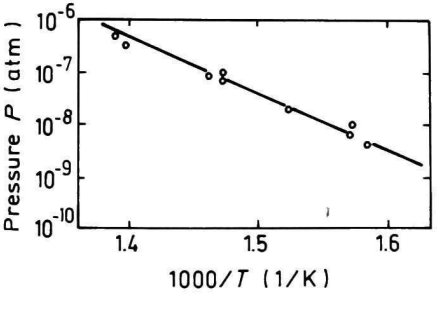

Fig. 9.5.6. Temperature dependence of Sb saturation vapor pressure (Nesmeyanov *et al.* [1960]).

Melting point $T_m = 800\,\mathrm{K}$.

9.6. Mechanical Properties, Elastic Constants, Lattice Vibrations, Other Properties

Density $5.77\ \mathrm{g\,cm^{-3}}$

Surface microhardness
(using Knoop's pyramid test) $220\ \mathrm{kg\,mm^{-2}}$

Cleavage plane {110}, {111}

Elastic constants at 300 K (Slutsky and Garland [1959])

C_{11} $6.67 \times 10^{11}\ \mathrm{dyn\,cm^{-2}}$

C_{12} $3.65 \times 10^{11}\ \mathrm{dyn\,cm^{-2}}$

C_{44} $3.02 \times 10^{11}\ \mathrm{dyn\,cm^{-2}}$

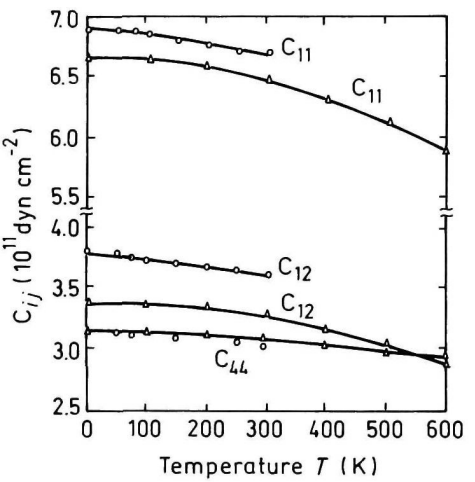

Fig. 9.6.1. Temperature dependences of elastic constants. (Circles – Slutsky and Garland [1959], triangles – Potter [1956]).

For $T = 300\ \mathrm{K}$

Bulk modulus (compressibility^{-1})

$$B_s = \frac{C_{11} + 2C_{12}}{3} \qquad B_s = 4.66 \times 10^{11}\ \mathrm{dyn\,cm^{-2}}$$

Shear modulus

$$C' = (C_{11} - C_{12})/2 \qquad C' = 1.51 \times 10^{11}\ \mathrm{dyn\,cm^{-2}}$$

[100] Young's modulus

$$Y_0 = \frac{(C_{11} + 2C_{12})(C_{11} - C_{12})}{(C_{11} + C_{12})} \qquad Y_0 = 4.09 \times 10^{11}\ \mathrm{dyn\,cm^{-2}}$$

[100] Poisson ratio

$$\sigma_0 = \frac{C_{12}}{C_{11} + C_{12}} \qquad \sigma_0 = 0.35$$

Acoustic Wave Speeds

Wave propagation direction	Wave character	Expression for wave speed	Wave speed (in units of $10^5\,\mathrm{cm\,s^{-1}}$)
[100]	V_L	$(C_{11}/\rho)^{1/2}$	3.4
	V_T	$(C_{44}/\rho)^{1/2}$	2.29
[110]	V_l	$[(C_{11}+C_{12}+2C_{44})/2\rho]^{1/2}$	3.76
	$V_{t\parallel}$	$V_{t\parallel}=V_T=(C_{44}/\rho)^{1/2}$	2.29
	$V_{t\perp}$	$[(C_{11}-C_{12})/2\rho]^{1/2}$	1.62
[111]	V_l'	$[(C_{11}+2C_{12}+4C_{44})/3\rho]^{1/2}$	3.88
	V_t'	$[(C_{11}-C_{12}+C_{44})/3\rho]^{1/2}$	1.87

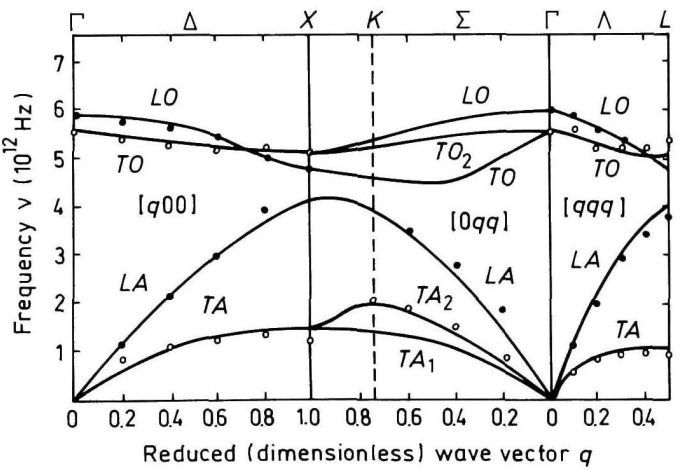

Fig. 9.6.2. Room temperature dispersion curves for acoustics and optical branch phonons. Solid lines are calculated according to the dynamic model (Ram and Kushwaha [1985]).

Phonon frequencies (in unit of 10^{12} Hz) (Price *et al.* [1971])

$\nu_{LO}(\Gamma)$	5.90
$\nu_{TO}(\Gamma)$	5.54
$\nu_{TA}(X_5)$	1.12
$\nu_{LA}(X_3)$	4.30
$\nu_{LO}(X_1)$	4.75
$\nu_{TO}(X_5)$	5.38
$\nu_{TA}(L_3)$	0.98
$\nu_{LA}(L_1)$	3.81
$\nu_{LO}(L_1)$	4.82
$\nu_{TO}(L_3)$	5.31

Piezoelectric constant e_{14}	$-7 \times 10^{-2}\,\mathrm{C\,m^{-2}}$
Electron g-factor:	− 50.6

References

Adachi, S., *J. Appl. Phys.* **66**, 12 (1989) 6030–6040.

Adomaitis, E., Z. Dobrovolskis, and A. Krotkus, *Appl. Phys.* **A38**, 2 (1985) 145–149.

Asauskas, R., Z. Dobrovolskis, and A. Krotkus, *Sov. Phys. Semicond.* **14**, 12 (1980) 1377–1380.

Aspnes, D. E. and A. A. Studna, *Phys. Rev.* **B27**, 2 (1983) 985–1009.

Baranskii, P. I. and O. P. Gorodnichii, *Phys. Status Solidi* **35**, 2 (1969) K123–K126.

Busch, G. and E. Steigmeier, *Helv. Phys. Acta.* **34**, 1 (1961) 1–28.

Dumke, W. P., *Phys. Rev.* **108**, 6 (1957) 1419–1425.

Euthymiou, P. C., P. A. Skountzos, C. E. Ravanos, and B. E. Hadjikontis, *Solid State Commun.* **37**, 9 (1981) 733–736.

Filipchenko, A. S. and L. P. Bolshakov, *Phys. Status Solidi (b)* **77**, 1 (1976) 53–58.

Gavrushko, V. V., O. V. Kosogov, and V. D. Lebedeva, *Sov. Phys. Semicond.* **12**, 12 (1978) 1398–1400.

Gibbons, D. F., *Phys. Rev.* **112**, 1 (1958) 136–140.

Gobeli, G. W. and H. Y. Fan, *Semiconductor Research, Second Quarterly Report*, Purdue Univ., 1956.

Gobeli, G. W. and H. Y. Fan, *Phys. Rev.* **119**, 2 (1960) 613–620.

Johnson, E. J., *Semiconductors and Semimetals*, R. K. Willardson and A. C. Beer, eds., Academic Press, N.Y., vol. 3, 1967, pp. 153–258.

Kanskaya, L. M., S. I. Kokhanosk, R. P. Seisyan and Al. L. Efros, *Sov. Phys. Semicond.* **15**, 9 (1981) 1079–1081.

Kosarev, V. V., P. V. Tamarin, S. S. Shalyt, *Phys. Stat. Solidi (b)* **44**, 2 (1971) 525–530.

Krotkus, A. and Z. Dobrovolskis, *Electrical Conductivity of Narrow-Gap Semiconductors*, Mokslas, Vilnus, 1988, (in Russian).

Littler, C. L., D. G. Seiler, *Appl. Phys. Lett.* **46**, 10 (1985) 986–988.
Litwin-Staszewska, E., W. Szymanska, and P. Piotrzkowski, *Phys. Status Solidi (b)* **106**, 2 (1981) 551–559.
Nesmeyanov, A. N., B. Z. Iofa, and A. S. Polyakov, *Russian J. Inorg. Chem.* **5** (1960) 119.
Neukermans, A. and G. S. Kino, *Phys. Rev.* **B7**, 6 (1973) 2703–2709.
Okhotin, A. S., A. S. Pushkarskii, and V. V. Gorbachev, *Thermophysical Properties of Semiconductors*, Moscow, "Atom" Publ. House, 1972, (in Russian).
Oszwaldowski, M. and M. Zimpel, *J. Phys. Chem. Solids* **49**, 10 (1988) 1179–1185.
Piesbergen, U., *Z. Naturforschung* **18a**, 2 (1963) 141–147.
Potter, R. F., *Phys. Rev.* **103**, 1 (1956) 47–50.
Price, D. L., J. M. Rowe, and R. M. Nickov, *Phys. Rev.* **B3**, 4 (1971) 1268–1279.
Prokhorov, E. D., N. I. Beletskii, and A. V. Dyadchenko, *Radiotekhnika i Elektronika* **22**, 6 (1977) 1313–1315, (in Russian).
Ram, R. K. and S. S. Kushwaha, *J. Phys. Soc. Jpn.* **54**, 2 (1985) 617–624.
Rode, D. L., *Phys. Rev.* **B3**, 10 (1971) 3287–3299.
Skountzos, P. A. and P. C. Euthymiou, *J. Appl. Phys.* **47**, 10 (1976) 4693–4696.
Slutsky, L. J. and C. W. Garland, *Phys. Rev.* **113**, 1 (1959) 167–169.
Sparks, P. W. and C. A. Swenson, *Phys. Rev.* **163**, 3 (1967) 779–790.
Van Camp, P. E., V. E. Van Doren, and J. T. Devreese, *Phys. Rev.* **B41**, 3 (1990) 1598–1602.
Ukhanov, Yu. I., *Optical Properties of Semiconductors*, Moscow, "Nauka" Publ. Co., 1977, (in Russian).
Vorobyev, L. E., V. I. Stafeev, V. A. Shalygin, and A. V. Shturbin, *Sov. Phys. Semicond.* **17**, 1 (1983) 81–84.
Wiley, J. D., *Semiconductors and Semimetals*, R. K. Willardson and A. C. Beer, eds., Academic Press, N.Y., vol. 10, 1975, p. 91.
Yaremenko, N. G., V. T. Potapov, and V. S. Ivleva, *Sov. Phys. Semicond.* **6**, 7 (1973) 1084–1090.
Zawadski, W., *Advances in Phys.* **23**, 3/4 (1974) 435–522.
Zimpel, M., M. Oszwaldowski, and J. Goc, *Acta Physica Polonica* **A75**, 2 (1989) 297–300.

APPENDICES

Appendix 1. Basic Physical Constants

Quantity	Symbol	Value
Avogadro number	N_{AV}	$6.0221 \times 10^{23}\,\mathrm{mol}^{-1}$
Bohr energy	E_B	$13.606\,\mathrm{eV}$
Bohr magneton	μ_B	$5.788 \times 10^{-5}\,\mathrm{eV\,T}^{-1}$
Bohr radius	a_B	$0.5292\,\text{Å}$
Boltzmann constant	k_B	$1.381 \times 10^{-23}\,\mathrm{J\,K}^{-1}$
Boltzmann constant $/q$	$k_B\,q^{-1}$	$8.617 \times 10^{-5}\,\mathrm{eV\,K}^{-1}$
Electronic charge	q	$1.602 \times 10^{-19}\,\mathrm{C}$
Electronvolt	eV	$1.602 \times 10^{-19}\,\mathrm{J}$
Fine structure constant	α_0	0.007297
Gas constant	R	$8.315\,\mathrm{J\,mol}^{-1}\,\mathrm{K}^{-1}$
Gravitational constant	γ	$6.673 \times 10^{-11}\,\mathrm{m}^3\,\mathrm{kg}^{-1} \times \mathrm{s}^{-2}$
Impedance of free space	$1/c\varepsilon_0 = \mu_0 c$	$376.7\,\Omega$
Mass of electron at rest	m_0	$0.9109 \times 10^{-30}\,\mathrm{kg}$
Mass of proton at rest	M_p	$1.672 \times 10^{-27}\,\mathrm{kg}$
Permeability in vacuum	μ_0	$1.256 \times 10^{-8}\,\mathrm{H\,cm}^{-1}$ $(4\pi \times 10^{-9})^{-1}$
Permittivity in vacuum	ε_0	$8.854 \times 10^{-12}\,\mathrm{F\,m}^{-1}$
Planck constant	h	$6.626 \times 10^{-34}\,\mathrm{J} \times \mathrm{s}$
Reduced Planck constant	$\hbar = h/(2\pi)$	$1.054 \times 10^{-34}\,\mathrm{J} \times \mathrm{s}$
Speed of light in vacuum	c	$2.997 \times 10^{8}\,\mathrm{m\,s}^{-1}$
Standard atmosphere		$1.013 \times 10^{5}\,\mathrm{N\,m}^{-2}$
Thermal voltage at 300 K	$k_B T q^{-1}$	$0.0258\,\mathrm{V}$
Wavelength of visible light	λ	0.4 to $0.7\,\mu\mathrm{m}$

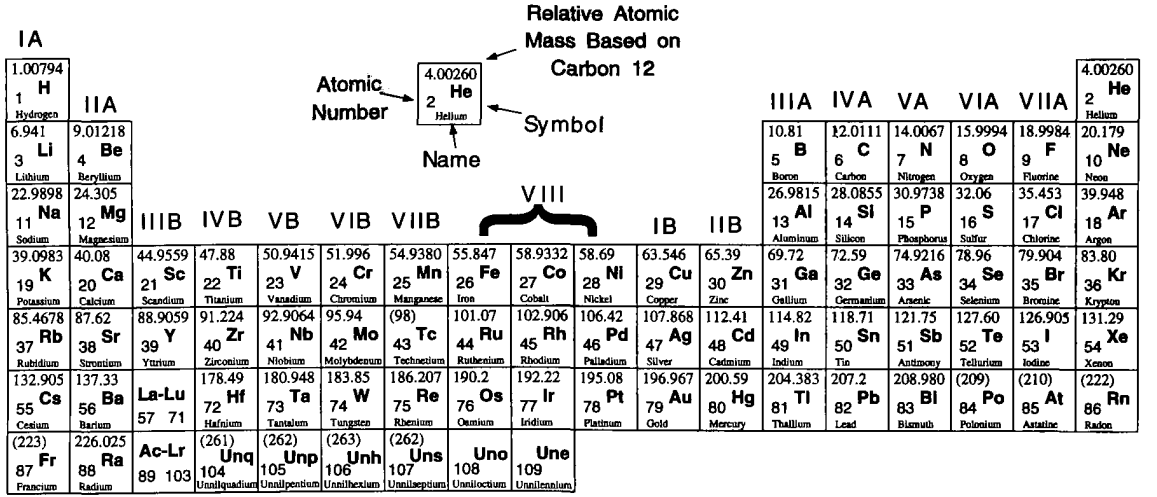

138.906 57 La Lanthanum	140.12 58 Ce Cerium	140.908 59 Pr Praseodymium	144.24 60 Nd Neodymium	(145) 61 Pm Promethium	150.36 62 Sm Samarium	151.96 63 Eu Europium	157.25 64 Gd Gadolinium	158.925 65 Tb Terbium	162.50 66 Dy Dysprosium	164.930 67 Ho Holmium	167.26 68 Er Erbium	168.934 69 Tm Thulium	173.04 70 Yb Ytterbium	174.967 71 Lu Lutetium
227.028 89 Ac Actinium	232.038 90 Th Thorium	231.036 91 Pa Protactinium	238.029 92 U Uranium	237.048 93 Np Neptunium	(244) 94 Pu Plutonium	(243) 95 Am Americium	(247) 96 Cm Curium	(247) 97 Bk Berkelium	(251) 98 Cf Californium	(252) 99 Es Einsteinium	(257) 100 Fm Fermium	(258) 101 Md Mendelevium	(259) 102 No Nobelium	(260) 103 Lr Lawrencium

Lactonoid series

Actinoid series

Masses in parentheses are masses of the most stable isotopes

Appendix 3. Greek Symbols

Letter	Lowercase	Capital
Alpha	α	A
Beta	β	B
Gamma	γ	Γ
Delta	δ	Δ
Epsilon	ε	E
Zeta	ζ	Z
Eta	η	H
Theta	θ	Θ
Iota	ι	I
Kappa	κ	K
Lambda	λ	Λ
Mu	μ	M
Nu	ν	N
Xi	ξ	Ξ
Omicron	o	O
Pi	π	Π
Rho	ρ	P
Sigma	σ	Σ
Tau	τ	T
Upsilon	υ	Y
Phi	ϕ	Φ
Chi	χ	X
Psi	ψ	Ψ
Omega	ω	Ω

Appendix 4. Diamond Crystal Structure

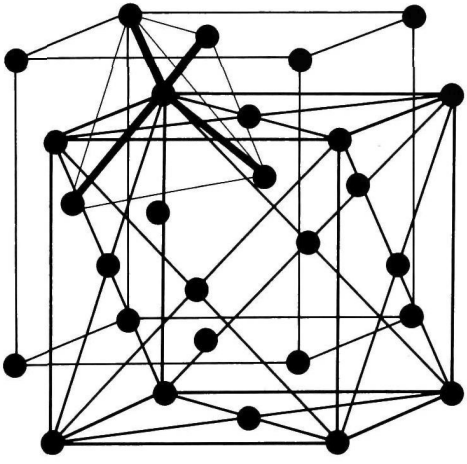

Thin lines show the tetrahedral atomic configuration.

Appendix 5. Zinc Blende Structure

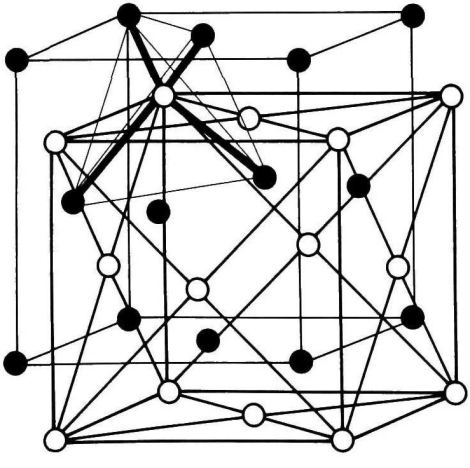

Thin lines show the tetrahedral atomic configuration.

Appendix 6. The First Brillouin Zone for the Face Centered Cubic (fcc) Lattice

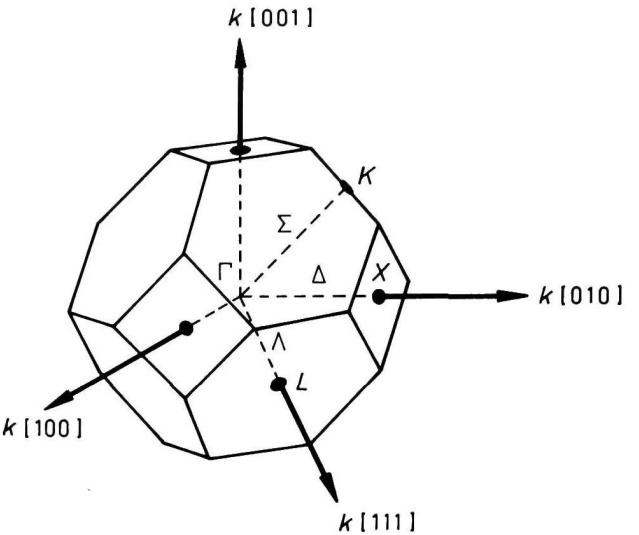

Symmetry points of the first Brillouin zone for the face centered cubic lattice

Notation	Location	Number of equivalent k-vectors	Symmetry operations	Point group of symmetry
Γ	(000)	1	$E, 8C_3, 3C_2, 6S_4, 6C_s$	T_d
X	$\frac{2\pi}{a}(101)$	3	$E, 3C_2, 2S_4, 2\sigma$	D_{2d}
L	$\frac{2\pi}{a}\left(\frac{1}{2}\frac{1}{2}\frac{1}{2}\right)$	4	$E, 2C_3, 3\sigma$	C_{3v}
W	$\frac{2\pi}{a}\left(10\frac{1}{2}\right)$	6	$E, 2S_4, C_2$	S_4
Δ	$(k00)$	6	$E, 2\sigma, C_2$	C_{2v}
Λ	(kkk)	4	$E, 2C_3, 3\sigma$	C_{3v}
Σ	$(k0k)$	12	E, σ	C_s
K	$\frac{2\pi}{a}\left(\frac{3}{4}0\frac{3}{4}\right)$	12	E, C_2	C_s